Host-Microbe Interactions
Impacting and Mediated
by Nervous Systems

Thesis by

Bryan B. Yoo

In Partial Fulfillment of the Requirements for

the degree of

Doctor of Philosophy

Caltech

CALIFORNIA INSTITUTE OF TECHNOLOGY

Pasadena, California

2020

Defended May 22, 2020

© 2020

Bryan B. Yoo
ORCID: 0000-0003-1450-2696

ACKNOWLEDGEMENTS

"The most valuable fruit ... was the profound conviction that living nature, far from being drained and exhausted, keeps back from all of us, great and small, immeasurable stretches of unknown territory; and that, even in the regions apparently most worked over, there remains still many unknown things to be cleared up."

Santiago Ramón y Cajal (Recollections of My Life, 1917)

Optimism, pessimism, and realism are essential characteristics of the psyche and are also largely applicable to the scientific process, from hypothesis to discovery to application. This process has made me unapologetically curious, fearlessly inspired, cautiously hesitant, and obsessively determined. These states of being have defined my journey into biology's abyss- a journey made only possible by those around me, from whom I have learned immensely from, remain eternally grateful for, and owe everything to.

To my advisor, Professor Sarkis Mazmanian: The trust you showed in me from the very beginning nourished my instincts and abilities. The intellectual freedom I had as a result enabled me to explore the depths of my scientific interests and helped me grow into who I am today. You have been so much more than a scientific mentor to me, and it has truly been an honor work with you and contribute to the work of the laboratory.

To Professors Marianne Bronner and Henry Lester: I am humbled to have been able to call on you for guidance. Thank you for continuing to be a source of inspiration through the sustaining work you do.

To Professor Viviana Gradinaru: Thank you for introducing me to neuroscience. None of this would have been possible without your invaluable support and gracious collaboration.

To Professor Rustem Ismagilov: Thank you for supporting me as a rotation student the summer before I officially began graduate school. Your outlook on science and your approach to problem-solving made indelible mark on me.

To past and present (more than just) colleagues: Thank you all for enriching my experience at Caltech. It is because of you that I was able to thrive in the peaks and persevere through the valleys of graduate school. It is our work *together* that helped me obtain this degree, and I am forever grateful for this. I will always cherish the conversations we had and the memories we made and look forward to the coming years when we can reminisce upon the time we shared together.

To my friends. You have made a tremendous impact on my life and have had an integral role in my successes while being there to help me navigate through my failures. You have not only been the light at the end of the tunnel, but my light through it. You connect my past with my present and will be with me in my future, and for that I am forever grateful. These are the names I would like to forever enshrine in this thesis: Adam Tarhouni, Afeef Ahmed, Andrea Taylor Lindsay, Andrew Strong, Armen Petrosian, Bobby Murphy, Diana Ajuria, Gabe Lupin, Kelsey Murphy, Kiah Lesher, Melissa Lupin, Moniza Ahmed, Nick Streets, Pitch Lindsay, and Stephanie Papes.

To my in-laws, mother, father, and sister: You have supported me every step of the way, accounting for many of the memories and meals I have had during graduate school. You have accepted me, truly as one of your own, and trusted me with your daughter and your sister. I hope that I continue to make you all proud. Seo Woo aka Alma, thank you for allowing me to be your big brother. I always wanted a younger sibling. You impress me every day and I am so proud to be a witness to your growth.

To my family: Your love is limitless, and I hope to always share the type of love you taught me. Mom and Dad, I was not the easiest child to raise, yet your support was and is unwavering. I am overwhelmed by the privilege and opportunity your hard work has afforded me and am awe-inspired by your dedication to our family to this day. I can never repay you for your unconditional love, but I hope to always make you proud. Elisa, thank you for being my older sister, for always engaging in (un)friendly banter, preparing me for it at the next level, and being someone whom I aspire to be more like. Brandon, thank you for coming into

my life and being a big brother that I can lean on. You tell it to me straight, and you know that I need that.

To my wife and life partner, Shin Young: You uprooted your beautiful life in Seoul and trusted a 26-year-old who just began another half decade stint as a student. You met me when I still had training wheels and helped me take them off as we embarked on a life together. Your love is robust and enduring and none of this would be possible without you. You deserve this doctorate degree just as much as I do. I love you.

"Asiye funzwa na mamae hufunzwa na ulimwengu" (in Swahili)
(Whomsoever is not taught by the mother will be taught with the world)

Thank you all for being my world.

ABSTRACT

Animals and microbes coevolved, and thus it is not surprising that the trillions of microorganisms that harmoniously inhabit the mammalian gastrointestinal tract (GIT), collectively termed the gut microbiome, continue to be implicated in healthy and disease states. However, less is known about the mechanisms by which these states are maintained, and how deviations from homeostasis (i.e., dysbiosis) occurr. This thesis explores the relationship between host-microbe interactions and the central and peripheral nervous systems. Specifically, the first chapter of this thesis explores how the microbiome differs is patients with multiple sclerosis and how these differences alter diseases outcomes in a mouse model of the disease. Next, we introduce the enteric nervous system (ENS), the intrinsic nervous system of the GI tract which is supposed as a major conduit of the bidirectional communication between the gut and the brain. Lastly, by adopting biotechnologies in gene delivery and genetically encoded tools for neuroscience, we introduce a molecular toolkit to characterize the ENS in a robust and efficient manner and modulate the ENS to uncover novel mechanisms by which innervation of the GI mediates host-microbe interactions.

PUBLISHED CONTENT AND CONTRIBUTIONS

Chapter II

Egle Cekanaviciute, **Bryan B. Yoo**, Tessel F. Runia, Justine W. Debelius, Sneha Singh, Charlotte A. Nelson, Rachel Kanner, Yadira Bencosme, Yun Kyung Lee, Stephen L. Hauser, Elizabeth Crabtree-Hartman, Ilana Katz Sand, Mar Gacias, Yunjiao Zhu, Patrizia Casaccia, Bruce A. C. Cree, Rob Knight, Sarkis K. Mazmanian, and Sergio E. Baranzini. (2017) "Gut bacteria from multiple sclerosis patients modulate human T cells and exacerbate symptoms in mouse models." *Proceedings of the National Academy of Sciences of the USA* 114 (40): 10713-10718.
DOI: 10.1073/pnas.1711235114

B.B.Y. and E.C. contributed equally to the work. B.B.Y. designed, performed, and analyzed *in vivo* animal work.

Chapter III

Bryan B. Yoo and Sarkis K. Mazmanian. (2017) "The Enteric Network: Interactions between the Immune and Nervous Systems of the Gut." *Immunity* 46 (6): 910-926.
DOI: 10.1016/j.immuni.2017.05.011

B.B.Y. conceived the topics, wrote the review, and drew the figures

Chapter IV

Ken Y. Chan, Min Y. Jang, **Bryan B. Yoo**, Alon Greenbaum, Namita Ravi, Wei-Li Wu, Luis Sánchez-Guardado, Carlos Lois, Sarkis K. Mazmanian, Benjamin E. Deverman, and Viviana Gradinaru. Engineered AAVs for efficient noninvasive gene delivery to the central and peripheral nervous systems." *Nature Neuroscience* 20 (8):1172-1179.
DOI: 10.1038/nn4593

B.B.Y helped characterize AAV-PHP.S in mice.

Bryan B. Yoo, Jessica A. Griffiths, Peter Thuy-Boun, Victor Cantu, Kelly Weldon, Collin Challis, Michael J. Sweredoski, Ken Y. Chan, Taren M. Thron, Gil Sharon, Annie

Moradian, Gregory Humphrey, Qiyun Zhu, Justin Shaffer, Dennis W. Wolan, Pieter C. Dorrestein, Rob Knight, Viviana Gradinaru, and Sarkis K. Mazmanian.
Tools to characterize the enteric nervous system and assay the consequences of its activation. *(Submitted for publication)*

B.B.Y. conceived the project, led the design of all experiments and executed them to obtain samples for analysis, interpreted the results, and wrote the manuscript.

TABLE OF CONTENTS

LIST OF FIGURES, ILLUSTRATIONS, AND TABLES

C h a p t e r   1

INTRODUCTION

Introduction

The human body consists of organs and organ systems that make, circulate, and utilize our life blood. However, often forgotten are the organisms that live on and within us that work in synergy with our body to maintain physiologies that are integral to our development, health, and survival. Over the years, the consortia of microbes that inhabit the gastrointestinal tract, collectively termed the gut microbiome, have been implicated in numerous physiologies associated with diverse cell types and organ systems, in both health and disease. Such implications range from maintenance and afflictions of the immune system (1), metabolism (2), and even behavior and neurological disease (3). Neuroimmunology, the study by which neurons in the brain and the periphery interact with the immune system, has been of particular interest to those that study the gut microbiome (4, 5). As the immune system continues to implicate neurological diseases (6, 7), and conversely, the nervous system implicates immunity (8, 9), the microbiome is well documented to have a modulatory effect on both the immune and nervous systems. However, the mechanisms of action by which the microbiome contributes to health and disease are complex and multifactorial, and thus deducing its contribution to the etiology of diseases remains difficult to dissect and is poorly understood.

The first aim of this thesis (Chapter 2) is to demonstrate the contribution of the microbiota in the progression and/or the protection against multiple sclerosis (MS), a neurodegenerative disease that results from the demyelination of neurons in the brain and the spinal cord. The cause of MS is unknown, however genetic and immunological mouse models of the disease have been developed. Furthermore, given the relapsing and remitting nature of the disease, environmental factors have been favorably hypothesized regarding its etiology. In this chapter we show that the microbiota differs between human patients with MS and their respective household controls. Additionally, we create a humanized gnotobiotic mouse model by transplanting the microbiome from MS patients into germ-free mice. In doing so, we find that the MS microbiome induces a more pro-inflammatory tissue environment, whereas the respective controls have a more anti-inflammatory tone. These humanized mice were induced with experimental autoimmune encephalomyelitis, an immunological mouse

models of MS. We found that those mice with microbiome transplants from MS patients exhibited worsened disease outcomes, implicating the microbiome and its modulation of the immune system as a mechanism by which MS and its associated sporadic exacerbations develop.

Although this study provides a link between the microbiota, immune system, and neurodegenerative disease, it does not explain how the underlying dysbiosis of the gut microbiome develops and persists. Animals have coevolved with the microbes that inhabit their gastrointestinal tract. Thus, there must have been evolutionary selective pressure on the luminal environment to exclude harmful and disease-causing microbes while allowing health promoting microbes to thrive. Understanding the mechanisms by which an "unhealthy" microbiome develops or how a "healthy" microbiome is sustained may hold the answer to novel therapeutic targets, treatments, and preventive measures.

Towards this end, we introduce the enteric nervous system (ENS) which is the network of neurons and glia that envelope the entire gastrointestinal tract. The GI ecosystem can be largely characterized by the exchange of molecules between and within luminal constituents and the host. Environmental and dietary molecules are necessary for host survival but, in addition, are important factors that affect gut microbes and the factors they produce. How these luminal components, as a whole, interact with the cells and molecules of the intestine elucidates complex and coordinated events that occur in the GI tract. Homeostatic communication across the intestinal epithelium involves contributions by diet and the microbiota, interacting with the mucosal immune system and the ENS. In the GI tract, multiple distinct cell types can produce a given modulatory molecule, and conversely, a given molecule is able to affect various cell types. This molecular synchrony, and deviations from it, impact expansive GI and non-GI physiologies. Yet understanding of cellular and molecular interconnections at this critical interface between the body and the environment remains largely unexplored. In Chapter 3 of this thesis, we review the diverse cellular anatomy of the GI system and discuss the molecules and receptors that various cell types use to communicate and function. The unique juxtaposition of a robust enteric

nervous and immune system, positioned in a location with the most extensive portal to our molecular universe, suggests a vital role for neuro-immune interactions in the gut whose effect goes beyond the host (i.e. microbes) and the confines of the GI tract.

In Chapter 4 of this thesis, we introduce an experimental toolbox to characterize and interrogate the ENS. As the ENS becomes more implicated in a diverse array of physiologies, we believe that it is crucial to thoroughly characterize the ENS and all of its subtleties. This is currently difficult to achieve due to the expansive nature of the GI tract and the limitations of antibody mediated labelling. Utilizing adeno-associated viral particles loaded with genetically encoded fluorescent reporters, we are able to characterize the cellular architecture of the ENS. Furthermore, by repurposing biotechnologies used in neuroscience research, we begin to define the consequence of *in vivo* ENS activation. Using a multi-omics assay approach, we discover activation mediated changes to the intestinal transcriptome and the luminal proteome, metagenome, and metabolome. From our research, we conclude that the ENS is capable of mediating a breadth of diverse cellular communications in the GI tract, of both host and microbial origin. These findings elucidate novel host-microbe interactions mediated by nervous systems and begin to uncover the potential etiological impact of the ENS in health and disease states.

We sincerely hope that the findings of this thesis introduce novel biological paradigms that inspire innovation in the way health is maintained and disease is treated.

References

1. Mowat AM, Agace WW (2014) Regional specialization within the intestinal immune system. *Nat Rev Immunol* 14(10):667–685.

2. Albenberg LG, Wu GD (2014) Diet and the intestinal microbiome: associations, functions, and implications for health and disease. *Gastroenterology* 146(6):1564–1572.

3. Sampson TR, Mazmanian SK (2015) Control of Brain Development, Function, and Behavior by the Microbiome. *Cell Host Microbe* 17(5):565–576.

4. Veiga-Fernandes H, Mucida D (2016) Neuro-Immune Interactions at Barrier Surfaces. *Cell* 165(4):801–811.

5. Sharkey KA, Beck PL, McKay DM (2018) Neuroimmunophysiology of the gut: advances and emerging concepts focusing on the epithelium. *Nature Reviews Gastroenterology and Hepatology* 15(12):765–784.

6. Fung TC, Olson CA, Hsiao EY (2017) Interactions between the microbiota, immune and nervous systems in health and disease. *Nat Neurosci* 20(2):145–155.

7. Vezzani A, Viviani B (2015) Neuromodulatory properties of inflammatory cytokines and their impact on neuronal excitability. *Neuropharmacology* 96:70–82.

8. Tracey KJ (2002) The inflammatory reflex. *Nature* 420(6917):853–859.

9. Steinman L (2004) Elaborate interactions between the immune and nervous systems. *Nat Immunol* 5(6):575–581.

C h a p t e r   2

GUT BACTERIA FROM MULTIPLE SCLEROSIS PATIENTS MODULATE HUMAN T CELLS AND EXACERBATE SYMPTOMS IN MOUSE MODELS

Egle Cekanaviciute, **Bryan B. Yoo**, Tessel F. Runia, Justine W. Debelius, Sneha Singh, Charlotte A. Nelson, Rachel Kanner, Yadira Bencosme, Yun Kyung Lee, Stephen L. Hauser, Elizabeth Crabtree-Hartman, Ilana Katz Sand, Mar Gacias, Yunjiao Zhu, Patrizia Casaccia, Bruce A. C. Cree, Rob Knight, Sarkis K. Mazmanian, and Sergio E. Baranzini. (2017) "Gut bacteria from multiple sclerosis patients modulate human T cells and exacerbate symptoms in mouse models."

ABSTRACT:

The gut microbiota regulates T cell functions throughout the body. We hypothesized that intestinal bacteria impact the pathogenesis of multiple sclerosis (MS), an autoimmune disorder of the central nervous system, and thus analyzed the microbiomes of 71 MS patients not undergoing treatment and 71 healthy controls. Although no major shifts in microbial community structure were found, we identified specific bacterial taxa that were significantly associated with MS. *Akkermansia muciniphila* and *Acinetobacter calcoaceticus*, both increased in MS patients, induced pro-inflammatory responses in human PBMCs and in mono-colonized mice. In contrast, *Parabacteroides distasonis*, which was reduced in MS patients, stimulated anti-inflammatory interleukin-10 (IL-10)-expressing human CD4+CD25+ T cells, and IL-10+FoxP3+ regulatory T cells (Tregs) in mice. Finally, microbiota transplants from MS patients into germ-free mice resulted in more severe symptoms of experimental autoimmune encephalomyelitis (EAE) and reduced proportions of IL-10+ Tregs compared to mice "humanized" with microbiota from healthy controls. This study identifies specific human gut bacteria that regulate adaptive autoimmune responses, suggesting therapeutic targeting of the microbiota as a novel treatment for MS.

SIGNIFICANCE:

For the first time, we have experimentally investigated the immunoregulatory effects of human gut microbiota in multiple sclerosis (MS). We have identified specific bacteria that are associated with MS and demonstrated that these bacteria regulate T lymphocyte-mediated adaptive immune responses and contribute to the pro-inflammatory environment *in vitro* and *in vivo*. Thus, our results expand the knowledge of the microbial regulation of immunity and may provide a basis for the development of microbiome-based therapeutics in autoimmune diseases.

Introduction

A major role of the human gut microbiota is to regulate both innate and adaptive immune responses during health and disease (1). Most studies of the human microbiome to date have focused on analyzing microbial population structures. However, it is equally important to investigate how variability in microbial abundance and composition affects host functions (2, 3). Exposing primary human immune cells to microbes or microbial products *in vitro* allows functional investigation of immunomodulatory effects by the gut microbiota (4-6).

There is growing evidence of population differences in the gut microbiota in multiple human autoimmune diseases (7, 8), including multiple sclerosis (MS) (9-12). While these studies in MS were performed with small sample sizes, and did not stratify patient groups by treatment with disease modifying drugs, consistent patterns of modest dysbiosis appear to be emerging. Furthermore, microbiota have been shown to mediate regulation of immune responses in experimental autoimmune encephalomyelitis (EAE), a mouse model of MS (13, 14). MS-like symptoms in EAE can be exacerbated by T helper 1 and 17 (Th1 and Th17) responses, and modulated by regulatory T lymphocytes (Tregs) (15, 16).

This led us to investigate structural and functional changes in intestinal microbiota as a potential component of MS pathogenesis. Specifically, we identified differences in microbial abundance between MS patients and controls, and investigated how particular MS-associated bacteria modulate T lymphocyte responses using both *in vitro* and *in vivo* model systems. Our results indicate that differences in specific gut bacteria are functionally associated with a shift towards a pro-inflammatory T cell profile that may exacerbate or perpetuate autoimmune responses, thus potentially identifying a novel environmental contributor to MS pathogenesis.

Results

MS microbiome elicits differential Treg responses and shows modest dysbiosis at genus level

To investigate whether MS-associated bacteria affect immune functions in the host, we stimulated peripheral blood mononuclear cells (PBMCs) from MS patients or healthy controls, using extracts from total bacteria isolated from the stool samples of the same subjects who were PBMC donors (thus, "self" bacterial extracts). We observed that PBMCs from MS patients showed an impaired ability to differentiate or expand CD25+FoxP3+ Treg populations (Figure 1A; Treg proportion expressed as fold difference over no-bacteria vehicle control). The total CD3+CD4+ T helper lymphocyte population (1.037±0.076 fold change in the percentage of CD3+CD4+ cells out of all live lymphocytes) was not altered by bacterial extract treatment, and the baseline proportion of CD25+FoxP3+ Tregs out of CD3+CD4+ T cells was not different between MS patients and healthy controls. These results suggest an immunoregulatory interaction between microbiota and PBMCs of MS patients that is functionally different compared to healthy controls.

We subsequently analyzed the microbiome by 16S rRNA gene sequencing of stool samples from 71 untreated relapsing-remitting MS patients and 71 healthy controls (demographic data, Supplemental Table S1). A subset of 79 subjects was sampled on two consecutive days to account for variability over time, and all subjects were used to compare the variability within and between subject groups (Supplemental Figure 1). We did not observe major global shifts in bacterial community structure in terms of alpha or beta diversity (Figure 1B, 1C), which is unsurprising given similar findings in other autoimmune diseases (7, 8). However, despite similar alpha and beta diversity (Figure 1B, 1C) we did observe differences at the level of individual microbial taxa between MS and control subjects (Figure 1D, Figure 2).

We identified 129 total genera and 1462 total operational taxonomic units (OTUs) in our samples. We systematically compared relative abundances of individual microbial taxa between MS patients and controls at the genus and OTU levels by negative binomial Wald test using Benjamini-Hochberg correction for multiple comparisons (17). Our analysis revealed differences in the relative abundance of 247 OTUs (16.89% of total) and 25 bacterial genera (19.38% of total) that were either significantly increased or reduced in MS

(Figure 2A, 2B). All genera that were significantly different between MS patients and healthy controls (Figure 2A points above the dotted line) are listed in Table 1, and all significantly different OTUs are listed in Supplemental Table S2.

We then selected individual significantly different taxa for functional studies to assess their potential contribution to autoimmune inflammation in MS. The specific taxa were selected based on the following criteria, here listed in order of importance: 1) identifiable to species level or genus level with high overlap between species; 2) culturable, in order to be able to study their functions *in vitro* and *in vivo;* 3) type strains available from ATCC to ensure reproducibility; and 4) previously associated with immunoregulatory effects.

Among the genera significantly increased in MS samples were *Acinetobacter* and *Akkermansia,* while one of the most significantly reduced genera in MS patients was *Parabacteroides*, with the majority of OTUs mapping to *P. distasonis* (Figure 2C, Supplemental Figure 2). Interestingly, *P. distasonis* was previously reported to induce a Treg phenotype in gnotobiotic mouse models (18, 19). All *Acinetobacter* species, including *A. baumannii, A. calcoaceticus* and *A. lwoffii,* are rare in the healthy human gut microbiome and share genome-wide homology (20, 21), making them indistinguishable by 16S amplicon sequencing. Thus, OTUs that mapped to the genus *Acinetobacter* did not allow for species-level discrimination. However, because *A. calcoaceticus* has been associated with MS in prior publications (22), we focused on this organism as a candidate for functional studies of immune regulation. Finally, all OTUs that mapped to the *Akkermansia* genus belonged to the species *A. muciniphila*, which has mostly been studied in the context of metabolism (23), but also contributes to inflammation during infection *(12, 24)*.

MS-associated bacterial species reduce Tregs and increase Th1 lymphocyte differentiation *in vitro*

We hypothesized that bacterial taxa altered in MS patients play functional roles in regulating immune responses. To test this hypothesis, we established an *in vitro* model system by exposing PBMCs from healthy donors to a suspension of heat-killed and sonicated individual

bacterial species (termed "bacterial extracts") under different stimulating conditions (e.g. Treg, Th1, etc), and used flow cytometry to evaluate T lymphocyte differentiation and proliferation. We observed that extracts from *A. calcoaceticus* reduced proportions of CD25+FoxP3+ Tregs among PBMCs (Figure 3A-B). These results suggest that intestinal *A. calcoaceticus* restrains immunoregulatory T cell development consistent with its relative increase in the MS cohort. Furthermore, we observed that *A. calcoaceticus* increased the proportion of effector CD4+ lymphocytes, which differentiated into IFNγ-producing Th1 cells (Figure 3C-D) thereby potentially exacerbating inflammation.

Analysis of *A. muciniphila*, another bacterial species increased in the MS microbiome, revealed an even more pronounced effect on stimulating Th1 differentiation. Extracts from *A. muciniphila* significantly increased healthy donor PBMC differentiation into Th1 lymphocytes (Figure 4A-D). Furthermore, we discovered that the mere presence of *A. muciniphila* in total stool bacteria was sufficient to increase Th1 lymphocyte differentiation *in vitro*. Specifically, exposing PBMCs to total bacterial extracts isolated from unrelated subjects with detectable levels of *A. muciniphila* increased the differentiation of IFNγ+ Th1 lymphocytes compared to bacterial extracts that did not have *A. muciniphila* (Figure 4E, 4G). Similarly, subjects with detectable *A. muciniphila* showed a significant increase in IFNγ+ Th1 differentiation in response to extracts of their own bacteria (Figure 4F, 4H). (The presence of *Acinetobacter* in total stool bacteria was not sufficient to skew PBMC responses to either increase Th1 or reduce Treg differentiation, likely due to its rarity and low relative abundance compared to other bacteria (data not shown)). In summary, we have identified *A. muciniphila* and *A. calcoaceticus* as examples of common and rare MS-associated bacterial species that favor pro-inflammatory T lymphocyte responses *in vitro*.

We next explored whether individual taxa that are less abundant in MS patients could promote immunoregulatory responses. Exposing healthy donor PBMCs to extracts from *P. distasonis* significantly increased the percentage of CD25+ T lymphocytes among the CD3+CD4+ T cell population (Figure 5A-B). Furthermore, we observed an enrichment of CD25+IL-10+ cells (Figure 5C-D), including CD25+IL-10+FoxP3- Tr1 cells (but not

CD25+FoxP3+ Tregs), which have been associated with strong immunoregulatory properties (14, 25). Thus, our results demonstrate that *P. distasonis* is sufficient to skew T lymphocytes toward a regulatory profile *in vitro.*

All immunoregulatory effects described here were at least partially specific to selected bacterial extracts. To show that exposure to any differentially abundant bacteria did not elicit similar effects, we analyzed the immune effects of *Eggerthella lenta,* which is significantly increased in MS patients, and found that it did not alter Th1 or Treg differentiation (Supplemental Figure 3 A, B). In addition, the specificity of *P. distasonis, A. calcoaceticus* and *A. muciniphila* functions is emphasized by the fact that these bacteria did not alter the differentiation of all lymphocyte populations indiscriminately, for example, *P. distasonis* had no effect on Th1 cells, and *A. muciniphila* had no effect on CD25+FoxP3+ Tregs (Supplemental Figure 3 C-E).

While regulation of immune functions by gut microbiota are likely multifaceted and complex, we speculate that the observed *P.distasonis*-associated reduction in immunoregulatory T cells could act in concert with the described increases in *A. calcoaceticus* and *A. muciniphila* and contribute to create an overall pro-inflammatory environment in MS patients.

Colonization of mice with single species of MS-associated bacteria recapitulates *in vitro* T lymphocyte differentiation profiles

To elucidate the role of individual MS-associated bacteria *in vivo,* we colonized antibiotic-treated or GF mice with single species *A. calcoaceticus, A. muciniphila,* and *P. distasonis.* Following colonization, we measured T lymphocyte differentiation in multiple peripheral lymphoid tissues. We were unable to observe an effect of *A. muciniphila* in monocolonized mice as described in our *in vitro* experiments, and we hypothesize that this discrepancy is likely due to differences in host (e.g., mice vs. human). However, we were able to replicate our key findings with the other two species analyzed.

In antibiotic-treated mice *A. calcoaceticus* inhibited FoxP3+ Treg differentiation, while *P. distasonis* stimulated CD4+IL-10+ lymphocyte differentiation (Supplemental Figure 4 A,B.) Furthermore, splenocytes from mice colonized with *P. distasonis* also displayed induction of CD4+IL10+ lymphocytes in response to their bacterial extracts, while this was not observed when splenocytes from control SPF mice were exposed to their own bacterial extracts (Supplemental Figure 4C).

Furthermore, monocolonization of GF mice with *A. calcoaceticus* increased T lymphocyte differentiation into IFNγ+ Th1 phenotype in cervical lymph nodes (Figure 6A), while monocolonization with *P. distasonis* led to significant increases in CD4+IL-10+ T lymphocyte population in mesenteric lymph nodes and spleens (Figure 6B, Supplemental Figure 5). Taken together, the *in vivo* monocolonization results form a consistent complement to our *in vitro* data.

Colonization of mice with MS donor microbiota inhibits Treg differentiation and exacerbates disease severity in experimental autoimmune encephalomyelitis (EAE)

To investigate whether the pro-inflammatory environment established by MS-associated bacteria is physiologically relevant, we randomly selected 3 MS and control donor pairs (each composed of an untreated RRMS patient and a household control) to perform fecal microbiota transplants into groups (n=6-8) of germ-free C57BL/6 mice. Six weeks after transplantation, mice were immunized with MOG_{35-55} to induce EAE. Remarkably, EAE disease scores were significantly increased in mice colonized with microbiota from MS patients when compared to animals colonized with microbiota from healthy controls and germ-free (GF) mice (Figure 7A). This result was recapitulated across all 3 donor pairs tested (Supplemental Figure 6), and accompanied by a lack of IL-10+ Treg induction in mesenteric lymph nodes from MS-microbiota colonized mice (Figure 7C-F, Supplemental Figure 7). RNAseq of spinal cords 35 days after EAE induction revealed hundreds of gene expression differences between GF mice humanized with MS and CTRL microbiota. Interestingly, when a specific analysis was performed to identify the cellular origin of these changes, a

noticeable enrichment towards genes expressed by microglia was observed (Supplemental Figure 8).

The inability of fecal bacteria from MS patients to promote Treg responses was observed both pre- and post- EAE induction, consistent with the microbiota showing no major differences in beta diversity at time points before and after the disease (Figure 7B).

Principal component analysis of beta diversity of the microbiota in recipient animals showed a significant separation by donor that was stabilized as early as 7 days after transplantation (Figure 7B, Supplemental Figure 9A). This separation was recapitulated by metrics of alpha diversity (Supplemental Figure 9B). Interestingly, some of the changes in relative abundance of individual bacterial genera, including a decrease in *Sutterella* and an increase in *Ruminococcus*, were also observed in mice colonized with microbiota from MS-discordant twins (Berer *et al.* accompanying manuscript; Supplemental Figure 9C). Although human and mouse microbiota are not directly comparable, the biological pathways represented by MS-associated taxa largely overlap in both groups (Supplemental Tables S3, S4).

Collectively, the MS microbial community *in vivo* enhances EAE disease progression and fails to induce IL-10+ Tregs relative to gut bacteria from healthy controls, suggesting a functional role for the microbiota in autoimmunity that may be independent of host factors.

Discussion

Summary and implications

Here we present a comparative structural analysis of the gut microbiome from patients with MS, followed by functional studies of MS-associated microbiota. While no major shifts in microbial diversity were identified, specific bacterial taxa were found to be significantly under- or over-represented in untreated MS patients compared to healthy controls. *In vitro* studies of MS-associated bacterial species revealed that even modest dysbiosis could drive a two-stage, immune deviation mechanism (either sequential or parallel), ultimately resulting in skewed T lymphocyte differentiation. *Acinetobacter* and *Akkermansia* species induce a

pro-inflammatory environment, mediated by reduction in CD25+FoxP3+ Tregs and expansion of Th1 lymphocytes. On the other hand, a potential concomitant decrease in *P. distasonis* mediates a relative loss of CD25+IL-10+ T lymphocytes. Furthermore, we show that MS-associated microbiota inhibits IL-10+ T lymphocyte responses *in vivo* and increases disease severity in a mouse model of MS.

Our results corroborate the concept of MS as a multi-hit model that combines genetic predisposition and environmental factors, one of which is the microbiota. The interaction between microbiota and the immune system is likely bidirectional, as suggested by impaired lymphocyte responses of MS patients to self microbiota, but no difference in control lymphocyte responses to either control or MS non-self microbiota (Supplemental Figure 10). Based on our findings, the main function of microbiota in MS is not to cause the disease directly, but rather to exacerbate it by creating a pro-inflammatory environment. A reduction in *Parabacteroides*, an increase in *Acinetobacter* and an increase in *Akkermansia* can together or separately contribute to inflammation and disease severity without being the only factors that account for the development of the disease. Thus, it is essential to view our findings not as an exclusive list of immunoregulatory microbiota, but rather as the first step in investigating the microbial species and pathways that contribute to the regulation of autoimmune inflammation in MS and other diseases.

In contrast to recent publications profiling the microbiome in MS and other chronic diseases (9, 10, 26, 27), we focused exclusively on patients that were not receiving disease-modifying therapeutics at the time of sample collection to decouple the effects of the disease and therapy, a valuable strategy highlighted in a recent report on Crohn's disease (8). In concordance with prior studies in MS, we did not observe global changes in microbial community structures. However, the larger sample size in our study allowed us to identify individual bacterial taxa that are potentially associated with autoimmunity. In addition, in contrast to studies on MS microbiota that were limited to identifying correlations between microbial taxa and host phenotypes (28, 29), we were able to investigate microbial immunoregulatory effects *in vitro* and *in vivo*.

Our taxa-specific investigation was focused on commensal microbiota, not infectious pathogens. *Akkermansia* and *Parabacteroides* are commensal and even *Acinetobacter*, even though it is typically contracted as an infection, is not considered a pathogen once it inhabits the human gut. We consciously chose to investigate the physiological contribution of commensals to systemic inflammation, as their ability to alter T lymphocyte differentiation is likely to create a systemic environment that may exacerbate inflammation in the host without overt infection, which constitutes a plausible model for MS etiology.

In our admittedly simplistic experimental setup, we used crude bacterial extracts without prior fractionation, thus relevant active components may consist of any bacterial products, either secreted or intracellular. Known bacterial metabolites with immunoregulatory effects fall into multiple categories, including polysaccharides (30), short-chain fatty acids (31), and aryl hydrocarbons (32). In addition, although we analyzed the effects of bacterial extracts on peripheral immune cells, some bacterial metabolites are able to cross the blood-CNS barrier and directly regulate CNS inflammation via microglia (33, 34) or astrocytes (32). Future research will likely be directed towards identifying the therapeutic potential of such products in MS and other complex diseases.

Potential mechanisms of microbial regulation of autoimmunity in MS

Our findings indicate that both rare and common microbiota may play a role in the exacerbation of autoimmune inflammation in MS. Notably, the presence of a relatively common bacterial species, *A. muciniphila,* in total stool bacteria was sufficient to recapitulate its functions of skewing PBMC responses towards pro-inflammatory Th1 phenotype. Apart from their *A. muciniphila* content, the subjects used for this analysis had very variable microbiomes based on 16S sequencing, which further supports the hypothesis that *A. muciniphila* is one of the keystone species sufficient to drive the microbiota towards Th1 induction. Despite this intriguing result, *A. muciniphila* is unlikely to be the only microbial species that is sufficient to induce Th1 differentiation. Instead, the discovery of *A. muciniphila* as a major pro-inflammatory regulator may be considered as the first step in

identifying other microbes and microbial pathways that are sufficient for inducing Th1 differentiation.

Contradictory to our *in vitro* results, the pro-inflammatory role of *A. muciniphila* was absent in monocolonized mice. This difference may be caused by a discrepancy in mouse and human immune cell responses to *A.muciniphila.* In addition, the main *in vivo* role of *A. muciniphila* may have little to do with its direct effects on T cells: it may instead shape the rest of the microbial community towards more pro-inflammatory phenotype. This function would explain why *A. muciniphila* is more abundant in untreated MS patients both in our study and a previous investigation of an independent cohort (12), and is sufficient to induce pro-inflammatory functions of total microbial community.

By contrast, *Acinetobacter* is an example of a species that is rare, but nonetheless was revealed to have a higher relative abundance in MS patients. Although it cannot be considered as a universal contributor to MS severity due to its rarity, we view it as one of multiple environmental contributors that are able to exacerbate the disease. Its role may be explained by drawing an analogy to genetics: same as a specific allele, a specific bacterial species may be rare overall, but significantly increased in MS patients compared to controls, and contribute to disease severity in those few MS patients in which it is present.

Our observed increases in *Acinetobacter,* which typically only colonizes the human gut during an infection, is consistent with previous reports of heightened serum antibody responses to *Acinetobacter* in MS patients compared to healthy controls (22, 35). Strikingly, *A. calcoaceticus* has also been shown to encode peptides that mimic the amino acid sequences of myelin basic protein (MBP) and myelin oligodendrocyte glycoprotein (MOG) (22), both of which are components of the myelin sheath that undergoes autoimmune destruction in MS (36). This suggests that molecular mimicry could potentially transform a normal immune response towards *Acinetobacter* into autoimmunity against myelin. Recently, another model of molecular mimicry mediated CNS autoimmunity was proposed when aquaporin 4-specific T lymphocytes from neuromyelitis optica patients were found to

recognize a peptide from *C. perfringens* and induce a Th17 bias (6) and this organism was found to be over abundant in NMO patients compared to HC (37).

Although intestinal *A. muciniphila* has been extensively studied in the context of diet and obesity (23, 38), its role in regulating immune responses is less well understood. Here we provide *in vitro* evidence that *A. muciniphila* promotes Th1 lymphocyte differentiation. Consistent with our observations, *A. muciniphila* has been reported to exacerbate inflammation during infection (24). In contrast, a recent study reported that EAE-resistant male TNFR2-/- mice harbor more *A. muciniphila* compared to disease-susceptible TNFR2-/- females (39). However, it remains to be addressed whether EAE susceptibility in this genotype is driven by the microbiome or by other factors that stem from gender and genetic differences. Notably, in a recently published study (12) as well as in the MS-discordant twin study that accompanies our manuscript (Berer *et al.)*, *Akkermansia* was reported to be elevated in untreated MS patients.

A growing body of literature has associated both CD25+FoxP3+ Tregs and IL-10 expressing T lymphocytes with alterations in gut microbiota. For example, monocolonization of GF mice with specific bacterial species is sufficient to drive CD25+FoxP3+ Treg differentiation and alter disease phenotype (3). Of interest, *P. distasonis* has also been shown to induce Treg differentiation in GF mice (2). In addition, our findings suggest that *in vivo* exposure to pure *P. distasonis* is associated with a subsequent immunoregulatory response to this bacterium *in vitro*. This observation is supported by the result that the immune cells of MS patients have impaired Treg differentiation in response to autologous ("self") bacteria. Thus, the initial exposure to *P. distasonis* or other "beneficial" bacteria found in healthy subjects may contribute to expanding regulatory T lymphocyte precursor populations, thus promoting anti-inflammatory responses upon subsequent exposure to the same bacteria.

Furthermore, we observed a consistent association between healthy control microbiota and CD25+IL-10+ lymphocyte differentiation both *in vitro* and *in vivo.* A similar result is presented in the MS-discordant twin study where blocking IL-10 results in increased EAE

incidence (Berer *et al.*). It has been previously reported that IL-10 deficient mice are susceptible to colitis induced by transplantation of normal mouse microbiota or simplified human microbiota (40, 41). Thus, CD25+IL-10+ lymphocyte differentiation in response to healthy microbiota, and especially to a common and highly abundant bacterial species like *P. distasonis*, may serve as a built-in control mechanism to dampen the pro-inflammatory characteristics of other microbial species. The loss of this mechanism due to MS-associated dysbiosis may then create a pro-inflammatory environment, which may further exacerbate the disease.

Microbial transfer of human phenotypes to gnotobiotic mice

While previous studies using GF mouse models have identified that the absence of gut bacteria ameliorates EAE (13, 14), here we show that gut bacteria transplanted from MS patients promotes more severe EAE symptoms relative to mice that were transplanted with fecal bacteria from household controls. Similar results of microbiota being sufficient to transfer a human donor phenotype to GF mice have been reported in the context of obesity (42) and IBD (43), and rheumatoid arthritis-associated bacteria were shown to exacerbate the disease in a mouse model of colitis (7). However, our study is the first to show that the gut microbiota is able to transfer the phenotype in a disease model unrelated to the digestive system and suggest a potentially causal role for the gut microbiota in MS.

We view GF mouse monocolonization as an experimental model to study microbial functions *in vivo*. However, its biological relevance has multiple caveats, because monocolonization may not represent bacterial functions within the entire microbial community of the gut, and it requires using a mouse host for bacteria that presumably have a function in human disease. Therefore, it is typical to find that *in vivo* studies using monocolonized mice do not completely replicate *in vitro* results from human cells. Instead, it may be advisable to consider all *in vitro* and *in vivo* findings together as the first step for future studies to identify which pathways and metabolites are important for Th1 and IL-10+ regulatory T lymphocyte production. It will open new avenues for the development of novel, microbiome-based therapeutic approaches for autoimmunity.

Figures, Tables, and Legends

Figure 1. MS patient microbiota alter self-Treg differentiation in spite of similar alpha and beta diversity to control microbiota. A. Quantification of CD25+FoxP3+ lymphocytes within CD3+CD4+ population in MS patients (n=7) and healthy controls (n=9), run in triplicate and results averaged, in response to extracts from total bacteria isolated from the stool samples of the same subjects who were PBMC donors (thus, "self" bacteria). CD25+ FoxP3+ lymphocyte induction expressed as fold difference over no-bacteria control. *P <0.05, two-tailed Mann-Whitney test. **B-D.** Comparison of microbial community composition of untreated MS patients (n=71) and healthy controls (n=71). **B**, Chao1 metric of alpha diversity. Error bars, mean±SEM. **C**, PCoA plot of beta diversity (unweighted Unifrac), **D**, mean relative abundance of microbial genera. Upper box, *Akkermansia.* Lower box, *Parabacteroides.*
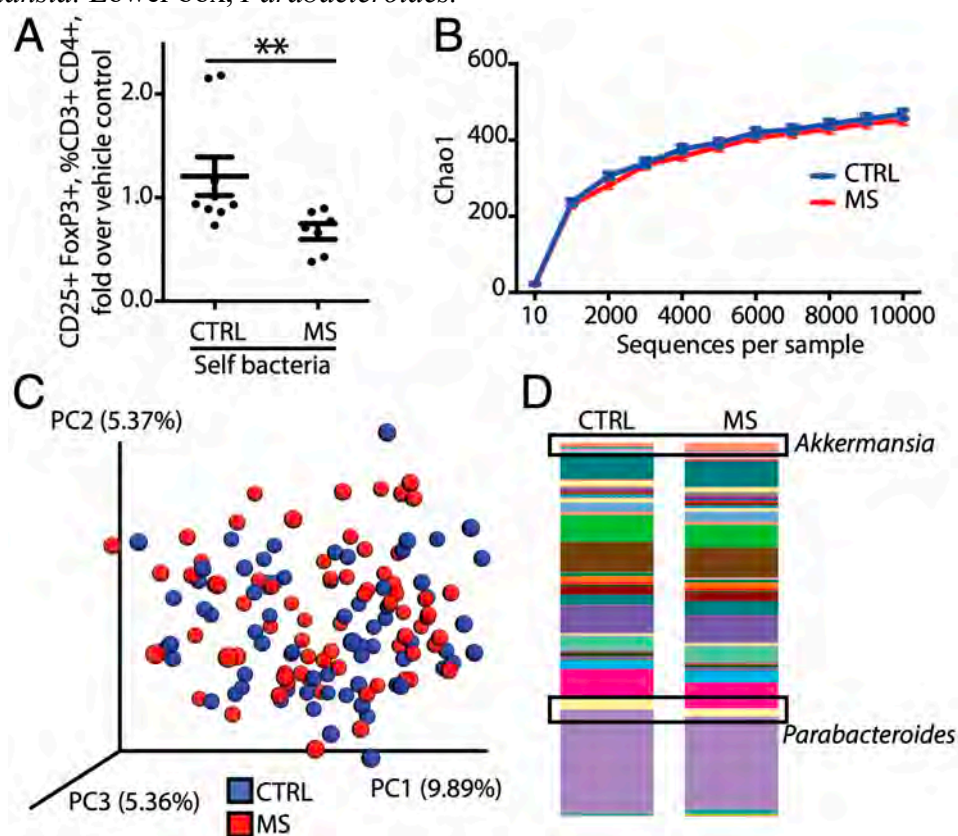
Figure 2. Relative abundances of individual microbial genera differ between MS patients and controls. A. Volcano plots of relative abundance distribution of microbial genera (left) and OTUs (right). X axis, log2 fold of relative abundance ratio between MS patients (n=71) and controls (n=71) after variance-stabilizing transformation. Y axis, negative log10 of *P* value, negative binomial Wald test, Benjamini-Hochberg correction for multiple comparisons. **B**. Summary of taxonomic differences between MS and control microbiome. **C.** Relative abundance plots of selected microbial genera (highlighted in **A)** that were found to be significantly different between MS and controls. Error bars, mean±SEM.

Taxonomic level	Reduced in MS	Increased in MS	Unchanged
Kingdom	0 (0%)	0 (0%)	2 (100%)
Phylum	0 (0%)	2 (18.18%)	9 (81.82%)
Class	1 (4.76%)	3 (14.29%)	17 (80.95%)
Order	1 (3.33%)	4 (13.34%)	25 (83.33%)
Family	1 (1.67%)	8 (13.33%)	51 (85%)
Genus	10 (7.75%)	15 (11.63%)	104 (80.62%)
OTU	161 (11.01%)	86 (5.88%)	1215 (83.11%)
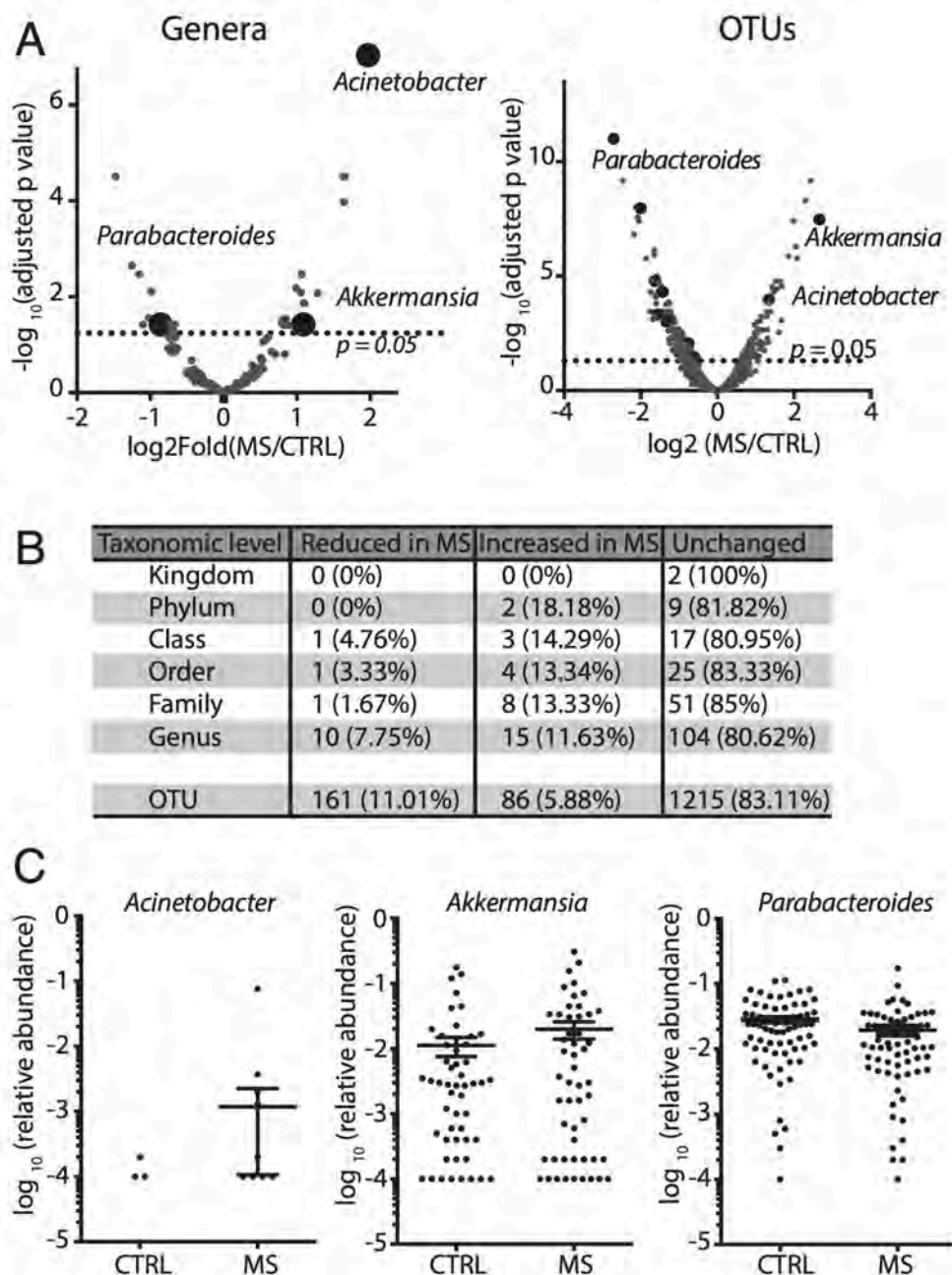
Figure 3. *Acinetobacter calcoaceticus* **inhibits Treg differentiation and stimulates Th1 differentiation** *in vitro*. **A, B.** Representative flow cytometry plots (**A**) and quantification (**B**) of CD25+FoxP3+ cell differentiation within CD3+CD4+ population in response to *Acinetobacter calcoaceticus (A. calc)* (n=6 PBMC donors*).* **C, D.** Representative flow cytometry plots (**C**) and quantification (**D**) of IFNγ+ Th1 lymphocytes within CD3+CD4+ population in response to *A. calcoaceticus (A. calc)* (n=11 PBMC donors). *$*P<0.05$, $**P<0.01$, two-tailed repeated measures *t* test. Error bars, mean±SEM.
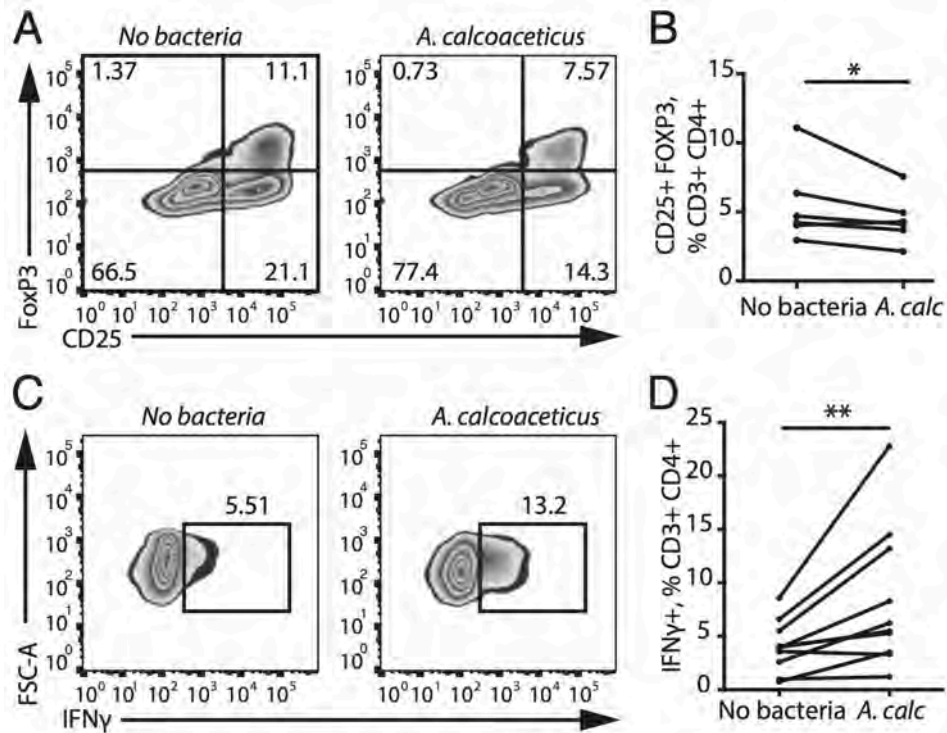
Figure 4. *Akkermansia muciniphila* **increases Th1 lymphocyte differentiation** *in vitro***.**
A-D. Representative flow cytometry plots (**A, B**) and quantification (**C, D**) of IFNγ+ and of Tbet+ Th1 lymphocytes within CD3+CD4+ population in response to *Akkermansia muciniphila (A. muci)*. n=6 PBMC donors for IFNγ experiment, 7 PBMC donors for Tbet experiment. *P<0.05, two-tailed repeated measures *t* test. **E-H**. Representative flow cytometry plots (**E, F**) and quantification (**G, H**) of IFNγ+ Th1 lymphocytes within CD3+CD4+ population in response to non-self or self bacteria from subjects with or without detected *A. muciniphila*. n=6 subjects without *A. muciniphila, n*=12 subjects with *A. muciniphila*. *P<0.05, two-tailed *t* test. **P<0.01, 2-way ANOVA for repeated measures. Error bars, mean±SEM.
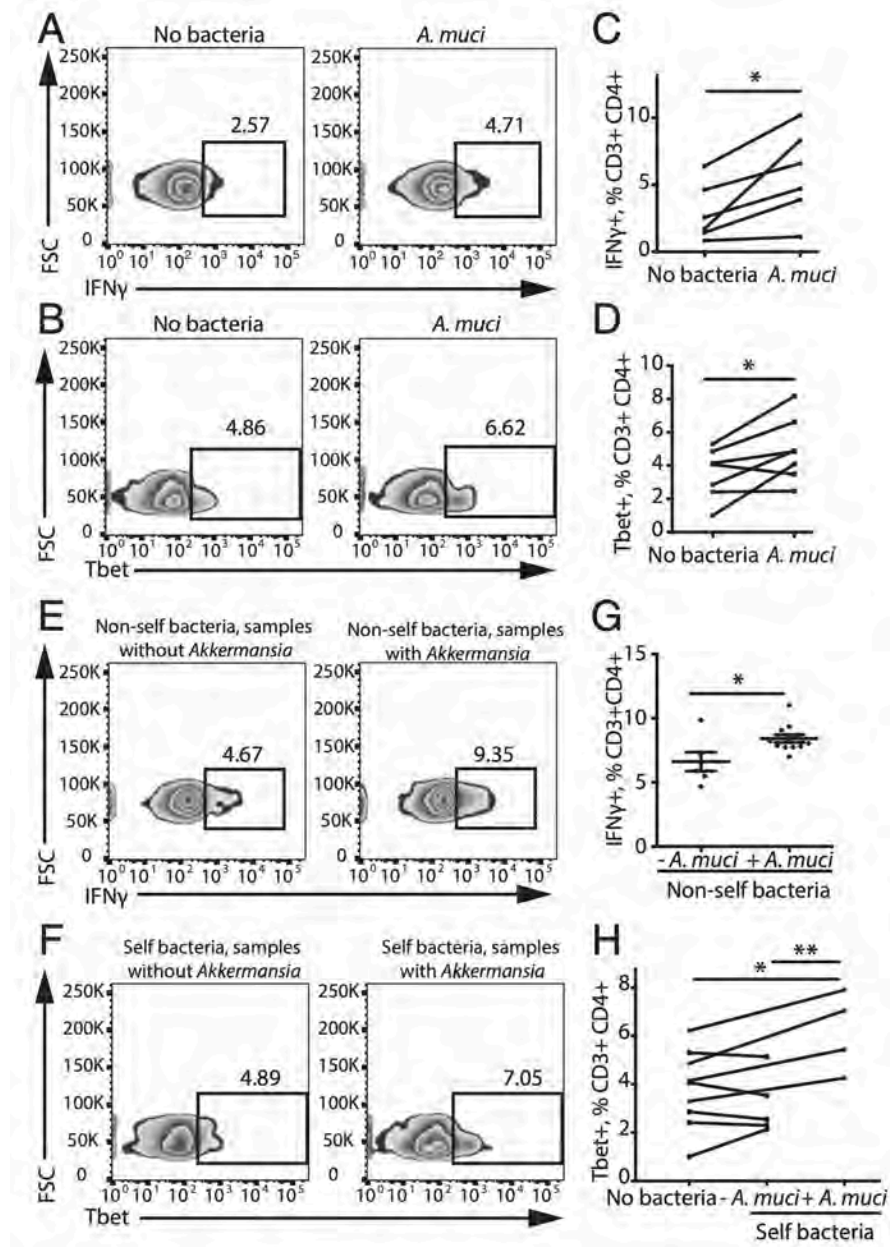
Figure 5. *Parabacteroides distasonis* **stimulates IL-10+ T regulatory lymphocyte differentiation** *in vitro.* **A-D**. Representative flow cytometry plots (**A, B**) and quantification (**C, D**) of CD25+ and CD25+IL-10+ lymphocytes within CD3+CD4+ population in response to *Parabacteroides distasonis (P.dist)*. n=6 PBMC donors. *$P<0.05$, **$P<0.01$, two-tailed repeated measures *t* test. Error bars, mean±SEM.
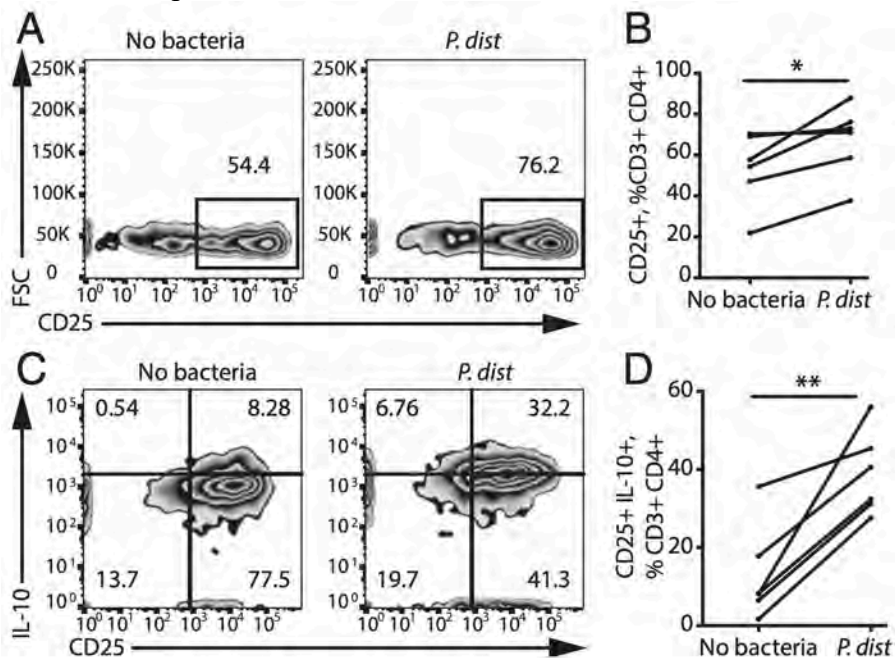
Figure 6. Monocolonization of GF mice with MS-associated bacteria mediates T lymphocyte differentiation. A-C. Representative flow cytometry plots (**A**) and quantification (**B, C**) of CD4+IFNγ+ lymphocytes (**B**) and CD4+IL-10+ lymphocytes (**C**) within live cell population in GF mice colonized with *Acinetobacter calcoaceticus, Akkermansia muciniphila* and *Parabacteroides distasonis.* GF mice and SPF mice are used as controls. n=3-8 mice per group. *P<0.05, **P<0.01, ***P<0.001, ****P<0.0001, 1-way ANOVA with Tukey adjustment for multiple comparisons. Error bars, mean±SEM.
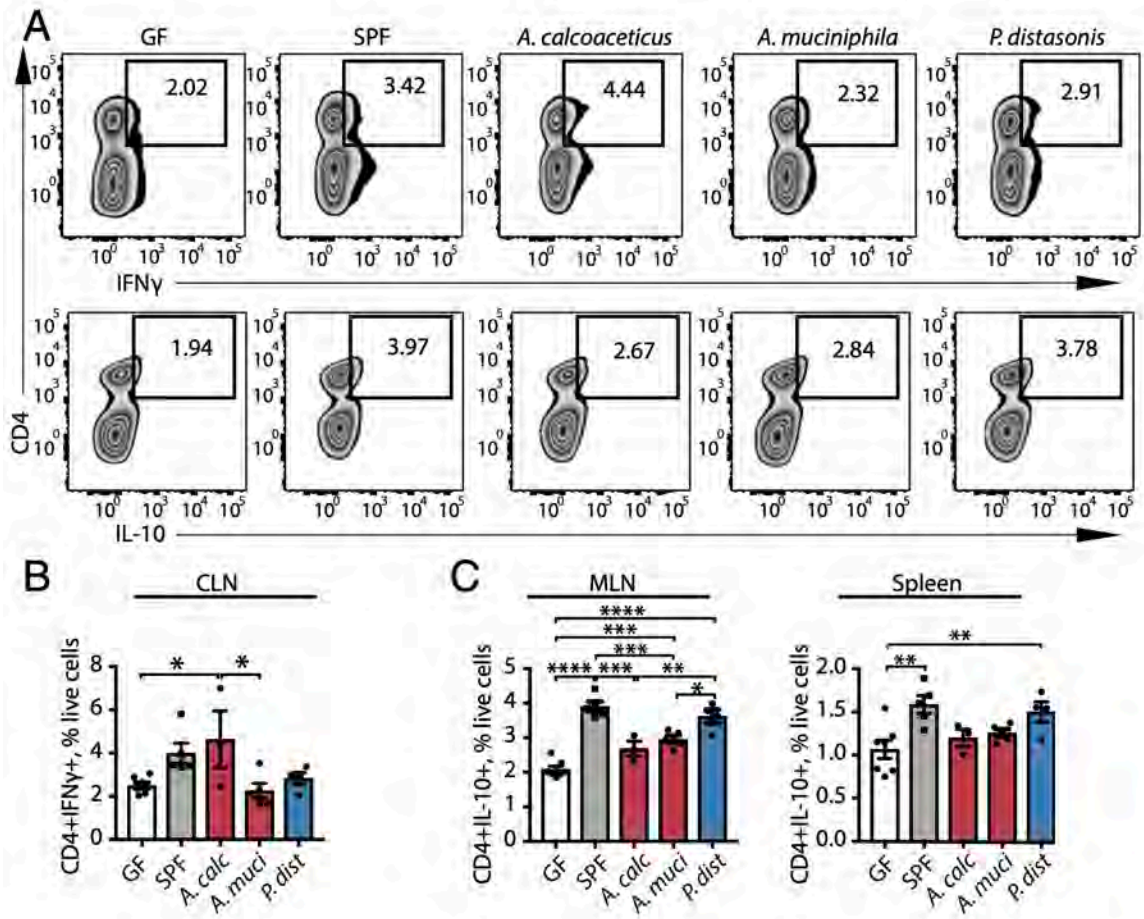
Figure 7. A. Clinical EAE scores of mice that had been colonized with healthy control or MS patient microbiota for at least 5 weeks, or kept GF, prior to induction of EAE at 9-10 weeks of age. Asterisks refer to significance both between MS vs. Control and MS vs. GF groups. n=6-8 mice per group. ****$P<0.0001$, 2-way ANOVA with Tukey adjustment for multiple comparisons. Error bars, mean±SEM. **B.** Principal coordinate analysis (PCoA) of mouse microbiota at different time points after colonization with fecal microbiota from donor pair #1. n=3-5 mice per group. EAE induction occurs at 35 days after transplantation. **C-F.** Representative flow cytometry plots **(C, D)** of FoxP3+ lymphocytes within CD4+ populations and IL-10+ lymphocytes within CD4+FoxP3+ populations. Frequencies of IL-10+ lymphocytes within CD4+FoxP3+ populations in mesenteric lymph nodes of mice sacrificed prior to EAE induction (E) and at peak of EAE progression (22 days after immunization) (F). *$P<0.05$, **$P<0.01$, ****$P<0.0001$, 1-way ANOVA with Tukey adjustment for multiple comparisons. Error bars, mean±SEM.
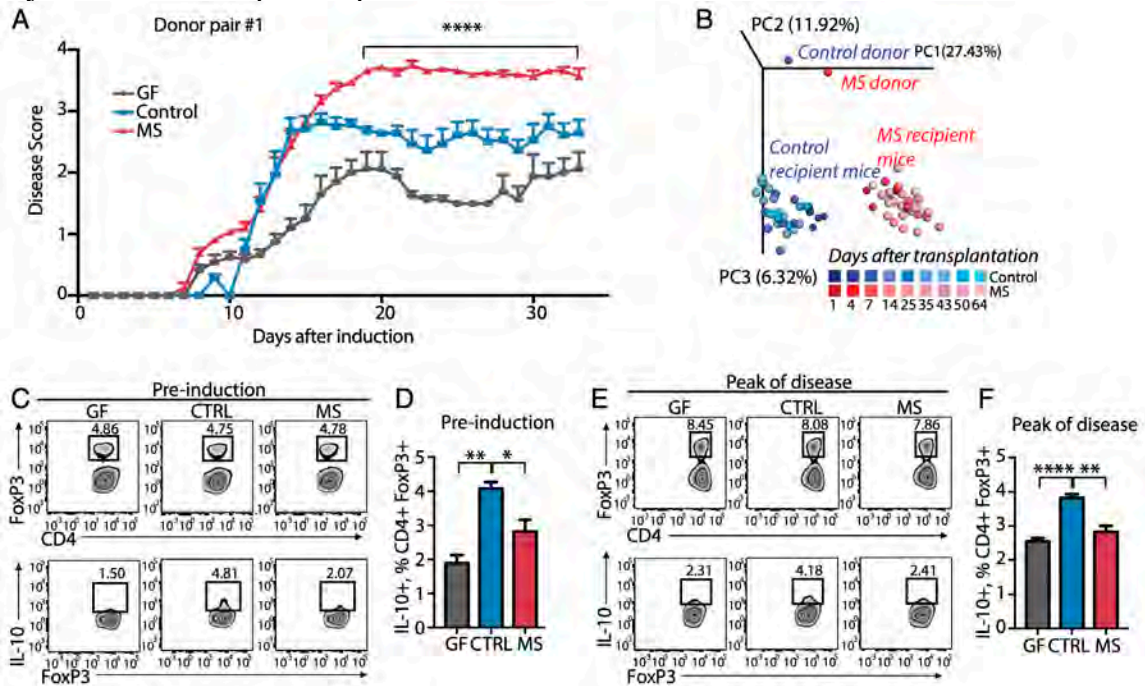
Supplemental Figures and Legends

Supplemental Figure 1. Microbial community variability within and between subjects. A. Comparison of microbial community composition in the same subject between consecutive days. Each color indicates a different subject. Controls and MS patients have been combined. Unweighted Unifrac measure of beta diversity. **B.** Comparison of variability in microbial community composition within and between groups of subjects. Unweighted Unifrac distances. CTRL_CTRL, within healthy control group. MS_MS, within MS patient group. CTRL_MS, between healthy controls and MS patients. ****P<0.01**, Mann-Whitney test, Bonferroni correction for multiple comparison.
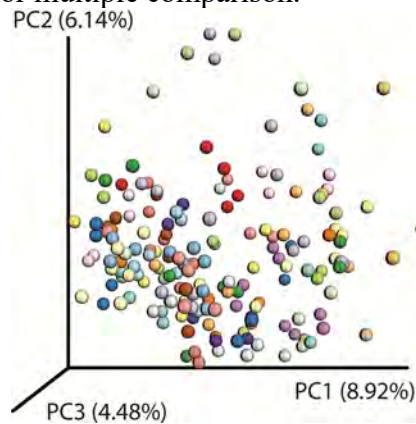
Supplemental Figure 2. Relative abundances of microbial genera in healthy controls. X axis, genera (ranked by relative abundance). Y axis, log10 of mean relative abundance in healthy controls after rarefaction to 10,000 reads per sample. n = 71.
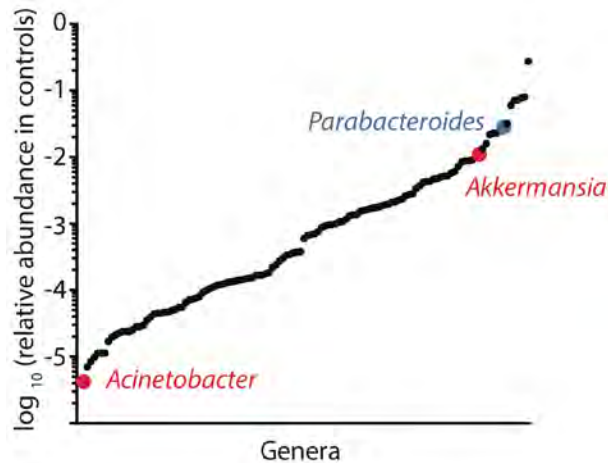
Supplemental Figure 3. Examples of selected bacterial species showing no immunoregulatory effect on human PBMCs. A. Quantification of CD25+FoxP3+ cell differentiation within CD3+CD4+ population in response to *Eggerthella lenta* (*E. len*). **B.** Quantification of IFNγ+ cell differentiation within CD3+CD4+ population in response to *Eggerthella lenta* (*E. len*). **C.** Quantification of CD25+IL10+ cell differentiation within CD3+CD4+ population in response to *Acinetobacter calcoaceticus* (*A. calc*). **D.** Quantification of IFNγ+ cell differentiation within CD3+CD4+ population in response to *Parabacteroides distasonis* (*P. dist*). **E.** Quantification of CD25+FoxP3+ cell differentiation within CD3+CD4+ population in response to *Akkermansia muciniphila* (*A. muci*). n=6 PBMC donors. Error bars, mean±SEM.
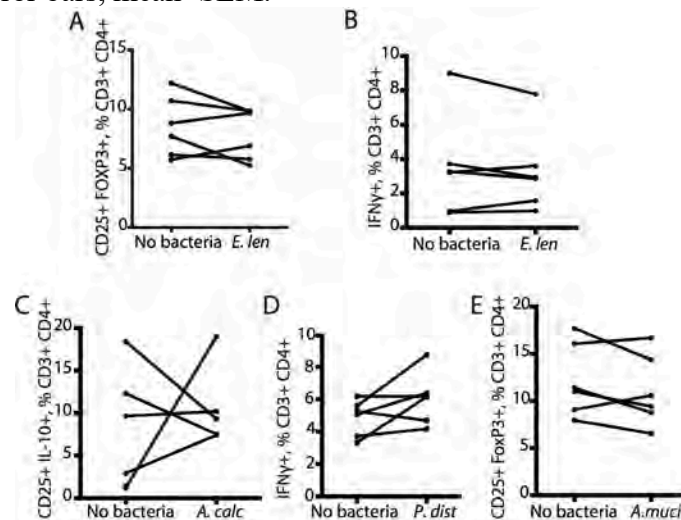
Supplemental Figure 4. Monocolonization of antibiotic-treated mice with individual bacterial species recapitulates *in vitro* T lymphocyte differentiation patterns. A. Quantification of FoxP3+ cell differentiation within CD4+ population in splenocytes of mice colonized with *A. calcoaceticus (A. calc)* after antibiotic treatment, compared to SPF control. **B.** Quantification of CD4+IL10+ cell differentiation within live cells in splenocytes of mice colonized with *P. distasonis (P. dist)* after antibiotic treatment, compared to SPF control. **C.** Quantification of CD4+IL10+ cell differentiation within live cells from splenocytes of mice colonized with *P. distasonis (P. dist)* or SPF control mice exposed to self bacterial extracts. *$P<0.05$, **$P<0.01$, two-tailed *t* test (**A, B**) or two-tailed repeated measures *t* test (**C**). n=5-7 mice per group. Error bars, mean ± SEM.
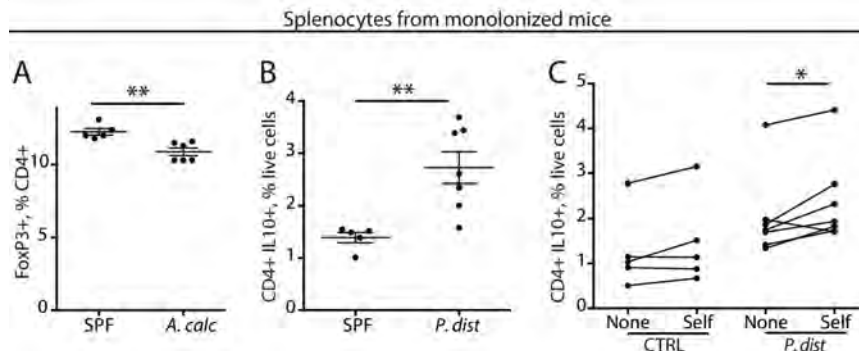
Supplemental Figure 5. The effects of monocolonization of GF mice with *Acinetobacter calcoaceticus*, *Akkermansia muciniphila* and *Parabacteroides distasonis* on T lymphocyte differentiation. A-C. Representative flow cytometry plots showing gating strategy (**A**) and quantification (**B, C**) of CD4+IFNγ+ Th1 lymphocytes (**B**) and CD4+IL-10+ lymphocytes (**C**) within live cell population in GF mice colonized with *Acinetobacter calcoaceticus, Akkermansia muciniphila* and *Parabacteroides distasonis.* GF mice and SPF mice used as controls. n=3-8 mice per group. *P<0.05, **P<0.01, ***P<0.001, ****P<0.0001, 1-way ANOVA with Tukey adjustment for multiple comparisons. Error bars, mean±SEM.
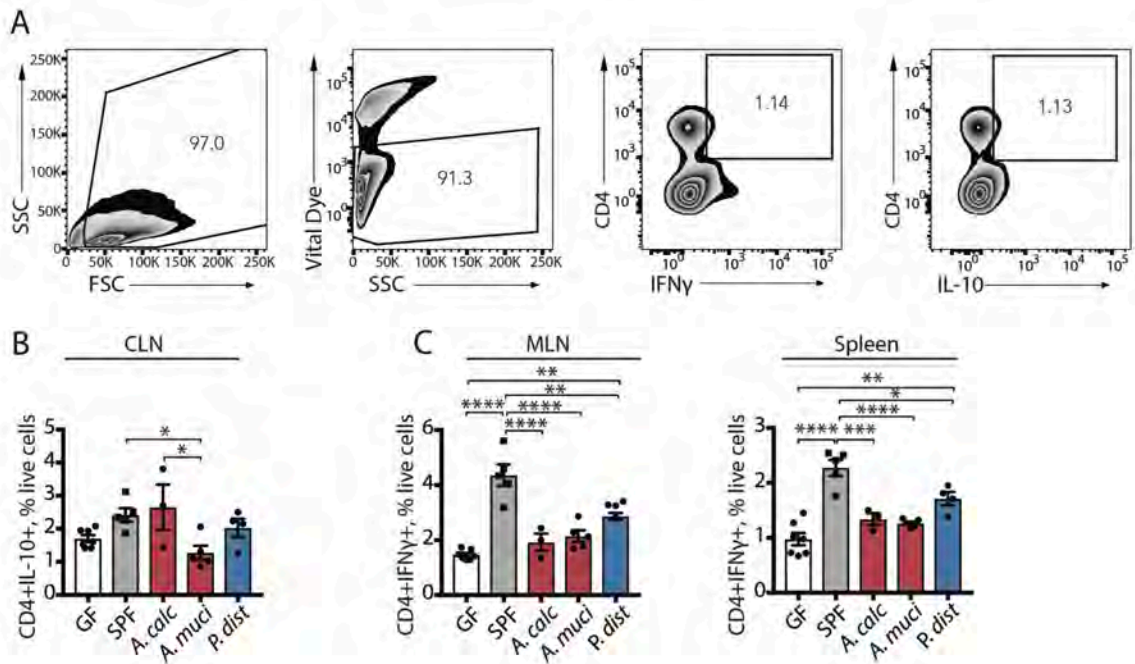
Supplemental Figure 6. Transfer of fecal microbiota from 3 different donor pairs (MS patient and healthy household control) into germ-free mice mediates EAE outcomes. (A-C) Clinical EAE scores of mice that had been colonized at 3-4 weeks of age with healthy control or MS patient microbiota from 3 independent donor pairs for at least 6 weeks prior to induction of EAE. n=3-8 mice per group. Error bars, mean ± SEM. * = Control vs. MS, # = Germ-free vs. MS. */#, $P < 0.05$, **/##, $P < 0.01$, ***/###, $P < 0.0001$, 2-way ANOVA with Tukey adjustment for multiple comparisons. Error bars, mean±SEM.
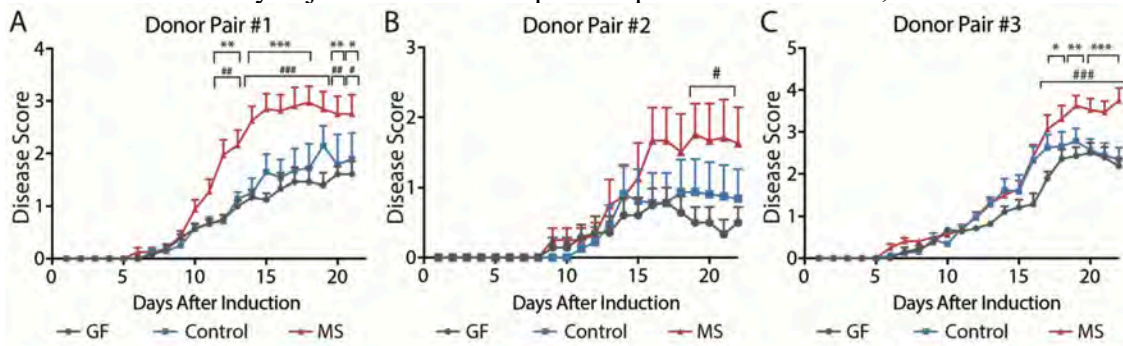
Supplemental Figure 7. Immunophenotyping of mesenteric and cervical lymph nodes of mice colonized with MS and control microbiota from donor pair 1. A. Flow cytometry gating strategy. **B-E.** Quantification of IFNγ+ Th1 and IL-17+ Th17 cell differentiation within CD4+FoxP3- population in mesenteric lymph nodes before induction of EAE (**B, C**) and at peak of disease (**D, E**). **F-K.** Quantification of IFNγ+ Th1, IL-17+ Th17 cell differentiation within CD4+FoxP3- population and IL-10+ cell differentiation within CD4+FoxP3+ population in cervical lymph nodes before induction of EAE (**F-H**) and at peak of disease (**I-K**). n=3-8 mice per group. Error bars, mean ± SEM.
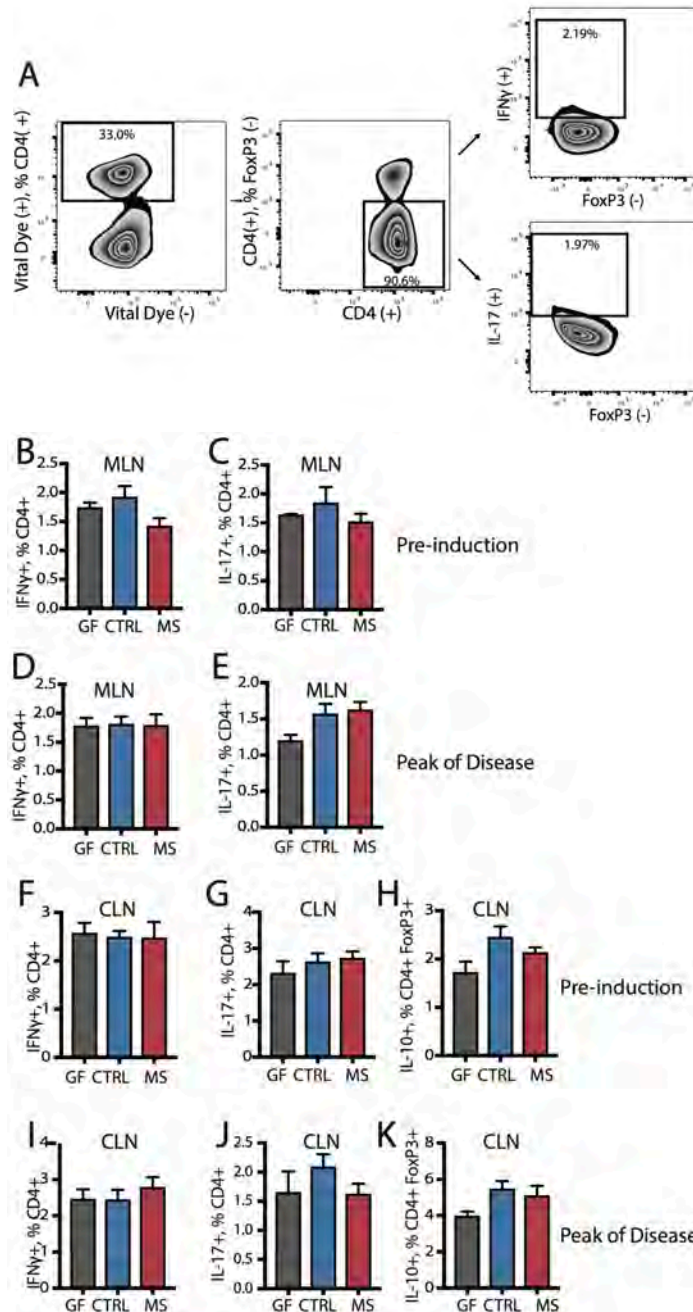
Supplemental Figure 8. Microglial gene expression in spinal cords of mice colonized with MS and control microbiota. Log_2fold difference in microglia-enriched genes at peak EAE compared to pre-induction in gnotobiotic mice colonized with microbiota from human donor pair #1.
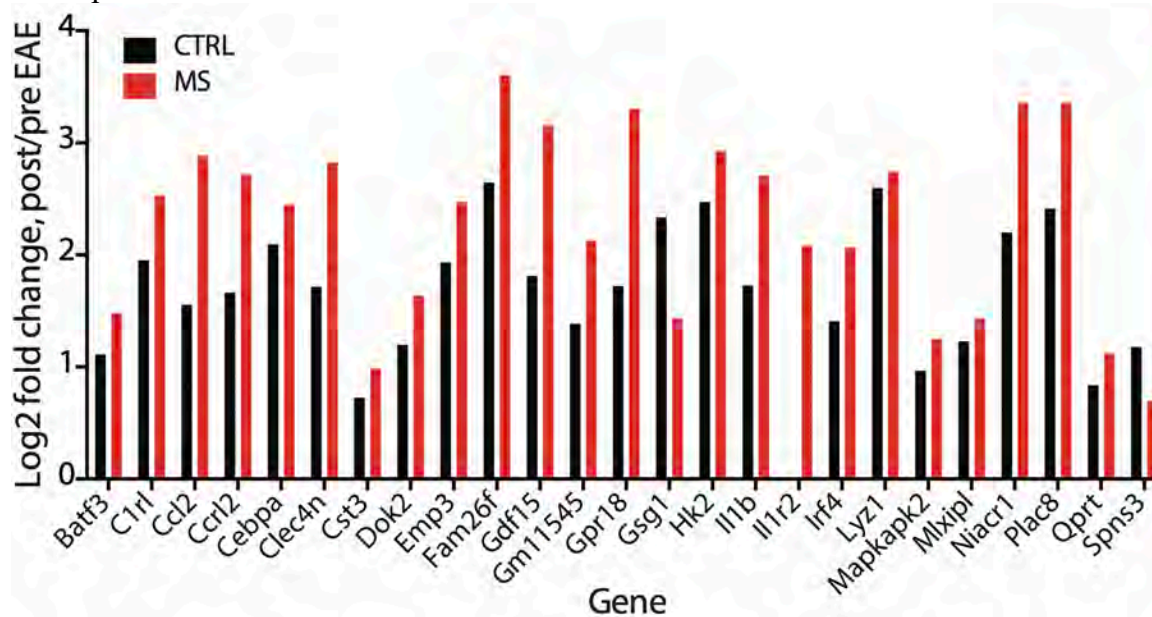
Supplemental Figure 9. Differences in microbiome composition of mice colonized with MS and control microbiota. A. Principal coordinate analysis (PCoA) of mouse microbiota at different time points after colonization with fecal microbiota from donor pair #1. Lines connect consecutive time points. **B.** Alpha diversity of microbiota of human donors and recipient mice from donor pair #1. **C.** Relative abundance of bacterial genera that were increased in mice colonized with either healthy control (*Sutterella*) or MS patient (*Ruminococcus*) microbiota in MS-Discordant Twin Study (Berer et al.).
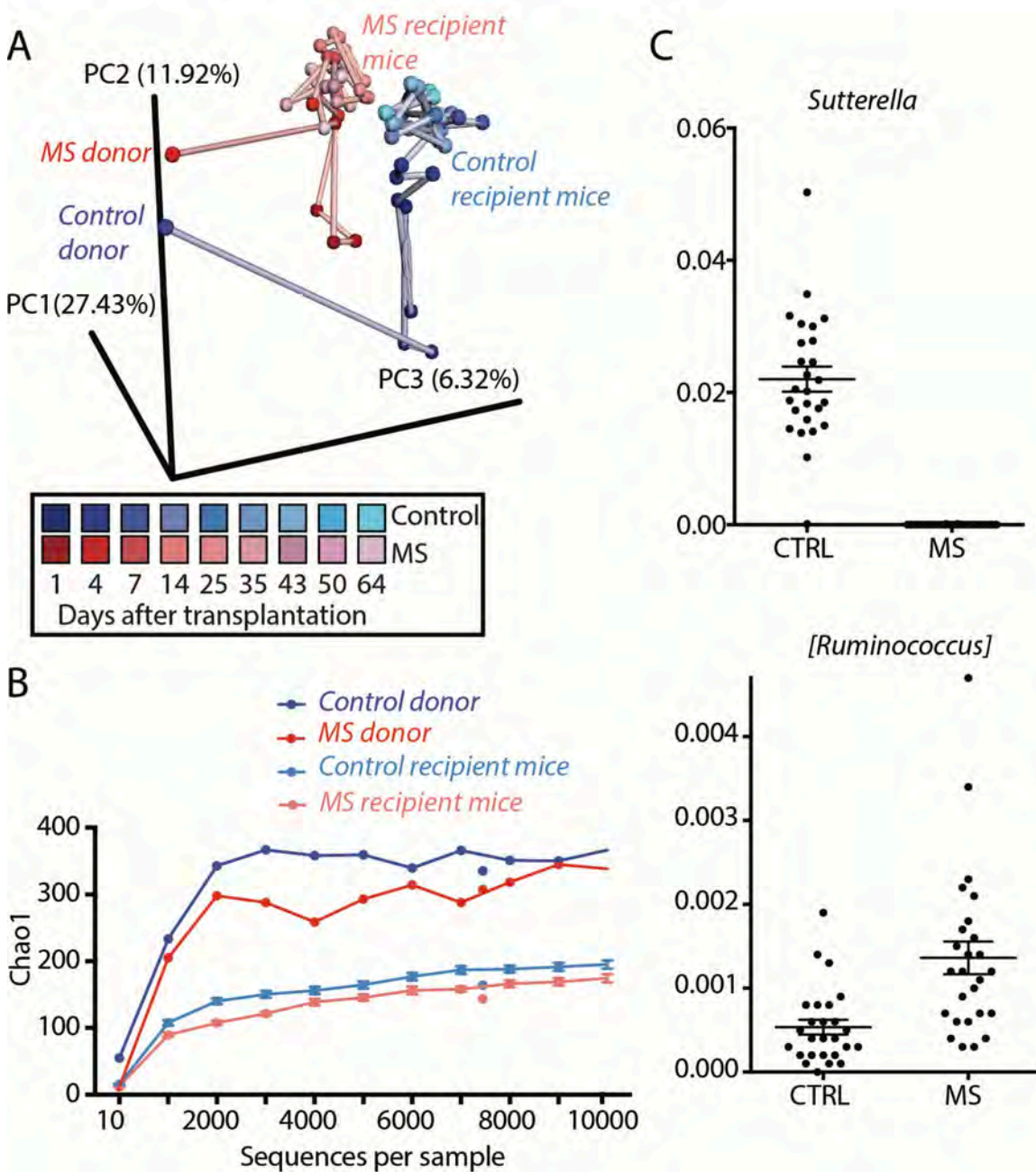
Supplemental Figure 10. CD25+ FoxP3+ Treg differentiation in response to non-self bacterial extracts. Quantification of CD25+FoxP3+ cell differentiation within CD3+CD4+ population in response to non-self bacterial extracts from healthy controls or MS patients. Lines connect averaged responses of the same donor. n = 5 PBMC donors, bacterial extracts from 6 MS patients and 6 healthy controls.
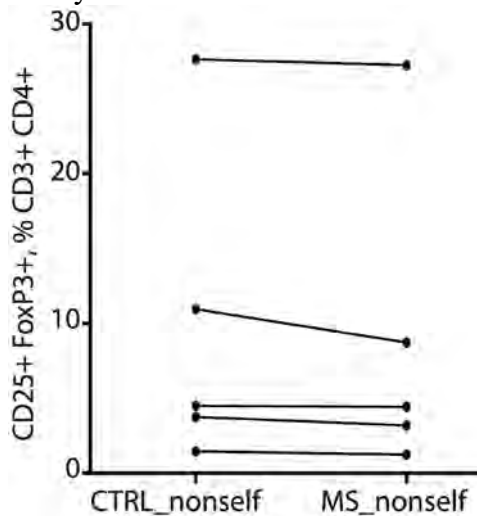
Supplemental Figure 11. Monocolonization of GF mice. A. Colony forming units (CFUs) 2 days after the colonization with *A. calcoaceticus* (AC), *A. muciniphila* (AM) and *P. distasonis* (PD) after culturing fecal bacteria from monocolonized mice on Brucella BL plates anaerobically. **B.** Gel image indicating bands specific to *A. muciniphila (A. muci)* and *P. distasonis (P. dist)*.
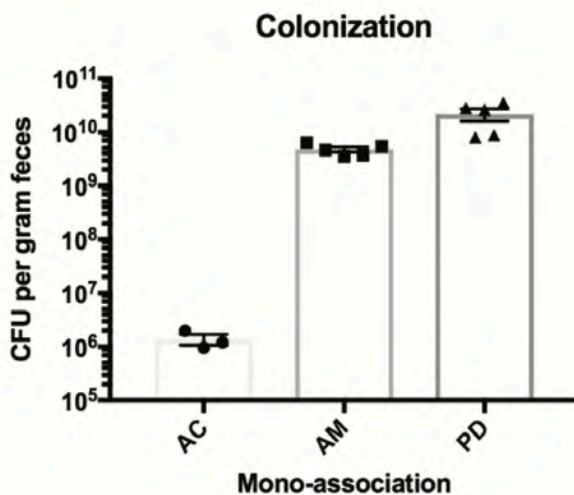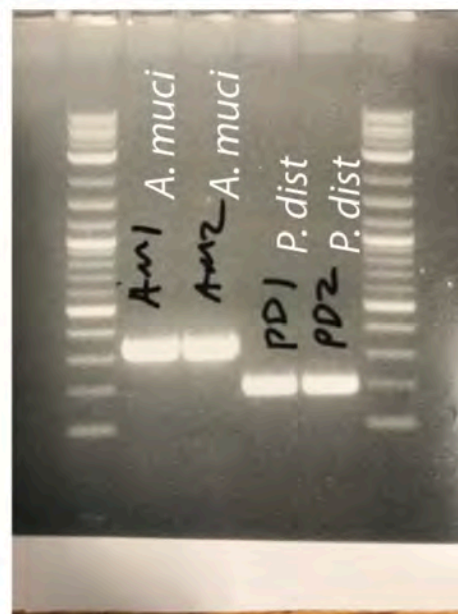
Supplemental Figure 12. Antibiotic-mediated reduction in alpha diversity of mouse microbial community. Chao1 metric of alpha diversity in mice 2 weeks after treatment with broad-spectrum antibiotics (ABX) compared to SPF controls. n = 4 mice per group. Error bars, mean±SEM.
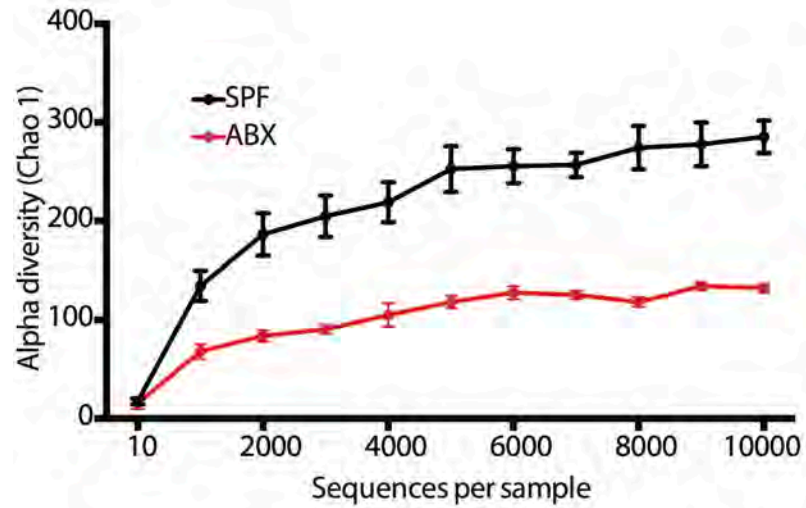
Supplemental Tables

Supplemental Table S1. Subject metadata.

age	sex	collection_site	disease_state	treatment_status	year_onset	BMI
N/A	male	UCSF	Control	Control	Control	N/A
51	female	UCSF	Control	Control	Control	N/A
N/A	male	UCSF	Control	Control	Control	N/A
38	male	UCSF	Control	Control	Control	25.83
65	female	UCSF	Control	Control	Control	26.81
64	male	UCSF	Control	Control	Control	16.97
NA	NA	UCSF	Control	Control	Control	NA
62	male	UCSF	Control	Control	Control	NA
51	male	UCSF	Control	Control	Control	28.08
45	male	UCSF	Control	Control	Control	NA
39	male	UCSF	Control	Control	Control	28.8
63	female	UCSF	Control	Control	Control	NA
64	male	UCSF	Control	Control	Control	NA
45	female	UCSF	Control	Control	Control	NA
43	male	UCSF	Control	Control	Control	NA
NA	male	UCSF	Control	Control	Control	NA
58	male	UCSF	Control	Control	Control	25.84
62	male	UCSF	Control	Control	Control	NA
64	male	UCSF	Control	Control	Control	NA
59	male	UCSF	Control	Control	Control	NA
38	male	UCSF	Control	Control	Control	NA
NA	male	UCSF	Control	Control	Control	NA
43	male	UCSF	Control	Control	Control	NA
56	male	UCSF	Control	Control	Control	NA
38	male	UCSF	Control	Control	Control	NA
32	male	UCSF	Control	Control	Control	24.39
68	male	UCSF	Control	Control	Control	31.07
NA	NA	UCSF	Control	Control	Control	NA
53	female	UCSF	Control	Control	Control	29.1
64	female	UCSF	Control	Control	Control	20.24
59	female	UCSF	Control	Control	Control	NA
64	male	UCSF	Control	Control	Control	NA
NA	male	UCSF	Control	Control	Control	NA
61	female	UCSF	Control	Control	Control	29.83
71	male	UCSF	Control	Control	Control	NA
53	male	UCSF	Control	Control	Control	NA
36	female	UCSF	Control	Control	Control	NA
31	male	UCSF	Control	Control	Control	NA
25	male	UCSF	Control	Control	Control	NA
25	female	UCSF	Control	Control	Control	NA

Supplemental Table S1 (continued)

22	male	UCSF	Control	Control	Control	NA
22	male	UCSF	Control	Control	Control	NA
39	male	UCSF	Control	Control	Control	NA
33	female	UCSF	Control	Control	Control	NA
29	male	UCSF	Control	Control	Control	NA
23	male	UCSF	Control	Control	Control	NA
29	male	UCSF	Control	Control	Control	NA
37	male	UCSF	Control	Control	Control	NA
NA	NA	UCSF	Control	Control	Control	NA
NA	NA	UCSF	Control	Control	Control	NA
43	male	UCSF	MS	No_Treatment	2000	21.5
51	female	UCSF	MS	No_Treatment	1998	25.8
48	male	UCSF	MS	No_Treatment	2001	24
55	female	UCSF	MS	No_Treatment	2002	29.7
38	female	UCSF	MS	No_Treatment	2002	18.9
60	female	UCSF	MS	No_Treatment	2001	18.7
57	female	UCSF	MS	No_Treatment	2001	19.6
43	female	UCSF	MS	No_Treatment	2015	47.1
28	male	UCSF	MS	No_Treatment	2013	23.5
45	male	UCSF	MS	No_Treatment	2008	28.2
31	male	UCSF	MS	No_Treatment	2015	27.6
24	male	UCSF	MS	No_Treatment	2011	24.6
36	male	UCSF	MS	No_Treatment	2013	25.1
29	male	UCSF	MS	No_Treatment	2016	20.9
33	female	UCSF	MS	No_Treatment	2016	20.9
44	male	UCSF	MS	No_Treatment		26.1
44	male	UCSF	MS	No_Treatment	1993	30.36
56	male	UCSF	MS	No_Treatment	1993	26.54
61	female	UCSF	MS	No_Treatment	1989	24.13
52	female	UCSF	MS	No_Treatment	1998	21.11
61	male	UCSF	MS	No_Treatment	1984	NA
38	female	UCSF	MS	No_Treatment	2004	NA
44	female	UCSF	MS	No_Treatment	1990	30.65
51	female	UCSF	MS	No_Treatment	1995	19.63
39	female	UCSF	MS	No_Treatment	2004	NA
57	female	UCSF	MS	No_Treatment	1996	17.72
37	female	UCSF	MS	No_Treatment	1998	22.87
64	female	UCSF	MS	No_Treatment	1983	21.19
42	female	UCSF	MS	No_Treatment	2003	NA
47	female	UCSF	MS	No_Treatment	2003	NA
59	male	UCSF	MS	No_Treatment	1997	NA
62	female	UCSF	MS	No_Treatment	1985	22.96

Supplemental Table S1 (continued)

61	female	UCSF	MS	No_Treatment	1993	NA
37	female	UCSF	MS	No_Treatment	1999	NA
41	female	UCSF	MS	No_Treatment	1996	24.28
21	female	UCSF	MS	No_Treatment	2013	NA
41	female	UCSF	MS	No_Treatment	2011	21.61
21	female	UCSF	MS	No_Treatment	2005	NA
36	female	UCSF	MS	No_Treatment	2014	NA
32	female	UCSF	MS	No_Treatment	2013	NA
30	female	UCSF	MS	No_Treatment	2014	21.97
39	male	UCSF	MS	No_Treatment	2013	NA
38	male	UCSF	MS	No_Treatment	2011	19.37
26	female	UCSF	MS	No_Treatment	2013	NA
32	male	UCSF	MS	No_Treatment	2014	NA
45	female	UCSF	MS	No_Treatment	NA	NA
47	female	UCSF	MS	No_Treatment	2015	21.66
33	male	UCSF	MS	No_Treatment	2015	NA
37	female	UCSF	MS	No_Treatment	2015	NA
49	female	Sinai	Control	Control	Control	23
30	female	Sinai	Control	Control	Control	20.1
28	female	Sinai	Control	Control	Control	24.4
27	female	Sinai	Control	Control	Control	24
29	female	Sinai	Control	Control	Control	20.6
37	female	Sinai	Control	Control	Control	24.4
37	female	Sinai	Control	Control	Control	21.3
43	female	Sinai	Control	Control	Control	18.3
55	female	Sinai	Control	Control	Control	23.8
57	male	Sinai	Control	Control	Control	20.2
25	female	Sinai	Control	Control	Control	19.5
62	male	Sinai	Control	Control	Control	33.2
28	female	Sinai	Control	Control	Control	24.1
32	female	Sinai	Control	Control	Control	20.9
35	male	Sinai	Control	Control	Control	25
51	female	Sinai	Control	Control	Control	21.9
30	male	Sinai	Control	Control	Control	42.3
50	female	Sinai	Control	Control	Control	24.7
55	female	Sinai	Control	Control	Control	46.9
53	female	Sinai	Control	Control	Control	22.1
30	female	Sinai	Control	Control	Control	26.6
48	male	Sinai	MS	No_Treatment	1997	22.69
22	female	Sinai	MS	No_Treatment	2014	45
29	male	Sinai	MS	No_Treatment	2011	27.17
44	female	Sinai	MS	No_Treatment	2009	21.66

Supplemental Table S1 (continued)

38	female	Sinai	MS	No_Treatment	2013	34.2
51	female	Sinai	MS	No_Treatment	2006	30.04
27	female	Sinai	MS	No_Treatment	2006	23.17
26	female	Sinai	MS	No_Treatment	2012	20.66
20	male	Sinai	MS	No_Treatment	2013	27.89
28	female	Sinai	MS	No_Treatment	2013	28.34
60	male	Sinai	MS	No_Treatment	2009	26
42	female	Sinai	MS	No_Treatment	2013	35.58
19	male	Sinai	MS	No_Treatment	2014	24.37
37	female	Sinai	MS	No_Treatment	2011	21.42
20	male	Sinai	MS	No_Treatment	2013	26.4
30	female	Sinai	MS	No_Treatment	2010	19.7
52	female	Sinai	MS	No_Treatment	2009	31.89
44	male	Sinai	MS	No_Treatment	2005	32.28
41	female	Sinai	MS	No_Treatment	2014	22.31
44	male	Sinai	MS	No_Treatment	2014	28
36	male	Sinai	MS	No_Treatment	2014	24.3
34	male	Sinai	MS	No_Treatment	2015	20.54

Supplemental Table S2. Differential abundance of microbial genera in MS patients and healthy controls.

	log2 fold change (MS/CTRL)	Adjusted p-value
k__Bacteria;p__Proteobacteria;c__Gammaproteobacteria;o__Pseudomonadales;f__Moraxellaceae;g__Acinetobacter	1.97	9.15E-08
k__Bacteria;p__Actinobacteria;c__Actinobacteria;o__Actinomycetales;f__Actinomycetaceae;g__Varibaculum	1.66	3.08E-05
k__Bacteria;p__Actinobacteria;c__Actinobacteria;o__Actinomycetales;f__Corynebacteriaceae;g__Corynebacterium	1.64	3.08E-05
k__Bacteria;p__Bacteroidetes;c__Bacteroidia;o__Bacteroidales;f__[Paraprevotellaceae];g__	-1.47	3.08E-05
k__Bacteria;p__Actinobacteria;c__Actinobacteria;o__Bifidobacteriales;f__Bifidobacteriaceae;g__Bifidobacterium	1.64	1.05E-04
k__Bacteria;p__Bacteroidetes;c__Bacteroidia;o__Bacteroidales;f__[Paraprevotellaceae];g__[Prevotella]	-1.25	2.23E-03
k__Bacteria;p__Firmicutes;c__Clostridia;o__Clostridiales;f__Veillonellaceae;g__Megamonas	1.06	3.38E-03
k__Bacteria;p__Proteobacteria;c__Gammaproteobacteria;o__Enterobacteriales;f__Enterobacteriaceae;g__Serratia	-1.15	3.38E-03
k__Bacteria;p__Firmicutes;c__Clostridia;o__Clostridiales;f__[Mogibacteriaceae];g__	9.89	6.68E-03
k__Bacteria;p__Firmicutes;c__Bacilli;o__Bacillales;f__Bacillaceae;g__Bacillus	-9.85	7.85E-03
k__Bacteria;p__Firmicutes;c__Clostridia;o__Clostridiales;f__Veillonellaceae;g__Megasphaera	1.05	8.06E-03
k__Bacteria;p__Proteobacteria;c__Gammaproteobacteria;o__Enterobacteriales;f__Enterobacteriaceae;g__Klebsiella	1.29	8.50E-03
k__Bacteria;p__Firmicutes;c__Clostridia;o__Clostridiales;f__Peptostreptococcaceae;g__	1.10	1.35E-02
k__Bacteria;p__Firmicutes;c__Clostridia;o__Clostridiales;f__Veillonellaceae;g__Acidaminococcus	-1.02	2.79E-02
k__Bacteria;p__Firmicutes;c__Erysipelotrichi;o__Erysipelotrichales;f__Erysipelotrichaceae;g__Clostridium	-8.08	2.90E-02
k__Bacteria;p__Firmicutes;c__Clostridia;o__Clostridiales;f__[Tissierellaceae];g__ph2	8.52	2.94E-02
k__Bacteria;p__Actinobacteria;c__Actinobacteria;o__Actinomycetales;f__Actinomycetaceae;g__Actinomyces	8.16	2.94E-02
k__Bacteria;p__Firmicutes;c__Clostridia;o__Clostridiales;f__[Mogibacteriaceae];g__Mogibacterium	7.99	3.55E-02
k__Bacteria;p__Verrucomicrobia;c__Verrucomicrobiae;o__Verrucomicrobiales;f__Verrucomicrobiaceae;g__Akkermansia	1.09	3.78E-02
k__Bacteria;p__Proteobacteria;c__Gammaproteobacteria;o__Enterobacteriales;f__Enterobacteriaceae;g__Aquamonas	-7.36	3.78E-02
k__Bacteria;p__Bacteroidetes;c__Bacteroidia;o__Bacteroidales;f__Porphyromonadaceae;g__Parabacteroides	-8.56	3.78E-02
k__Bacteria;p__Firmicutes;c__Clostridia;o__Clostridiales;f__Veillonellaceae;g__Phascolarctobacterium	-1.10	3.78E-02
k__Bacteria;p__Proteobacteria;c__Gammaproteobacteria;o__Pseudomonadales;f__Pseudomonadaceae;g__	-6.65	3.78E-02
k__Bacteria;p__Firmicutes;c__Clostridia;o__Clostridiales;f__Clostridiaceae;g__SMB53	8.22	3.86E-02
k__Bacteria;p__Firmicutes;c__Erysipelotrichi;o__Erysipelotrichales;f__Erysipelotrichaceae;g__Bulleidia	8.84	3.86E-02

Supplemental Table S3. Results of differential abundance analysis of MS and control microbiota, OTU level, Wald negative binomial test to calculate statistical significance.

OTU	log2 fold change (MS/Control)	p value	FDR adjusted p value	taxonomy
851323	-2.709	7.08E-15	9.83E-12	k__Bacteria; p__Bacteroidetes; c__Bacteroidia; o__Bacteroidales; f__Porphyromonadaceae; g__Parabacteroides; s__
4443143	2.437	1.18E-12	6.77E-10	k__Bacteria; p__Firmicutes; c__Clostridia; o__Clostridiales; f__Ruminococcaceae; g__Ruminococcus; s__
3910247	-2.468	1.46E-12	6.77E-10	k__Bacteria; p__Bacteroidetes; c__Bacteroidia; o__Bacteroidales; f__[Paraprevotellaceae]; g__[Prevotella]; s__
365385	2.299	1.40E-11	4.86E-09	k__Bacteria; p__Actinobacteria; c__Actinobacteria; o__Bifidobacteriales; f__Bifidobacteriaceae; g__Bifidobacterium; s__bifidum
2990918	-2.120	3.33E-11	9.23E-09	k__Bacteria; p__Actinobacteria; c__Coriobacteriia; o__Coriobacteriales; f__Coriobacteriaceae; g__Collinsella; s__stercoris
4442459	-2.003	4.62E-11	1.07E-08	k__Bacteria; p__Bacteroidetes; c__Bacteroidia; o__Bacteroidales; f__Porphyromonadaceae; g__Parabacteroides; s__
437137	-2.082	1.37E-10	2.72E-08	k__Bacteria; p__Proteobacteria; c__Betaproteobacteria; o__Burkholderiales; f__Alcaligenaceae; g__Sutterella; s__
4306262	2.664	1.89E-10	3.29E-08	k__Bacteria; p__Verrucomicrobia; c__Verrucomicrobiae; o__Verrucomicrobiales; f__Verrucomicrobiaceae; g__Akkermansia; s__muciniphila
4435982	1.990	2.71E-10	3.90E-08	k__Bacteria; p__Proteobacteria; c__Gammaproteobacteria; o__Pseudomonadales; f__Pseudomonadaceae; g__Pseudomonas; s__veronii
211720	-2.045	2.81E-10	3.90E-08	k__Bacteria; p__Proteobacteria; c__Alphaproteobacteria; o__RF32; f__; g__; s__
4476065	-2.177	1.20E-09	1.51E-07	k__Bacteria; p__Firmicutes; c__Clostridia; o__Clostridiales; f__Ruminococcaceae; g__Ruminococcus; s__
184678	2.050	4.35E-09	5.04E-07	k__Bacteria; p__Firmicutes; c__Clostridia; o__Clostridiales; f__Ruminococcaceae; g__Faecalibacterium; s__prausnitzii
197698	-1.650	6.77E-09	7.22E-07	k__Bacteria; p__Firmicutes; c__Clostridia; o__Clostridiales; f__; g__; s__
197517	-1.652	1.17E-08	1.16E-06	k__Bacteria; p__Bacteroidetes; c__Bacteroidia; o__Bacteroidales; f__[Barnesiellaceae]; g__; s__
1039584	1.858	1.41E-08	1.31E-06	k__Bacteria; p__Firmicutes; c__Clostridia; o__Clostridiales; f__[Tissierellaceae]; g__Anaerococcus; s__
2403301	2.076	2.00E-08	1.67E-06	k__Bacteria; p__Firmicutes; c__Clostridia; o__Clostridiales; f__Lachnospiraceae; g__; s__
520657	-1.857	2.04E-08	1.67E-06	k__Bacteria; p__Bacteroidetes; c__Bacteroidia; o__Bacteroidales; f__Prevotellaceae; g__Prevotella; s__stercorea
215097	-1.573	1.29E-07	9.98E-06	k__Bacteria; p__Proteobacteria; c__Betaproteobacteria; o__Burkholderiales; f__Alcaligenaceae; g__Sutterella; s__
172163	-1.585	1.39E-07	1.02E-05	k__Bacteria; p__Firmicutes; c__Clostridia; o__Clostridiales; f__; g__; s__
198190	-1.634	2.34E-07	1.62E-05	k__Bacteria; p__Bacteroidetes; c__Bacteroidia; o__Bacteroidales; f__Porphyromonadaceae; g__Parabacteroides; s__distasonis
4305923	1.652	2.52E-07	1.65E-05	k__Bacteria; p__Tenericutes; c__Mollicutes; o__RF39; f__; g__; s__
182044	1.527	2.73E-07	1.65E-05	k__Bacteria; p__Firmicutes; c__Clostridia; o__Clostridiales; f__Ruminococcaceae; g__; s__
128300	-1.727	2.68E-07	1.65E-05	k__Bacteria; p__Firmicutes; c__Bacilli; o__Lactobacillales; f__Lactobacillaceae; g__Lactobacillus; s__
187248	-1.532	3.48E-07	2.01E-05	k__Bacteria; p__Firmicutes; c__Clostridia; o__Clostridiales; f__Lachnospiraceae; g__; s__
328472	1.677	5.23E-07	2.79E-05	k__Bacteria; p__Actinobacteria; c__Actinobacteria; o__Actinomycetales; f__Actinomycetaceae; g__Varibaculum; s__
4319785	-1.469	5.05E-07	2.79E-05	k__Bacteria; p__Bacteroidetes; c__Bacteroidia; o__Bacteroidales; f__[Paraprevotellaceae]; g__; s__
196381	1.437	5.87E-07	3.02E-05	k__Bacteria; p__Firmicutes; c__Clostridia; o__Clostridiales; f__Lachnospiraceae; g__; s__
296394	1.541	7.37E-07	3.65E-05	k__Bacteria; p__Firmicutes; c__Clostridia; o__Clostridiales; f__Ruminococcaceae; g__; s__
4425368	1.470	7.69E-07	3.68E-05	k__Bacteria; p__Firmicutes; c__Clostridia; o__Clostridiales; f__Veillonellaceae; g__Megasphaera; s__
4404187	1.471	1.07E-06	4.92E-05	k__Bacteria; p__Firmicutes; c__Clostridia; o__Clostridiales; f__Lachnospiraceae; g__; s__
186233	-1.426	1.17E-06	4.92E-05	k__Bacteria; p__Bacteroidetes; c__Bacteroidia; o__Bacteroidales; f__Porphyromonadaceae; g__Parabacteroides; s__distasonis
178713	-1.552	1.10E-06	4.92E-05	k__Bacteria; p__Firmicutes; c__Clostridia; o__Clostridiales; f__Ruminococcaceae; g__; s__
190913	-1.738	1.15E-06	4.92E-05	k__Bacteria; p__Bacteroidetes; c__Bacteroidia; o__Bacteroidales; f__Bacteroidaceae; g__Bacteroides; s__
4428714	-1.619	1.74E-06	7.10E-05	k__Bacteria; p__Tenericutes; c__Mollicutes; o__RF39; f__; g__; s__
562244	-1.611	2.10E-06	8.34E-05	k__Bacteria; p__Proteobacteria; c__Betaproteobacteria; o__Burkholderiales; f__Alcaligenaceae; g__Sutterella; s__
703635	1.345	2.70E-06	1.04E-04	k__Bacteria; p__Proteobacteria; c__Gammaproteobacteria; o__Pseudomonadales; f__Moraxellaceae; g__Acinetobacter; s__
1082607	1.340	3.71E-06	1.39E-04	k__Bacteria; p__Actinobacteria; c__Actinobacteria; o__Actinomycetales; f__Corynebacteriaceae; g__Corynebacterium; s__
1028632	-1.275	3.89E-06	1.42E-04	k__Bacteria; p__Proteobacteria; c__Gammaproteobacteria; o__Enterobacteriales; f__Enterobacteriaceae; g__; s__
345951	-1.249	4.10E-06	1.46E-04	k__Bacteria; p__Proteobacteria; c__Gammaproteobacteria; o__Enterobacteriales; f__Enterobacteriaceae; g__; s__

Supplemental Table S3 (continued)

4339144	-1.594	4.54E-06	1.58E-04	k__Bacteria;p__Bacteroidetes;c__Bacteroidia;o__Bacteroidales;f__[Odoribacteraceae];g__Butyricimonas;s__
299770	-1.338	4.96E-06	1.68E-04	k__Bacteria;p__Bacteroidetes;c__Bacteroidia;o__Bacteroidales;f__Prevotellaceae;g__Prevotella;s__stercorea
195029	-1.278	5.16E-06	1.70E-04	k__Bacteria;p__Firmicutes;c__Clostridia;o__Clostridiales;f__;g__;s__
4227110	1.383	1.18E-05	3.48E-04	k__Bacteria;p__Proteobacteria;c__Gammaproteobacteria;o__Enterobacteriales;f__Enterobacteriaceae;g__Citrobacter;s__freundii
300829	1.287	1.08E-05	3.48E-04	k__Bacteria;p__Firmicutes;c__Clostridia;o__Clostridiales;f__Clostridiaceae;g__Clostridium;s__
587933	-1.258	1.25E-05	3.48E-04	k__Bacteria;p__Firmicutes;c__Erysipelotrichi;o__Erysipelotrichales;f__Erysipelotrichaceae;g__Coprobacillus;s__
847711	-1.274	1.19E-05	3.48E-04	k__Bacteria;p__Firmicutes;c__Clostridia;o__Clostridiales;f__Christensenellaceae;g__;s__
4333943	-1.306	1.23E-05	3.48E-04	k__Bacteria;p__Proteobacteria;c__Alphaproteobacteria;o__RF32;f__;g__;s__
354574	-1.522	1.11E-05	3.48E-04	k__Bacteria;p__Proteobacteria;c__Deltaproteobacteria;o__Desulfovibrionales;f__Desulfovibrionaceae;g__Bilophila;s__
4365130	-1.581	1.23E-05	3.48E-04	k__Bacteria;p__Bacteroidetes;c__Bacteroidia;o__Bacteroidales;f__Porphyromonadaceae;g__Parabacteroides;s__distasonis
179159	-1.748	1.20E-05	3.48E-04	k__Bacteria;p__Firmicutes;c__Clostridia;o__Clostridiales;f__;g__;s__
2368865	-1.431	1.28E-05	3.48E-04	k__Bacteria;p__Firmicutes;c__Clostridia;o__Clostridiales;f__;g__;s__
4461030	-1.518	1.31E-05	3.50E-04	k__Bacteria;p__Proteobacteria;c__Gammaproteobacteria;o__Enterobacteriales;f__Enterobacteriaceae;g__;s__
3531225	-1.222	1.35E-05	3.54E-04	k__Bacteria;p__Proteobacteria;c__Gammaproteobacteria;o__Enterobacteriales;f__Enterobacteriaceae;g__;s__
4415390	-1.513	1.46E-05	3.76E-04	k__Bacteria;p__Firmicutes;c__Clostridia;o__Clostridiales;f__Lachnospiraceae;g__;s__
4356080	-1.551	1.80E-05	4.54E-04	k__Bacteria;p__Bacteroidetes;c__Bacteroidia;o__Bacteroidales;f__[Barnesiellaceae];g__;s__
4299126	1.290	2.52E-05	5.81E-04	k__Bacteria;p__Proteobacteria;c__Alphaproteobacteria;o__RF32;f__;g__;s__
4426298	-1.317	1.99E-05	4.93E-04	k__Bacteria;p__Actinobacteria;c__Actinobacteria;o__Bifidobacteriales;f__Bifidobacteriaceae;g__Bifidobacterium;s__animalis
4413619	1.153	2.64E-05	5.81E-04	k__Bacteria;p__Firmicutes;c__Clostridia;o__Clostridiales;f__Lachnospiraceae;g__;s__
173810	-1.275	2.07E-05	5.05E-04	k__Bacteria;p__Firmicutes;c__Clostridia;o__Clostridiales;f__Ruminococcaceae;g__;s__
319275	-1.295	2.28E-05	5.47E-04	k__Bacteria;p__Firmicutes;c__Clostridia;o__Clostridiales;f__Ruminococcaceae;g__Faecalibacterium;s__prausnitzii
4436046	-1.263	2.37E-05	5.57E-04	k__Bacteria;p__Firmicutes;c__Clostridia;o__Clostridiales;f__Lachnospiraceae;g__Dorea;s__
566243	-1.190	2.61E-05	5.81E-04	k__Bacteria;p__Proteobacteria;c__Gammaproteobacteria;o__Enterobacteriales;f__Enterobacteriaceae;g__;s__
4442899	-1.614	2.57E-05	5.81E-04	k__Bacteria;p__Firmicutes;c__Clostridia;o__Clostridiales;f__;g__;s__
4449851	-1.687	3.52E-05	7.64E-04	k__Bacteria;p__Proteobacteria;c__Gammaproteobacteria;o__Enterobacteriales;f__Enterobacteriaceae;g__;s__
363389	-1.130	3.68E-05	7.73E-04	k__Bacteria;p__Firmicutes;c__Clostridia;o__Clostridiales;f__Clostridiaceae;g__Clostridium;s__
524661	-1.206	3.62E-05	7.73E-04	k__Bacteria;p__Bacteroidetes;c__Bacteroidia;o__Bacteroidales;f__Bacteroidaceae;g__Bacteroides;s__
191251	-1.309	4.09E-05	8.47E-04	k__Bacteria;p__Bacteroidetes;c__Bacteroidia;o__Bacteroidales;f__Porphyromonadaceae;g__Parabacteroides;s__
4470870	1.679	4.21E-05	8.60E-04	k__Bacteria;p__Bacteroidetes;c__Bacteroidia;o__Bacteroidales;f__[Barnesiellaceae];g__;s__
554163	1.118	4.49E-05	9.02E-04	k__Bacteria;p__Proteobacteria;c__Gammaproteobacteria;o__Enterobacteriales;f__Enterobacteriaceae;g__;s__
324882	1.052	4.79E-05	9.50E-04	k__Bacteria;p__Firmicutes;c__Clostridia;o__Clostridiales;f__[Mogibacteriaceae];g__;s__
326626	-1.203	4.92E-05	9.60E-04	k__Bacteria;p__Bacteroidetes;c__Bacteroidia;o__Bacteroidales;f__Bacteroidaceae;g__Bacteroides;s__
440605	-1.336	4.98E-05	9.60E-04	k__Bacteria;p__Firmicutes;c__Clostridia;o__Clostridiales;f__Christensenellaceae;g__;s__
4378683	-1.109	5.41E-05	1.03E-03	k__Bacteria;p__Firmicutes;c__Clostridia;o__Clostridiales;f__Lachnospiraceae;g__;s__
317315	-1.162	5.48E-05	1.03E-03	k__Bacteria;p__Firmicutes;c__Clostridia;o__Clostridiales;f__;g__;s__
367946	-1.149	5.86E-05	1.08E-03	k__Bacteria;p__Firmicutes;c__Clostridia;o__Clostridiales;f__Ruminococcaceae;g__;s__
195998	0.974	7.19E-05	1.31E-03	k__Bacteria;p__Firmicutes;c__Clostridia;o__Clostridiales;f__;g__;s__
1071450	-1.172	1.02E-04	1.84E-03	k__Bacteria;p__Proteobacteria;c__Gammaproteobacteria;o__Pseudomonadales;f__Pseudomonadaceae;g__Pseudomonas;s__fragi
4449244	-1.010	1.12E-04	2.00E-03	k__Bacteria;p__Fusobacteria;c__Fusobacteriia;o__Fusobacteriales;f__Fusobacteriaceae;g__Fusobacterium;s__
234443	1.073	1.15E-04	2.02E-03	k__Bacteria;p__Bacteroidetes;c__Bacteroidia;o__Bacteroidales;f__Rikenellaceae;g__;s__
650171	1.301	1.26E-04	2.18E-03	k__Bacteria;p__Actinobacteria;c__Actinobacteria;o__Actinomycetales;f__Corynebacteriaceae;g__Corynebacterium;s__
110192	-1.139	1.27E-04	2.18E-03	k__Bacteria;p__Firmicutes;c__Clostridia;o__Clostridiales;f__Ruminococcaceae;g__Oscillospira;s__
505565	1.183	1.33E-04	2.23E-03	k__Bacteria;p__Firmicutes;c__Clostridia;o__Clostridiales;f__[Tissierellaceae];g__Anaerococcus;s__
839282	-1.084	1.34E-04	2.23E-03	k__Bacteria;p__Firmicutes;c__Bacilli;o__Lactobacillales;f__Leuconostocaceae;g__;s__

Supplemental Table S3 (continued)

ID	Value			Taxonomy
216111	-1.123	1.38E-03	2.28E-03	k__Bacteria;p__Firmicutes;c__Clostridia;o__Clostridiales;f__Lachnospiraceae;g__;s__
2749126	-0.977	1.43E-04	2.34E-03	k__Bacteria;p__Proteobacteria;c__Gammaproteobacteria;o__Enterobacteriales;f__Enterobacteriaceae;g__;s__
7366	-1.164	1.46E-04	2.35E-03	k__Bacteria;p__Proteobacteria;c__Betaproteobacteria;o__Burkholderiales;f__Oxalobacteraceae;g__Oxalobacter;s__formigenes
361966	-1.284	1.50E-04	2.39E-03	k__Bacteria;p__Firmicutes;c__Clostridia;o__Clostridiales;f__Ruminococcaceae;g__Faecalibacterium;s__prausnitzii
4338624	-1.035	1.69E-04	2.67E-03	k__Bacteria;p__Proteobacteria;c__Betaproteobacteria;o__Burkholderiales;f__Alcaligenaceae;g__Sutterella;s__
210262	-1.092	1.80E-04	2.80E-03	k__Bacteria;p__Firmicutes;c__Clostridia;o__Clostridiales;f__;g__;s__
3235048	1.607	1.84E-04	2.82E-03	k__Bacteria;p__Firmicutes;c__Clostridia;o__Clostridiales;f__Ruminococcaceae;g__Ruminococcus;s__
573061	-1.032	1.85E-04	2.82E-03	k__Bacteria;p__Proteobacteria;c__Deltaproteobacteria;o__Desulfovibrionales;f__Desulfovibrionaceae;g__Desulfovibrio;s__
516553	-0.923	1.89E-04	2.85E-03	k__Bacteria;p__Firmicutes;c__Clostridia;o__Clostridiales;f__Lachnospiraceae;g__;s__
348642	1.056	1.93E-04	2.88E-03	k__Bacteria;p__Firmicutes;c__Clostridia;o__Clostridiales;f__Lachnospiraceae;g__[Ruminococcus];s__gnavus
1097961	0.980	2.00E-04	2.95E-03	k__Bacteria;p__Bacteroidetes;c__Bacteroidia;o__Bacteroidales;f__Porphyromonadaceae;g__Porphyromonas;s__
289883	-1.048	2.07E-04	3.02E-03	k__Bacteria;p__Firmicutes;c__Bacilli;o__Bacillales;f__Bacillaceae;g__Bacillus;s__
9846	0.991	2.19E-04	3.17E-03	k__Bacteria;p__Proteobacteria;c__Gammaproteobacteria;o__Enterobacteriales;f__Enterobacteriaceae;g__Citrobacter;s__
194654	-0.957	2.28E-04	3.26E-03	k__Bacteria;p__Firmicutes;c__Clostridia;o__Clostridiales;f__Ruminococcaceae;g__;s__
2017729	-0.916	2.38E-04	3.38E-03	k__Bacteria;p__Firmicutes;c__Clostridia;o__Clostridiales;f__Lachnospiraceae;g__;s__
25695	-1.040	2.48E-04	3.47E-03	k__Bacteria;p__Firmicutes;c__Clostridia;o__Clostridiales;f__Ruminococcaceae;g__;s__
188735	-1.149	2.73E-04	3.79E-03	k__Bacteria;p__Bacteroidetes;c__Bacteroidia;o__Bacteroidales;f__Bacteroidaceae;g__Bacteroides;s__
4375000	-1.017	2.97E-04	4.09E-03	k__Bacteria;p__Proteobacteria;c__Gammaproteobacteria;o__Enterobacteriales;f__Enterobacteriaceae;g__;s__
691423	-0.934	3.39E-04	4.56E-03	k__Bacteria;p__Proteobacteria;c__Gammaproteobacteria;o__Enterobacteriales;f__Enterobacteriaceae;g__;s__
208479	-1.112	3.36E-04	4.56E-03	k__Bacteria;p__Bacteroidetes;c__Bacteroidia;o__Bacteroidales;f__[Odoribacteraceae];g__Butyricimonas;s__
2530636	0.993	3.52E-04	4.69E-03	k__Bacteria;p__Firmicutes;c__Clostridia;o__Clostridiales;f__Veillonellaceae;g__Megamonas;s__
187780	-1.222	3.67E-04	4.85E-03	k__Bacteria;p__Firmicutes;c__Clostridia;o__Clostridiales;f__Ruminococcaceae;g__;s__
424038	0.957	3.80E-04	4.94E-03	k__Bacteria;p__Firmicutes;c__Clostridia;o__Clostridiales;f__[Tissierellaceae];g__Anaerococcus;s__
188333	-0.901	3.81E-04	4.94E-03	k__Bacteria;p__Firmicutes;c__Clostridia;o__Clostridiales;f__Lachnospiraceae;g__[Ruminococcus];s__gnavus
308760	-1.145	3.91E-04	5.02E-03	k__Bacteria;p__Tenericutes;c__Mollicutes;o__RF39;f__;g__;s__
180414	-1.050	3.97E-04	5.06E-03	k__Bacteria;p__Firmicutes;c__Clostridia;o__Clostridiales;f__Lachnospiraceae;g__Blautia;s__
4020502	-0.873	4.03E-04	5.09E-03	k__Bacteria;p__Bacteroidetes;o__Bacteroidales;f__Bacteroidaceae;g__Bacteroides;s__
184534	-1.048	4.12E-04	5.15E-03	k__Bacteria;p__Firmicutes;c__Clostridia;o__Clostridiales;f__Christensenellaceae;g__;s__
176062	1.313	4.36E-04	5.26E-03	k__Bacteria;p__Firmicutes;c__Clostridia;o__Clostridiales;f__;g__;s__
4428313	-0.917	4.34E-04	5.26E-03	k__Bacteria;p__Firmicutes;c__Bacilli;o__Lactobacillales;f__Lactobacillaceae;g__Lactobacillus;s__
1599042	-0.980	4.31E-04	5.26E-03	k__Bacteria;p__Firmicutes;c__Clostridia;o__Clostridiales;f__Ruminococcaceae;g__;s__
4402645	-1.099	4.26E-04	5.26E-03	k__Bacteria;p__Firmicutes;c__Clostridia;o__Clostridiales;f__;g__;s__
195556	-0.997	4.57E-04	5.46E-03	k__Bacteria;p__Firmicutes;c__Clostridia;o__Clostridiales;f__Ruminococcaceae;g__;s__
730906	-1.059	4.60E-04	5.46E-03	k__Bacteria;p__Firmicutes;c__Clostridia;o__Clostridiales;f__Ruminococcaceae;g__;s__
178759	-0.978	4.80E-04	5.60E-03	k__Bacteria;p__Tenericutes;c__RF3;o__ML615J-28;f__;g__;s__
178845	-1.256	4.79E-04	5.60E-03	k__Bacteria;p__Firmicutes;c__Clostridia;o__Clostridiales;f__Ruminococcaceae;g__;s__
153075	0.896	4.88E-04	5.65E-03	k__Bacteria;p__Firmicutes;c__Clostridia;o__Clostridiales;f__;g__;s__
179989	0.898	6.17E-04	7.08E-03	k__Bacteria;p__Firmicutes;c__Clostridia;o__Clostridiales;f__Lachnospiraceae;g__Blautia;s__
360890	1.102	6.25E-04	7.11E-03	k__Bacteria;p__Firmicutes;c__Clostridia;o__Clostridiales;f__Lachnospiraceae;g__Blautia;s__
18735	0.833	6.36E-04	7.18E-03	k__Bacteria;p__Firmicutes;c__Clostridia;o__Clostridiales;f__Lachnospiraceae;g__Blautia;s__
232030	-0.913	6.65E-04	7.45E-03	k__Bacteria;p__Firmicutes;c__Clostridia;o__Clostridiales;f__Lachnospiraceae;g__Coprococcus;s__
4434579	1.329	6.82E-04	7.58E-03	k__Bacteria;p__Bacteroidetes;c__Bacteroidia;o__Bacteroidales;f__Prevotellaceae;g__Prevotella;s__
2730944	-0.928	7.09E-04	7.81E-03	k__Bacteria;p__Bacteroidetes;c__Bacteroidia;o__Bacteroidales;f__Bacteroidaceae;g__Bacteroides;s__coprophilus
4473788	-0.984	8.00E-04	8.69E-03	k__Bacteria;p__Firmicutes;c__Clostridia;o__Clostridiales;f__Lachnospiraceae;g__;s__

Supplemental Table S3 (continued)

ID	Value	p	q	Taxonomy
366147	-1.073	8.03E-04	8.69E-03	k__Bacteria;p__Bacteroidetes;c__Bacteroidia;o__Bacteroidales;f__[Paraprevotellaceae];g__Paraprevotella;s__
2740950	-1.243	8.08E-04	8.69E-03	k__Bacteria;p__Firmicutes;c__Clostridia;o__Clostridiales;f__Lachnospiraceae;g__Coprococcus;s__
4476877	1.088	8.28E-04	8.72E-03	k__Bacteria;p__Bacteroidetes;c__Bacteroidia;o__Bacteroidales;f__[Odoribacteraceae];g__Odoribacter;s__
178859	0.861	8.18E-04	8.72E-03	k__Bacteria;p__Firmicutes;c__Clostridia;o__Clostridiales;f__Ruminococcaceae;g__Ruminococcus;s__
4374084	-0.754	8.32E-04	8.72E-03	k__Bacteria;p__Bacteroidetes;c__Bacteroidia;o__Bacteroidales;f__Porphyromonadaceae;g__Parabacteroides;s__distasonis
1566691	-0.920	8.35E-04	8.72E-03	k__Bacteria;p__Proteobacteria;c__Gammaproteobacteria;o__Pseudomonadales;f__Pseudomonadaceae;g__Pseudomonas;s__
4347159	1.205	8.59E-04	8.89E-03	k__Bacteria;p__Actinobacteria;c__Actinobacteria;o__Bifidobacteriales;f__Bifidobacteriaceae;g__Bifidobacterium;s__adolescentis
269937	-1.088	8.99E-04	9.24E-03	k__Bacteria;p__Bacteroidetes;c__Bacteroidia;o__Bacteroidales;f__Prevotellaceae;g__Prevotella;s__stercorea
191913	-0.872	9.55E-04	9.70E-03	k__Bacteria;p__Firmicutes;c__Clostridia;o__Clostridiales;f__Lachnospiraceae;g__;s__
810831	-1.010	9.57E-04	9.70E-03	k__Bacteria;p__Proteobacteria;c__Gammaproteobacteria;o__Enterobacteriales;f__Enterobacteriaceae;g__;s__
329820	0.946	9.68E-04	9.74E-03	k__Bacteria;p__Firmicutes;c__Erysipelotrichi;o__Erysipelotrichales;f__Erysipelotrichaceae;g__[Eubacterium];s__biforme
329096	-0.790	9.79E-04	9.77E-03	k__Bacteria;p__Proteobacteria;c__Gammaproteobacteria;o__Enterobacteriales;f__Enterobacteriaceae;g__;s__
842596	0.832	1.03E-03	1.02E-02	k__Bacteria;p__Firmicutes;c__Clostridia;o__Clostridiales;f__Lachnospiraceae;g__Coprococcus;s__
216010	0.821	1.09E-03	1.06E-02	k__Bacteria;p__Firmicutes;c__Clostridia;o__Clostridiales;f__[Mogibacteriaceae];g__;s__
185558	0.814	1.08E-03	1.06E-02	k__Bacteria;p__Firmicutes;c__Clostridia;o__Clostridiales;f__;g__;s__
13986	-0.857	1.09E-03	1.06E-02	k__Bacteria;p__Firmicutes;c__Clostridia;o__Clostridiales;f__Lachnospiraceae;g__;s__
4476780	1.161	1.21E-03	1.16E-02	k__Bacteria;p__Bacteroidetes;c__Bacteroidia;o__Bacteroidales;f__Rikenellaceae;g__;s__
4318470	-0.760	1.21E-03	1.16E-02	k__Bacteria;p__Bacteroidetes;c__Bacteroidia;o__Bacteroidales;f__Bacteroidaceae;g__Bacteroides;s__
2835813	-0.943	1.46E-03	1.38E-02	k__Bacteria;p__Firmicutes;c__Clostridia;o__Clostridiales;f__Ruminococcaceae;g__;s__
188881	0.867	1.51E-03	1.43E-02	k__Bacteria;p__Firmicutes;c__Clostridia;o__Clostridiales;f__Christensenellaceae;g__;s__
4471245	-1.074	1.56E-03	1.45E-02	k__Bacteria;p__Firmicutes;c__Clostridia;o__Clostridiales;f__Ruminococcaceae;g__Oscillospira;s__
297414	-1.110	1.55E-03	1.45E-02	k__Bacteria;p__Firmicutes;c__Clostridia;o__Clostridiales;f__Lachnospiraceae;g__Dorea;s__
4457872	-1.089	1.59E-03	1.47E-02	k__Bacteria;p__Bacteroidetes;c__Bacteroidia;o__Bacteroidales;f__Prevotellaceae;g__Prevotella;s__copri
552376	0.816	1.61E-03	1.47E-02	k__Bacteria;p__Proteobacteria;c__Gammaproteobacteria;o__Enterobacteriales;f__Enterobacteriaceae;g__Enterobacter;s__
473883	-0.876	1.61E-03	1.47E-02	k__Bacteria;p__Firmicutes;c__Bacilli;o__Lactobacillales;f__Streptococcaceae;g__Streptococcus;s__alactolyticus
325850	1.122	1.66E-03	1.50E-02	k__Bacteria;p__Proteobacteria;c__Alphaproteobacteria;o__RF32;f__;g__;s__
146586	-0.906	1.67E-03	1.50E-02	k__Bacteria;p__Firmicutes;c__Clostridia;o__Clostridiales;f__Ruminococcaceae;g__Oscillospira;s__
4381553	-1.097	1.68E-03	1.51E-02	k__Bacteria;p__Bacteroidetes;c__Bacteroidia;o__Bacteroidales;f__Bacteroidaceae;g__Bacteroides;s__
2751958	0.892	1.75E-03	1.55E-02	k__Bacteria;p__Firmicutes;c__Clostridia;o__Clostridiales;f__[Tissierellaceae];g__Anaerococcus;s__
180121	-0.833	1.74E-03	1.55E-02	k__Bacteria;p__Firmicutes;c__Clostridia;o__Clostridiales;f__Ruminococcaceae;g__;s__
4379449	-0.836	1.77E-03	1.56E-02	k__Bacteria;p__Firmicutes;c__Erysipelotrichi;o__Erysipelotrichales;f__Erysipelotrichaceae;g__Clostridium;s__saccharogumia
2957436	-0.775	1.80E-03	1.56E-02	k__Bacteria;p__Firmicutes;c__Clostridia;o__Clostridiales;f__Lachnospiraceae;g__Dorea;s__
174901	-0.823	1.80E-03	1.56E-02	k__Bacteria;p__Firmicutes;c__Clostridia;o__Clostridiales;f__Lachnospiraceae;g__;s__
163243	-1.159	1.81E-03	1.56E-02	k__Bacteria;p__Firmicutes;c__Clostridia;o__Clostridiales;f__Ruminococcaceae;g__Ruminococcus;s__
214331	0.807	1.84E-03	1.58E-02	k__Bacteria;p__Firmicutes;c__Clostridia;o__Clostridiales;f__[Mogibacteriaceae];g__Mogibacterium;s__
194626	-0.739	1.85E-03	1.58E-02	k__Bacteria;p__Firmicutes;c__Clostridia;o__Clostridiales;f__Ruminococcaceae;g__;s__
4448331	-0.851	1.86E-03	1.58E-02	k__Bacteria;p__Proteobacteria;c__Gammaproteobacteria;o__Enterobacteriales;f__Enterobacteriaceae;g__;s__
4393466	0.944	1.96E-03	1.65E-02	k__Bacteria;p__Firmicutes;c__Clostridia;o__Clostridiales;f__Clostridiaceae;g__SMB53;s__
4474593	-0.741	1.99E-03	1.65E-02	k__Bacteria;p__Bacteroidetes;c__Bacteroidia;o__Bacteroidales;f__Bacteroidaceae;g__Bacteroides;s__fragilis
294246	-0.900	1.99E-03	1.65E-02	k__Bacteria;p__Firmicutes;c__Clostridia;o__Clostridiales;f__Ruminococcaceae;g__;s__
4476604	-1.118	2.02E-03	1.67E-02	k__Bacteria;p__Firmicutes;c__Clostridia;o__Clostridiales;f__Lachnospiraceae;g__[Ruminococcus];s__gnavus
320915	-0.789	2.05E-03	1.69E-02	k__Bacteria;p__Cyanobacteria;c__4C0d-2;o__YS2;f__;g__;s__
2814830	-0.755	2.05E-03	1.70E-02	k__Bacteria;p__Firmicutes;c__Clostridia;o__Clostridiales;f__;g__;s__
4353913	-0.677	2.10E-03	1.71E-02	k__Bacteria;p__Firmicutes;c__Clostridia;o__Clostridiales;f__Ruminococcaceae;g__;s__

Supplemental Table S3 (continued)

13994	0.722	2.12E-03	1.71E-02	k__Bacteria;p__Firmicutes;c__Clostridia;o__Clostridiales;f__;g__;s__
323135	-1.169	2.18E-03	1.75E-02	k__Bacteria;p__Firmicutes;c__Clostridia;o__Clostridiales;f__;g__;s__
175761	1.227	2.20E-03	1.75E-02	k__Bacteria;p__Firmicutes;c__Clostridia;o__Clostridiales;f__Ruminococcaceae;g__Ruminococcus;s__
4439487	-0.863	2.24E-03	1.78E-02	k__Bacteria;p__Firmicutes;c__Clostridia;o__Clostridiales;f__Ruminococcaceae;g__;s__
4458306	0.870	2.28E-03	1.79E-02	k__Bacteria;p__Firmicutes;c__Clostridia;o__Clostridiales;f__Veillonellaceae;g__Veillonella;s__dispar
218710	0.738	2.28E-03	1.79E-02	k__Bacteria;p__Firmicutes;c__Clostridia;o__Clostridiales;f__;g__;s__
182073	-1.051	2.31E-03	1.80E-02	k__Bacteria;p__Firmicutes;c__Clostridia;o__Clostridiales;f__;g__;s__
3090117	-0.834	2.38E-03	1.85E-02	k__Bacteria;p__Bacteroidetes;c__Bacteroidia;o__Clostridiales;f__Ruminococcaceae;g__;s__
4396298	-0.884	2.46E-03	1.90E-02	k__Bacteria;p__Firmicutes;c__Clostridia;o__Clostridiales;f__Ruminococcaceae;g__;s__
190864	-0.728	2.49E-03	1.91E-02	k__Bacteria;p__Firmicutes;c__Clostridia;o__Clostridiales;f__;g__;s__
358639	0.735	2.55E-03	1.94E-02	k__Bacteria;p__Firmicutes;c__Clostridia;o__Clostridiales;f__Ruminococcaceae;g__;s__
4447188	-1.000	2.67E-03	2.02E-02	k__Bacteria;p__Bacteroidetes;c__Bacteroidia;o__Bacteroidales;f__Bacteroidaceae;g__Bacteroides;s__uniformis
1028501	0.807	2.69E-03	2.03E-02	k__Bacteria;p__Firmicutes;c__Clostridia;o__Clostridiales;f__Veillonellaceae;g__Dialister;s__
296052	0.730	2.74E-03	2.05E-02	k__Bacteria;p__Firmicutes;c__Clostridia;o__Clostridiales;f__Lachnospiraceae;g__;s__
4336939	-0.839	2.73E-03	2.05E-02	k__Bacteria;p__Firmicutes;c__Clostridia;o__Clostridiales;f__Ruminococcaceae;g__;s__
514257	0.954	2.77E-03	2.05E-02	k__Bacteria;p__Firmicutes;c__Clostridia;o__Clostridiales;f__;g__;s__
10180	-0.775	2.78E-03	2.05E-02	k__Bacteria;p__Proteobacteria;c__Gammaproteobacteria;o__Enterobacteriales;f__Enterobacteriaceae;g__Aquamonas;s__haywardensis
510295	0.762	2.84E-03	2.09E-02	k__Bacteria;p__Firmicutes;c__Clostridia;o__Clostridiales;f__Ruminococcaceae;g__;s__
125624	-1.032	2.87E-03	2.10E-02	k__Bacteria;p__Firmicutes;c__Clostridia;o__Clostridiales;f__Lachnospiraceae;g__;s__
198221	0.817	2.99E-03	2.17E-02	k__Bacteria;p__Firmicutes;c__Clostridia;o__Clostridiales;f__Ruminococcaceae;g__;s__
544996	-0.900	3.00E-03	2.17E-02	k__Bacteria;p__Firmicutes;c__Clostridia;o__Clostridiales;f__Ruminococcaceae;g__Oscillospira;s__
120281	-1.063	3.04E-03	2.19E-02	k__Bacteria;p__Firmicutes;c__Clostridia;o__Clostridiales;f__Lachnospiraceae;g__Blautia;s__producta
199490	-0.852	3.08E-03	2.20E-02	k__Bacteria;p__Firmicutes;c__Clostridia;o__Clostridiales;f__Lachnospiraceae;g__;s__
593868	-0.904	3.10E-03	2.21E-02	k__Bacteria;p__Tenericutes;c__Mollicutes;o__RF39;f__;g__;s__
4349519	0.832	3.17E-03	2.25E-02	k__Bacteria;p__Firmicutes;c__Clostridia;o__Clostridiales;f__[Tissierellaceae];g__Anaerococcus;s__
215468	0.757	3.28E-03	2.31E-02	k__Bacteria;p__Firmicutes;c__Clostridia;o__Clostridiales;f__Ruminococcaceae;g__;s__
563572	0.707	3.35E-03	2.35E-02	k__Bacteria;p__Firmicutes;c__Clostridia;o__Clostridiales;f__Lachnospiraceae;g__;s__
111135	-0.764	3.43E-03	2.39E-02	k__Bacteria;p__Proteobacteria;c__Betaproteobacteria;o__Burkholderiales;f__Alcaligenaceae;g__Sutterella;s__
19674	0.745	3.49E-03	2.42E-02	k__Bacteria;p__Firmicutes;c__Clostridia;o__Clostridiales;f__Ruminococcaceae;g__;s__
311950	-1.030	3.53E-03	2.44E-02	k__Bacteria;p__Bacteroidetes;c__Bacteroidia;o__Bacteroidales;f__Bacteroidaceae;g__Bacteroides;s__plebeius
4473763	-0.722	3.59E-03	2.47E-02	k__Bacteria;p__Bacteroidetes;c__Bacteroidia;o__Bacteroidales;f__Bacteroidaceae;g__Bacteroides;s__fragilis
187468	0.668	3.65E-03	2.49E-02	k__Bacteria;p__Firmicutes;c__Clostridia;o__Clostridiales;f__Lachnospiraceae;g__Blautia;s__
232828	-0.717	3.74E-03	2.54E-02	k__Bacteria;p__Firmicutes;c__Clostridia;o__Clostridiales;f__Ruminococcaceae;g__;s__
176306	-0.922	3.77E-03	2.55E-02	k__Bacteria;p__Firmicutes;c__Clostridia;o__Clostridiales;f__Lachnospiraceae;g__;s__
179663	-0.766	3.80E-03	2.56E-02	k__Bacteria;p__Firmicutes;c__Clostridia;o__Clostridiales;f__Ruminococcaceae;g__;s__
4477861	-1.078	3.97E-03	2.66E-02	k__Bacteria;p__Bacteroidetes;c__Bacteroidia;o__Bacteroidales;f__Bacteroidaceae;g__Bacteroides;s__
4378081	-0.950	4.01E-03	2.68E-02	k__Bacteria;p__Bacteroidetes;c__Bacteroidia;o__Bacteroidales;f__Bacteroidaceae;g__Bacteroides;s__
332241	0.778	4.13E-03	2.74E-02	k__Bacteria;p__Firmicutes;c__Clostridia;o__Clostridiales;f__Ruminococcaceae;g__;s__
4419459	1.001	4.32E-03	2.85E-02	k__Bacteria;p__Firmicutes;c__Clostridia;o__Clostridiales;f__;g__;s__
728119	-0.936	4.33E-03	2.85E-02	k__Bacteria;p__Proteobacteria;c__Gammaproteobacteria;o__Pseudomonadales;f__Pseudomonadaceae;g__Pseudomonas;s__
4454586	-0.959	4.44E-03	2.91E-02	k__Bacteria;p__Bacteroidetes;c__Bacteroidia;o__Bacteroidales;f__[Odoribacteraceae];g__Odoribacter;s__
851634	0.808	4.47E-03	2.91E-02	k__Bacteria;p__Bacteroidetes;c__Bacteroidia;o__Bacteroidales;f__[Prevotellaceae];g__Prevotella;s__
561607	-0.769	4.48E-03	2.91E-02	k__Bacteria;p__Firmicutes;c__Clostridia;o__Clostridiales;f__Ruminococcaceae;g__;s__
180352	-0.656	4.54E-03	2.92E-02	k__Bacteria;p__Firmicutes;c__Clostridia;o__Clostridiales;f__;g__;s__

Supplemental Table S3 (continued)

192983	-0.792	4.55E-03	2.92E-02	k__Bacteria;p__Firmicutes;c__Clostridia;o__Clostridiales;f__Lachnospiraceae;g__;s__
1102370	0.986	4.61E-03	2.95E-02	k__Bacteria;p__Firmicutes;c__Clostridia;o__Clostridiales;f__Ruminococcaceae;g__;s__
176726	0.695	4.69E-03	2.98E-02	k__Bacteria;p__Firmicutes;c__Clostridia;o__Clostridiales;f__Lachnospiraceae;g__;s__
4413347	0.659	4.84E-03	3.07E-02	k__Bacteria;p__Actinobacteria;c__Actinobacteria;o__Bifidobacteriales;f__Bifidobacteriaceae;g__Bifidobacterium;s__
194297	1.088	4.91E-03	3.09E-02	k__Bacteria;p__Firmicutes;c__Clostridia;o__Clostridiales;f__Ruminococcaceae;g__Ruminococcus;s__
4409730	0.958	4.95E-03	3.11E-02	k__Bacteria;p__Firmicutes;c__Clostridia;o__Clostridiales;f__Peptostreptococcaceae;g__;s__
2829179	-0.948	4.97E-03	3.11E-02	k__Bacteria;p__Firmicutes;c__Clostridia;o__Clostridiales;f__Veillonellaceae;g__Acidaminococcus;s__
195015	-0.637	5.13E-03	3.19E-02	k__Bacteria;p__Firmicutes;c__Clostridia;o__Clostridiales;f__Lachnospiraceae;g__Lachnospira;s__
193763	-0.700	5.29E-03	3.28E-02	k__Bacteria;p__Firmicutes;c__Clostridia;o__Clostridiales;f__;g__;s__
364289	0.861	5.64E-03	3.46E-02	k__Bacteria;p__Firmicutes;c__Clostridia;o__Clostridiales;f__Peptococcaceae;g__rc4-4;s__
585914	-0.607	5.63E-03	3.46E-02	k__Bacteria;p__Bacteroidetes;c__Bacteroidia;o__Bacteroidales;f__Porphyromonadaceae;g__Parabacteroides;s__distasonis
809658	0.793	5.84E-03	3.57E-02	k__Bacteria;p__Proteobacteria;c__Deltaproteobacteria;o__Desulfovibrionales;f__Desulfovibrionaceae;g__Desulfovibrio;s__
195186	0.696	5.91E-03	3.60E-02	k__Bacteria;p__Firmicutes;c__Clostridia;o__Clostridiales;f__Lachnospiraceae;g__Blautia;s__
134265	-0.831	6.18E-03	3.75E-02	k__Bacteria;p__Bacteroidetes;c__Bacteroidia;o__Bacteroidales;f__Prevotellaceae;g__Prevotella;s__
797229	-0.815	6.39E-03	3.85E-02	k__Bacteria;p__Proteobacteria;c__Gammaproteobacteria;o__Enterobacteriales;f__Enterobacteriaceae;g__;s__
185141	0.612	6.53E-03	3.92E-02	k__Bacteria;p__Firmicutes;c__Clostridia;o__Clostridiales;f__Ruminococcaceae;g__;s__
4425669	-0.965	6.65E-03	3.98E-02	k__Bacteria;p__Firmicutes;c__Clostridia;o__Clostridiales;f__Lachnospiraceae;g__Coprococcus;s__
262095	-0.684	6.77E-03	4.03E-02	k__Bacteria;p__Firmicutes;c__Erysipelotrichi;o__Erysipelotrichales;f__Erysipelotrichaceae;g__;s__
175180	0.842	6.89E-03	4.09E-02	k__Bacteria;p__Firmicutes;c__Clostridia;o__Clostridiales;f__;g__;s__
157424	-0.764	7.00E-03	4.14E-02	k__Bacteria;p__Firmicutes;c__Clostridia;o__Clostridiales;f__Veillonellaceae;g__;s__
292921	-0.796	7.06E-03	4.15E-02	k__Bacteria;p__Bacteroidetes;c__Bacteroidia;o__Bacteroidales;f__Prevotellaceae;g__Prevotella;s__copri
281015	0.623	7.18E-03	4.20E-02	k__Bacteria;p__Proteobacteria;c__Gammaproteobacteria;o__Enterobacteriales;f__Enterobacteriaceae;g__;s__
158771	-0.661	7.37E-03	4.28E-02	k__Bacteria;p__Firmicutes;c__Clostridia;o__Clostridiales;f__;g__;s__
192210	-0.677	7.36E-03	4.28E-02	k__Bacteria;p__Firmicutes;c__Clostridia;o__Clostridiales;f__;g__;s__
362793	0.701	7.44E-03	4.30E-02	k__Bacteria;p__Firmicutes;c__Clostridia;o__Clostridiales;f__Ruminococcaceae;g__Oscillospira;s__
721569	-0.703	7.48E-03	4.31E-02	k__Bacteria;p__Firmicutes;c__Clostridia;o__Clostridiales;f__Ruminococcaceae;g__;s__
182483	-0.989	7.52E-03	4.32E-02	k__Bacteria;p__Firmicutes;c__Erysipelotrichi;o__Erysipelotrichales;f__Erysipelotrichaceae;g__[Eubacterium];s__biforme
175844	-0.894	7.92E-03	4.52E-02	k__Bacteria;p__Bacteroidetes;c__Bacteroidia;o__Bacteroidales;f__[Barnesiellaceae];g__;s__
174840	-0.790	8.07E-03	4.59E-02	k__Bacteria;p__Firmicutes;c__Clostridia;o__Clostridiales;f__Ruminococcaceae;g__;s__
259604	0.650	8.17E-03	4.63E-02	k__Bacteria;p__Firmicutes;c__Clostridia;o__Clostridiales;f__[Tissierellaceae];g__WAL_1855D;s__
357930	0.802	8.54E-03	4.82E-02	k__Bacteria;p__Firmicutes;c__Clostridia;o__Clostridiales;f__Veillonellaceae;g__Dialister;s__
145401	0.616	8.72E-03	4.90E-02	k__Bacteria;p__Firmicutes;c__Clostridia;o__Clostridiales;f__Lachnospiraceae;g__Blautia;s__

Supplemental Table S4. Top pathways that separate MS and control samples in the human dataset and at least 1 mouse dataset.

Pathway	Human	Mouse 1	Mouse 2
Cellular Processes;Cell Motility;Bacterial chemotaxis	●	●	●
Cellular Processes;Cell Motility;Flagellar assembly	●	●	●
Cellular Processes;Transport and Catabolism;Lysosome	●	●	
Environmental Information Processing;Membrane Transport;ABC transporters	●		●
Metabolism;Amino Acid Metabolism;Histidine metabolism	●	●	●
Metabolism;Biosynthesis of Other Secondary Metabolites;Streptomycin biosynthesis	●	●	●
Metabolism;Carbohydrate Metabolism;Fructose and mannose metabolism	●	●	●
Metabolism;Carbohydrate Metabolism;Starch and sucrose metabolism	●	●	●
Metabolism;Enzyme Families;Peptidases	●		●
Metabolism;Glycan Biosynthesis and Metabolism;Lipopolysaccharide biosynthesis proteins	●		●
Metabolism;Lipid Metabolism;Sphingolipid metabolism	●	●	●
Metabolism;Metabolism of Terpenoids and Polyketides;Polyketide sugar unit biosynthesis	●	●	●
Unclassified;Metabolism;Carbohydrate metabolism	●		●

Supplemental Table S5: Top pathways that separate MS and control samples in the human dataset and at least 1 mouse dataset, calculated only the differentially expressed OTUs.

Pathway	Human	Mouse 1	Mouse 2
Cellular Processes;Transport and Catabolism;Lysosome	●	●	
Environmental Information Processing;Membrane Transport;Transporters	●	●	●
Metabolism;Biosynthesis of Other Secondary Metabolites;Streptomycin biosynthesis	●	●	●
Metabolism;Carbohydrate Metabolism;Fructose and mannose metabolism	●	●	
Metabolism;Carbohydrate Metabolism;Pentose phosphate pathway	●	●	
Metabolism;Glycan Biosynthesis and Metabolism;Other glycan degradation	●	●	
Metabolism;Metabolism of Terpenoids and Polyketides;Polyketide sugar unit biosynthesis	●	●	●
Metabolism;Xenobiotics Biodegradation and Metabolism;Chloroalkane and chloroalkene degradation	●		●
Metabolism;Xenobiotics Biodegradation and Metabolism;Drug metabolism - other enzymes	●	●	
Unclassified;Cellular Processes and Signaling;Other ion-coupled transporters	●	●	
Unclassified;Cellular Processes and Signaling;Pores ion channels	●	●	
Unclassified;Cellular Processes and Signaling;Sporulation	●	●	●
Unclassified;Genetic Information Processing;Restriction enzyme	●	●	
Unclassified;Metabolism;Energy metabolism	●	●	
Unclassified;Metabolism;Others	●		●
Unclassified;Poorly Characterized;Function unknown	●		●

Materials and Methods

Human fecal sample collection

Fecal samples were collected from 71 adult patients with relapsing-remitting multiple sclerosis that had not received treatment for at least 3 months prior to the time of collection and 71 controls without autoimmune disorders at the University of California, San Francisco (UCSF) and the Icahn School of Medicine at Mt Sinai (New York, NY). The inclusion criteria specified no use of antibiotics or cancer therapeutics in 3 months prior to the study. Detailed patient information is available in Supplemental Table 1. All individuals signed a written informed consent in accordance with th?.AZQ sampling procedure approved by the UCSF and Icahn School of Medicine at Mt Sinai Institutional Review Boards. Samples were collected using culture swabs (BD #220135) and stored at -80C until DNA extraction or bacterial isolation.

16S rRNA amplicon sequencing and computational analysis of human and mouse microbiome samples

DNA was extracted from samples using MoBio Power Fecal DNA extraction kit (MoBio #12830) and amplicons of V4 region of the prokaryotic 16S rRNA gene were sequenced using the Earth Microbiome Project standard protocol (44). Analysis was performed using QIIME v1.9 as described (45). Essentially, amplicon sequences were quality-filtered and grouped to "species-level" OTUs using SortMeRNA method (46) using GreenGenes version 13.8 97% dataset for closed reference. Sequences that did not match reference sequences in the GreenGenes database were dropped from the analysis. Taxonomy was assigned to the retained OTUs based on the GreenGenes reference sequence, and the GreenGenes tree was used for all downstream phylogenetic community comparisons. Samples were filtered to at least 10000 sequences per sample, and OTUs were filtered to retain only OTUs present in at least 5% of samples and covering at least 100 total reads. After filtering samples were rarefied to 10000 sequences per sample. Alpha diversity was calculated using the Chao1 method (47). For analysis of beta diversity, pairwise distance matrices were generated using the phylogenetic metric unweighted UniFrac (48) and used for principal coordinate analysis (PCoA). For comparison of individual taxa, samples were not rarefied. Instead, OTU abundances were normalized using variance-stabilizing transformation and taxa distributions

were compared using Wald negative binomial test from R software package DESeq2 as described previously (17, 49) with Benjamini-Hochberg correction for multiple comparisons. All statistical analyses of differences between individual bacterial species were performed using QIIME v.1.9 or R (packages DESeq2 and phyloseq).

Comparison of functional pathways expressed by microbiota

$$KO_j = \sum_{i=1}^{m}\left(W_{otu\ i\rightarrow ko\ j} \times C_{otu\ i}\right) \quad (Equation\ 1)$$

$$Pathway_k = \sum_{j=1}^{n} KO_j \times B\ where\ B = \begin{cases} 0, if\ KO_j\ not\ in\ Pathway_k \\ 1, if\ KO_j\ in\ Pathway_k \end{cases} \quad (Equation\ 2)$$

A matrix of containing samples and OTU counts was obtained for all datasets using QIIME (described above). We transformed the raw OTU counts (C_{otu}) into KEGG Ortholog (KO) values by taking the product of C_{otu} and pre-established OTU contribution weights ($W_{otu\text{-}>ko}$) (50). This resulted in matrix of samples and KO values (*Equation 1*). The KO values were then transformed into pathway values by simply taking the sum of all KOs that contribute to a pathway (*Equation 2*). Once every sample had a pathway value for each pathway, we ran a logistic regression to determine which pathways were the most important in separating MS and control samples. The MS and controls samples separated very well in all three datasets (0.81 AUC (area under the curve) Human, 0.98 AUC Mouse 1, and 0.94 AUC Mouse 2). For each dataset, the pathway coefficients were used to calculate the odds ratio of each pathway. We then took the top 10% of pathways in each of the datasets and checked to see if there was any overlap between the human and mouse datasets. Next, we repeated the same analysis using only the fraction of OTUs that were differentially expressed in MS and control samples. Using this small subset of OTUs, the MS and control samples still separated (0.70 AUC Human and 1.0 AUC in both Mouse datasets).

Bacterial extract preparation for stimulation of human PBMCs

We used a combined experimental approach based on previously published studies to prepare bacterial extracts (51) and combine them with human PBMCs (4), followed by standard Th1 and Treg differentiation protocols (52, 53). All PBMC responses to bacterial extracts were compared to no-bacteria vehicle controls that contained the same protease and phosphatase inhibitors. PBMCs were immunostained and analyzed using standard flow cytometry protocols (described in detail in Supplemental Materials and Methods).

Total bacteria were isolated from patient or control stool samples by suspending ~0.5mg stool sample in 1.5ml PBS, passing it three times through a 40um cell strainer and washing twice with 1.5ml PBS by spinning at 8000rpm. Individual bacterial species were ordered directly from ATCC. *Parabacteroides distasonis* (ATCC #8503) was grown on pre-reduced OxyPRAS Brucella Blood Agar plates (Oxyrase #P-BRU-BA) or in MTGE broth (Anaerobe Systems #AS-778) for 2 days anaerobically. *Akkermansia muciniphila* (ATCC #BAA-835) was grown on Tryptic Soy Blood Agar plates (Anaerobe Systems, #AS-542) or in OxyPRAS BHI broth (Oxyrase #BHI-HK) for 3 days anaerobically. *Acinetobacter calcoaceticus* (ATCC #23055) was grown on OxyPRAS Brucella Blood Agar plates or in Brucella Broth (Anaerobe Systems #AS-105) for 2 days aerobically.

Human PBMC isolation and stimulation with bacterial extracts

Peripheral blood mononuclear cells were isolated from healthy controls or RRMS patients and stored at -80C in cryovials at 10^7 cells/ml concentration in FBS containing 10% DMSO. Before plating, cells were washed in PBS twice, re-counted, and plated at 10^6 cells/ml concentration in RPMI media supplemented with 10% FBS and 1% penicillin/streptomycin/glutamine.

After isolation bacteria were resuspended in PBS supplemented with protease inhibitor (Roche #4693159001) and phosphatase inhibitor (Roche #4906845001), heat-inactivated at 65C for 1h and sonicated for 10min as described previously (48). Protein concentration in the resulting suspension was measured using the Pierce BCA protein assay kit (Thermo Scientific #23227). Bacterial extracts were added to PBMCs at 0.1µg/ml (*A. calcoaceticus*)

or at 1µg/ml *(A. muciniphila, P. distasonis),* to represent their relative abundances, 1h after plating as described previously (4). Each experiment contained at least 6 independent donor samples and was repeated at least twice with no more than 50% overlap between donors. .

For human Treg differentiation, cells were stimulated with anti-human CD3 (BD #555336, 0.3 µg/ml), anti-human CD28 (BD #555725, 2 µg/ml) and recombinant human TGF-β1 (R&D #240B002, 2.5ng/ml) for 4 days (50), in presence of bacterial extracts. For human Th1 differentiation, cells were stimulated with anti-human CD3 (BD #555336, 2 µg/ml), anti-human CD28 (BD #555725, 2 µg/ml), anti-human IL-4 (BioLegend #500702, 5 µg/ml) and recombinant human IL-12 (Thermo Fisher Scientific #NBP143214, 20ng/ml) for 3 days (49), in presence of bacterial extracts. After 3 days the culture media was changed and Th1 cells were restimulated for 4 hours with 1µM ionomycin and 50ng/ml PMA in presence of 2 µM monensin, in absence of bacterial extracts.

Flow cytometry of human PBMCs

Live/dead cell gating was achieved using Live/Dead Fixable Aqua kit (ThermoFisher #L34957). BD Cytofix/Cytoperm kit (BD #554722) was used for staining of intracellular cytokines, and FoxP3/Transcription factor staining buffer set (eBioscience #00-5523-00) for transcription factors. The following antibodies were used for human PBMC staining: anti-CD3-PE.Cy7 (BD #563423), anti-CD4-PerCP.Cy5.5 (BioLegend #300530 or BD #560650) and anti-CD25-PE (BD #555432) or anti-CD25-BV421 (BD #562442) or anti-CD25-APC (BD #555434), anti-IFNγ-FITC (BioLegend #502506), anti-Tbet-PE (BD #561265), anti-FoxP3-AlexaFluor-488 (BD #560047), and anti-IL-10-PE (eBioscience #12-7108). Flow cytometry was performed on BD Fortessa cell analyzer and analyzed using FlowJo software (TreeStar). For both mouse and human PBMC flow cytometry, cells were gated to identify the lymphocyte population based on forward and side scatter, followed by gating for single cell and live cell populations. Unstained, single color, and fluorescence-minus-one controls were used to identify stained populations.

Verification of germ-free or antibiotic-treated mouse status

The level of bacterial colonization in GF mice was verified in feces by quantifying colony forming units in anaerobic conditions (Supplemental Figure 11A). Colonization specificity was verified by PCR (Supplemental Figure 11B). In bacterial monocolonization experiments, mice were euthanized and immunophenotyping was performed 3-4 weeks after colonization. GF mice remained in isolators for the duration of the experiment and transferred out when euthanized. GF mice that were subsequently associated with fecal microbes or single species of bacteria were taken out of isolators at 3-4 weeks of age and colonized with a single oral gavage. In experiments without EAE induction, GF control groups were kept in isolators until mice were euthanized for immunophenotyping. In experiments with EAE induction, GF mice were removed from the isolators in order to induce EAE, and maintained GF outside of the isolators by supplementing drinking water with erythromycin and gentamycin until the end of the experiment. In order to ensure that the GF animals remained GF both inside and outside the isolators, their stool samples were repeatedly plated on Brucella blood agar plates and cultured both aerobically and anaerobically. GF mice were determined to be clean after no colonies could be observed on the plates after a week of incubation.

To ensure that broad-spectrum antibiotic treatment depletes stool bacteria, total bacteria isolated from mouse stool was cultured on Brucella Blood Agar plates and no colonies were observed. Antibiotic-mediated depletion of microbiota was further verified by comparing community richness in antibiotic-treated mice and SPF controls (Supplemental Figure 12; Chao1 metric of alpha diversity).

Mouse colonization with microbiota

Germ-free (GF) mice were bred and maintained in sterile isolators that were assayed every two weeks for GF status by bacterial plating and PCR. Fecal material from human donor samples or individual bacteria species at 10^8 CFU/mouse was diluted to a final solution of 1.5% sodium bicarbonate. For colonization experiments following antibiotic treatment, mice were treated with 1% solution of Amphotericin B in drinking water for 3 days, followed by 2 weeks of antibiotic solution composed of 1% Amphotericin B, 1mg/ml ampicillin, 1mg/ml

neomycin, 1mg/ml metronidazole, and 0.5mg/ml vancomycin in drinking water; 1% Amphotericin B solution was used as a control. After 2 weeks, we replaced the drinking solution by sterile water and mice were gavaged by specific bacteria of interest in a solution of 1.5% sodium bicarbonate at 10^8 CFU/mouse every 2-3 days for 2 weeks. SPF mice were gavaged with mock culture medium every 2-3 days for 2 weeks to mimic the esophageal trauma.

Induction of EAE

EAE was induced 6-7 weeks after colonization, corresponding to 9-10 weeks of age. Mice were subcutaneously immunized in the upper and lower back with 0.1ml MOG_{35-55} emulsion (1mg/ml) mixed with Complete Freud's Adjuvant and killed mycobacterium tuberculosis H37Ra (2-5mg/ml), followed by two 0.1ml intraperitoneal injections of pertussis toxin (4μg/ml) approximately 2 and 26 hours later (Hooke Laboratories #EK-2110). Mice were scored daily in a blinded fashion for motor deficits as follows: 0, no deficit; 1, limp tail only; 2, limp tail and hind limb weakness; 3, complete hind limb paralysis; 4, complete hind limb paralysis and partial/complete forelimb paralysis; 5, moribund.

Mouse immune cell isolation and intracellular cytokine staining

Mesenteric lymph nodes, cervical lymph nodes, and spleens were dissected and processed by grinding tissues through a 100um cell strainer. Single cell suspensions were incubated for 4-5 hours with 50ng/ml PMA, 2μg/ml ionomycin in presence of 2μg/ml protein transport inhibitor (GolgiPlug, BD #51-2301KZ). Cells were then incubated in 5% mouse serum for 15 min and stained for 20 min at 4ºC with Live/Dead Fixable Violet kit (Life Technologies #L34964) or Live/Dead Fixable Aqua kit (ThermoFisher #L34957) and anti-CD4-PE-Cy7 (eBioscience #25-0042-82). Cells were fixed and permeabilized with FoxP3/Transcription factor buffer set (eBioscience #00-5523-00), and stained with anti-Foxp3-APC (eBioscience, #17-5773-82) and anti-IL10-PE (eBioscience #12-7101-82), anti-IFNγ-FITC (eBioscience, #11-7311-82), anti-IL17-PerCP/Cy5.5 (eBioscience #45-7177-82).

RNAseq analysis in gnotobiotic mouse spinal cords

RNA was isolated from whole spinal cord and sequenced at the New York Genome Center. Samples were pair-end sequenced and each sample generated 100 million reads (50 million read-pairs). Raw reads were then aligned to the Ensemble reference genome (mapping rate = 80%). Differential expression of transcripts was analyzed using the DESeq2 package. We identified transcripts with baseMean (average count value normalized to library size) > 5 and a log2 fold change of at least 1.5 between the spinal cord of EAE mice transplanted with MS stool samples compared to mice transplanted with control stools. This gene list was used to interrogate cell-enrichment gene lists that were generated using the data from Zhang et al. (J Neurosci. 2014 Sep 3;34(36):11929-47)

A gene whose expression was at least 10 folds higher in one cell type than in any other cell type was considered cell-specific. Six cell-specific lists were generated: astrocytes, myelinating oligodendrocytes, neurons, oligodendrocyte precursor cells, microglia and endothelial cells.

Statistical analysis of *in vitro* data

Statistical significance of expression changes in markers of T lymphocyte differentiation and proliferation was determined using two-tailed Student's *t* test to compare samples from different donors, two-tailed repeated measures *t* test to compare samples from the same donor, and one or two-way ANOVA to compare samples from different donors in different groups based on bacterial presence. When data was non-normally distributed, two-tailed nonparametric Mann-Whitney test was used instead. Benjamini-Hochberg adjustment was used to account for multiple comparisons. GraphPad Prism 6 software was used to analyze and plot the data. $P < 0.05$ was considered statistically significant.

Acknowledgments

References

1.   Lee YK & Mazmanian SK (2010) Has the microbiota played a critical role in the evolution of the adaptive immune system? *Science* 330(6012):1768-1773.

2.   Faith JJ, Ahern PP, Ridaura VK, Cheng J, & Gordon JI (2014) Identifying gut microbe-host phenotype relationships using combinatorial communities in gnotobiotic mice. *Sci Transl Med* 6(220):220ra211.

3.   Round JL & Mazmanian SK (2010) Inducible Foxp3+ regulatory T-cell development by a commensal bacterium of the intestinal microbiota. *Proc Natl Acad Sci U S A* 107(27):12204-12209.

4.   Lozupone CA*, et al.* (2013) Alterations in the gut microbiota associated with HIV-1 infection. *Cell Host Microbe* 14(3):329-339.

5.   Chu H*, et al.* (2016) Gene-microbiota interactions contribute to the pathogenesis of inflammatory bowel disease. *Science* 352(6289):1116-1120.

6.   Varrin-Doyer M*, et al.* (2012) Aquaporin 4-specific T cells in neuromyelitis optica exhibit a Th17 bias and recognize Clostridium ABC transporter. *Ann Neurol* 72(1):53-64.

7.   Scher JU*, et al.* (2013) Expansion of intestinal Prevotella copri correlates with enhanced susceptibility to arthritis. *Elife* 2:e01202.

8.   Gevers D*, et al.* (2014) The treatment-naive microbiome in new-onset Crohn's disease. *Cell host & microbe* 15(3):382-392.

9.   Cantarel BL*, et al.* (2015) Gut microbiota in multiple sclerosis: possible influence of immunomodulators. *J Investig Med* 63(5):729-734.

10.   Miyake S*, et al.* (2015) Dysbiosis in the Gut Microbiota of Patients with Multiple Sclerosis, with a Striking Depletion of Species Belonging to Clostridia XIVa and IV Clusters. *PLoS One* 10(9):e0137429.

11.   Tremlett H*, et al.* (2016) Gut microbiota composition and relapse risk in pediatric MS: A pilot study. *J Neurol Sci* 363:153-157.

12.   Jangi S*, et al.* (2016) Alterations of the human gut microbiome in multiple sclerosis. *Nat Commun* 7:12015.

13.   Berer K*, et al.* (2011) Commensal microbiota and myelin autoantigen cooperate to trigger autoimmune demyelination. *Nature* 479(7374):538-541.

14.   Lee YK, Menezes JS, Umesaki Y, & Mazmanian SK (2011) Proinflammatory T-cell responses to gut microbiota promote experimental autoimmune encephalomyelitis. *Proceedings of the National Academy of Sciences of the United States of America* 108 Suppl 1:4615-4622.

15.   Simmons SB, Pierson ER, Lee SY, & Goverman JM (2013) Modeling the heterogeneity of multiple sclerosis in animals. *Trends Immunol* 34(8):410-422.

16.   Carbajal KS*, et al.* (2015) Th Cell Diversity in Experimental Autoimmune Encephalomyelitis and Multiple Sclerosis. *J Immunol* 195(6):2552-2559.

17.   McMurdie PJ & Holmes S (2014) Waste not, want not: why rarefying microbiome data is inadmissible. *PLoS Comput Biol* 10(4):e1003531.

18.   Kverka M*, et al.* (2011) Oral administration of Parabacteroides distasonis antigens attenuates experimental murine colitis through modulation of immunity and microbiota composition. *Clin Exp Immunol* 163(2):250-259.

19.   Geuking MB*, et al.* (2011) Intestinal bacterial colonization induces mutualistic regulatory T cell responses. *Immunity* 34(5):794-806.

20.   Peleg AY, Seifert H, & Paterson DL (2008) Acinetobacter baumannii: emergence of a successful pathogen. *Clin Microbiol Rev* 21(3):538-582.

21.   Almeida LA & Araujo R (2013) Highlights on molecular identification of closely related species. *Infect Genet Evol* 13:67-75.

22.   Hughes L (2003) Cross-reactivity between related sequences found in Acinetobacter sp., Pseudomonas aeruginosa, myelin basic protein and myelin oligodendrocyte glycoprotein in multiple sclerosis. *Journal of Neuroimmunology* 144(1-2):105-115.

23.   Everard A*, et al.* (2014) Microbiome of prebiotic-treated mice reveals novel targets involved in host response during obesity. *ISME J* 8(10):2116-2130.

24.   Ganesh BP, Klopfleisch R, Loh G, & Blaut M (2013) Commensal Akkermansia muciniphila exacerbates gut inflammation in Salmonella Typhimurium-infected gnotobiotic mice. *PLoS One* 8(9):e74963.

25. Hua J, Davis SP, Hill JA, & Yamagata T (2015) Diverse Gene Expression in Human Regulatory T Cell Subsets Uncovers Connection between Regulatory T Cell Genes and Suppressive Function. *J Immunol* 195(8):3642-3653.

26. Devkota S (2016) MICROBIOME. Prescription drugs obscure microbiome analyses. *Science* 351(6272):452-453.

27. Chen J*, et al.* (2016) Multiple sclerosis patients have a distinct gut microbiota compared to healthy controls. *Sci Rep* 6:28484.

28. Tremlett H*, et al.* (2016) Associations between the gut microbiota and host immune markers in pediatric multiple sclerosis and controls. *BMC Neurol* 16(1):182.

29. Tremlett H*, et al.* (2016) Gut microbiota in early pediatric multiple sclerosis: a case-control study. *Eur J Neurol* 23(8):1308-1321.

30. Wang Y*, et al.* (2014) A commensal bacterial product elicits and modulates migratory capacity of CD39(+) CD4 T regulatory subsets in the suppression of neuroinflammation. *Gut Microbes* 5(4):552-561.

31. Arpaia N*, et al.* (2013) Metabolites produced by commensal bacteria promote peripheral regulatory T-cell generation. *Nature* 504(7480):451-455.

32. Rothhammer V*, et al.* (2016) Type I interferons and microbial metabolites of tryptophan modulate astrocyte activity and central nervous system inflammation via the aryl hydrocarbon receptor. *Nat Med* 22(6):586-597.

33. Erny D*, et al.* (2015) Host microbiota constantly control maturation and function of microglia in the CNS. *Nat Neurosci* 18(7):965-977.

34. Sampson TR*, et al.* (2016) Gut Microbiota Regulate Motor Deficits and Neuroinflammation in a Model of Parkinson's Disease. *Cell* 167(6):1469-1480 e1412.

35. Hughes LE*, et al.* (2001) Antibody responses to Acinetobacter spp. and Pseudomonas aeruginosa in multiple sclerosis: prospects for diagnosis using the myelin-acinetobacter-neurofilament antibody index. *Clin Diagn Lab Immunol* 8(6):1181-1188.

36. Derfuss T & Meinl E (2012) Identifying autoantigens in demyelinating diseases: valuable clues to diagnosis and treatment? *Curr Opin Neurol* 25(3):231-238.

37.   Cree BA, Spencer CM, Varrin-Doyer M, Baranzini SE, & Zamvil SS (2016) Gut microbiome analysis in neuromyelitis optica reveals overabundance of Clostridium perfringens. *Ann Neurol* 80(3):443-447.

38.   Derrien M, Belzer C, & de Vos WM (2016) Akkermansia muciniphila and its role in regulating host functions. *Microb Pathog*.

39.   Miller PG, Bonn MB, Franklin CL, Ericsson AC, & McKarns SC (2015) TNFR2 Deficiency Acts in Concert with Gut Microbiota To Precipitate Spontaneous Sex-Biased Central Nervous System Demyelinating Autoimmune Disease. *J Immunol* 195(10):4668-4684.

40.   Sellon RK*, et al.* (1998) Resident enteric bacteria are necessary for development of spontaneous colitis and immune system activation in interleukin-10-deficient mice. *Infect Immun* 66(11):5224-5231.

41.   Eun CS*, et al.* (2014) Induction of bacterial antigen-specific colitis by a simplified human microbiota consortium in gnotobiotic interleukin-10-/- mice. *Infect Immun* 82(6):2239-2246.

42.   Ridaura VK*, et al.* (2013) Gut microbiota from twins discordant for obesity modulate metabolism in mice. *Science* 341(6150):1241214.

43.   Sokol H*, et al.* (2008) Faecalibacterium prausnitzii is an anti-inflammatory commensal bacterium identified by gut microbiota analysis of Crohn disease patients. *Proc Natl Acad Sci U S A* 105(43):16731-16736.

Chapter 3

THE ENTERIC NETWORK: INTERACTIONS BETWEEN THE IMMUNE AND NERVOUS SYSTEMS OF THE GUT

SUMMARY:

The enteric nervous system (ENS), located along the gastrointestinal (GI) tract, enervates an organ that contains a rich collection of cells from the immune system, and is exposed to an ever-changing environment. Collectively, interactions between the nervous and immune systems enable the gut to respond to a variety of dietary products it absorbs, a spectrum of pathogens it encounters, and the diverse microbiome it harbors. The ENS senses and reacts to the dynamic ecosystem of the GI tract by translating chemical cues from the environment into neuronal impulses that propagate throughout the gut, and into other organs in the body including the central nervous system (CNS). This review will describe current understanding of the anatomy and physiology of the GI tract, focusing on ENS and the mucosal immune system. We highlight emerging literature that the ENS is essential for aspects of microbe-induced immune responses in the GI tract. While most basic and applied research in neuroscience has focused on the brain, the strategic location of the ENS in proximity to a rich immune system and the external environment suggest novel paradigms for nervous system function await discovery.

Introduction

The gastrointestinal (GI) tract spans 5 meters in length and has an epithelial surface area of ~32 square meters (1). It is resident to 70-80% of the body's immune cells (2), over 100 million neurons (3) and 50,000 extrinsic nerve endings. The microbiome consists of as many as 40 trillion cells and at least hundreds of different species (4, 5). An important function of the GI tract is to sense and respond to external cues. Diverse cellular interactions are responsible for interpreting external cues, and these interactions must be amenable to the change and flux in the molecular environment of the GI tract. Thus, there are countless components that necessitate GI function, and equally complex aberrations that can affect it. Accordingly, 70 million people in the United States (>20% of the population) are affected by digestive diseases every year (6), and GI dysfunction is often a comorbidity with numerous non-intestinal conditions. As such, interactions between interdependent, cellular pathways in the gut and the periphery may underlie process involved in health and disease.

Overview of GI Compartments

Anatomy of the GI tract

The GI tract consists of the stomach, small and large intestines. Anatomically, the tissue of the GI tract can generally be compartmentalized by the mesentery and serosa, muscularis, submucosa, lamina propria, epithelium, and lumen (Figure 1).

In the mesentery, recently considered a distinct organ (7), major extrinsic arteries, veins, lymphatics, and nerve fibers enter and exit the tissue. Connective tissue immobilizes the GI tract within the peritoneum, and adipose tissue insulates nerves and vasculature. The mesentery is contiguous with the serosa, which is the outermost layer of mesothelium that encapsulates and lubricates the GI tract so that peristaltic contractions are uninhibited. The mesentery also encloses the mesenteric lymph nodes (MLNs), which are the draining lymph nodes of the intestines.

The outermost layers of intestinal tissue proper are collectively called the muscularis. This region is made up of an outer longitudinal and inner circular muscle layer. These layers are orthogonal to each other, providing stretch and shear flexibility, and are also resident to many immune cells (8). Between these two layers of smooth muscle lies the myenteric plexus which is the network of neurons and glia that extend throughout GI tract. Luminal to the muscularis, vasculature spreads throughout the submucosal layer, bringing within it, circulating immune cells that infiltrate and exit the tissue. The submucosal plexus also sends neuronal impulses and senses inputs to and from cells in the myenteric plexus and mucosa. Immune structures such as Peyer's patches and lymphoid follicles emanate from the submucosa and extend into the mucosa. The lamina propria and innermost epithelial layer make up the mucosa. The lamina propria contains many innate and adaptive immune cells, but also is made of the connective tissue that is important for GI structural identity. Furthermore, the vascular, neuronal, and glial processes extend throughout the lamina propria, and the diverse cells and molecules associated with these structures are important for enteric function. The epithelium is the single layer of cells that separates intestinal tissue from the lumen. As will be described later, distinct subtypes of intestinal epithelial cells (IECs) are responsible for absorption, communication, and protection, and these roles are mediated by diverse effector molecules that function apically and basolaterally. Finally, the lumen hosts the molecules excreted and consumed by the host and the microbiome that has adapted to survive the GI tract.

Intestinal Epithelium

The intestinal epithelium is composed of distinct IEC types that mediate communication between the host and the luminal environment. The four most abundant IECs are enterocytes, goblet cells, Paneth cells, and enteroendocrine cells (EECs). Enterocytes are the primary absorptive cells in the epithelium and they increase their surface area with apical microvilli structures. Goblet cells are responsible for producing and secreting mucin proteins into the lumen. Mucins are

heavily glycosylated proteins that not only provide a protective barrier from the lumen, but also provide a medium to facilitate molecular exchange between the epithelium and the environment (9). Paneth cells reside mainly in ileal intestinal crypts and secrete potent antimicrobial products via release of granule contents (10). As such, antimicrobial peptides (AMPs) are secreted when the epithelium senses microbe associated molecular patterns, and downregulated in germ-free (GF) mice (mice free of all microorganisms) (11-13). Finally, enteroendocrine cells (EECs) produce a variety of modulatory, neuroendocrine molecules. These cells have been commonly referred to as the "taste" cells of the gut (14), as they are popularly known for their chemosensation and production of molecules that control aspects of feeding, such as appetite.

Other IECs are important for directing innate and adaptive immunological responses to luminal antigens. In particular, microfold cells (M-cells) aid in the immunological sampling of antigens across the epithelium (15). M-cells are also capable of transporting intact bacteria across the epithelium and to gut-associated lymphoid tissues (GALT) (16). Thus, M-cells are often found in close association with dendritic cells (DCs) on the luminal side of Peyer's patches and lymphoid follicles. This gives immune cells prime position to induce an adaptive immune response. The intestinal stem cell compartment is vital to sustain immense epithelial turnover in response to high levels of oxidative stress and damage. Finally, cup and tuft cells are not well characterized, but the latter has recently been shown to be important for inducing type 2 immune responses against parasitic helminths (17, 18).

Transport of molecules to and from the lumen occurs both transepithelially (through epithelial cells) and paracellularly (between epithelial cells) (19). Paracellular transport is mediated by selective cellular junctions known as tight junctions. Transepithelial transport can occur through primary or secondary active transport mechanisms– the former requires ATP and carrier proteins and the latter employs concentration gradients (20). Furthermore, receptor-mediated transcytosis also

occurs across the epithelium. Although a variety of apical stimuli are important in mediating IEC function, as will be discussed, basolateral signals can also incite effector functions in IECs. Thus, the epithelium mediates critical barrier functions, though in a dynamic fashion interacting with both the luminal (e.g., gut bacteria) and basolateral (e.g., immune and neuronal cells) compartments of the gut.

The Enteric Nervous System

The mammalian nervous system is divided into two arms: the central nervous system (CNS) and the peripheral nervous system (PNS). The CNS encompasses the brain and the spinal cord, and the PNS includes the ganglia, aggregates of neural cell bodies where nerve bundles arise from, in the head, neck, and viscera. The autonomic (involuntary) nervous system is characterized as sympathetic or parasympathetic, and the main neurotransmitters produced are the catecholamines (CCh- norepinephrine, epinephrine, and dopamine) and acetylcholine (ACh), respectively. Extrinsic connectivity from the CNS to the ENS is comprises of both sympathetic and parasympathetic nerve fibers. Upon leaving the hindbrain, the parasympathetic vagus nerve travels through the diaphragm and synapses onto the GI tract. Sympathetic visceral ganglia also innervate the intestines, and in both instances, nerves can synapse directly onto the myenteric ganglia, smooth muscle, and mucosa (21). Parasympathetic pelvic nerves originate in the spinal cord and leave via the sacral spinal nerve where it ultimately innervates the distal colon and rectum. Furthermore, parasympathetic nerves can innervate sympathetic ganglia and modulate their sympathetic output onto the GI tract. The intrinsic ENS is the expansive network of neurons and glia along the GI tract that can be affected by their connectivity to extrinsic sympathetic and parasympathetic nerves (22). Thus, communication between the CNS and ENS is bidirectional.

Receptors on enteric neurons mediate important GI functions. Mechanoreceptors are responsive to mucosal abrasion and tension receptors are responsive to stretch. Chemoreceptors respond to the chemical stimuli of the lumen, such as pH,

osmolarity, and nutrients. Furthermore, various receptors are responsible for regulating fluid exchange within the gut (23). Subsets of neurons can generally be categorized by their connectivity. Intrinsic primary afferent neurons (IPAN), are large, multi-axonal, and sensory neurons that are responsible for detecting molecular and mechanical aberrations of the GI tract. These neurons relay sensory impulses to other IPANS, interneurons, and ultimately intrinsic motor neurons that induce effector functions. They comprise 10-30% of the neurons in both the myenteric and submucosal plexuses. Intrinsic intestinofugal afferent neurons (IFANs) send neuronal impulses from the GI tract to extrinsic, visceral ganglia where efferent nerves send sympathetic impulses back to the ENS and complete the reflex arc (10). Interneurons synapse with other interneurons as well as motor neurons. They are responsible for connecting sensory and motor neurons, and thus propagates a neuronal impulse. Muscle motor neurons are found along the entire GI tract in the longitudinal and circular muscle layers and mucosa, and they mainly respond to signals initiated by mechanoreceptors and tension receptors. Vasodilator and secretomotor neurons manage fluid and molecular exchange between the GI vasculature, tissue, and the lumen (11, 12)(Figures 1 and 2).

Enteric glial cells (EGCs) are significant constituents of the ENS and have been shown to be important benefactors towards mucosal health (13). EGCs in the myenteric and submucosal plexuses have been shown to envelop enteric neurons and associate with blood vessels and lymphatics (14). As will be described in later sections, important EGC-derived signaling molecules implicate the functional development of certain cell types important in GI immunity.

Cells, Molecules, and Receptors Implicated in GI Neuro-immunity

Brief Overview of the GI Immune System

The extensive GI lymphatic system mediates the flux of immune cells that occupies the lamina propria. Intestinal granulocytes rapidly produce toxic molecules against

intracellular and extracellular bacteria and parasites, while natural killer (NK) cells attach virally infected cells. Macrophages, specifically, are important GI innate immune cells that are involved in early microbial surveillance, and subsequent attraction and activation of other immune cell types. B and T cells carry out adaptive immune functions, and this is predicated on activation by antigen presenting cells (APCs) such as macrophages and dendritic cells (DCs). Interestingly, it has been reported that DCs express IEC tight junction proteins that allows them to extend protrusions between IECs and directly sample gut luminal antigens (15). Intraepithelial lymphocytes (IELs) and innate lymphoid cells (ILCs) have a common progenitor that is distinct from B and T lymphocytes (16), do not require any prior activation or maturation to carryout effector immune function, and have been appreciated for their role in GI immune homeostasis (17, 18), and more recently in the context of the microbiota (19). The GI immune system with respect to its microbiome has been extensively reviewed (20); thus we will focus on the specific cells and molecules that reveal potential neuro-immune responses to gut bacteria in subsequent sections.

Catecholamines

Catecholamines (CChs) are a class of neuroactive molecules secreted at sympathetic nerve endings. The bone marrow, thymus, spleen, and peripheral lymph nodes are innervated by sympathetic nerves (24), and accordingly, functional adrenergic receptors are expressed on virtually all leukocytes (25). Thus, immunologists have long been intrigued by the role of sympathetic, catecholaminergic signaling in the immune system, and their effects have been long been studied (26). Recently, Gabanyi *et. al*. discovered potential mechanisms by which the ENS functions to polarize intestinal macrophages, spatially and immunologically (27), thus, positing on the role of sympathetic innervation of the GI tract. In this study, intestinal macrophages, were found to be phenotypically compartmentalized in the muscularis and mucosa layers of the GI tract, putting them in close proximity to extrinsic innervation and submucosal nerve fibers, respectively. Muscularis macrophages

were found to be phenotypically similar to M2 (regulatory) macrophages, whereas those isolated in the lamina propria were similar to M1 (proinflammatory) macrophages. Naïve peritoneal macrophages became more similar to muscularis macrophages when cultured with enteric neurospheres, and this was dependent upon engagement of the β-2 adrenergic receptor (β2AR) (Figure 4). Furthermore, sympathetic ganglia are activated during *Salmonella* infection, and this induces a β2AR activation-dependent expression of genes associated with muscularis macrophages. In another study, *ex vivo* catecholaminergic treatment of Peyer's patches exhibit lower rates of *Salmonella* translocation (28), potentially mitigating infection. These studies suggest that adrenergic signaling occurs in the GI tract. However, tyrosine hydroxylase (an enzyme critical for CCh biosynthesis from tyrosine) immunoreactivity persists in the GI tract after extrinsic denervation (29), and this suggests that intrinsic, catecholaminergic synthesis, and signaling may also be involved in modulating GI immune responses.

In addition to the direct effects that CChs may have in regulating immune response, similar effects may occur by modulating their availability in the GI tract. UDP-glucuronyltransferase is an enzyme that has been studied in the liver, kidneys, brain, and GI tract (30) for their ability to transfer glucuronic acid onto endogenous and xenobiotic molecules, making them more hydrophilic and often excreted in the urine and feces. However, hormones are also glucuronidated, giving them their rapid systemic effect. 90% of the dopamine found in the lumen of the GF mouse is glucuronidated, and 90% of the dopamine found in the GI tract of SPF mice is not. Colonizing GF mice with an SPF microbiota or a consortia of *Clostridia* species can reverse skewing towards glucuronidated products (31). Interestingly, microbes isolated from the rodent GI tract have been shown to have endogenous beta-glucuronidase (GUS) activity (32), and thus, colonizing GF mice with *E. coli* that produce functional GUS enzymes is sufficient for decreasing levels of glucuronidated CChs. Conversely, mutant *E. coli* that is deficient in GUS production cannot (31). Thus, gut microbes, and specifically, microbial GUS

activity, can shape the molecular activity and availability of CChs, and this may affect how leukocytes behave in the GI tract.

Interestingly, bacteria also produce endogenous adrenergic receptors, QseC and QseE, through which epinephrine and norepinephrine regulate expression of virulence genes in enteric pathogens (33-35). Pathogenicity is diminished in mutant strains of *Citrobacter rodentium* (an enteric pathogen) that are deficient in QseC and QseE. Also, wildtype *C. rodentium* is also ineffective in colonizing mice that do not express dopamine beta-hydroxylase (36), the enzyme required for norepinephrine and epinephrine synthesis. However, whether glucuronidated CChs are ineffective in modulating virulence, or whether bacteria that produce GUS can enhance virulence in a mouse is unknown. Regardless, this intriguingly links host CCh biosynthetic pathways to bacterial infections, and may provide novel, antibiotic-independent strategies towards mitigating intestinal bacterial infections. In all, CChs in the GI tract are impactful signaling molecules that affect cells of multiple phyla. However, the way in which the cellular source of CChs impacts its effect on the immune system is still poorly understood.

Acetylcholine

Acetylcholine (ACh) is the primary parasympathetic neurotransmitter that is released by preganglionic nerve fibers (these fibers arise from ganglia along the spinal cord) and the vagus nerve. ACh has been studied for its powerful anti-inflammatory effects in the periphery, and vagal stimulation was sufficient in suppressing systemic inflammation in response to endotoxin (37). It was later discovered that endotoxemic mice deficient in α7-nicotinic acetylcholine receptor (α7-nAchR) display increased systemic levels of TNFα, IL-1β, and IL-6, and these mice could not suppress TNFα levels upon vagal stimulation. Specifically, α7-nAChR expression on macrophages was necessary for the observed ACh-mediated TNFα suppression (38). In another study that followed, splenic nerve stimulation also produced similar inhibition of the inflammatory TNFα response to LPS (39). However, vagal innervation results in

ACh release on the celiac ganglion which in turn sends noradrenergic signals to the spleen via the splenic nerve (40). Thus, the question remained on how vagal and splenic nerve stimulation is able to produce similar effects, when the vagus nerve does not directly innervate the spleen and the splenic nerve does not produce acetylcholine, all the while, the immunoregulatory effects appeared to function through ACh receptors. In a paradigm shifting study in neuro-immunology, ACh-producing T cells were discovered to mediate these effects. These T cells secrete ACh in response to the activation of their β-adrenergic receptors, and the resulting ACh activates α7-nAchR on macrophages to suppress TNFα production (41). The functional discovery of ACh-producing T cells has demonstrated the remarkable molecular reflexes at the interface of the peripheral nervous and immune systems, and such discoveries have immensely expanded the breadth and appreciation of previously known neuro-immune interactions. However, research regarding cholinergic pathways in the GI tract are only just beginning to appear in the literature. For example, it has recently been shown that specific depletion of ACh producing T cells results in reduced intestinal AMP levels and relative changes to the microbiota (42). Mice deficient in type 3 muscarinic ACh receptors (M_3-AChR) have a leaky intestinal barrier, higher basal levels of IFNγ, IL-17A, and TNFα, and exhibit delayed clearance of *C. rodentium* (43). Interestingly, these mice also express lower levels of IL-4 and IL-13, resulting in the delayed clearance of intestinal parasites (44).

Although the vagus and pelvic nerves have connections along the length of the GI tract, with some nerve endings directly innervating the mucosa, they are not the only source of intestinal ACh. Intrinsic neurons are also immunoreactive against choline acetyltransferase (ChAT), the rate limiting enzyme in ACh synthesis (45). Furthermore, these extrinsic nerve endings often synapse onto neurons in the myenteric plexus, and thus, it is possible that ACh may induce activation of noncholinergic neurons in the ENS, and subsequent release of other neuromodulatory compounds. Also, because the ENS can initiate its own neuronal reflexes independent of extrinsic inputs, it is possible that the intrinsic circuitry alone can

influence immune function. Thus, it is plausible that similar neuro-immune paradigms existing in the spleen and the periphery could also exist in the GI tract.

IECs, like immune cells, are in close proximity to neuronal projections in the mucosa. However, unlike immune cells, every IEC is in direct association with the lumen. This apical and basolateral dichotomy makes IECs an interesting and potential mediator of neuro-immune communications that occur between the mucosa and the microbiota. Specifically, ACh has been well studied for its effects on Paneth and goblet cells (Figure 3). AchR activation is important for both Paneth and goblet cell degranulation. As such, bethanechol, an mAChR agonist stimulates degranulation (46), while the mAChR antagonist atropine suppresses this function (47). Similarly, AChR activation on goblet cells induces mucin secretion (48, 49). AChR activation in mice also results in increased goblet-cell-associated antigen passages (GAPs), which allow goblet cells to take up luminal antigens and deliver them to DCs in the lamina propria (50). This is particularly interesting because it directly implicates ACh in the immunological sampling of luminal contents and microbes. Finally, like goblet and Paneth cells, cholinergic stimulation of EECs induces its secretion of neuroendocrine molecules (51). Although all IECs come from the common intestinal stem cell progenitor, Math1 is a distinct transcription factor that determines differentiation of Paneth, goblet, and EECs but not absorptive enterocytes (52). Thus, it may also be true that ACh sensitivity of certain IECs is a functional determination that is developmentally programmed. Ultimately, ACh is a powerful mediator of intestinal function, but again, it is unclear what the endogenous source of ACh is, and if this distinction affects its functional output on IECs, the ENS, and GI immune cells.

Enteroendocrine Cells

Many different subtypes of EECs exist along the epithelium of the GI tract. Their main function is to secrete a variety of endocrine molecules in response to luminal and GI cues (53, 54). Intriguingly, EECs produce molecules that not only affect the ENS but are also produced by it (55). As such, the molecules glucagon like peptide

1 (GLP-1) (56) and cholecystokinin (CCK) (57) are known mediators of EEC function, but also modulate ENS activity. Furthermore, enteric neurons have been shown to "synapse" onto EECs (58), and EECs have been shown to secrete their intracellular stores of effector molecules in response to membrane depolarization (59, 60) and heightened calcium levels (61). However, the functionality of these physical neuro-epithelial circuits is unknown. Specifically, the secretory output of an EEC in response to an action potential from a synapsed enteric neuron is unknown.

Other GI constituents can affect aspects of EEC function. For example, T cell receptor mutant mice have lower numbers of CCK producing EECs in the colon (62), potentially linking adaptive immune function to EEC peptide production. GF mice have fewer EECs (63), and *C. rodentium* infection decreased levels of 5-HT-producing EECs (64). Furthermore, EECs express functional TLRs (65), and treatment of mice with TLR agonists induce CCK release, and this may not be limited to just CCK (66).

As previously described, EECs are oriented such that apical stimuli are translated into basolateral signals (Figure 3). Perhaps EECs represent a direct means by which microbes can actively remodel the neuromodulatory environment across the epithelium, potentially changing the activity of sensory neurons in the mucosa. Given the similarity of the molecules that EECs and the ENS utilize to communicate, and their potential effects on the immune system, perhaps EECs translate luminal cues to the GI neuro-immune system.

Neuropeptides

Neuropeptides are small protein molecules that are generally used to communicate between neurons. However, EECs (67) in addition to enteric neurons (68) produce and secrete neuropeptides, and environmental factors such as the microbiota have been shown to influence their levels in the CNS (69, 70) and GI tract (63).

It has been well documented that neuropeptides can have significant impact on immunological function. Peyer's patches are innervated (Figure 1) by intrinsic, peptidergic neurons (71), and immunoglobulin synthesis and lymphocyte proliferation in peripheral lymph nodes and GALT are affected by neuropeptide exposure (72). Substance P (SP) was the first example of an immunomodulatory neuropeptide that enhanced the production of IL-1, TNFα, and IL-6 from human monocytes (73). SP also regulates intestinal ion and fluid transport across the epithelium, and these effects were through its preferred receptor, neurokinin 1 receptor, and these effects were abolished by blocking neural transmission with tetrodotoxin. Interestingly, engagement of mast cell histamine receptors was increased the effect that SP has on fluid secretion (74). Often, intestinal inflammation is concomitant with excessive ion and fluid secretion, leading to symptoms such as diarrhea. Expectedly, SP was found to be more abundant in the GI tract of patients with ulcerative colitis and Crohn's disease (75). Subsequent research showed that many other neuropeptides and their associated receptors are important for immunity. For example, in macrophages, neuropeptide Y (NPY) and peptide YY (PYY) enhance phagocytosis (76) and mice that are deficient in the NPY receptor 1 display impaired macrophage response to endotoxin. Furthermore, these mice also have fewer naïve CD4+ T cells in peripheral lymph nodes, and reduced IFNγ production following DSS-colitis (77). This suggests that immune cells harbor receptors for neuropeptides, and these receptors have an important role in shaping the maturation of the immune system. In another study, Th1 and Th2-lineage polarized T cell lines were created to have T cell receptors specific for an exogenous peptide. Thus, antigen exposure should lead to the production of cytokines representative of each respective lineage. Surprisingly, neuropeptide exposure to these T cells is able to induce both canonical and non-canonical production of T helper cytokines, without exposure of the antigen (78). These results point to intriguing neuropeptide-mediated, immunological plasticity and innate-like function from adaptive lymphocytes. These initial studies broadened the known impact that neuropeptides can have, but also elucidated the complexity of their immunological effects.

In contrast to SP and NPY, vasoactive intestinal peptide (VIP) has been the best studied anti-inflammatory peptide. VIP induces regulatory (79) and tolerogenic DCs (80, 81), both of which are able to induce differentiation of Tregs (82). Furthermore, VIP inhibits TGF-B1 (83) and enhances IL-10 (84) production in murine macrophages. Also in macrophages, TLR2 and TLR4 stimulation upregulates expression of VIP receptor type 2 (85) and conversely, VIP inhibits LPS mediated upregulation of TLRs, as well as monocyte to macrophage differentiation (86).

In the GI tract, VIP mitigates trinitrobenzene sulfonic acid (TNBS)-induced intestinal inflammation, a mouse model of colitis. As is in macrophages, it also inhibits TNBS mediated upregulation of TLRs in macrophages, DCs, lymphocytes, and colon protein extracts (87, 88). Furthermore, VIP ameliorates intestinal barrier dysfunction in *C. rodentium*-induced colitis in mice (89). Toxin B from the colitogenic bacterium, *Clostridium difficile*, can activate VIP producing neurons in the submucosa (90). However, over time, *C. difficile* infection decreases overall levels of VIP (91), and perhaps by depleting VIP, *C. difficile* can ultimately exacerbate enteric infection. Finally, VIP-deficient mice have multiple GI abnormalities, including deficits in goblet cell secretion (92).

Hirschsprung's disease is often comorbid with enterocolitis (93-96). Although the precise etiology of this colitic pathology is unknown, patients with Hirschprung's disease often display mutations in the aforementioned RET tyrosine kinase. In mice, RET deficiency results in symptoms similar to patients with Hirschsprung's disease, and VIP is among the most downregulated genes (92, 97). Thus, neuropeptide balance is imperative for proper immune function and GI homeostasis, and skewing in either direction leads to irregularities in physiology, and potential disease pathologies.

Serotonin and Histamine

Serotonin (5-HT) is produced by various cell types in the GI tract and has multiple physiological roles. 5-HT was first identified for his roles in vasoconstriction and was initially found stored in platelets (98). In the GI tract, mast cells and enterochromaffin cells, a specific EEC, were established as major sources of 5-HT (99). Currently, various leukocyte types, including macrophages, DCs, B and T cells, have been found to express either tryptophan hydroxylase (TPH-1, the rate limiting enzyme in 5-HT biosynthesis), or 5-HT transporters (SERT) which are necessary mediators of extracellular 5-HT uptake (100-102). Furthermore, a variety of 5-HT receptors have been identified in lymphoid tissues (103), and as a result their expression and function have been extensively studied in a variety of immune cells (104). In general, serotonergic signaling in leukocytes appears to promote immune function, whether by enhancing DC-mediated T cell activation (101, 105), or affecting macrophage polarization (106) and phagocytosis (107).

5-HT has been one of the earliest known molecules involved in GI peristalsis (108), and it does so by directly modulating ENS activity (109, 110). Mast cells also secrete histamine which has also been implicated in the activation of IPANs (111, 112). As such, increased histamine and 5-HT levels correlate with increased activation of submucosal neurons, and these increases are dampened by 5-HT and histamine receptor antagonists (113). Although this is compelling, the significance and physiological implications of mast cell mediated ENS activation is poorly understood. Interestingly, vagal stimulation decreases intracellular stores of 5-HT in enterochromaffin cells, and this appears to be mediated by adrenergic receptor activation (114). Also, adrenergic receptor activation on mast cells can enhance IgE mediated degranulation of 5-HT and histamine (115). However, amitriptyline, a 5-HT and norepinephrine uptake inhibitor, inhibits mast cell secretion of histamine but not 5-HT (116), suggesting that intrinsic production of 5-HT, as opposed to the reuptake of 5-HT, in mast cells may be important for adrenergic receptor-mediated 5-HT secretion. These data show that similar mechanisms observed in the cholinergic anti-inflammatory pathway may affect the levels of 5-HT in the GI tract, but similar

shortcomings in mechanistic understanding persist, such as the contribution of adrenergic signals from extrinsic sympathetic nerves versus those that are produced intrinsically. Nonetheless, these results show that molecules that are traditionally associated with leukocytes are capable of modulating the ENS, providing more evidence of neuro-immune interactions exist in the GI tract.

Potentially linking the microbiota to these neuro-immune interactions is a study by Yano *et al.* that illustrated how indigenous, spore-forming bacteria, which are primarily *Clostridia,* are sufficient in rescuing 5-HT deficiency in GF mice (117). Consistent with this finding, short chain fatty acids (SCFAs), which are fermentation products of dietary fibers metabolized by the intestinal microbiota, are also sufficient in upregulating 5-HT (117, 118). Interestingly, *Clostridia*, and specifically butyrate producing strains, are important for the induction of regulatory T cells (Tregs) (119-121). Patients with depression have lower levels of Tregs and serum 5-HT, and these Tregs also expressed lower levels of the 5-HT1a receptor (122). Furthermore, anti-CD25 depletion of Tregs resulted in reductions in 5-HT and led to depression-like behaviors in mice. Perhaps it is possible that specific gut bacteria are capable of modulating CNS-associated phenotypes by inducing immunological changes that are mediated by neuromodulatory compounds. These types of studies would provide powerful, mechanistic understanding of how gut bacteria incite changes beyond the GI tract and implicate more global physiologies. At the moment, it is appreciated that mucosal 5-HT is an important paracrine signaling molecule in the GI tract, however, it is less understood how the diverse cell types contribute to such a unified physiological response that is dependent on 5-HT.

Enteric Glial Cells, Neurotrophic Factors, and Associated Immune Reactions
In the GI tract, the most abundant neurotrophic factors (NTFs) are the glial cell-derived neurotrophic factor (GDNF) family of ligands (GFLs, which include GDNF, Neurturin, and Artemin), and they are produced by EGCs and smooth muscle cells (123-125). Neurotrophic factors (NTFs) are small protein molecules that can sustain

neurons and modulate their function, but unlike their name suggests, their effect spans multiple cell types. Firstly, EGCs modulate neurotransmission by inducing production of neuropeptides. For example, GDNF promotes enteric neuron release of NPY (126) (Figure 2), and GDNF-, NTN-, GFRα1- (receptor for GDNF), and RET- (co-receptor for GFL receptors-α1-3) deficient mice have defects in stimulus evoked release of VIP and SP. These mice also display significant reduction GI contractibility (127, 128), suggesting that EGC-mediated changes in neuropeptide levels are sufficient to cause dysregulated ENS activity. But, as previously described, GFL modulation of neuropeptides may also illustrate their indirect effects on neuro-immune interactions in the GI tract. Additionally, EGC derived NTFs have recently been shown to directly affect the development of specific GI immunological compartments. It has been known that GFL-mediated RET signaling is necessary for proper development of Peyer's patches (129, 130), but in a more recent study by Ibiza et al., GFL-mediated RET signaling was found to be necessary for the functional development of IL-22 producing innate lymphoid cell type 3 (ILC3) (131). These cells are the first innate immune cell to expand in the GI tract following bacterial infection (132), and via IL-22, have broadly protective effects on the intestinal epithelium (133-136)Ibiza and colleagues found that GFLs directly activate RET expressed on ILC3s, and depletion of RET diminishes intestinal IL-22 levels and exacerbates enteric inflammation (Figure 4). ILC3s were shown in close proximity to EGCs, and as previous studies showed (137), TLR activation induced expression of GFLs. Importantly, glial specific depletion of MyD88 displayed marked reductions in GFLs and IL-22, and recapitulated inflammatory pathologies observed in ILC3 RET knockout mice (131). These findings are the first to show that that EGCs directly sense the microbial environment to induce GFL production, and this sensing is necessary for the development of GI immunity. This seminal study elucidated mechanisms by which components of the ENS can directly shape the immunological environment in the GI tract.

EGCs and NTFs are also implicated in intestinal neuropathies and inflammatory pathologies. Ablation of EGCs results in epithelial and neuronal damage as well as severe intestinal inflammation (138). Agangliosis (a lack of enteric ganglia) occurs in mice that are deficient in GDNF (139) and RET (the coreceptor GDNF family receptors-α1-3) (140), and also in humans with Hirschspring's disease. Interestingly, Hirschsprung's disease is associated with germline mutations in GDNF (123, 141), and its pathology is often comorbid with enterocolitis (96). EGC proliferation is also linked to intestinal inflammation (142, 143) and accordingly, GDNF is increased during enteric parasitic infections (144), found in intestinal biopsies from humans with colitogenic *Clostridium difficile* infection, and upregulated in humans who suffer from ulcerative colitis and Crohn's disease (145). However, in culture, IL-1β appears to dampen their proliferation while IL-10 enhances it (143). Although this may appear contradictory, it is possible that intestinal inflammation incites potential immunoregulatory functions in EGCs through proliferation and upregulation of GFLs, but persistent, hyperinflammatory responses may result in inhibition of these processes altogether, thus leading to enteric pathology and disease. In all, it is apparent that GFLs have a significant role in maintaining intestinal immune homeostasis. It also appears that enteric neurons have the potential to interface with the GI immune system via the actions of GFLs, but it is currently unknown whether these compartments are in fact, interdependent.

Cytokines

Cytokines and chemokines are the main effector molecules of immune cells. However, enteric neurons and glia are also capable of producing cytokines. As previously alluded to, EGCs express functional TLRs (131, 146) and an increase in IL-1β is observed upon LPS stimulation of EGCs. Furthermore, ENS cultures produce TNFα and IL-6 in response to LPS, and this production is abrogated when NF-kB signaling is inhibited (147). Curiously, IL-6 and the IL-6 receptor promote the growth and survival of enteric neurons in culture (148), but just as IL-6 has both pro- and anti-inflammatory effects in the peripheral immune system (149), it may

also have dichotomous effects on the ENS.

As detailed previously, neurotransmitters and neuropeptides alter immune function. However, reciprocally, cytokines are capable of modulating neuron activity. The abundance and close proximity of neuronal varicosities to immune cells should make this unsurprising, but it is important in the study of immune responses to consider the effector functions of cytokine molecules on non-immune cell types. For example, IL-1β is heightened in the intestines of inflammatory bowel diseases (IBD) patients (150), and in accordance with prior discussions, IL-1β also induces SP production in the ENS (151). Furthermore, IL-1β engagement to its cognate receptor in *ex vivo* ENS preparations suppresses electric-field stimulation (EFS)-evoked release of acetylcholine and norepinephrine (152), and IL-1β and IL6 can excite enteric secretomotor neurons (Figure 4). The latter also appears to occur by suppressing extrinsic noradrenergic and nicotinic activity (153). Thus, it is possible that enteric inflammatory symptoms are not only a product of proinflammatory cytokines, but also a result of IL-1β mediated upregulation of SP, and subsequent increases in secretomotor activity, fluid secretion, and decreased anti-inflammatory signaling from cholinergic and adrenergic neurons. This would explain many of the aforementioned phenotypes in IBD patients, including the heightened levels of SP, IL-1β, and TNFα (154).

Microbes, and the Enteric Immune and Nervous Systems

Microbiota

The intestinal microbiota is the collection of microorganisms in the GI tract, and its constituents are known to be representative of the animals' diet, habitat, and even phylogenetic order(155). It has long been appreciated that the indigenous microbiota of the GI tract is important for its development and susceptibility to enteric infections(156), but it was not until much later that researchers demonstrated how

commensal bacteria have an active role in maintaining GI immune homeostasis. In 1996, it was found that anaerobic bacteria in human feces was specifically enriched in coating by immunoglobulin A (IgA) (157). A few years later, Macpherson *et. al*. discovered T cell-independent mechanisms of IgA binding to commensal gut microbes, suggesting an evolutionary innate, immunological adaptation to the intestinal microbiota(158). In 2001, Hooper *et. al*. showed that *Bacteroides thetaiotaomicrion* modulate host genes important for IEC homeostasis (159). In 2005, Mazmanian *et. al*. discovered that polysaccharide A (PSA) from *Bacteroides fragilis* is sufficient for the development of adaptive immune responses(160). These influential studies expanded the knowledge and incited curiosity towards the microbiome, but more importantly, they empirically defined homeostatic roles of the intestinal microbiota that were not previously appreciated.

GF animals were first studied and characterized using rats in the 1950s (161) to study dental hygiene, and were later used to study microbial colonization resistance (162). More recently research groups have implicated the microbiota in stress, anxiety, behavioral developmental disorders, and neurological deficits (163-166). This has popularized hypotheses on the "gut-brain axis". However, the role of the ENS and GI-resident immune functions are currently understudied as conduits for the gut-brain axis. Furthermore, the abundance of immune cells in the GI tract and the vast connectivity of the ENS (and its direct connectivity to the CNS) make it unlikely that the "gut-brain axis" is independent of these interactions.

The microbiota has been shown to be altered during intestinal inflammation and immunological disease. Severity of inflammation is mediated and ameliorated by pathogenic and commensal bacteria, respectively (167, 168). As mentioned in previous sections, microbes or microbial products can actively change TLR expression in most cellular compartments of the GI tract, and this alters the host's ability to sense and respond to the microbiota. Antibiotic depletion of the microbiota alters TLR expression in mice, and also results in concomitant in changes to GI

motility and sensitivity to ACh (169). TLR4 mutant mice have fewer neurons in the ENS and this result is also recapitulated in MyD88 knockout and antibiotic-treated mice (170). Furthermore, GF animals display morphological defects to the ENS and these deficits are ameliorated by housing them in soiled cages from conventional mice with a normal flora (171). The microbiota is also necessary for normal excitability of neurons in the ENS (172). EGC growth, maturation, and signaling is also affected by the microbiota. For example, GF mice and antibiotic-mediated depletion of the microbiota results in truncated glial cells that fail to extend through the mucosa and into villi structures (173). Antibiotic-treatments also reduce levels of GDNF/GFRα1 and RET, and these deficiencies can be reversed by Toll-like receptor (TLR) 2 stimulation (174). Furthermore, TLR2-deficient mice also display lower levels of GDNF, impaired RET signaling, and heightened inflammation in response to dextran sulfate sodium (DSS)-induced colitis. Accordingly, these phenotypes can be mitigated by exogenous GDNF administration (174). Exact mechanisms by which microbiota modulates neural activity in the GI tract are unknown. However, these findings suggest that there exists an active, post-developmental role of the microbiota on ENS form and function, and this potentially explains disparities seen in their molecular output.

Short Chain Fatty Acids

The most studied SCFAs are butyrate, propionate, and acetate (175, 176), and these microbial metabolites are initially sensed by the intestinal epithelium, but can also diffuse across the epithelium (177) where they can be sensed next by enteric nervous and immune systems (Figure 3). G-protein coupled receptors (GPR) 41 and 43 are activated by acetate and propionate (178, 179), whereas GPR109A is specific for butyrate (180).

IECs from mice deficient in GPR41 or GPR43 cannot produce inflammatory chemokine and cytokine profiles in response to TNBS-induced colitis and *C. rodentium* infection, and these mice also exhibit delayed clearance of *C. rodentium*

itself (181). In an EEC line, GPR43 is necessary for propionate-mediated secretion of PYY and GLP-1 and these results are consistent *in* vivo (182). Also, PYY inhibits gastrointestinal transit and GPR41 deficiency is associated with decreased PYY production (183). Accordingly, SCFA-mediated induction of PYY inhibits in colonic motility (184). Furthermore, selective agonists for GPR41 and GPR 43 induce GLP1 secretion from colonic crypt cultures, and purified GPR41+ cells exhibit higher expression levels for peptide hormone precursors (185).

Intriguingly, it was found that enteric neurons in both the submucosa and myenteric plexus express GPR41. In contrast, immune cells in the lamina propria preferentially expressed GPR43. (185, 186) Tregs isolated from the colon and small intestines express high levels of GPR43 through which propionate enhances their immunosuppressive capabilities (187). Accordingly, propionate administration alleviates symptoms during experimental autoimmune encephalomyelitis, a mouse model of multiple sclerosis. The mitigating effects of propionate were also found to be concomitant with small intestinal Treg induction (188). Mucosal mast cells (189) and neutrophils (190) also express GPR43. In neutrophils, bacterial-derived SCFAs enhance chemotaxis (191) and propionate induces degranulation (192). Activation of GPR109A reduces intestinal inflammation and colon cancer susceptibility in mice (193). In human monocytes, activation of GPR109A by nicotinic acid has anti-inflammatory effects (194), and this is further illustrated by the ability of butyrate to inhibit mast cell activation and degranulation (195). Butyrate and butyrate-producing bacteria, as previously described, are also sufficient for inducing differentiation of Tregs in mice (120, 121). Finally, butyrate is also capable of inducing action potentials in both submucosal and myenteric neurons of the ENS (196, 197), and this is associated with increases in intrinsic, cholinergic neurons of the myenteric plexus (198). This is in agreement with prior evidence showing the potent anti-inflammatory effects of ACh, and thus it is possible that ENS sensing of butyrate may be an important aspect of coordinating intrinsic, ACh-mediated neuro-immune responses.

Lactobacilli and Bacteroides

Many *Lactobacillus* species have been studied for their immunoregulatory role. Species such as *L. rhamnosus*, *L salivarius*, *L. reuteri*, *L. planatrum*, *L. fermentum*, and *L. casei* have been shown to induce Tregs and decrease levels of inflammatory cytokines, such as IFNγ and TNFα (199-201). *Lactobacilli* have also been studied for their neuromodulatory capabilites. Rats colonized with *L. reuteuri* display lower thresholds for IPAN activation, higher frequency of action potentials (197, 202), and shorter hyperpolarizing potentials, all of which are proxies of increased IPAN excitability. However, in an influential study describing the gut-brain axis, Bravo *et al.* discovered that commensal microbes modulate physiologies beyond the GI tract and influence behaviors commonly associated with affections in the CNS. Specifically, *L. rhamnosus* can reduce stress-induced corticosterone levels and decrease expression of γ-aminobutyric acid (GABA) receptors in the CNS, leading to concomitant reduction in anxiety and depression-like symptoms in mice. These behavioral and neurochemical phenotypes were abolished following chemically-induced vagotomy (203). In accordance, it was later shown that *L. rhamnosus* increases the rate of spontaneous firing in vagal afferent nerves (204). Furthermore, certain strains of *L. rhamnosus* are known to produce GABA under certain conditions (205), and *L. reuteuri* can produce GABA from its precursor, glutamate (206, 207). Thus, direct production of neuroactive molecules by gut microbes has the potential of modulating ENS activity, but this has not been specifically addressed.

The *Bacteroides* genus has also been studied for its immunoregulatory roles in the GI tract, and the species have predominantly been focused on *B. thetaiotaomicron* (208) and *B. fragilis* (168). As described previously, *B. fragilis* has been studied for its role in inducing IL-10 producing FoxP3 Tregs (209, 210). Interestingly, *B. fragilis* mono-associated mice also display enhanced IPAN excitability, and PSA was both sufficient and necessary for this phenotype (202). These data illustrate the active role that bacteria and bacterial-associated molecules have on the excitability and activity

of intrinsic sensory neurons in the ENS, but whether microbe-induced ENS activation is necessary for modulating GI immunity is unknown.

Trichinella spiralis

Trichinella spiralis is a parasitic nematode that infects the intestines (211) and induces IL-1 production (212). In mice, *T. spiralis* infection causes hypophagia, the decrease in food intake (213). This infection is also associated with increased CCK and 5-HT expression in EECs, both of which have been implicated in hypophagia (214, 215). Furthermore, CCK and IL-4 induce contractions in the longitudinal muscle (216, 217), and increased contractibility of the GI tract has been implicated in T. spiralis expulsion (218). Interestingly, prior *T. spiralis* infection increases sensitivity of mouse enteric neurons to T. spiralis antigens, and this heightened sensitivity is abrogated by histamine receptor antagonism (219). IgE binding to mast cells induces histamine secretion (220) and enhances *T. spiralis* explusion (221). Taken together, these studies put forth a potential histamine-mediated, adaptive, neuro-immune response to pathogenic microorganisms that may be important for their clearance.

Perspective

The GI tract is poised to sense and respond to diverse fluxes of intestinal cues. These cues are intrinsic, extrinsic, and environmental. In the viscera, nerves from CNS and PNS synapse onto the GI tract. At the mucosa, the host readily and selectively absorbs molecules within and across the epithelium. And in the lumen, the microbiota is under constant selective pressure from many host factors such as diet, environmental exposure, immunity, and exocrine function. Altogether, the exchange of molecular information in the GI tract illustrates potential intestinal "reflex loops" that would describe how our body utilizes the ENS to physiologically sense and respond to changes in the environment.

Peristaltic waves are the rhythmic contractions that result in the passage of contents from the environment through the host. Segmentation contractions are bouts of content mixing that is required for efficient digestion, but also maximizes moments when nutrients are readily accessible for host absorption. It would be fascinating if the ENS coordinated GI physiology such that absorptive and secretory events coincide with immunological sampling of the lumen. However, mechanisms by which functional enteric circuits integrate with microbe-mediated GI immune responses are poorly understood. For example, it is unknown if the ENS senses the microbial environment and initiates an immune response, or whether the ENS senses immune responses to subsequently modify, amplify, or propagate those signals. It is also unknown how the ENS reciprocally affects the luminal environment to potentially shape and alter the microbiota, and whether this effect is mediated by an immune response. Further characterization of the connectivity of the ENS with itself and other cell types will help understand how molecules in the GI tract dictate the body's ability to immunologically mature and adapt to the microbiota. However, to truly dissect mechanisms by which the ENS mediates, potentiates, or responds to microbe-induced GI immunological changes, spatial and temporal manipulation of the ENS is required. Accordingly, modern advances in neuroscience, such as optogenetics and chemogenetics, have recently been implemented in the context of the ENS (222-224). While emerging discoveries on neuro-immune interactions in the GI tract indicate ENS participation in GI immune development (27, 131), effects of the microbiota on these immunological changes remain unstudied. Thus, future studies uncoupling the effects of the ENS on GI immune function will provide the foundation to study how the microbiota affects these interactions. Furthermore, it remains an intriguing possibility that enteric neuro-immune interactions may be the preferred route by which the microbiota has more global effects on CNS-related behavior.

Communication between the microbiome and the mucosa is essential for the maintenance of intestinal homeostasis. Microbes or microbial products can directly

affect epithelial cells, but also have mechanisms to pass through them. The direct effect of this on immune cells is well documented, but how the ENS may be involved in the process is not. Given the diversity and reciprocity of extracellular signaling molecules in the GI tract, the ENS has evolved over time to receive and interpret these diverse cues, and transmit them throughout the GI tract and ultimately, the entire body. As such, the ENS is best adapted to coordinate physiologically related responses between different cell types and propagate them over vast regions of the GI tract. The cellular biology of the GI tract is inherently complex, necessitating the development and testing of interdisciplinary hypotheses, a challenge with immense implications for human physiology.

ACKNOWLEDGMENTS

Figures, Tables, and Legends

Figure 1. Anatomy of the GI Tract

The GI tract is comprised of distinct cross-sectional compartments. Extrinsic, sympathetic and parasympathetic nerve fibers enter the GI tract through the mesentery and can extend throughout all layers of intestinal tissue. The myenteric plexus and submucosal plexus form the dense nerve network that innervates the entire length and depth of the GI tract. Various immune cells are resident to the muscularis, but are also highly abundant in the lamina propria, especially in Peyer's patches and lymphoid follicles. These immune cells are also in close proximity to neurons and glia. The epithelium shown here is made up of 5 different cell types. These include absorptive enterocytes, EECs, goblet cells, Paneth cells, and M-cells.
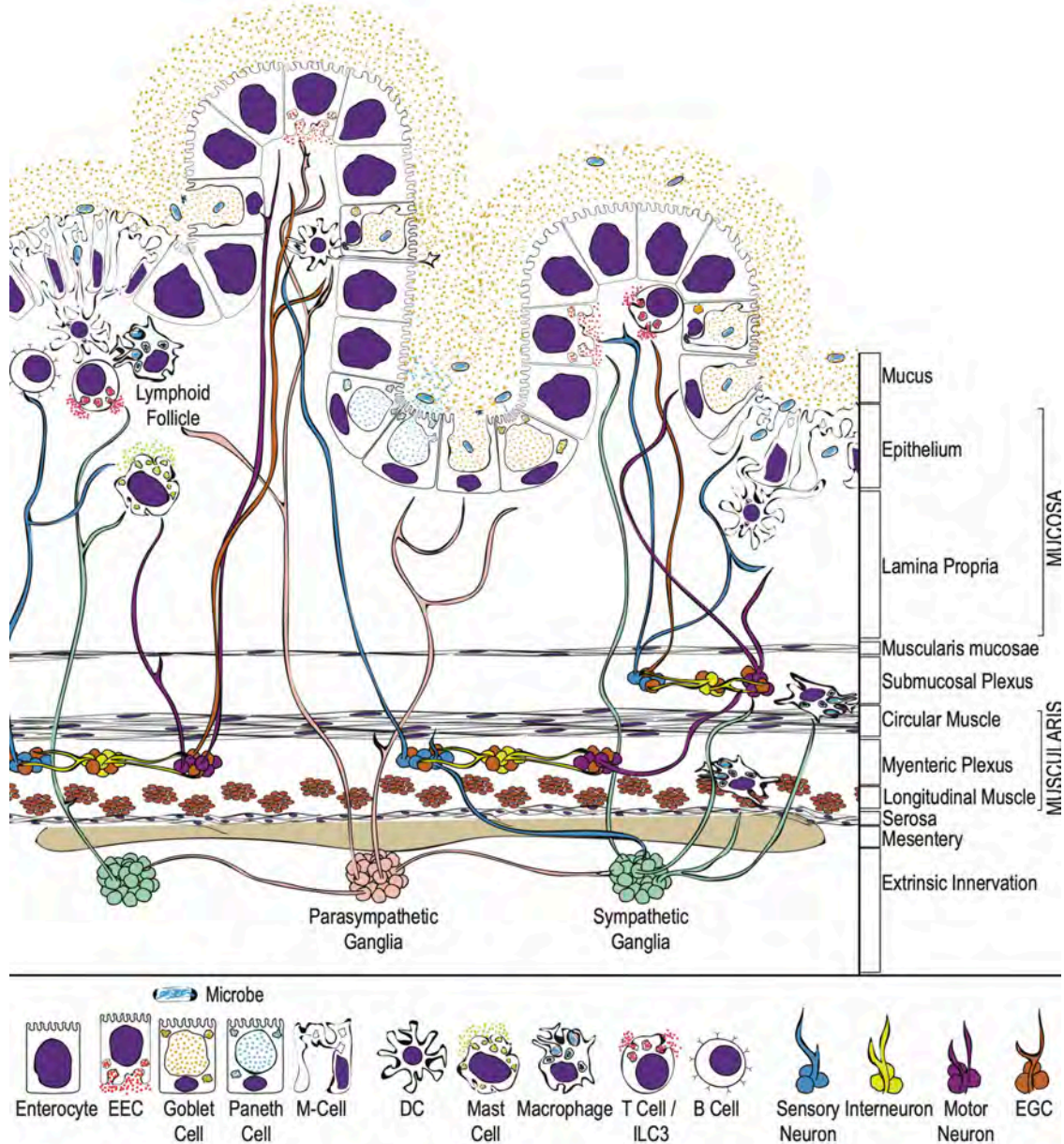
Figure 2. Connectivity of Enteric Neurons and Glia
Enteric neurons are located in either the submucosal or myenteric plexuses. Both plexuses are located in between two muscle layers (see Figure 1). Parasympathetic nerve fibers release acetylcholine and sympathetic nerves release norepinephrine. These extrinsic nerve fibers can innervate enteric neurons but also associate with the cells in the smooth muscle, lamina propria, and the epithelium. Enteric neurons can innervate one another or extend towards the lamina propria, and specific intestinofugal (IFANs) can synapse onto sympathetic ganglia. Enteric glial cells make and release neurotrophic factors, associate with enteric neurons, and extend throughout the mucosa. The table associated with this figure lists specific interactions that have been described.
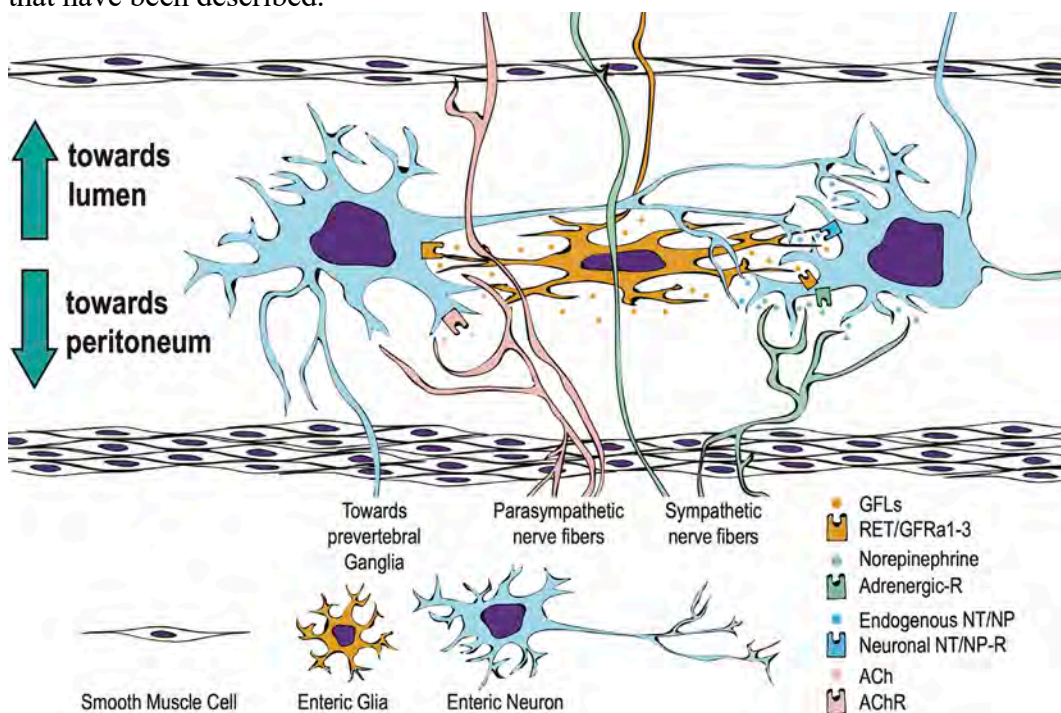
GDNF	increased NPY, 5-HT, proliferation	Anitha et al., 2006; Beck et al., 1996; Gianino, 2003
GDNF-/-, NTN-/-, GFRa1-/-, RET-/-	decreased VIP, SP, GI contractability	Gianino, 2003; Heuckeroth et al., 1999
EGC-/-	increases inflammation, enteric neuropathy	Bush et al., 1998
GDNF	decreases inflammation	Brun et al., 2013
GDNF-/-, RET-/-	agangliosis	Sanchez et al., 1996; Schuchardt et al., 1994)
Purines	Activation	Gulbranson et al., 2010

Figure 3. Interactions at the Intestinal Epithelium

The intestinal epithelium is where luminal constituents are actively or passively transported into the tissue. Extrinsic nerves and neurons are found near the epithelium, and thus the molecules that cross the epithelium and those that are secreted basolaterally can potentially have an effect on their activity. Microbes or microbial parts can cross the epithelium and affect other cell types through M-cells, immunoglobulin-mediated transcytosis, goblet cell-associated passages (GAPs), and by general leakiness of the epithelium. Dendritic cells (DCs) and macrophages can phagocytose microbial antigens and secrete cytokines that can have an effect on neurons as well. Parasympathetic fibers release acetylcholine (ACh) and induce secretion of intracellular stores of molecules. In goblet cells, ACh also increases rates of DC luminal sampling via GAPs. EECs can also release neuroendocrine molecules in response to TLR stimulation and SCFAs. These molecules released basolaterally can potentially regulate the activity of neurons. Enteric glial cells can also project towards the epithelium, potentially allowing microbes to impact their function. Enteric neurons can be activated by commensal and pathogenic bacteria, as well as short chain fatty acids that diffuse across the epithelium. The table associated with this figure lists specific interactions that have been described.
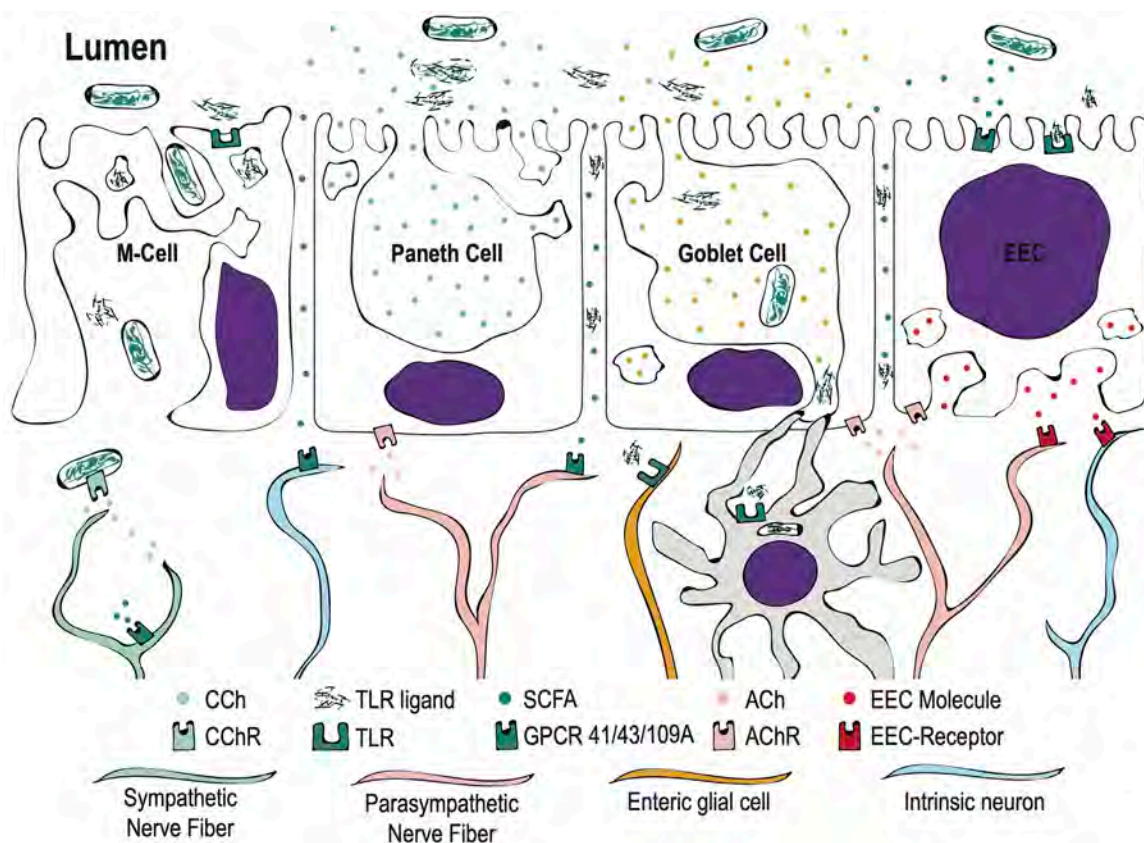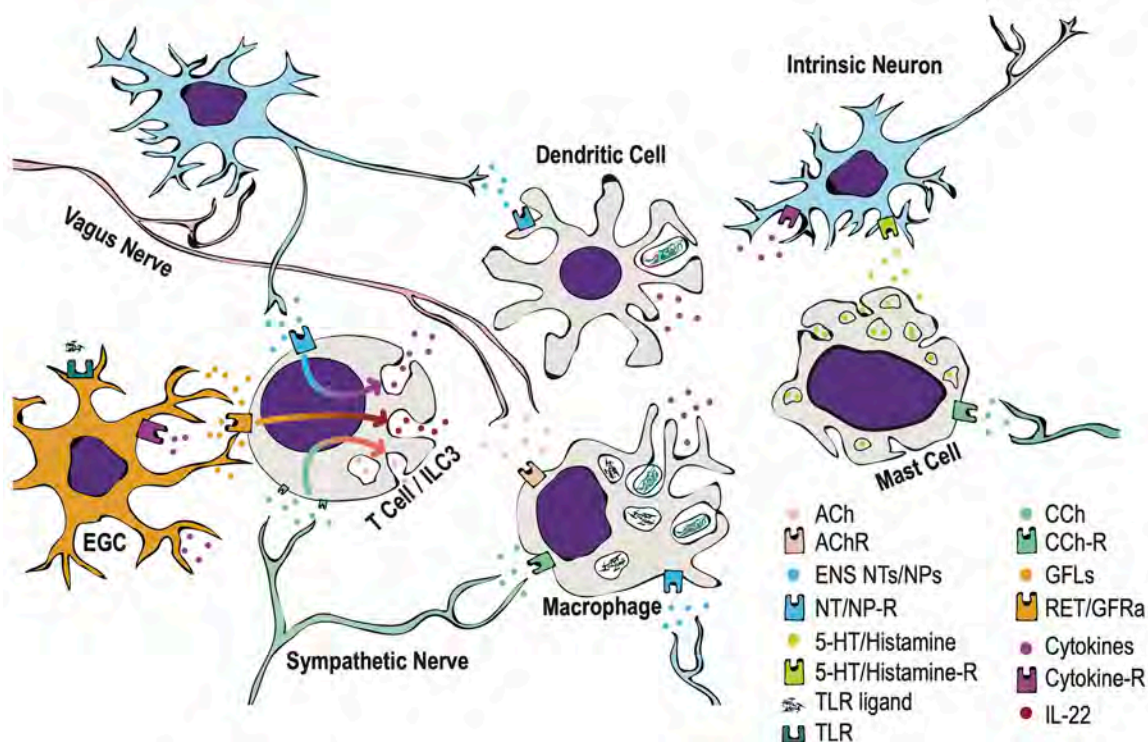
GF Mice	less neurons and decreased ENS excitability	Collins et al., 2014; McVey Neufeld et al., 2013
Antibiotics	decreases motility and GI sensitivity to ACh	Grasa et al., 2015
TLR4-/-	fewer neurons in ENS	Anitha et al., 2012
Microbiota	increases EGC growth	Kabouridis et al., 2015
Antibiotics	decreases GDNF, GFRa1, RET	Brun et al., 2013
TLR2-/-	decreases GDNF, RET	Brun et al., 2013
TLR-ligand	increase GDNF	Brun et al., 2013
Microbiota, *Clostridia*, GUS enzyme	increases CCh availability	Asano et al., 2012
Clostridia, SCFAs	5-HT from enterochromaffin cells	Yano et al., 2015; Reigstad et al., 2015)
GPR 41, GPR43 activation	PYY and GLP-1 release	Psichas et al., 2014; Nohr et al., 2013
GPR41-/-, GPR43-/-	deficient inflammatory chemokine/cytokine profiles in response to C. rodentium infection and delayed clearance	Kim et al., 2013
Butyrate	decreases monocyte activation and mast cell degranulation	Digby et al., 2012; Diakos et al., 2006
Butyrate	Activates intrinsic ENS	Neunlist and Dobreva, 1999
Butyrate	increases cholinergic neurons in myenteric plexus	Soret et al., 2010
L. reuteuri	increased IPAN excitability	Kunze et al., 2009
L. rhamnosus	lowers anxiety via vagus nerve, increases vagal firing	Bravo et al., 2011; Perez-Burgos et al., 2013
B. fragilis PSA	increased IPAN excitability	Mao et al., 2013
GLP-1, CCK	Activate ENS	Amato et al., 2010; Ngu, 1985

CCh	increase virulence	Hadjifrangiskou et al., 2011; Moreira and Spreandio, 2012; Njoroge and Sperandio, 2012
mAChR agonist bethanechol	increases Paneth cell degranulation	Satoh et al. 1992
mAChR antagonist atropine	decreases Paneth cell degranulation	Satoh, 1988
AChR agonist carbahol	increases Goblet cell mucin secretion	Gustafsson et al., 2012; Birchenough et al., 2016
AChR agonist carbahol	increases Goblet cell associated passages (GAPs)	McDole et al. 2012
mAChR agonist bethanechol	increases EEC secretion	Anini and Brubaker, 2003

Figure 4. Interactions Between GI Immune Cells and the ENS

Extrinsic nerves, intrinsic neurons, and enteric glial cells (EGCs) are in close proximity to each other and to the immune cells in the GI tract. Thus, the molecules that are produced by one cell can have an effect on another cell, given that the latter expresses a receptor to recognize the molecule. By these parameters, interactions between neurons/glia and immune cells are, in theory, abundant, and some of these putative interactions are presented here. Immune cells can be influenced by neurotransmitters and neuropeptides produced by intrinsic neurons of the ENS (as well as those produced by extrinsic nerve fibers), and cytokines produced by immune cells can have a reciprocal effect on neurons. The table associated with this figure lists specific interactions that have been described.

LPS	increases IL-1B from EGCs, and TNFa and IL-6 from ENS	Barajon et al., 2009; Burgueno et al., 2016
Clostridia, Butyrate, Lactobacilli, B. fragilis	Regulatory T cells	Atarashi et al., 2013; Furusawa et al. 2013; Foligne et al., 2007; Madsen et al., 1999; Valeur et al., 2004; Roud and Mazmanian, 2010, Chu et al., 2016
MyD88-/- on EGCs	decreases IL-22	Ibiza et al., 2016
GFL	increases IL-22 from ILC3	Ibiza et al., 2016

IL-1B	suppresess proliferation	Ruhl et al. 2001
IL-10	enhances proliferation	Ruhl et al. 2001
IL-1B	increases SP	Hurst et al., 1993
IL-1B	suppresses ACh, Norepinephrine from extrinsic nerves	Collins et al., 1992
IL-1B, IL-6	activate secretomotor neurons	Xia et al., 1999
VIP	increases IL-10	Delgado et al., 1999
VIP	Regulatory DCs and T cells	Chorny et al., 2005; Delgado et al., 2005b; Ganea et al., 2006; Delgado et al., 2005a
Intrinsic peptidergic neurons	innervate Peyer's Patches	Vulchanove et al., 2007
SP	increases Peyers patch, MLN, lymphocyte proliferation and IgA synthesis	Stanisz et al. 1986
VIP, Somatostatin	decrease Peyers patch, MLN, lymphocyte proliferation	Stanisz et al. 1986
SP	higher in ulcerative colitis and Crohn's disease	Mantyh et al., 1988
SP	increases TNFa, IL-6, IL-1B	Lotz et al., 1988
NPY and PYY	enhance macrophage phagocytosis	la Fuente et al., 1993
Neuropeptides	affect T cell cytokine profile	Levite, 1998; Wheway et al., 2005
5-HT, Histamine	IPAN activation	Rosas-Ballina et al., 2008
5-HT	increases DC mediated T cell activation	Yamasaki et al., 1983
5-HT	enhances macrophage polzarization and phagocytosis	Gabanyi et al., 2016
5-HT receptors	expressed on lymphoid tissues	D.R. Brown and Price, 2008
Mast cells	major producers of 5-HT and histamine	Bergquist et al., 1994
Leukocytes	make or store 5-HT	Borovikova et al. 2000

AR activation	increases mast cell degranuilation of 5-HT	H. Wang et al., 2003
B2AR activation	polarizes regulatory macrophages	Rosas-Ballina et al., 2011
CCh	decreases bacterial translocation in Peyer's patches	McLean et al., 2015
Splenic Nerve stimulation	decreases TNFa	McLean et al., 2015
dopamine	decreases lymphocyte proliferation	McLean et al., 2016
Vagal stimulation	decreases TNFa, IL-6, IL-1B	Leon-Ponte et al., 2007; O'Connell et al., 2006
a7nAChR-/-	increases TNFa, IL-6, IL-1B (emphasis on macrophage)	las Casas-Engel et al., 2013; Csaba et al., 1975
B-AR on ACh producing T cells, a7nAChR on macrophages	decreases TNFa	Stefulj et al., 2000
M3-ACh3-/-	increased TNFa, IFNg, IL-17a	Song et al., 2015; Starodub and Wood, 2000; Buhner et al., 2009
M3-ACh3-/-	delayed clearance of C. rodentium	Espamer and Asero, 1952
M3-ACh3-/-	decreased IL-4 and IL-13, delayed parasite clearance	Rudd et al., 2005; O'Connell et al., 2006; Meredith et al., 2005

REFERENCES

1. Helander HF, Fåndriks L (2014) Surface area of the digestive tract – revisited. *Scand J Gastroenterol* 49(6):681–689.

2. Kagnoff MF (1987) *Immunology of the digestive system* (Physiology of the gastrointestinal tract).

3. Furness JB, Callaghan BP, Rivera LR, Cho H-J (2014) The Enteric Nervous System and Gastrointestinal Innervation: Integrated Local and Central Control. *The Enteric Nervous System*, Advances in Experimental Medicine and Biology. (Springer New York, New York, NY), pp 39–71.

4. Sender R, Fuchs S, Milo R (2016) Are We Really Vastly Outnumbered? Revisiting the Ratio of Bacterial to Host Cells in Humans. *Cell* 164(3):337–340.

5. Lozupone CA, Stombaugh JI, Gordon JI, Jansson JK, Knight R (2012) Diversity, stability and resilience of the human gut microbiota. *Nature* 489(7415):220–230.

6. Peery AF, et al. (2012) Burden of Gastrointestinal Disease in the United States: 2012 Update. *Gastroenterology* 143(5):1179–1187.e3.

7. Coffey JC, O'Leary DP (2016) The mesentery: structure, function, and role in disease. *The Lancet Gastroenterology & Hepatology* 1(3):238–247.

8. Kalff JC, Schwarz NT, Walgenbach KJ, Schraut WH, Bauer AJ (1998) Leukocytes of the intestinal muscularis: their phenotype and isolation. *J Leukoc Biol* 63(6):683–691.

9. Johansson MEV, Hansson GC (2016) Immunological aspects of intestinal mucus and mucins. *Nat Rev Immunol* 16(10):639–649.

10. Bevins CL, Salzman NH (2011) Paneth cells, antimicrobial peptides and maintenance of intestinal homeostasis. *Nat Rev Micro* 9(5):356–368.

11. Satoh Y, Ishikawa K, Ono K, Vollrath L (2004) Quantitative Light Microscopic Observations on Paneth Cells of Germ-Free and Ex-Germ-Free Wistar Rats. *Digestion* 34(2):115–121.

12.   Ayabe T, et al. (2000) Secretion of microbicidal α-defensins by intestinal Paneth cells in response to bacteria. *Nat Immunol* 1(2):113–118.

13.   Vaishnava S, et al. (2011) The Antibacterial Lectin RegIII Promotes the Spatial Segregation of Microbiota and Host in the Intestine. *Science* 334(6053):255–258.

14.   Sternini C, Anselmi L, Rozengurt E (2008) Enteroendocrine cells: a site of "taste" in gastrointestinal chemosensing. *Current Opinion in Endocrinology, Diabetes and Obesity* 15(1):73–78.

15.   Lelouard H, Fallet M, de Bovis B, Méresse S, Gorvel JP (2012) Peyer's Patch Dendritic Cells Sample Antigens by Extending Dendrites Through M Cell-Specific Transcellular Pores. *Gastroenterology* 142(3):592–601.e3.

16.   Clark MA, Hirst BH, Jepson MA (1998) M-Cell Surface β1 Integrin Expression and Invasin-Mediated Targeting of Yersinia pseudotuberculosis to Mouse Peyer's Patch M Cells. *Infect Immun* 66(3):1237–1243.

17.   Gerbe F, et al. (2016) Intestinal epithelial tuft cells initiate type 2 mucosal immunity to helminth parasites. *Nature* 529(7585):226–230.

18.   Howitt MR, et al. (2016) Tuft cells, taste-chemosensory cells, orchestrate parasite type 2 immunity in the gut. *Science* 351(6279):1329–1333.

19.   Pácha J (2000) Development of Intestinal Transport Function in Mammals. *Physiol Rev* 80(4):1633–1667.

20.   Bröer S (2008) Amino Acid Transport Across Mammalian Intestinal and Renal Epithelia. *Physiol Rev* 88(1):249–286.

21.   Hansen GH, et al. (1999) Transcytosis of immunoglobulin A in the mouse enterocyte occurs through glycolipid raft- and Rab17-containing compartments. *YGAST* 116(3):610–622.

22.   Furness JB, Costa M (1980) TYPES OF NERVES IN THE ENTERIC NERVOUS SYSTEM. *Commentaries in the Neurosciences* (Elsevier), pp 235–252.

23.   Derrien M (2004) Akkermansia muciniphila gen. nov., sp. nov., a human intestinal mucin-degrading bacterium. *INTERNATIONAL JOURNAL OF*

SYSTEMATIC AND EVOLUTIONARY MICROBIOLOGY 54(5):1469–1476.

24. Rescigno M, et al. (2001) Dendritic cells express tight junction proteins and penetrate gut epithelial monolayers to sample bacteria. *Nat Immunol* 2(4):361–367.

25. Serafini N, Vosshenrich CAJ, Di Santo JP (2015) Transcriptional regulation of innate lymphoid cell fate. *Nat Rev Immunol* 15(7):415–428.

26. Abadie C, Foucart S, Pagé P, Nadeau R (1997) Interleukin-1β and tumor necrosis factor-α inhibit the release of [3H]-Noradrenaline from isolated human atrial appendages. *Naunyn-Schmiedeberg's Arch Pharmacol* 355(3):384–389.

27. Gabanyi I, et al. (2016) Neuro-immune Interactions Drive Tissue Programming in Intestinal Macrophages. *Cell* 164(3):378–391.

28. Brown DR, Price LD (2008) Catecholamines and sympathomimetic drugs decrease early SalmonellaTyphimurium uptake into porcine Peyer's patches. *FEMS Immunology & Medical Microbiology* 52(1):29–35.

29. Li ZS (2004) Enteric Dopaminergic Neurons: Definition, Developmental Lineage, and Effects of Extrinsic Denervation. *Journal of Neuroscience* 24(6):1330–1339.

30. King C, Rios G, Green M, Tephly T (2000) UDP-Glucuronosyltransferases. *CDM* 1(2):143–161.

31. Asano Y, et al. (2012) Critical role of gut microbiota in the production of biologically active, free catecholamines in the gut lumen of mice. *American Journal of Physiology - Gastrointestinal and Liver Physiology* 303(11):G1288–G1295.

32. Gadelle D, Raibaud P, Sacquet E (1985) beta-Glucuronidase activities of intestinal bacteria determined both in vitro and in vivo in gnotobiotic rats. *Applied and Environmental Microbiology* 49(3):682–685.

33.   Hadjifrangiskou M, et al. (2011) A central metabolic circuit controlled by QseC in pathogenic Escherichia coli. *Molecular Microbiology* 80(6):1516–1529.

34.   Njoroge J, Sperandio V (2012) Enterohemorrhagic Escherichia coli Virulence Regulation by Two Bacterial Adrenergic Kinases, QseC and QseE. *Infect Immun* 80(2):688–703.

35.   Moreira CG, Sperandio V (2012) Interplay between the QseC and QseE Bacterial Adrenergic Sensor Kinases in Salmonella enterica Serovar Typhimurium Pathogenesis. *Infect Immun* 80(12):4344–4353.

36.   Moreira CG, et al. (2016) Bacterial Adrenergic Sensors Regulate Virulence of Enteric Pathogens in the Gut. *mBio* 7(3):94.

37.   Borovikova LV, et al. (2000) Vagus nerve stimulation attenuates the systemic inflammatory response to endotoxin. *Nature* 405(6785):458–462.

38.   Wang H, et al. (2002) Nicotinic acetylcholine receptor α7 subunit is an essential regulator of inflammation. *Nature* 421(6921):384–388.

39.   Rosas-Ballina M, et al. (2008) Splenic nerve is required for cholinergic antiinflammatory pathway control of TNF in endotoxemia. *Proceedings of the National Academy of Sciences* 105(31):11008–11013.

40.   Berthoud H-R, Powley TL (1993) Characterization of vagal innervation to the rat celiac, suprarenal and mesenteric ganglia. *Journal of the Autonomic Nervous System* 42(2):153–169.

41.   Rosas-Ballina M, et al. (2011) Acetylcholine-Synthesizing T Cells Relay Neural Signals in a Vagus Nerve Circuit. *Science* 334(6052):98–101.

42.   Dhawan S, et al. (2016) Acetylcholine-producing T cells in the intestine regulate antimicrobial peptide expression and microbial diversity. *American Journal of Physiology - Gastrointestinal and Liver Physiology* 311(5):G920–G933.

43.   McLean LP, et al. (2015) Type 3 Muscarinic Receptors Contribute to Clearance of Citrobacter rodentium. *Inflammatory Bowel Disease* 21(8):1860–1871.

44.   McLean LP, et al. (2016) Type 3 muscarinic receptors contribute to intestinal mucosal homeostasis and clearance of Nippostrongylus brasiliensisthrough induction of T H2 cytokines. *American Journal of Physiology - Gastrointestinal and Liver Physiology* 311(1):G130–G141.

45.   Furness JB (2012) The enteric nervous system and neurogastroenterology. *Nature Reviews Gastroenterology and Hepatology* 9(5):286–294.

46.   Satoh Y, Ishikawa K, Oomori Y, Takeda S, Ono K (1992) Bethanechol and a G-protein activator, NaF/AlCl3, induce secretory response in Paneth cells of mouse intestine. *Cell Tissue Res* 269(2):213–220.

47.   Satoh Y (1988) Atropine inhibits the degranulation of Paneth cells in ex-germ-free mice. *Cell Tissue Res* 253(2). doi:10.1007/BF00222296.

48.   Gustafsson JK, et al. (2012) An ex vivo method for studying mucus formation, properties, and thickness in human colonic biopsies and mouse small and large intestinal explants. *American Journal of Physiology - Gastrointestinal and Liver Physiology* 302(4):G430–G438.

49.   Birchenough GMH, Nystrom EEL, Johansson MEV, Hansson GC (2016) A sentinel goblet cell guards the colonic crypt by triggering Nlrp6-dependent Muc2 secretion. *Science* 352(6293):1535–1542.

50.   McDole JR, et al. (2012) Goblet cells deliver luminal antigen to CD103+ dendritic cells in the small intestine. *Nature* 483(7389):345–349.

51.   Anini Y, Brubaker PL (2003) Muscarinic Receptors Control Glucagon-Like Peptide 1 Secretion by Human Endocrine L Cells. *Endocrinology* 144(7):3244–3250.

52.   Yang Q (2001) Requirement of Math1 for Secretory Cell Lineage Commitment in the Mouse Intestine. *Science* 294(5549):2155–2158.

53.   Gribble FM, Reimann F (2016) Enteroendocrine Cells: Chemosensors in the Intestinal Epithelium. *Annu Rev Physiol* 78(1):277–299.

54.   Gunawardene AR, Corfe BM, Staton CA (2011) Classification and functions of enteroendocrine cells of the lower gastrointestinal tract. *International Journal of Experimental Pathology* 92(4):219–231.

55. Merchant JL (2007) Tales from the crypts: regulatory peptides and cytokines in gastrointestinal homeostasis and disease. *J Clin Invest* 117(1):6–12.

56. Amato A, et al. (2010) Peripheral motor action of glucagon-like peptide-1 through enteric neuronal receptors. *Neurogastroenterology & Motility* 22(6):664–e203.

57. Ngu MC (1985) Activation of enteric nerve pathways in the guinea-pig duodenum by cholecystokinin octapeptide and pentagastrin. *The Journal of Physiology* 364:31–43.

58. Bohórquez DV, et al. (2015) Neuroepithelial circuit formed by innervation of sensory enteroendocrine cells. *J Clin Invest* 125(2):782–786.

59. Reimann F, Tolhurst G, Gribble FM (2012) G-Protein-Coupled Receptors in Intestinal Chemosensation. *Cell Metabolism* 15(4):421–431.

60. Matsumura K, Miki T, Jhomori T, Gonoi T, Seino S (2005) Possible role of PEPT1 in gastrointestinal hormone secretion. *Biochem Biophys Res Commun* 336(4):1028–1032.

61. Hira T, Nakajima S, Eto Y, Hara H (2008) Calcium-sensing receptor mediates phenylalanine-induced cholecystokinin secretion in enteroendocrine STC-1 cells. *FEBS Journal* 275(18):4620–4626.

62. Rubin DC, et al. (2000) Altered enteroendocrine cell expression in T cell receptor alpha chain knock-out mice. *Microsc Res Tech* 51(2):112–120.

63. Duca FA, Swartz TD, Sakar Y, Covasa M (2012) Increased Oral Detection, but Decreased Intestinal Signaling for Fats in Mice Lacking Gut Microbiota. *PloS one* 7(6):e39748.

64. O'Hara JR, Skinn AC, MacNaughton WK, Sherman PM, Sharkey KA (2006) Consequences of Citrobacter rodentium infection on enteroendocrine cells and the enteric nervous system in the mouse colon. *Cell Microbiol* 8(4):646–660.

65. Bogunovic M, et al. (2007) Enteroendocrine cells express functional Toll-like receptors. *American Journal of Physiology - Gastrointestinal and Liver Physiology* 292(6):G1770–G1783.

66. Palazzo M, et al. (2007) Activation of enteroendocrine cells via TLRs induces hormone, chemokine, and defensin secretion. *J Immunol* 178(7):4296–4303.

67. Nogueira AM, Barbosa AJ (1994) Immunocytochemical study of intestinal endocrine cells in germ-free mice. *Eur J Histochem* 38(3):213–218.

68. Mongardi Fantaguzzi C, Thacker M, Chiocchetti R, Furness JB (2009) Identification of neuron types in the submucosal ganglia of the mouse ileum. *Cell Tissue Res* 336(2):179–189.

69. Schéle E, et al. (2013) The Gut Microbiota Reduces Leptin Sensitivity and the Expression of the Obesity-Suppressing Neuropeptides Proglucagon (Gcg) and Brain-Derived Neurotrophic Factor (Bdnf) in the Central Nervous System. *Endocrinology* 154(10):3643–3651.

70. Covasa M, Duca FA, Swartz TD (2016) Gut Microbiota Restores Central Neuropeptide Deficits Present in Germ Free Animals. *The FASEB Journal*.

71. Vulchanova L, CASEY M, CRABB G, KENNEDY W, BROWN D (2007) Anatomical evidence for enteric neuroimmune interactions in Peyer's patches. *J Neuroimmunol* 185(1-2):64–74.

72. Stanisz AM, Befus D, Bienenstock J (1986) Differential effects of vasoactive intestinal peptide, substance P, and somatostatin on immunoglobulin synthesis and proliferations by lymphocytes from Peyer's patches, mesenteric lymph nodes, and spleen. *J Immunol* 136(1):152–156.

73. Lotz M, Vaughan JH, Carson DA (1988) Effect of Neuropeptides on Production of Inflammatory Cytokines by Human-Monocytes. *Science* 241(4870):1218–1221.

74. Wang L, Stanisz AM, WERSHIL BK, GALLI SJ, PERDUE MH (1995) Substance P induces ion secretion in mouse small intestine through effects on enteric nerves and mast cells. *American Journal of Physiology - Gastrointestinal and Liver Physiology* 269(1):G85–G92.

75. Mantyh CR, et al. (1988) Receptor binding sites for substance P, but not substance K or neuromedin K, are expressed in high concentrations by

arterioles, venules, and lymph nodules in surgical specimens obtained from patients with ulcerative colitis and Crohn disease. *Proceedings of the National Academy of Sciences* 85(9):3235–3239.

76. la Fuente De M, Bernaez I, Del Rio M, Hernanz A (1993) Stimulation of murine peritoneal macrophage functions by neuropeptide Y and peptide YY. Involvement of protein kinase C. *Immunology* 80(2):259–265.

77. Wheway J, et al. (2005) A fundamental bimodal role for neuropeptide Y1 receptor in the immune system. *Journal of Experimental Medicine* 202(11):1527–1538.

78. Levite M (1998) Neuropeptides, by direct interaction with T cells, induce cytokine secretion and break the commitment to a distinct T helper phenotype. *Proceedings of the National Academy of Sciences* 95(21):12544–12549.

79. Chorny A, et al. (2005) Vasoactive intestinal peptide induces regulatory dendritic cells with therapeutic effects on autoimmune disorders. *Proceedings of the National Academy of Sciences* 102(38):13562–13567.

80. Ganea D, Gonzalez-Rey E, Delgado M (2006) A Novel Mechanism for Immunosuppression: from Neuropeptides to Regulatory T Cells. *Jrnl Neuroimmune Pharm* 1(4):400–409.

81. Delgado M, Gonzalez-Rey E, Ganea D (2005) The Neuropeptide Vasoactive Intestinal Peptide Generates Tolerogenic Dendritic Cells. *J Immunol* 175(11):7311–7324.

82. Delgado M (2005) Vasoactive intestinal peptide generates CD4+CD25+ regulatory T cells in vivo. *J Leukoc Biol* 78(6):1327–1338.

83. Sun W, Tadmori I, Yang L, Delgado M, Ganea D (2000) Vasoactive intestinal peptide (VIP) inhibits TGF-β1 production in murine macrophages. *J Neuroimmunol* 107(1):88–99.

84. Delgado M, Ganea D (2001) Inhibition of Endotoxin-Induced Macrophage Chemokine Production by Vasoactive Intestinal Peptide and Pituitary

Adenylate Cyclase-Activating Polypeptide In Vitro and In Vivo. *J Immunol* 167(2):966–975.

85.   Herrera JL, et al. (2009) Toll-like receptor stimulation differentially regulates vasoactive intestinal peptide type 2 receptor in macrophages. *Journal of Cellular and Molecular Medicine* 13(9b):3209–3217.

86.   Foster N, Lea SR, Preshaw PM, Taylor JJ (2006) Pivotal Advance: Vasoactive intestinal peptide inhibits up-regulation of human monocyte TLR2 and TLR4 by LPS and differentiation of monocytes to macrophages. *J Leukoc Biol* 81(4):893–903.

87.   Abad C, et al. (2003) Therapeutic effects of vasoactive intestinal peptide in the trinitrobenzene sulfonic acid mice model of Crohn's disease. *Gastroenterology* 124(4):961–971.

88.   Gomariz RP, et al. (2005) Time-course expression of Toll-like receptors 2 and 4 in inflammatory bowel disease and homeostatic effect of VIP. *J Leukoc Biol* 78(2):491–502.

89.   Conlin VS, et al. (2009) Vasoactive intestinal peptide ameliorates intestinal barrier disruption associated with Citrobacter rodentium-induced colitis. *American Journal of Physiology - Gastrointestinal and Liver Physiology* 297(4):G735–G750.

90.   Neunlist M, et al. (2003) Toxin B of Clostridium difficileactivates human VIP submucosal neurons, in part via an IL-1β-dependent pathway. *American Journal of Physiology - Gastrointestinal and Liver Physiology* 285(5):G1049–G1055.

91.   Nassif A, et al. (1995) Clostridium difficilesuppresses colonic vasoactive intestinal peptide associated with altered motility. *Mediators Inflamm* 4(6):452–453.

92.   Lelievre V, et al. (2007) Gastrointestinal dysfunction in mice with a targeted mutation in the gene encoding vasoactive intestinal polypeptide: A model for the study of intestinal ileus and Hirschsprung's disease. *Peptides* 28(9):1688–1699.

93.   Fujimoto T, Reen DJ, Puri P (1988) Inflammatory Response in Enterocolitis in the Piebald Lethal Mouse Model of Hirschsprung's Disease. *Pediatr Res* 24(2):152–155.

94.   Austin KM (2012) The pathogenesis of Hirschsprung's disease-associated enterocolitis. *Seminars in Pediatric Surgery* 21(4):319–327.

95.   Imamura A, Puri P, O'Briain DS, Reen DJ (1992) Mucosal immune defence mechanisms in enterocolitis complicating Hirschsprung's disease. *Gut* 33(6):801–806.

96.   Murphy F, Puri P (2005) New insights into the pathogenesis of Hirschsprung's associated enterocolitis. *Ped Surgery Int* 21(10):773–779.

97.   Heanue TA, Pachnis V (2006) Expression profiling the developing mammalian enteric nervous system identifies marker and candidate Hirschsprung disease genes. *Proceedings of the National Academy of Sciences* 103(18):6919–6924.

98.   RAPPORT MM, GREEN AA, PAGE IH (1948) Serum vasoconstrictor, serotonin; isolation and characterization. *J Biol Chem* 176(3):1243–1251.

99.   Erspamer V, Asero B (1952) Identification of Enteramine, the Specific Hormone of the Enterochromaffin Cell System, as 5-Hydroxytryptamine. *Nature* 169(4306):800–801.

100.   Rudd ML, Nicolas AN, Brown BL, Fischer-Stenger K, Stewart JK (2005) Peritoneal macrophages express the serotonin transporter. *J Neuroimmunol* 159(1-2):113–118.

101.   O'Connell PJ, et al. (2006) A novel form of immune signaling revealed by transmission of the inflammatory mediator serotonin between dendritic cells and T cells. *Blood* 107(3):1010–1017.

102.   Meredith EJ, et al. (2005) The serotonin transporter (SLC6A4) is present in B-cell clones of diverse malignant origin: probing a potential anti-tumor target for psychotropics. *The FASEB Journal* 19(9):1187–1189.

103. Stefulj J, Jernej B, Cicin-Sain L, Rinner I, Schauenstein K (2000) mRNA Expression of Serotonin Receptors in Cells of the Immune Tissues of the Rat. *Brain Behav Immun* 14(3):219–224.

104. Shajib MS, Khan WI (2014) The role of serotonin and its receptors in activation of immune responses and inflammation. *Acta Physiologica* 213(3):561–574.

105. Leon-Ponte M, Ahern GP, O'Connell PJ (2006) Serotonin provides an accessory signal to enhance T-cell activation by signaling through the 5-HT7 receptor. *Blood* 109(8):3139–3146.

106. las Casas-Engel de M, et al. (2013) Serotonin Skews Human Macrophage Polarization through HTR 2Band HTR 7. *J Immunol* 190(5):2301–2310.

107. Csaba G, Kapa E, Cserhalmi M (1975) Hormone receptor studies on frog macrophage cells by means of histamine, serotonin and indoleacetic acid. *Endokrinologie* 65(2):219–223.

108. Bülbring E, Lin RCY (1958) The effect of intraluminal application of 5-hydroxytryptamine and 5-hydroxytryptophan on peristalsis; the local production of 5-HT and its release in relation to intraluminal pressure and propulsive activity. *The Journal of Physiology* 140(3):381–407.

109. Costa M, Furness JB (2015) THE SITES OF ACTION OF 5-HYDROXYTRYPTAMINE IN NERVE-MUSCLE PREPARATIONS FROM THE GUINEA-PIG SMALL INTESTINE AND COLON. *British Journal of Pharmacology* 65(2):237–248.

110. Hillsley K, GRUNDY D (2004) Sensitivity to 5-hydroxytryptamine in different afferent subpopulations within mesenteric nerves supplying the rat jejunum. *The Journal of Physiology* 509(3):717–727.

111. Song J, et al. (2015) Mast Cell-dependent Mesenteric Afferent Activation by Mucosal Supernatant From Different Bowel Segments of Guinea Pigs With Post-infectious Irritable Bowel Syndrome. *J Neurogastroenterol Motil* 21(2):236–246.

112. Starodub AM, Wood JD (2000) Histamine suppresses A-type potassium current in myenteric neurons from guinea pig small intestine. *J Pharmacol Exp Ther* 294(2):555–561.

113. Buhner S, et al. (2009) Activation of Human Enteric Neurons by Supernatants of Colonic Biopsy Specimens From Patients With Irritable Bowel Syndrome. *Gastroenterology* 137(4):1425–1434.

114. Ahlman H, Lundberg J, Dahlstrom A, Kewenter J (1976) A Possible Vagal Adrenergic Release of Serotonin from Enterochromaffin Cells in the Cat. *Acta Physiologica Scandinavica* 98(3):366–375.

115. Yamasaki Y, Shimamura O, Kizu A, Nakagawa M, Ijichi H (1983) Modulation by alpha 2-adrenergic stimulation of IgE-mediated 14C-serotonin release from rat mast cells. *Agents Actions* 13(4):310–317.

116. THEOHARIDES TC, BONDY PK, TSAKALOS ND, ASKENASE PW (1982) Differential release of serotonin and histamine from mast cells. *Nature* 297(5863):229–231.

117. Yano JM, et al. (2015) Indigenous Bacteria from the Gut Microbiota Regulate Host Serotonin Biosynthesis. *Cell* 161(2):264–276.

118. Reigstad CS, et al. (2015) Gut microbes promote colonic serotonin production through an effect of short-chain fatty acids on enterochromaffin cells. *The FASEB Journal* 29(4):1395–1403.

119. Atarashi K, et al. (2011) Induction of Colonic Regulatory T Cells by Indigenous Clostridium Species. *Science* 331(6015):337–341.

120. Atarashi K, et al. (2013) Treg induction by a rationally selected mixture of Clostridia strains from the human microbiota. *Nature* 500(7461):232–236.

121. Furusawa Y, et al. (2013) Commensal microbe-derived butyrate induces the differentiation of colonic regulatory T cells. *Nature* 504(7480):446–450.

122. Li Y, et al. (2010) Altered expression of CD4+CD25+ regulatory T cells and its 5-HT1a receptor in patients with major depression disorder. *Journal of Affective Disorders* 124(1-2):68–75.

123. Bar KJ, Facer P, Williams NS, Tam PK, Anand P (1997) Glial-derived neurotrophic factor in human adult and fetal intestine and in Hirschsprung's disease. *Gastroenterology* 112(4):1381–1385.

124. Brun P, et al. (2015) Toll like receptor-2 regulates production of glial-derived neurotrophic factors in murine intestinal smooth muscle cells. *Molecular and Cellular Neuroscience* 68:24–35.

125. Han TY, Lourenssen S, Miller KG, Blennerhassett MG (2015) Intestinal smooth muscle phenotype determines enteric neuronal survival via GDNF expression. *Neuroscience* 290:357–368.

126. Anitha M, et al. (2006) Glial-Derived Neurotrophic Factor Modulates Enteric Neuronal Survival and Proliferation Through Neuropeptide Y. *Gastroenterology* 131(4):1164–1178.

127. Gianino S (2003) GDNF availability determines enteric neuron number by controlling precursor proliferation. *Development* 130(10):2187–2198.

128. Heuckeroth RO, et al. (1999) Gene Targeting Reveals a Critical Role for Neurturin in the Development and Maintenance of Enteric, Sensory, and Parasympathetic Neurons. *Neuron* 22(2):253–263.

129. Veiga-Fernandes H, et al. (2007) Tyrosine kinase receptor RET is a key regulator of Peyer's Patch organogenesis. *Nature* 446(7135):547–551.

130. Patel A, et al. (2012) Differential RET Signaling Pathways Drive Development of the Enteric Lymphoid and Nervous Systems. *Science Signaling* 5(235):ra55–ra55.

131. Ibiza S, et al. (2016) Glial-cell-derived neuroregulators control type 3 innate lymphoid cells and gut defence. *Nature* 535(7612):440–443.

132. Sonnenberg GF, Monticelli LA, Elloso MM, Fouser LA, Artis D (2011) CD4+ Lymphoid Tissue-Inducer Cells Promote Innate Immunity in the Gut. *Immunity* 34(1):122–134.

133. Liang SC, et al. (2006) Interleukin (IL)-22 and IL-17 are coexpressed by Th17 cells and cooperatively enhance expression of antimicrobial peptides. *Journal of Experimental Medicine* 203(10):2271–2279.

134. Zheng Y, et al. (2008) Interleukin-22 mediates early host defense against attaching and effacing bacterial pathogens. *Nature Medicine* 14(3):282–289.

135. Sugimoto K, et al. (2008) IL-22 ameliorates intestinal inflammation in a mouse model of ulcerative colitis. *J Clin Invest*. doi:10.1172/JCI33194.

136. Lindemans CA, et al. (2015) Interleukin-22 promotes intestinal-stem-cell-mediated epithelial regeneration. *Nature* 528(7583):560–564.

137. Brun P, et al. (2013) Toll-Like Receptor 2 Regulates Intestinal Inflammation by Controlling Integrity of the Enteric Nervous System. *Gastroenterology* 145(6):1323–1333.

138. Bush TG, et al. (1998) Fulminant Jejuno-Ileitis following Ablation of Enteric Glia in Adult Transgenic Mice. *Cell* 93(2):189–201.

139. Sánchez MP, et al. (1996) Renal agenesis and the absence of enteric neurons in mice lacking GDNF. *Nature* 382(6586):70–73.

140. Schuchardt A, D'Agati V, Larsson-Blomberg L, Costantini F, Pachnis V (1994) Defects in the kidney and enteric nervous system of mice lacking the tyrosine kinase receptor Ret. *Nature* 367(6461):380–383.

141. Angrist M, Bolk S, Halushka M, Lapchak PA, Chakravarti A (1996) Germline mutations in glial cell line-derived neurotrophic factor (GDNF) and RET in a Hirschsprung disease patient. *Nat Genet* 14(3):341–344.

142. Bradley JS Jr, Parr EJ, Sharkey KA (1997) Effects of inflammation on cell proliferation in the myenteric plexus of the guinea-pig ileum. *Cell Tissue Res* 289(3):455–461.

143. Ruhl A, Franzke S, Stremmel W (2001) IL-1beta and IL-10 have dual effects on enteric glial cell proliferation. *Neurogastroenterology & Motility* 13(1):89–94.

144. Starke-Buzetti WA, Oaks JA (2008) Increased glial-derived neurotrophic factor in the small intestine of rats infected with the tapeworm, Hymenolepis diminuta. *International Journal of Experimental Pathology* 89(6):458–465.

145. Boyen von GB, et al. (2011) Distribution of enteric glia and GDNF during gut inflammation. *BMC Gastroenterol* 11(1):622.

146. Barajon I, et al. (2009) Toll-like Receptors 3, 4, and 7 Are Expressed in the Enteric Nervous System and Dorsal Root Ganglia. *J Histochem Cytochem* 57(11):1013–1023.

147. Burgueño JF, et al. (2016) TLR2 and TLR9 modulate enteric nervous system inflammatory responses to lipopolysaccharide. *J Neuroinflammation* 13(1):286–15.

148. Schäfer K-H, Mestres P, Marz P, Rose-John S (1999) The IL-6/sIL-6R Fusion Protein Hyper-IL-6 Promotes Neurite Outgrowth and Neuron Survival in Cultured Enteric Neurons. *Journal of Interferon & Cytokine Research* 19(5):527–532.

149. Scheller J, Chalaris A, Schmidt-Arras D, Rose-John S (2011) The pro- and anti-inflammatory properties of the cytokine interleukin-6. *Biochimica et Biophysica Acta (BBA) - Molecular Cell Research* 1813(5):878–888.

150. Ligumsky M, Simon PL, Karmeli F, Rachmilewitz D (1990) Role of interleukin 1 in inflammatory bowel disease--enhanced production during active disease. *Gut* 31(6):686–689.

151. HURST SM, Stanisz AM, Sharkey KA, COLLINS SM (1993) Interleukin 1β-induced increase in substance P in rat myenteric plexus. *Gastroenterology* 105(6):1754–1760.

152. COLLINS SM, et al. (1992) Effect of Inflammation of Enteric Nerves Cytokine-Induced Changes in Neurotransmitter Content and Release. *Ann NY Acad Sci* 664(1 Neuro-immuno-):415–424.

153. Xia Y, et al. (1999) IL-1β and IL-6 excite neurons and suppress nicotinic and noradrenergic neurotransmission in guinea pig enteric nervous system. *J Clin Invest* 103(9):1309–1316.

154. Xavier RJ, Podolsky DK (2007) Unravelling the pathogenesis of inflammatory bowel disease. *Nature* 448(7152):427–434.

155. Ley RE, et al. (2008) Evolution of Mammals and Their Gut Microbes. *Science* 320(5883):1647–1651.

156. Dubos RJ, Schaedler RW (1960) THE EFFECT OF THE INTESTINAL FLORA ON THE GROWTH RATE OF MICE, AND ON THEIR SUSCEPTIBILITY TO EXPERIMENTAL INFECTIONS. *Journal of Experimental Medicine* 111(3):407–417.

157. vanderWaaij LA, Limburg PC, Mesander G, vanderWaaij D (1996) In vivo IgA coating of anaerobic bacteria in human faeces. *Gut* 38(3):348–354.

158. Macpherson AJ, et al. (2000) A primitive T cell-independent mechanism of intestinal mucosal IgA responses to commensal bacteria. *Science* 288(5474):2222–.

159. Hooper LV, et al. (2001) Molecular Analysis of Commensal Host-Microbial Relationships in the Intestine. *Science* 291(5505):881–884.

160. Mazmanian SK, Liu CH, Tzianabos AO, Kasper DL (2005) An Immunomodulatory Molecule of Symbiotic Bacteria Directs Maturation of the Host Immune System. *Cell* 122(1):107–118.

161. Orland FJ, et al. (2016) Use of the Germfree Animal Technic in the Study of Experimental Dental Caries. *Journal of Dental Research* 33(2):147–174.

162. Van der Waaij D, Berghuis-de Vries JM, Lekkerkerk-van der Wees JEC (2009) Colonization resistance of the digestive tract in conventional and antibiotic-treated mice. *J Hyg (Lond)* 69(3):405–411.

163. Heijtz RD, et al. (2011) Normal gut microbiota modulates brain development and behavior. *Proceedings of the National Academy of Sciences* 108(7):3047–3052.

164. Hsiao EY, et al. (2013) Microbiota Modulate Behavioral and Physiological Abnormalities Associated with Neurodevelopmental Disorders. *Cell* 155(7):1451–1463.

165. Hoban AE, et al. (2016) Regulation of prefrontal cortex myelination by the microbiota. *Transl Psychiatry* 6(4):e774–e774.

166. Sampson TR, et al. (2016) Gut Microbiota Regulate Motor Deficits and Neuroinflammation in a Model of Parkinson's Disease. *Cell* 167(6):1469–1480.e12.

167. Aas J, Gessert CE, Bakken JS (2003) Recurrent Clostridium difficileColitis: Case Series Involving 18 Patients Treated with Donor Stool Administered via a Nasogastric Tube. *CLIN INFECT DIS* 36(5):580–585.

168. Mazmanian SK, Round JL, Kasper DL (2008) A microbial symbiosis factor prevents intestinal inflammatory disease. *Nature* 453(7195):620–625.

169. Grasa L, et al. (2015) Antibiotic-Induced Depletion of Murine Microbiota Induces Mild Inflammation and Changes in Toll-Like Receptor Patterns and Intestinal Motility. *Microb Ecol* 70(3):835–848.

170. Anitha M, Vijay Kumar M, Sitaraman SV, Gewirtz AT, Srinivasan S (2012) Gut Microbial Products Regulate Murine Gastrointestinal Motility via Toll-Like Receptor 4 Signaling. *Gastroenterology* 143(4):1006–1016.e4.

171. Collins J, Borojevic R, Verdu EF, Huizinga JD, Ratcliffe EM (2013) Intestinal microbiota influence the early postnatal development of the enteric nervous system. *Neurogastroenterology & Motility* 26(1):98–107.

172. McVey Neufeld KA, Mao YK, Bienenstock J, Foster JA, Kunze WA (2013) The microbiome is essential for normal gut intrinsic primary afferent neuron excitability in the mouse. *Neurogastroenterol Motil* 25(2):183–e88.

173. Kabouridis PS, et al. (2015) Microbiota Controls the Homeostasis of Glial Cells in the Gut Lamina Propria. *Neuron* 85(2):289–295.

174. Brun P, et al. (2013) Toll-Like Receptor 2 Regulates Intestinal Inflammation by Controlling Integrity of the Enteric Nervous System. *Gastroenterology* 145(6):1323–1333.

175. Wolin M (1981) Fermentation in the rumen and human large intestine. *Science* 213(4515):1463–1468.

176. Campbell JM, Fahey GC, Wolf BW (1997) Selected indigestible oligosaccharides affect large bowel mass, cecal and fecal short-chain fatty acids, pH and microflora in rats. *J Nutr* 127(1):130–136.

177. Charney AN, Micic L, Egnor RW (1998) Nonionic diffusion of short-chain fatty acids across rat colon. *Am J Physiol* 274(3 Pt 1):G518–24.

178. Brown AJ, et al. (2003) The Orphan G Protein-coupled Receptors GPR41 and GPR43 Are Activated by Propionate and Other Short Chain Carboxylic Acids. *J Biol Chem* 278(13):11312–11319.

179. Tazoe H, et al. (2008) Roles of short-chain fatty acids receptors, GPR41 and GPR43 on colonic functions. 59 Suppl 2:251–262.

180. Thangaraju M, et al. (2009) GPR109A Is a G-protein-Coupled Receptor for the Bacterial Fermentation Product Butyrate and Functions as a Tumor Suppressor in Colon. *Cancer Research* 69(7):2826–2832.

181. Kim MH, Kang SG, Park JH, Yanagisawa M, Kim CH (2013) Short-Chain Fatty Acids Activate GPR41 and GPR43 on Intestinal Epithelial Cells to Promote Inflammatory Responses in Mice. *Gastroenterology* 145(2):396–406.e10.

182. Psichas A, et al. (2014) The short chain fatty acid propionate stimulates GLP-1 and PYY secretion via free fatty acid receptor 2 in rodents. *Int J Obes Relat Metab Disord* 39(3):424–429.

183. Samuel BS, et al. (2008) Effects of the gut microbiota on host adiposity are modulated by the short-chain fatty-acid binding G protein-coupled receptor, Gpr41. *Proceedings of the National Academy of Sciences* 105(43):16767–16772.

184. Saffar AA, Hellstrosm PM, Nylander G (2009) Correlation between Peptide YY-Induced Myoelectric Activity and Transit of Small-Intestinal Contents in Rats. *Scand J Gastroenterol* 20(5):577–582.

185. Nøhr MK, et al. (2013) GPR41/FFAR3 and GPR43/FFAR2 as Cosensors for Short-Chain Fatty Acids in Enteroendocrine Cells vs FFAR3 in Enteric Neurons and FFAR2 in Enteric Leukocytes. *Endocrinology* 154(10):3552–3564.

186. Karaki S-I, et al. (2006) Short-chain fatty acid receptor, GPR43, is expressed by enteroendocrine cells and mucosal mast cells in rat intestine. *Cell Tissue Res* 324(3):353–360.

187. Smith PM, et al. (2013) The Microbial Metabolites, Short-Chain Fatty Acids, Regulate Colonic Treg Cell Homeostasis. *Science* 341(6145):569–573.

188. Haghikia A, et al. (2015) Dietary Fatty Acids Directly Impact Central Nervous System Autoimmunity via the Small Intestine. *Immunity* 43(4):817–829.

189. Karaki S-I, et al. (2006) Short-chain fatty acid receptor, GPR43, is expressed by enteroendocrine cells and mucosal mast cells in rat intestine. *Cell Tissue Res* 324(3):353–360.

190. Le Poul E, et al. (2003) Functional Characterization of Human Receptors for Short Chain Fatty Acids and Their Role in Polymorphonuclear Cell Activation. *J Biol Chem* 278(28):25481–25489.

191. Eftimiadi C, et al. (1987) Short-chain fatty acids produced by anaerobic bacteria alter the physiological responses of human neutrophils to chemotactic peptide. *J Infect* 14(1):43–53.

192. Carretta MD, Conejeros I, Hidalgo MA, Burgos RA (2013) Propionate induces the release of granules from bovine neutrophils. *Journal of Dairy Science* 96(4):2507–2520.

193. Singh N, et al. (2014) Activation of Gpr109a, Receptor for Niacin and the Commensal Metabolite Butyrate, Suppresses Colonic Inflammation and Carcinogenesis. *Immunity* 40(1):128–139.

194. Digby JE, et al. (2012) Anti-Inflammatory Effects of Nicotinic Acid in Human Monocytes Are Mediated by GPR109A Dependent Mechanisms. *Arterioscler Thromb Vasc Biol* 32(3):669–676.

195. Diakos C, et al. (2006) n-Butyrate inhibits Jun NH(2)-terminal kinase activation and cytokine transcription in mast cells. *Biochem Biophys Res Commun* 349(2):863–868.

196. Neunlist M, Dobreva G, Schemann M (2004) Characteristics of mucosally projecting myenteric neurones in the guinea-pig proximal colon. *The Journal of Physiology* 517(2):533–546.

197.   Kunze WA, et al. (2009) Lactobacillus reuterienhances excitability of colonic AH neurons by inhibiting calcium-dependent potassium channel opening. *Journal of Cellular and Molecular Medicine* 13(8b):2261–2270.

198.   Soret R, et al. (2010) Short-Chain Fatty Acids Regulate the Enteric Neurons and Control Gastrointestinal Motility in Rats. *Gastroenterology* 138(5):1772–1782.e4.

199.   Madsen KL, Doyle JS, Jewell LD, Tavernini MM, Fedorak RN (1999) Lactobacillus species prevents colitis in interleukin 10 gene–deficient mice. *Gastroenterology* 116(5):1107–1114.

200.   Valeur N, Engel P, Carbajal N, Connolly E, Ladefoged K (2004) Colonization and Immunomodulation by Lactobacillus reuteri ATCC 55730 in the Human Gastrointestinal Tract. *Applied and Environmental Microbiology* 70(2):1176–1181.

201.   Foligne B (2007) Correlation between in vitro and in vivo immunomodulatory properties of lactic acid bacteria. *World J Gastroenterol* 13(2):236.

202.   Mao YK, et al. (2013) Bacteroides fragilis polysaccharide A is necessary and sufficient for acute activation of intestinal sensory neurons. *Nature Communications* 4(1):735.

203.   Bravo JA, et al. (2011) Ingestion of Lactobacillus strain regulates emotional behavior and central GABA receptor expression in a mouse via the vagus nerve. *Proceedings of the National Academy of Sciences* 108(38):16050–16055.

204.   Perez-Burgos A, et al. (2013) Psychoactive bacteria Lactobacillus rhamnosus(JB-1) elicits rapid frequency facilitation in vagal afferents. *American Journal of Physiology - Gastrointestinal and Liver Physiology* 304(2):G211–G220.

205.   Lin Q (2013) Submerged fermentation of Lactobacillus rhamnosus YS9 for γ-aminobutyric acid (GABA) production. *Braz J Microbiol* 44(1):183–187.

206. Siragusa S, et al. (2007) Synthesis of -Aminobutyric Acid by Lactic Acid Bacteria Isolated from a Variety of Italian Cheeses. *Applied and Environmental Microbiology* 73(22):7283–7290.

207. Barrett E, Ross RP, O'Toole PW, Fitzgerald GF, Stanton C (2012) γ-Aminobutyric acid production by culturable bacteria from the human intestine. *J Appl Microbiol* 113(2):411–417.

208. Kelly D, et al. (2003) Commensal anaerobic gut bacteria attenuate inflammation by regulating nuclear-cytoplasmic shuttling of PPAR-γ and RelA. *Nat Immunol* 5(1):104–112.

209. Round JL, Mazmanian SK (2010) Inducible Foxp3+ regulatory T-cell development by a commensal bacterium of the intestinal microbiota. *Proceedings of the National Academy of Sciences* 107(27):12204–12209.

210. Chu H, et al. (2016) Gene-microbiota interactions contribute to the pathogenesis of inflammatory bowel disease. *Science* 352(6289):1116–1120.

211. Wright KA (1979) Trichinella spiralis: An Intracellular Parasite in the Intestinal Phase. *The Journal of Parasitology* 65(3):441.

212. Stadnyk AW, Kearsey JA (1996) Pattern of proinflammatory cytokine mRNA expression during Trichinella spiralis infection of the rat. *Infect Immun* 64(12):5138–5143.

213. McDermott JR (2006) Immune control of food intake: enteroendocrine cells are regulated by CD4+ T lymphocytes during small intestinal inflammation. *Gut* 55(4):492–497.

214. Burton-Freeman B, Gietzen DW, Schneeman BO (1999) Cholecystokinin and serotonin receptors in the regulation of fat-induced satiety in rats. *AJP: Regulatory, Integrative and Comparative Physiology* 276(2):R429–R434.

215. Hayes MR, Chory FM, Gallagher CA, Covasa M (2006) Serotonin type-3 receptors mediate cholecystokinin-induced satiation through gastric distension. *AJP: Regulatory, Integrative and Comparative Physiology* 291(1):R115–R123.

216. Lv Y, et al. (2010) CCK mediated the inhibitory effect of oxytocin on the contraction of longitudinal muscle strips of duodenum in male rats. *Pflugers Arch* 460(6):1063–1071.

217. Zhao A, et al. (2014) Dependence of IL-4, IL-13, and Nematode-Induced Alterations in Murine Small Intestinal Smooth Muscle Contractility on Stat6 and Enteric Nerves. *J Immunol* 171(2):948–954.

218. Vallance BA, Blennerhassett PA, COLLINS SM (1997) Increased intestinal muscle contractility and worm expulsion in nematode-infected mice. *American Journal of Physiology - Gastrointestinal and Liver Physiology* 272(2):G321–G327.

219. Frieling T, Palmer JM, Cooke HJ, Wood JD (1994) Neuroimmune communication in the submucous plexus of guinea pig colon after infection with Trichinella spiralis. *Gastroenterology* 107(6):1602–1609.

220. Ishizaka T, Hirata F, Ishizaka K, Axelrod J (1980) Stimulation of phospholipid methylation, Ca2+ influx, and histamine release by bridging of IgE receptors on rat mast cells. *Proceedings of the National Academy of Sciences* 77(4):1903–1906.

221. Ahmad A, Wang CH, Bell RG (1991) A role for IgE in intestinal immunity. Expression of rapid expulsion of Trichinella spiralis in rats transfused with IgE and thoracic duct lymphocytes. *J Immunol* 146(10):3563–3570.

222. Rakhilin N, et al. (2016) Simultaneous optical and electrical in vivo analysis of the enteric nervous system. *Nature Communications* 7(1):31.

223. Chang RB, Strochlic DE, Williams EK, Umans BD, Liberles SD (2015) Vagal Sensory Neuron Subtypes that Differentially Control Breathing. *Cell* 161(3):622–633.

224. Grubišić V, Gulbransen BD (2017) Enteric glial activity regulates secretomotor function in the mouse colon but does not acutely affect gut permeability. *The Journal of Physiology* 595(11):3409–3424.

C h a p t e r   4

TOOLS TO CHARACTERIZE THE ENTERIC NERVOUS SYSTEM AND ASSAY THE CONSEQUENCES OF ITS ACTIVATION

Bryan B. Yoo, Jessica A. Griffiths, Peter Thuy-Boun, Victor Cantu, Kelly Weldon, Collin Challis, Michael J. Sweredoski, Ken Y. Chan, Taren M. Thron, Gil Sharon, Annie Moradian, Gregory Humphrey, Qiyun Zhu, Justin Shaffer, Dennis W. Wolan, Pieter C. Dorrestein, Rob Knight, Viviana Gradinaru, and Sarkis K. Mazmanian. "Tools to characterize the gastrointestinal nervous system and the host-microbe interactions mediated by its modulation."

ABSTRACT:

The gastrointestinal (GI) tract coordinates physiological responses throughout the body. These responses are initiated by different exposures to environments and are shaped by behavioral tendencies such as diet (direct) and stress (indirect). The signals are integrated in the GI tract, where complex molecular interactions occur between and among diverse cell types including those of both host and microbial origin. Here, we sought to further characterize and interrogate the GI nervous system by delivering recombinant adeno-associated (rAAV) viral vectors encoding fluorescent reporters and/or chemogenetic modulators to specifically map and activate enteric neurons with spatial and temporal resolution. We show that rAAV-mediated multi-color labelling of enteric neurons is an effective and efficient method to histologically characterize the enteric nervous system (ENS). To characterized neuronal cell physiology, we delivered GCamP6F, a fluorescent calcium reporter, and performed live, *in vivo* microscopy in anesthetized mice. We report that germ-free mice have reduced neuronal innervation in the gut, with altered neuronal firing patterns compared to mice with a complex microbiome. Designer receptors exclusively activated by designer drugs (DREADDs) were utilized to induce activation of GI neurons that express choline acetyltransferase (ChAT$^+$) and tyrosine hydroxylase (TH$^+$). Using a multi-omics assaying approach, we measured changes to the intestinal transcriptome, host and microbial proteome, metagenome, and metabolome. In doing so, we uncover novel associations between the activation of specific neuronal subsets in the GI tract and changes to the intestinal microbiota and molecular physiology. Importantly, activation of specific neuronal subsets specifically in the gut results in physiological changes reminiscent of increased intestinal motility, diarrhea-like symptoms, and altered secretory components. The experimental tools described herein and the findings they produced encourage the study of cellular and physiological responses mediated by the neural inputs in the GI tract and motivates novel hypotheses regarding human health and disease etiology.

INTRODUCTION:

The gastrointestinal (GI) tract consists of a diversity of cells. These cells (immune, epithelial, endothelial, endocrine, muscle, neuronal, adipocytes, and microbial) and their associated molecules are responsible for conducting and coordinating many physiological processes (1). This complex cellular network requires synergy in their molecular communication; however, the extent and scope of this communication is not well understood.

The GI tract receives extrinsic neuronal signals from over 100,000 nerve fibers that originate in from the sympathetic (SNS) and parasympathetic (PNS) arms of the peripheral nervous system (2). The GI tract is also innervated by an expansive intrinsic nervous system that has over 100 million neurons organized into distinct compartments of the GI tract, namely the myenteric and submucosal plexuses- this is collectively termed the enteric nervous system (ENS) (3). In recent years, extrinsic and intrinsic innervation of the GI tract has been implicated in various host responses, from digestion (4) and immunity (5, 6), to even behavior (7). Our understanding of how the GI tract coordinates diverse physiological processes remains limited; however, recent advances made in the development of experimental neuroscience tools has positioned the study of neurogastroenterology to experience momentous progress– such tools will help define the nature of neural communication in the gut.

Towards this end, we introduce novel experimental paradigms using bioengineered viral constructs to broadly characterize the ENS, and model the complex, coordinated physiologies altered by *in vivo* activation of the GI nervous system. Adeno-associated viruses (AAVs) have been characterized for their ability to delivery genes to eukaryotic cells (8). Using an engineered AAV capsid variant AAV-AAV-PHP.S (9) that has enhanced tropism for the ENS, we achieved robust expression of genetically encoded fluorescent reporters and neural activators. We also expressed the fluorescent calcium reporter GCaMP6F in enteric neurons to measure ENS activity in live animals by confocal microscopy. In doing so, we present methodological advances to immunohistochemistry (IHC) and calcium

imaging that allow us to broadly assay ENS cellular architecture in intact GI tissue and measure its activity, *in vivo*.

Lastly, we investigate how activation of different neuronal subsets within the ENS affects diverse cellular and molecular responses. ChAT and TH are the rate limiting enzymes in acetylcholine and catecholamine biosynthesis, respectively and are the key chemical mediators of neurotransmission in the PNS and SNS. However, the extent to which they impact GI physiology via the ENS is less understood. To begin filling this gap in knowledge, we transduced GI neurons with chemogenetic modulators (10) in transgenic mice that express the Cre recombinase at the ChAT and TH loci (ChAT-Cre and TH-Cre, respectively). We discover that stimulating neural activity in the GI tract via DREADDs alters the transcriptional and molecular landscape of the intestines, with complementing alterations to the gut microbiota, the consortia of microorganisms that inhabit the GI tract. The experimental tools described herein advance promote the study of the GI nervous system and its complex etiological impact on diseases of the GI tract and the periphery.

RESULTS:

Use of AAV-delivered Fluorescent Proteins Enables Vast, High-Resolution Labelling of the ENS

The general morphology and neurochemistry of the ENS has been well-characterized (1). However, current methods of immunohistochemistry (IHC) are hindered by many physical aspects of the GI tract: its relatively large size (~40cm long in a mouse), dynamic nature (i.e., with or without luminal contents, relaxed vs. contracted smooth muscle), and regional anatomic differences (i.e., small vs. large intestine, proximal vs. medial vs. distal regions). Furthermore, the ENS is localized to two distinct plexuses of the GI tract. Current studies often only characterize myenteric neurons by microdissection of the longitudinal muscle/myenteric plexus (LMMP) tissue layer (11), a severe manipulation of the tissue that overlooks the organization of submucosal neurons.

To address these limitations, we took a viral approach to label the ENS and employed tissue clearing techniques to enhance visualization of intact GI tissue. The AAV capsid variant AAV-PHP.S was used as it was optimized for systemic delivery (12) and characterized for its heightened tropism to the peripheral nervous system (9), specifically the ENS. Here, AAV-PHP.S genetic cargo that expresses under the ubiquitous CAG promoter or the neuron specific, human Synapsin 1 (hSYN1) promoter. This efficiently transduced cells throughout the ENS with a single delivery, inducing expression of genetic constructs in both myenteric and submucosal compartments of the ENS. AAV9 has been used in the past for viral delivery to the ENS (13). In comparison, AAV-PHP.S exhibits greater infectivity in the GI tract as seen by increased cellular expression of nuclear localized CAG-mNeonGreen (Figure 1A). Furthermore, 90% (±1.5%) of neurons labelled with antibodies against protein gene product 9.5 (PGP9.5), a pan-neuronal protein, co-localize with the expression of constructs driven under the hSYN1 promoter and delivered in AAV-PHP.S (Figure 1B).

The physical length of the GI tract also makes thorough characterization of the ENS by IHC intractable and costly. With AAV-mediated labeling, a single

systemic injection of AAV-PHP.S:hSYN1-mNeonGreen at 10^{12} viral genomes (vg) is sufficient to label expansive regions of ENS as seen in the small (Supplemental Figure 1A and 1B) and large intestines (Figure 1C). This minimizes the technical variability inherent to IHC and enables uniform imaging of millimeters of tissue at a micron resolution across many samples. From these images, it is apparent that there is spatial diversity in ENS structure, even within a distinct intestinal region (insets in Figure 1C). Coupling viral-labeling with tissue clearing methods, such as passive clarity technique (PACT) or a sorbitol-based clearing method (ScaleS) (14-16), we were able to preserve the structure of intestinal tissue. This garnered a more holistic understanding of the ENS such as how extrinsic nerves synapse with the ENS (Supplemental Figure 1C), how ENS architecture changes when it associates with Peyer's patches (small intestinal lymphoid tissues) (Supplemental Figure 1D), or even the differences that occur when the tissue is fixed with or without luminal contents (Supplemental Figure 1E-1G).

Furthermore, when equal vector genomes of three separate viruses encoding either PHP.S:hSYN1-mTurquoise, PHP.S:hSYN1-mNeonGreen, or PHP.S:hSYN1-mRuby (together AAV-PHP.S:hSYN1-XFP) are delivered together at a dose of 10^{12} vg, stochastic and combinatorial viral transduction of cells results in multi-color labelling of neurons. This accentuates cellular boundaries (Figure 1D) and morphologies (Figure 1E) more clearly than IHC. This method is also tunable by the design of genetic promoters. This versatility can be seen by the labeling of enteric glial cell bodies with virally-expressed tdTomato driven by the glial fibrillary acidic protein (GFAP) promoter (Figure 1F).

Lastly, tissue clearing also facilitated confocal imaging by enabling the capture of both myenteric and submucosal neurons within the same image stack (Figure 1G)– an important aspect of ENS phenotyping that is commonly overlooked. These histological advances allow for the direct imaging of the ENS in intact GI tissue via whole mount microscopy, eliminating the need to microdissect distinct layers of the GI tract, prepare thin sections, and use antibodies altogether. In all, this

labelling paradigm provides an effective and economical method to label the ENS at a high resolution, with or without the use of transgenic animals.

Characterizing and Quantifying ENS Architecture and Physiology

The small and large intestines have developed both divergent and synergistic functions and the ENS plays a critical role in regulating these physiologies (17). However, it remains poorly understood how the cellular architecture and physiology of the ENS contributes to the functional diversity within the GI tract. For example, the intestinal immune system has evolved regional specialization to effectively cope with the constant exposure to environmental, dietary, and microbial antigens (18). Furthermore, digestion of dietary lipids, proteins, and carbohydrates occurs in the proximal small intestine and absorption occurs distally (19), whereas gut bacteria mediate the digestion and fermentation of soluble fibers in the large intestines (20). Thus, as the role of the ENS in regulating complex intestinal physiologies continues to be explored, the need for thorough GI phenotyping becomes increasingly important. However, current characterization of the ENS focuses on only a single region of the myenteric plexus, resulting in an incomplete understanding of GI innervation and therefore its contribution to overall health and disease states.

To address this, wild-type mice were transduced with AAV-PHP.S:hSYN1-XFP, as described above, to label enteric neurons (Figure 2A). We found no significant differences in the relative abundance of viral vector genomes from the regions sampled in the small and large intestines (SI and LI) (Supplemental Figure 2A), outside of a small ~1.5cm section of the medial large intestinal tissue which as excluded from further characterization. Seven regions of the small intestine and two regions of the large intestine were sampled, proximally to distally. Using ScaleS tissue clearing methods, we imaged and enumerated neurons in both myenteric and submucosal plexuses, normalizing these counts to the number of crypts to account for the variability of similar tissue regions between animals at the time of fixation. Importantly, no difference was found in crypt diameter along the GI tract

(Supplemental Figure 2B), ensuring that normalizing neuron counts in this way was appropriate.

Here, we characterized ENS architecture in all assayed regions by quantifying the number of neurons and ganglia, as well as the size of ganglia (i.e., the number of neurons in each ganglion) in the myenteric and submucosal plexuses (Figure 2B-2G). Notably in the SI, the number of neurons and ganglia increase in the distal portions of the myenteric plexus compared to proximal regions while the converse is true for neurons and ganglia in the submucosal plexus (i.e., lower numbers in the distal regions relative to proximal regions) (Figure 2B and 2C). Additionally, the size of the ganglia increased in the distal regions of the SI myenteric plexus, but this was not observed in the submucosal plexus (Figure 2D). Although the number of neurons is unchanged in the proximal and distal regions of the LI neural plexuses (Figure 2E), the number of myenteric ganglia is increased (Figure 2F) while the size of each ganglion decreases in the distal LI (Figure 2G). Interestingly, LI submucosal neurons are localized to the natural folds that form in the colon (Figure 2A, lower right panels), and these ganglia appear smaller in the distal colon. Importantly, our labeling method enables simultaneous analysis of myenteric and submucosal neurons and motivates the characterization of multiple intestinal regions, uncovering changes to neural architecture throughout the GI tract.

Next, we developed a method to measure baseline calcium transients in the ENS of live mice. Existing methods to measure calcium levels in the ENS include *ex vivo* preparations of intestinal tissue (21) or surgically implanting an abdominal window to obtain *in vivo* ENS calcium recordings (22). These methods face significant limitations such as they involve extensive manipulation of tissue to obtain access to the LMMP, uncouple the ENS from its extrinsic neural connectivity, and require technically difficult and permanent surgical procedures.

In our method, we systemically delivered a fluorescent calcium reporter, GCaMP6F (23), to the ENS through viral delivery with AAV-PHP.S. Unstimulated calcium transients in the proximal large intestine were recorded in individual neurons by *in vivo* confocal microscopy (Figure 2H and Supplemental Video 1). Analysis of

neuronal calcium fluxes show an average spike rate of 29.1 spikes/minute with an interquartile range of 19.0 - 37.7 spikes/minute (min. = 7.0 spikes/min., max. = 63.0 spikes/min) (Figure 2I). Time between calcium spikes was calculated for each cell, and the average peak interval was 2.6 seconds with an interquartile range of 1.6 - 3.2 seconds (min. = 1.0 seconds, max. = 8.6 seconds) (Figure 2J). Heatmaps (Figure 2K) and traces (Figure 2L) constructed from GCaMP6F fluorescence intensities also depict the heterogeneity of neuronal firing among cells and within them (i.e., tonic vs. phasic, small vs. large fluorescence delta, duration of spike). This underscores the granularity and resolution of our methods in achieving single cell measurements of neuronal activity. The relative ease of the histological and live imaging techniques described above, facilitated by viral transduction of fluorescent reporters, can be applied broadly to many disease models to provide meaningful, *in vivo*, characterization of basal ENS activity– an important aspect of ENS phenotyping as it becomes increasingly implicated in health and disease.

Characterizing the Effect of the Intestinal Microbiome on ENS Architecture and Physiology

The complex community of microorganisms that inhabit the GI tract is collectively known as the intestinal microbiota. It impacts both GI and host function. In an effort to illuminate how the microbiota affects cellular architecture of the ENS, previous studies have shown that germ-free (GF) animals, void of all microorganisms, display stunted development in the GI tract evidenced by lower innervation (24-26). We aimed to benchmark our viral-mediated labelling to prior IHC studies and further characterize the effects of microbial influence on the ENS.

To this end, GF and specific pathogen free (SPF) (mice harboring a complex microbiota) mice were infected with PHPS-hSyn-XFP, as described above (Figure 3A). To ensure equal infectivity of GF and SPF mice, we found that the relative abundance of viral vector DNA from the small and large intestines was similar between the two groups (Supplemental Figure 3A). Seven regions of the small intestine and three regions of the large intestine were sampled, proximally to distally.

Using ScaleS tissue clearing methods, we imaged and enumerated neurons in both myenteric and submucosal plexuses, normalizing these counts to the number of crypts. Importantly, no difference was found in crypt diameter between GF and SPF (Supplemental Figure 3B), ensuring that normalizing neuron counts to the number of crypts was appropriate.

Notably, GF mice were found have fewer myenteric and submucosal neurons in the along many regions of the small intestine (Figure 3B and 3C) and the medial large intestine (Figure 3D and 3E). GF mice also have fewer neurons per cluster of neurons, or ganglion (Supplemental Figure 4C and 4D). However, there was generally no difference between GF and SPF mice when quantifying the normalized number of ganglia, except in the submucosal neurons of the proximal small intestine (Supplemental Figure 4E and 4F).

To better understand when the microbiota is most important in shaping ENS architecture, an antibiotic cocktail (ABX) containing ampicillin, vancomycin, neomycin, and metronidazole was administered, *ad libitum*, to GF and SPF mice at different developmental timepoints to deplete the microbiome. ABX treatment generally reduced the numbers of neurons in the SPF small intestine down to the levels of GF mice (Supplemental Figure 4A-4F), irrespective of when antibiotics were first administered (prenatally, or 3 and 8 weeks postnatally). The adult ENS has been shown to be actively maintained by a balance of apoptosis and neurogenesis (27), and our findings indicate that the microbiome also influences postnatal remodeling of the ENS.

Next, we developed a method to measure baseline calcium transients in the ENS of live mice. Existing methods to measure calcium levels in the ENS include *ex vivo* preparations of intestinal tissue (21) or surgically implanting an abdominal window to obtain *in vivo* ENS calcium recordings (22). These methods face significant limitations such as severe manipulation of tissue to obtain the LMMP, uncoupling the ENS from its extrinsic innervation, and use of a technically difficult surgical procedure.

We systemically delivered virally encoded GCaMP6 to GF and SPF mice as previously mentioned. Prior studies have shown that enteric neurons from GF mice exhibit reduced excitability as measured by lower resting potentials and heightened refractory periods (28, 29). These studies clearly show a link between the microbiome and ENS electrophysiology, but were limited to the study of a single cell type. To expand upon these findings, we recorded *in vivo*, intracellular calcium influx in enteric neurons from GF and SPF mice. Average fluorescence did not change between the GF and SPF ENS (Supplemental Figure 5A), however, GF mice have modestly higher rates of calcium influx than do SPF mice (Figure 3F), indicating higher baseline activity. Accordingly, time between calcium maxima for all measured peaks (peak interval) is decreased in GF mice (Supplemental Figure 5B). Although there is no difference in the average peak interval per cell, there are significant differences in the its variance (F-test) between GF and SPF (Figure 3G and Supplemental Figure 5B). This method of measuring GCaMP6F allows for a more global characterization of *in vivo* ENS activity, with extrinsic nerves intact. A heatmap generated from GCaMP6F signals from GF and SPF mice (Figure 3H and 3I) and example traces of raw fluorescent data (Supplemental Figure 5C and 5D), suggest potential dysregulation of ENS activity indicated by variability in the time between calcium maxima.

Characterizing and Modulating Neuronal Subpopulations of the ENS in ChAT-Cre and TH-Cre Transgenic Mice

Research in the central nervous system was initially predicated on IHC characterization; however, as genetically encoded neuroscience tools (e.g. AAVs, neuronal reporters and modulators) became available for neuroscience, neural populations were re-characterized using transgenic mouse models so that they could be leveraged, in tandem, to systematically characterize neural circuits. Similarly, a deeper understanding of the ENS will depend on histological recharacterization that can be coupled to functional modulation.

We started this process by histologically characterizing the ENS in ChAT- and TH-Cre animals. Cholinergic and catecholaminergic neurons are fundamental to the peripheral nervous system, innervating the body's internal organs and relaying information to and from the CNS. Though ChAT$^+$ and TH$^+$ neurons are intrinsic to the GI tract, they have yet to be systematically characterized for their active role in modifying local GI physiology. To do so, genetic constructs can be engineered to have the transgene be in double-floxed inverse orientation (DIO), such that the transgene is flipped and expressed only in the presence of Cre-recombinase (Cre). Thus, packaging these Cre-dependent vectors into AAV-PHP.S and delivering them to transgenic mouse lines that express Cre at the ChAT and TH genomic loci allow for their expression in potential subsets of neurons that are neurochemically distinct. In lieu of viral transduction, similar labelling can be achieved through transgenic crosses (e.g. Rosa26-DIO reporter strains crossed with Cre-mice); however, this requires extensive mouse husbandry and ultimate antibody use to verify neuron specificity.

To this end, we transduced ChAT-Cre or TH-Cre mice with AAV-PHP.S:hSYN1-DIO-XFP to visualize these subsets of neurons. Surprisingly, the labelled cells in each mouse line occupied spatially distinct layers of the GI tract as ChAT-Cre$^+$ neurons were localized to the myenteric plexus whereas TH-Cre$^+$ neurons were primarily localized to the submucosal plexus (Figure 4A-4B). Also, distal regions of the small intestine in TH-Cre mice show increasing proportion of myenteric neurons, though much lower than what is found in ChAT-Cre mice (Figure 4B). Conversely in the large intestine, the ratio of myenteric and submucosal neurons does not change between ChAT- and TH-Cre mice. These data suggest that spatial localization of enteric neurons is genetically encoded and thus may also be functionally distinct. To the best of our knowledge, this is the first characterization of the unique spatial distributions of ChAT- and TH-Cre$^+$ neurons in the ENS. As previously mentioned, characterization of submucosal neurons in the ENS has been technically limited. Without the tools implemented in this experiment, identifying and defining this overlooked compartment of neurons in the ENS would not have

been possible. Furthermore, the abundance of neuron-specific, Cre-expressing mouse lines affords tremendous opportunity for (re)discovery.

Activation of ChAT-Cre[+] and TH-Cre[+] Neurons in the GI Tract Alters the Intestinal Transcriptome

The spatial organization of TH and ChAT neurons hinted at distinct functional effects in the GI. To address this question, ChAT- and TH-Cre mice were infected with Cre-dependent genetic constructs encoding activating DREADDs (AAV-PHP.S:hSYN1-DIO-hM3Dq-mRuby2). hM3Dq is a modified neurotransmitter receptor that is designed to induce neuronal activation when exposed to Compound 21 (C21), its "designer drug" that activates only this receptor (30). Accordingly, C21 induces a long calcium transient in a Cre-expressing neuron, as shown by the gradual increase in GCaMP6F fluorescence in an intestinal explant (Figure 4C). Thus, this method enables activation of subsets enteric neurons with temporal resolution.

We next developed a novel experimental paradigm to test and assay the direct and indirect impact of chronic neuronal activation on various intestinal biological processes in a freely moving animal. To do this, ChAT- and TH-Cre mice were infected with activating DREADDs or a control virus expressing the reporter protein alone (AAV-PHP.S:hSYN1-DIO-mRuby2). C21 was administered intraperitoneally, once daily for 10 consecutive days to all mice (Figure 4D). One hour following the last C21 injection, 1cm of tissue from the distal small intestine (dSI) and proximal large intestinal (pLI) was harvested, and bulk tissue gene expression was profiled by QuantSeq, a 3' mRNA-sequencing technology. We hypothesized that the ENS is involved in propagating signals to the cells that reside in the GI tract, and thus chronic ENS activation would alter the intestinal transcriptome. Furthermore, we believed that the transcriptional changes induced in ChAT- and TH-Cre mice would be generally different given their distinct spatial localization of enteric neurons.

In neurons, the rapid and transient expression of immediate early genes (IEGs) is widely used as a measure of heightened neural activity (31). Accordingly, the IEGs *Fos*, *Egr1*, *Jun*, *Klf2* (Figure 4E-4H) were among the most significantly

upregulated transcript in the small and large intestines of both ChAT- and TH-Cre mice- further justifying our experimental paradigm as a model for *in vivo* ENS activation (Figure 4I). Moreover, IEGs are upregulated during growth and differentiation of highly active cell-types such as immune cells (32, 33), smooth muscle cells (34), and intestinal epithelial cells (35). As IEGs often function as transcriptional regulators in both neurons and non-neuronal cell types, this result shows how activation of the GI nervous system can induce broad mechanisms of transcriptional regulation throughout the intestinal transcriptome (Figure 4E-4H).

In the dSI, DREADD activation produced similar numbers of differentially expressed genes (DEGs; $p_{adj.}<0.05$) in ChAT-Cre mice (162 DEGs) (Figure 4G) and TH-Cre mice (165 DEGs) (Figure 4E). Interestingly, ~73% of the DEGs were upregulated upon ChAT-Cre activation (118 up, 44 down) and only ~42% of the DEGs were upregulated upon TH-Cre activation (69 up, 96 down). This parallels the number of upregulated IEGs in the dSI of ChAT-Cre mice (29 IEGs) compared to those in TH-Cre mice (5 IEGs) (Figure 4I), with a few IEGs (i.e., *Hbegf, Soca3, Mcl1*) actually being downregulated in TH-Cre mice (Figure 4G). In the pLI of both ChAT- (253 DEGs- 169 up, 84 down) (Figure 4F) and TH-Cre mice (192 DEGs – 130 up, 62 down) (Figure 4H), similar proportions transcripts were upregulated (~67-68%).

We then sought to contextualize our DEGs with the broader landscape oc cellular function and known signaling pathways using Gene Set Enrichment Analysis (GSEA) to identify differences in gene ontology (GO) annotations between treatment groups (Figure 4J-4M). Remarkably, the most enriched GO term in the dSI of ChAT-Cre mice was "regulation of smooth muscle cell proliferation" (Figure 4J), whereas in TH-Cre mice it was the "response to bacteria" (Figure 4L). This is evidence that ENS activation alters the intestinal transcriptome, from IEGs and transcriptional regulators to their downstream gene targets, and the functional consequence of neural activation may be influenced by their spatial localization. In the proximal large intestine, we see more similarity in the ChAT- and TH-Cre mice GO pathways that are affected by DREADD activation (Figure 4K and 4M). Strikingly, this supports

the fact that spatial localization may drive transcriptomic signatures of ChAT$^+$ and TH$^+$ neurons, given the fact that these neuronal subsets are both highly abundant in the myenteric plexus of the pLI (Figure 4B). Interestingly, the enriched biological processes upregulated in ChAT-Cre mice, where neurons exist in both myenteric and submucosal plexuses, portray the breadth of changes that neuronal activation has on the diverse cell types that exist in the GI tract, including endothelial, epithelial, immune, and fat cells (Figure 4J).

GI Neural Activation Alters Host and Microbial Proteome in the GI Lumen

The gut mucosa serves as a portal to the molecular environment, where the host, microbes, and dietary constituents exchange chemical signals and ultimately alter intestinal and peripheral physiology (36). To determine how activation of the neuronal subsets alters the luminal environment and if this alters host-microbe interactions, we first performed label-free proteomics (LC-MS/MS) on cell-free supernatants of cecal contents in ChAT- and TH-Cre mice. The cecum a large compartment at the juncture of the small and large intestines and has an abundance of microbes and luminal contents to assay. Samples were collected one hour following the final C21 dose (Figure 4D). In doing so, we assayed for host- and microbe-associated proteins and tested whether *in vivo* ENS activation altered the luminal environment.

Pancreatic digestive enzymes were the most significantly upregulated proteins in lumen of the activated mice (Figure 5A). These include chymopasin (CTRL), chymotrypsinogen 1 (CTRB1), and pancreatic lipase related protein 2 (PNLIPRP2). Accordingly, network analysis of upregulated proteins showed that KEGG pathways associated with digestion represent the majority of the network (Figure 5B). This also implicates cholinergic, viscerofugal neurons that send signals from the GI tract to other organs of the digestive system, such as the pancreas (3).

Interestingly, Niemann-Pick C1-Like 1 protein (NPCL1) is upregulated in the cecum of ChAT-Cre mice. NPCL1 is expressed on the apical surface of enterocytes (37) and is an integral protein involved in the absorption of free cholesterol in the

lumen, the precursor of bile acids. Goblet-cell related proteins also trended upwards, specifically Mucin-19 (MUC19) and Zymogen granule 16 (ZG16) (Figure 5A), a protein localized to secretory granules (38). Conversely, one of the most downregulated proteins was an aldehyde dehydrogenase (Q3U367) encoded by the *Aldh9A1* gene. It is involved in the catalytic conversion of putrescine (39), a molecule produced by the urea cycle and gut bacteria (40), to gamma-aminobutyric acid (GABA), a major inhibitory neurotransmitter. Acetylcholine produced by cholinergic neurons is known to be excitatory. However, this is the first example of enteric downregulation of GABA biosynthesis by cholinergic activation, potentially augmenting the excitatory signal in the GI tract.

Activation of TH^+ neurons also altered the luminal proteome. Interestingly, 88% (52/59) of the differentially abundant proteins ($p_{adj} < 0.25$, $p_{nom} < 0.021$) are distinct from those identified in activated ChAT-Cre mice ($p_{adj} < 0.25$, $p_{nom} < 0.042$). Also 90% of these proteins were upregulated (53/59), whereas only 18% of proteins in ChAT-Cre mice were upregulated (20/112), suggesting that activation of distinct neuronal subsets is associated with largely distinct changes in GI function. There are also heightened protein-protein interactions in activated TH-Cre samples, evidenced by increased levels of network nodes and connections (Figure 5C and 5D). When $TH-Cre^+$ neurons were activated, Filamin B (FLNB) and spectrin beta chain, non-erythrocytic 1 (SPTB2) were some of the most significantly enriched proteins (Figure 5C). These proteins are associated with the intestinal brush border and membrane vesicles (41, 42). Accordingly, vesicle-mediated transport was a major protein network identified (Figure 5D) and relatedly, coatomer proteins also trend upwards (COPA and COPB2) (Figure 5C). These vesicle associated proteins are known to package apolipoproteins, which are secreted luminally from enterocytes. Other enriched protein interaction networks that emerged were associated with the immune system, metabolic pathways, and ribosomes (Figure 5D). For example, immune related proteins such as IgA (in ChAT-Cre) and IgG2b and complement c3 (in TH-Cre) trend upwards (Figure 5A and 5C). These findings are in accordance with the immune-related biological processes identified in analysis of gene expression after

activation (Figure 4J-4M). It also provides novel mechanistic insights of the regulation of luminal immunoglobulins which have an important role in regulating host physiology through the intestinal microbiome (43-46).

Perhaps the most intriguing observation from this experiment was the strong depletion of acidic mammalian chitinase (CHIA) upon activation of TH-Cre mice (Figure 5C). Chitin is a natural polysaccharide that is a major component of fungal cell walls. However, to the best of our knowledge, intestinal chitinases are poorly studied in mice and CHIA has not been investigated for its role in regulating fungal populations. Because our peptide samples are made up of host and microbial proteins, the identified peptide sequences were also searched against microbial protein databases. Remarkably, the decrease in CHIA abundance was accompanied by a large increase in the proportion of fungal-associated peptides in the microbiome (representing ~59% of peptides mapped to any microbe) (Figure 5E). Furthermore, ~45% of the enriched eukaryotic proteins are involved in fermentation, the process that is responsible for chitin biosynthesis (Supplemental Figure 6A). In contrast, fungal peptides represented only ~0.4% of enriched peptides in the lumen of ChAT-Cre mice (Figure 5F) and all enriched GO terms are bacterial (Supplemental Figure 6B).

Taken together, the described activation-mediated alterations to the luminal proteomic environment model the molecular exchanges and physiological changes that occur at the interface of the GI tract and the environment. Furthermore, it is through these experiments that we uncover initial insights towards novel host-microbe interactions. It is clear that neuron-mediated host responses in the GI tract are vast and complex. Continued characterization with additional Cre-expressing mouse lines will highlight the breadth of changes that can result, enabling mechanistic studies regarding the ENS' role in modulating physiology.

Changes to the Gut Microbiome upon Activation of the GI Nervous System

Given that we observed robust changes in the gut proteome, including factors associated with microbial communities in the gut, we reasoned that neuronal

activation in the ENS would also result in changes to the composition and structure of the gut microbiome. For example, digestive enzymes can alter the nutrient composition and availability not only for the host, but also for the gut microbiome. Also, changes to GI immunity could have a potent effect on the resulting diversity and abundance of microbes in the GI tract. We believe the methods described in this study can be used to model host-microbe interactions and dysbiosis that are influenced by the neural activation of the GI tract.

To address this, we performed shotgun metagenomics on feces (pre-C21 samples, and at 1, 5, and 9 days after initial C21 dose) and cecal contents (10 days after initial dose) (Figure 4D). In ChAT-Cre mice, Faith's phylogenetic diversity decreases by day 9 in the feces and also in the cecum on day 10 (Figure 6A). This can also be seen by the large number taxa that are less abundant in activated samples (Supplemental Figures 7 and 8). In TH-Cre mice, phylogenetic diversity remained unchanged between groups. However, there is a trend towards a decrease in diversity from pre-C21 samples to 5 days post activation, and this decrease recovers by day 9 in the feces (Figure 5A and Supplemental Figure 8B). We then measured differences in the composition of microbial communities using weighted UniFrac distances were calculated and principle coordinate analyses (PCA) were performed. There is clear separation between control and activated groups in the feces and cecal contents of ChAT-Cre mice and this shift was largely absent in samples from TH-Cre mice (Figure 6B-6G). Interestingly, over the experimental time course, Verrucomicrobia was largely enriched in activated ChAT-Cre mice (Figure 6H). To discover differentially abundant bacterial taxa, we used linear discriminant analysis effect size (LEfSe) (47) and then visualized the data into cladograms depicting the phylogenetic relationship of differentially abundant taxa (Figure 6I and 6K). Family level changes to cecal bacterial communities are described in ChAT- and TH-Cre mice (Figure 6J and 6L). *Akkermansia muciniphila* appears to drive the increase in Verrucomicrobia in activated ChAT-Cre mice (Figure 6M) and this increase is absent in respective TH-Cre mice (Figure 6N). *A. muciniphila* is known to metabolize host-derived mucus as a growth substrate, and this corresponds to the increase in luminal mucin

proteins (MUC19) in activated ChAT-Cre mice. *A. muciniphila* is implicated in many diseases, such as obesity (48, 49), multiple sclerosis (50, 51), and seizures (52). Here we show that activation of ChAT$^+$ neurons may affect the abundance of this microbe that appears to be intricately linked to human health.

Lastly, metagenomic analysis allows for the investigation of gene families and pathways that are differentially abundant in the microbiota. Only ChAT-Cre mice showed activation-mediated changes in beta-diversity of both gene families and pathways (Figure 6O-6R), and these shifts occurred in the cecum and feces collected 9 days after activation. The colors of the arrows represent different gene families and pathways and their direction is indicative of the influence that each feature has on the separation of control and activated groups. Thus, the most distinguishing features are highly represented in the control groups and downregulated in activated ChAT-Cre mice. The families and pathways that distinguish the control groups (Supplemental Figure 8C and 8D) are mainly associated with bacterial activity, such as nucleotide biosynthesis and metabolism, and protein translation and transport. The downregulation of these gene families and pathways in activated ChAT-Cre mice supports the corresponding decreases in bacterial diversity (Figure 6A).

From these data, it is apparent that neuronal activation has an active role in shaping the gut microbiome at a community, species, and genetic resolution. Thus, health-promoting communities or pathological dysbiosis may be predicated on nuanced differences and perturbations to the innervation and activation of the GI tract, integrating both host and microbes' impact on GI and peripheral physiology.

Metabolomic Changes Upon Neural Stimulation

Lastly, we assayed for small molecular changes in the cell-free supernatants of GI cecal contents by performing untargeted metabolomics using LC-MS/MS. Metabolomics offers unique insight to host and microbial metabolism of luminal constituents, complementing the changes already observed in the host and microbial proteome and microbiome.

In ChAT- and TH-Cre mice, we see a strong, activation-dependent clustering of cecal samples (Figure 7A-7B) taken one hour following the last C21 injection. In the fecal samples of ChAT-Cre mice, we see the separation of control and activated groups by day 5 following the initial C21 injection, and this separation persists at 9 days (Figure 7C-7F). Interestingly, we also observed a decrease in diversity in feces and cecal contents of these mice at the end of the experimental time course (Figure 6A). In TH-Cre fecal samples, there appeared to be a plate effect driving the separation of control and activated groups on one axis of the PCA. Thus, the samples were plotted on axes that minimized this experimental bias, and it appears that the samples also begin cluster by day 9 post-activation (Figure 7G-7J). Furthermore, there is clear separation between cecal metabolites in ChAT- and TH-Cre mice upon GI activation (Supplemental Figure 9A and 9B) and such separation occurs in the feces by Day 9 of the activation time course (Supplemental Figure 9C-9F). All of this suggests there are distinct metabolites that are altered in the feces and cecal contents of ChAT- and TH-Cre mice following activation.

The Global Natural Products Social Molecular Networking (GNPS) (53) tool is an open-access mass spectroscopy repository and analysis pipeline, from which we are able to visualize the data by producing molecular networks based on MS2 spectral similarities of small molecules and their analogs, both annotated via spectral matches against all available public reference spectral libraries and the purchased NIST17 CID library and unannotated. The feature based molecular networking workflow on GNPS (54) was utilized in order to analyze the spectra associated with the feature tables produced using the open source software MZmine version 2.51 (55). In the cecal contents of ChAT and TH-Cre mice, metabolic networks consisting of both annotated and unannotated molecules are shown (Figure 7K and 7L). Annotated, non-networked metabolites were chosen for their differential abundance in either control or activated samples.

Annotations, when available, help the discovery of potential direct and indirect consequences of neural activation on the luminal metabolome (Figure 7M-7N and Supplemental Table 1). All annotations produced by GNPS using spectral

matching against the reference libraries for this dataset are considered either level 2 or level 3 based on the Metabolomics Standards Initiative (MSI) (56). In both ChAT- and TH-Cre mice, the molecular networks largely consist of level 3 annotations of compounds belonging to the bile acid molecular family and their conjugates, as well as unannotated analogs. Spectral matches to primary and secondary bile acid families show changes upon activation status. Primary bile acids are known to be host associated, while secondary bile acids have shown to be metabolized by gut (57, 58).

Interestingly, metabolites with their closest spectral match being the primary bile acid cholic acid (ID: 108, 114, 215, 219, 221, 224, 259) are significantly enriched in the cecum of activated ChAT-Cre mice (Figure 7K and Supplemental Table 1). Additional metabolites that closely resemble the spectra of tauro-conjugated primary bile acids trend upwards, such as taurocholic acid (ID: 234, 238) and taurohyocholic acid (ID: 235). Conversely, features with spectral matches to the family of secondary bile acids and bile acid metabolites such as ursodeoxycholic acid (ID: 13), deoxycholic acid (ID: 100), beta-hyodeoxycholic acid (ID: 1, 143) and 12-ketodeoxycholic acid (ID: 19, 138) are decreased in activated mice (Figure 7K and Supplemental Table 1). Remarkably, this finding is concomitant with the decrease in microbial diversity observed in the cecum of ChAT-Cre mice (Figure 6A). This suggests that in ChAT-Cre mice, activation of the ENS is capable of modulating bile acids in the GI tract by influencing of their secretion and/or metabolism via the microbiota. It is noteworthy that increases in primary bile acids coincide with increases in the cholesterol transporter, NPCL1. Cholesterol, as previously mentioned, is an necessary precursor in bile acid biosynthesis. In TH-Cre mice, there are no significant differences in bile acid abundances. However, there were strong increases to non-networked metabolites in activated TH-Cre mice whose closest spectral matches were linoelaidic acid (ID: 626), oleanolic acid methyl ester (ID:378), and coproporphyrin I (ID: 378), and metabolites that spectrally resemble xanthine (ID: 259), genistein (ID: 846), and trans-Ferulic acid (ID: 707) were decreased (Figure 7L and Supplemental Table 1). All annotations identified using GNPS should be verified in future analyses with exact standards to attain level 2 MSI

annotation. Characterization small molecular changes in the lumen of the GI tract can help describe the functional metabolic consequences ENS activity, and such insights can help model the metabolic output not only in the GI tract, but also in systemic circulation.

DREADD Activation Alters GI Physiology

We hypothesized that gross physiological changes would accompany the abundant molecular alterations observed. First, water content of fecal pellets was measured over the 5 hours following neural activation. Water content of individual fecal pellets reached a maximum in ChAT-Cre mice 1-2 hours after a single dose of C21, but this increase was absent in TH-Cre mice (Figure 8A-8F). Linear regression analyses of percent water content 0-2 hours after C21 administration determined a significant increase in the slope of the best fit line of ChAT activated mice vs ChAT control and TH activated mice (Figure 8D and 8F). However, no differences were identified in TH control mice vs TH activated and ChAT control mice (Figure 8C and 8E). Finally, average percent water content of fecal pellets per mouse, over the 5 hour time course, was significantly increased by ~10% only in activated ChAT-Cre mice (Figure 8G). Next, activation-mediated secretion was assayed by measuring the mass of luminal contents, normalized to the body weight of the animal, 1 hour after C21 administration. Using this measure of secretion, there was a 71% increase in TH-Cre mice and a 65% increase in ChAT-Cre mice (Figure 8H). This is surprising because the increase in water abundance was only observed in the cecal contents of ChAT-Cre mice. Thus, alternative explanations, such as heightened water resorption in activated TH mice, the inhibition of it in activated ChAT mice, or a difference in the composition of ions and molecules secreted in the lumens of TH and ChAT mice, could explain these seemingly contrasting results. Lastly, transit time is decreased in both activated TH and ChAT-Cre (Figure 8I) mice, and accordingly, the rate of fecal output is significantly increased (Figure 8J). To determine potential confounding behavioral changes, open field testing was performed. This test identified a decrease

in locomotion in only activated ChAT-Cre mice as seen by a 35% and 33% decrease in distance travelled and movement duration (Supplemental Figure 10A and 10B).

DISCUSSION

We present a viral approach towards delivering genetically encoded fluorescent reporters and neural modulators to characterize the ENS and activate the neural inputs to the GI tract. To date, broad histological characterization of the ENS has been restricted by the limitations of current antibody labeling approaches (59). Viral-mediated expression of AAV-PHP.S allows for vast infectivity of enteric neurons with a single systemic injection, without the use of transgenic animals, and makes it much simpler to perform histology of the ENS in intact GI tissue.

Dysbiosis of the gut microbiota continues to be implicated in seemingly dissimilar diseases such as those of the immune and nervous systems (60). Similarly, innervation of the GI tract is responsible for mediating communications both internally (i.e., intestinal immunity) and externally (i.e., the CNS) (61). In this study, chronic enteric neural activation altered the gut microbiome, at the gene and protein level. Furthermore, GI activation altered metabolic byproducts of families of host molecules known to be mediated by the microbiome, such as bile acids. If enteric innervation and activation can explain both dynamic changes of the microbiome and long-lasting alterations to it, then perhaps gut bacteria do not only affect disease, but also serve as novel biomarkers for those with ENS-originating etiologies. Thus, as medicine continues to adopt microbiome-based interventions, it is important to understand and address the underlying mechanism of dysbiosis. Additionally, characterizing the luminal molecular environment and its ability to influence microbial taxa, genes, and metabolic pathways will be important towards the development of drugs that target the microbiome. Further studies, such as the transfer of gut microbes from "activated" mice or disease model outcomes with or without GI neural activation are necessary to dissect the role of the microbiome as a direct effector of physiology and/or a biomarker for neural dysregulation.

Neurogastroenterology research is at an inflection point where tools in neuroscience can be adapted for studies in the GI tract. This study provides a methodological proof-of-principle necessary to begin dissecting the histological and

functional complexity of the GI nervous system. The GI tract, in particular, is an ideal tissue to model the diverse interactions between neurons and non-neural cell types. As such, recent studies have highlighted the role of ENS signaling and integrating signals from other cell types including immune cells, enteroendocrine cells, and even the gut microbiome (5, 62-66). The genetic tools and multi-omics assay approach used in this study holistically outline the breadth of complex, multicellular interactions that are responsible for the molecular and microbial output of the GI tract and encourage the study of the ENS as a central motivator of physiology.

Figures and Legends

Figure 1. Advantages of Viral labeling in the ENS

Figure 1A
Viral-mediated expression of nuclear localized (NLS) GFP driven by the ubiquitous CAG promoter. Quantification of virally labelled cells in AAV9 vs. AAV-PHP.S in the longitudinal muscle, myenteric plexus, and circular muscle of the stomach. (N = 4-5 mice, each data point represents the average from 3 representative fields).
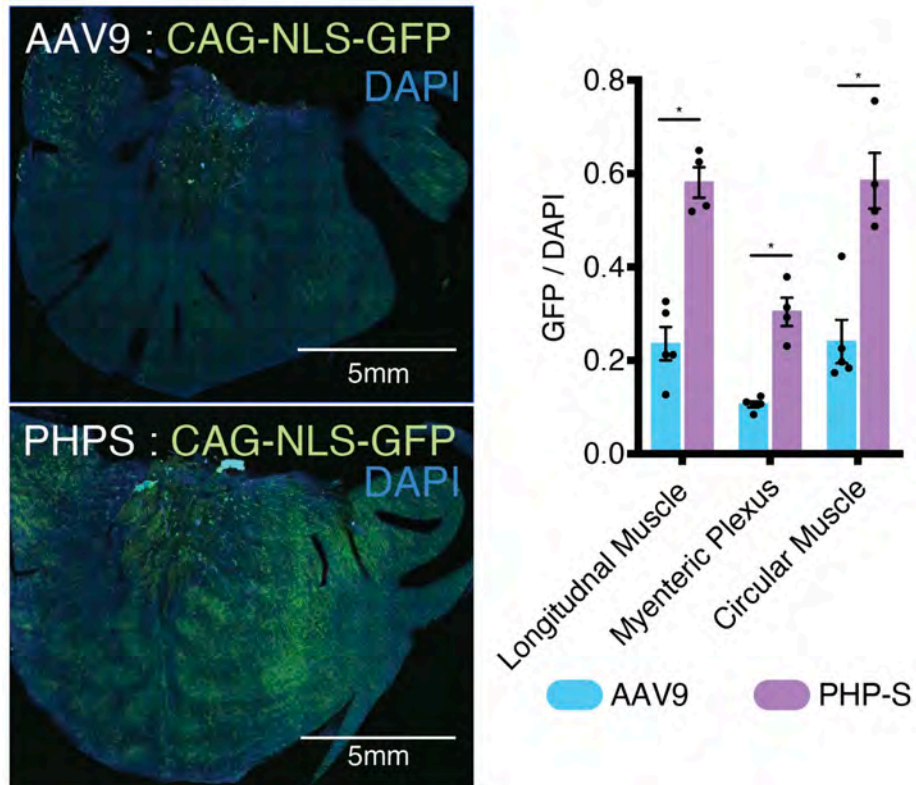
Figure 1B

Representative images of small and large intestines in mice infected with AAV-PHP.S:hSYN1-TdTomato and immunolabelled with the pan-neuronal antibody, PGP9.5. Inset: quantification of TdTomato$^+$ cells / PGP9.5$^+$ cells (N = 3 mice, each data point represent the average from 3 representative fields).
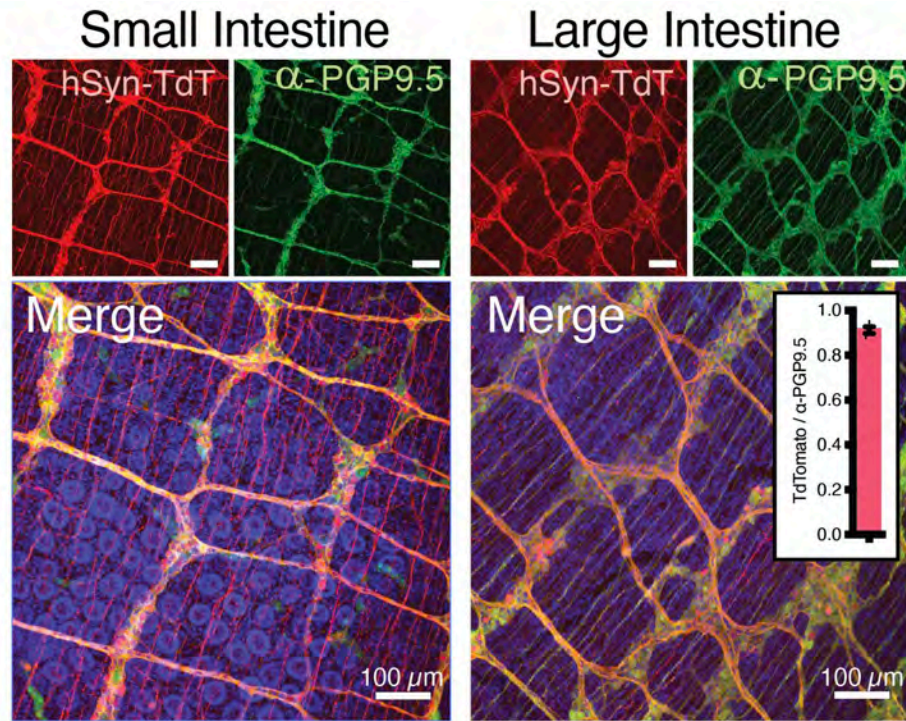
Figure 1C

Tiled, whole mount microscopy showing widespread labelling in the proximal large intestine (>1cm of tissue) from a single injection (10^{12} VGs-vector containing AAVs).
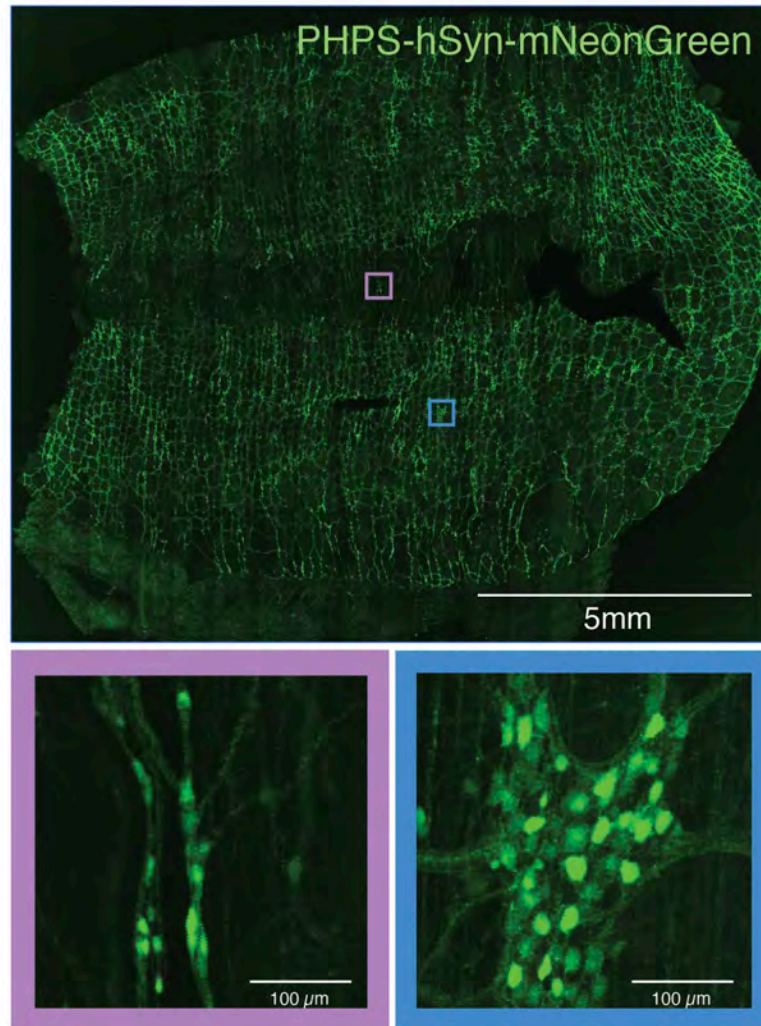
Figure 1D

PaCT tissue clearing coupled with multicolor labelling of the intestine, showing structural and anatomical resolution in Z.
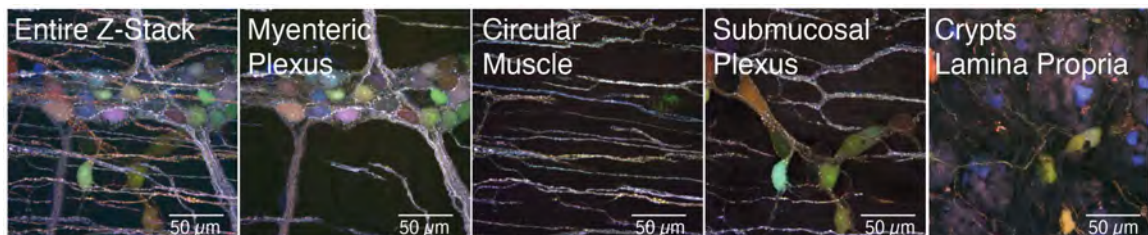
Figure 1E
Left: Antibody-labelled myenteric plexus of the proximal large intestine. Right: Viral-mediated multicolor labelling of a comparable region. AAV-PHP.S:hSYN1-(mTurq2/mNeonGreen/TdTomato) (AAV-PHP.S:hSYN1-XFP, 3e^{11} VGs each).
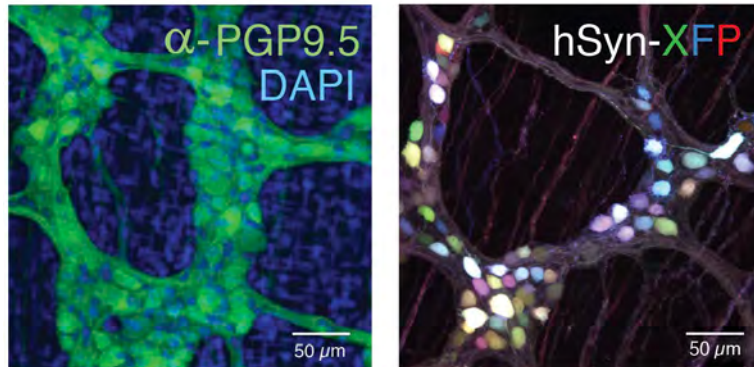
Figure 1F
High resolution confocal microscopy showing cell morphology when labelled with AAV-PHP.S:hSYN1-XFP vs. traditional IHC with PGP9.5.
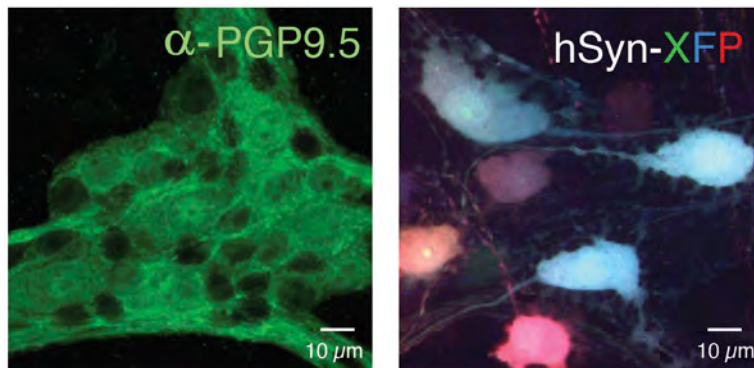
Figure 1G
Left: IHC with anti-PGP9.5 and anti-GFAP Right: Viral expression of AAV-PHP.S:hSYN1-mNeonGreen and AAV-PHP.S-GFAP-TdTomato
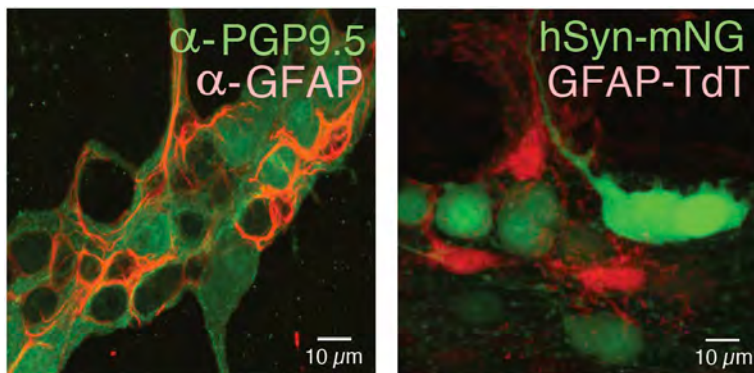
Figure 2. Quantifying ENS Architecture and Measuring ENS Activity with GCaMP6F

Figure 2A
Representative images from proximal and distal, small and large intestines of AAV-PHP.S:hSYN1-XFP infected mice.
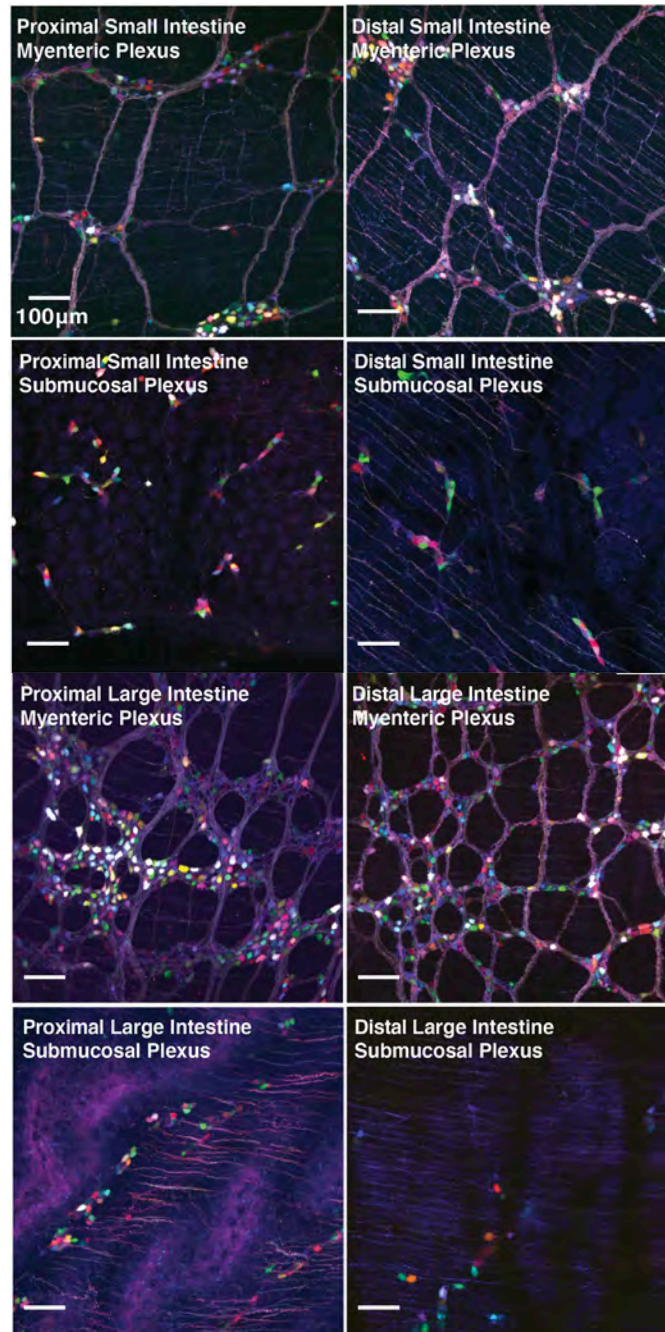
Figure 2B-2G

Quantification of neurons in 7 regions from the small intestine, and 2 regions from the large intestine, sampled proximally to distally (N = 3-4 mice per group, per intestinal region. Data points are averages from 2-3 images per mouse, per region; *: $p<0.05$, **: $p<0.01$, ***: $p<0.001$, ****: $p<0.001$, 2-way ANOVA with Sidak's multiple comparisons test)
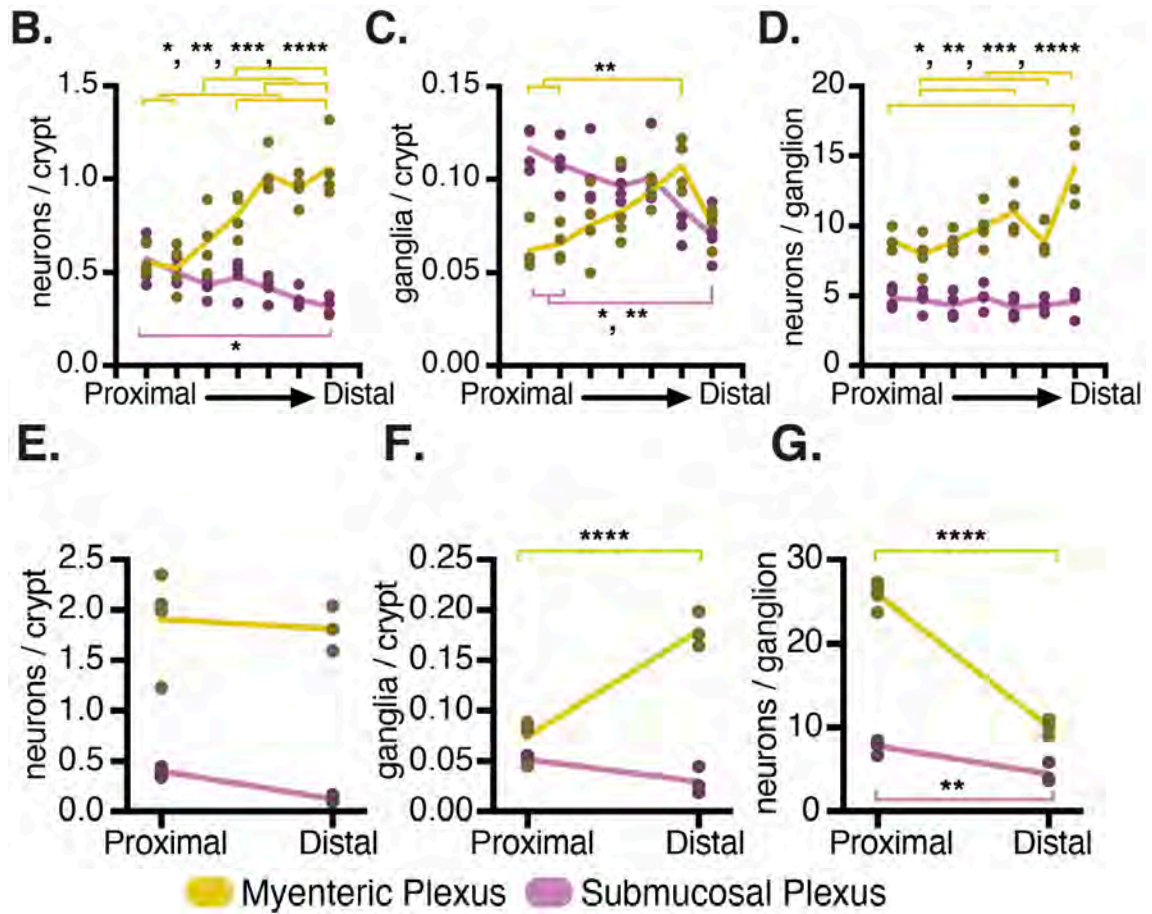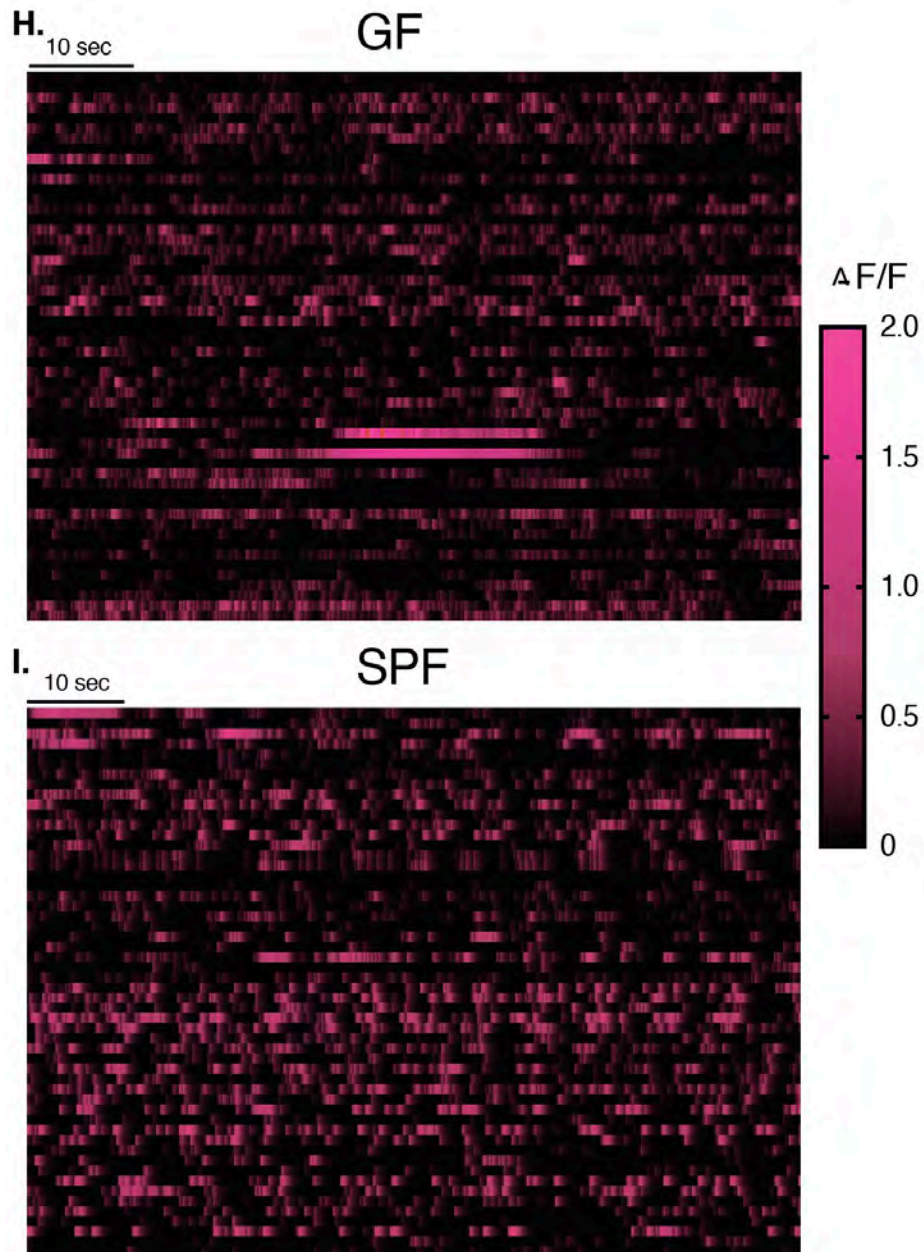
Figure 2H

Experimental setup to capture GCaMP6F fluorescence in a live, anesthetized animal.
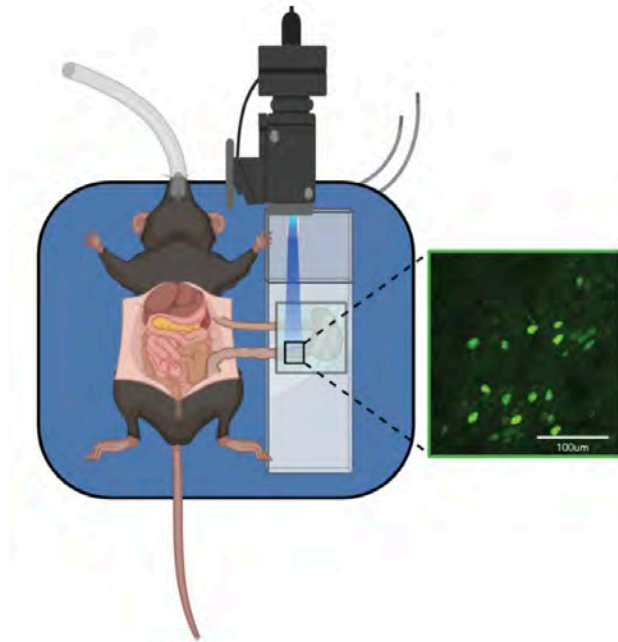
Figure 2I

Frequency distribution of calcium spike rate
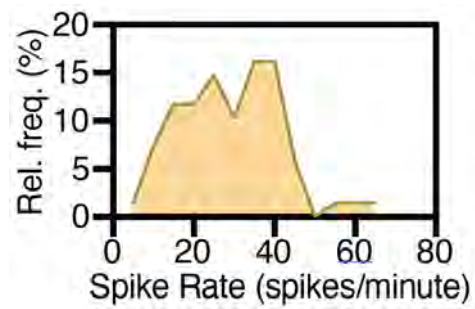
Figure 2J

Frequency distribution of calcium peak interval
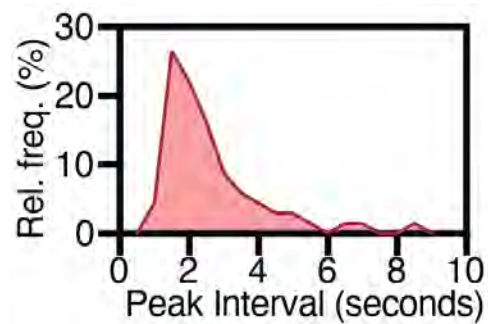
Figure 2K

Heatmap of GCaMP6F fluorescence (dF/F) over time. Each row represents fluorescent time course of a single cell. Data was cutoff at 83.64 seconds.
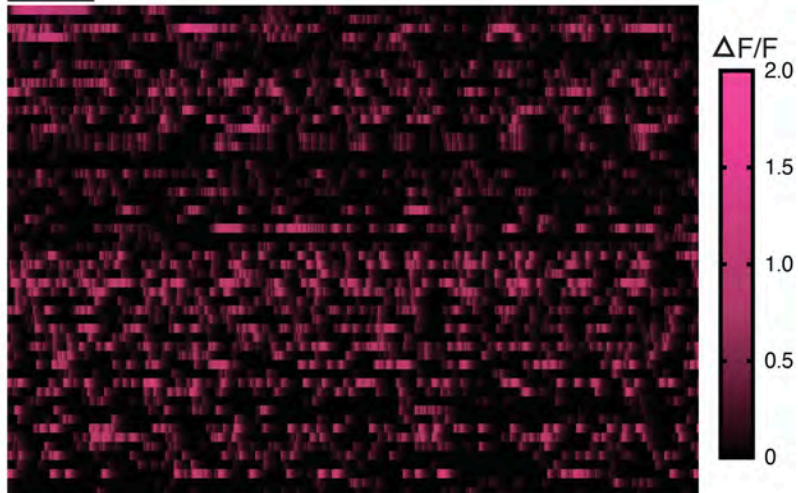
Figure 2L

Representative GCaMP6F fluorescent traces.
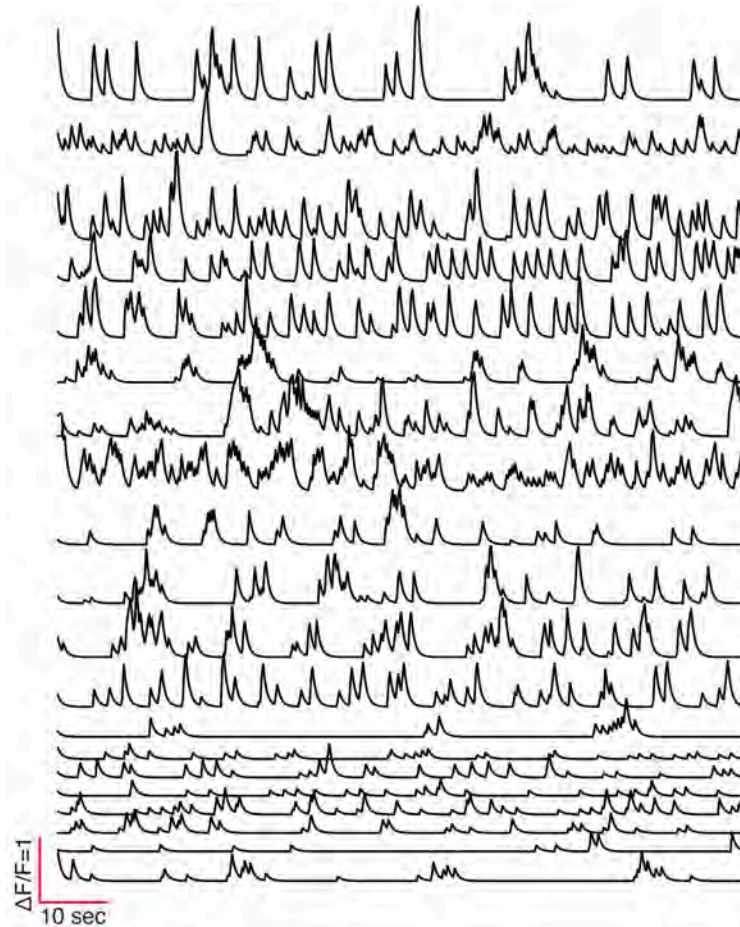
Figure 3. Microbiota influences ENS cellular architecture and activity

Figure 3A
Representative images from small intestines of PHPS-hSyn-XFP infected SPF and
GF mice.
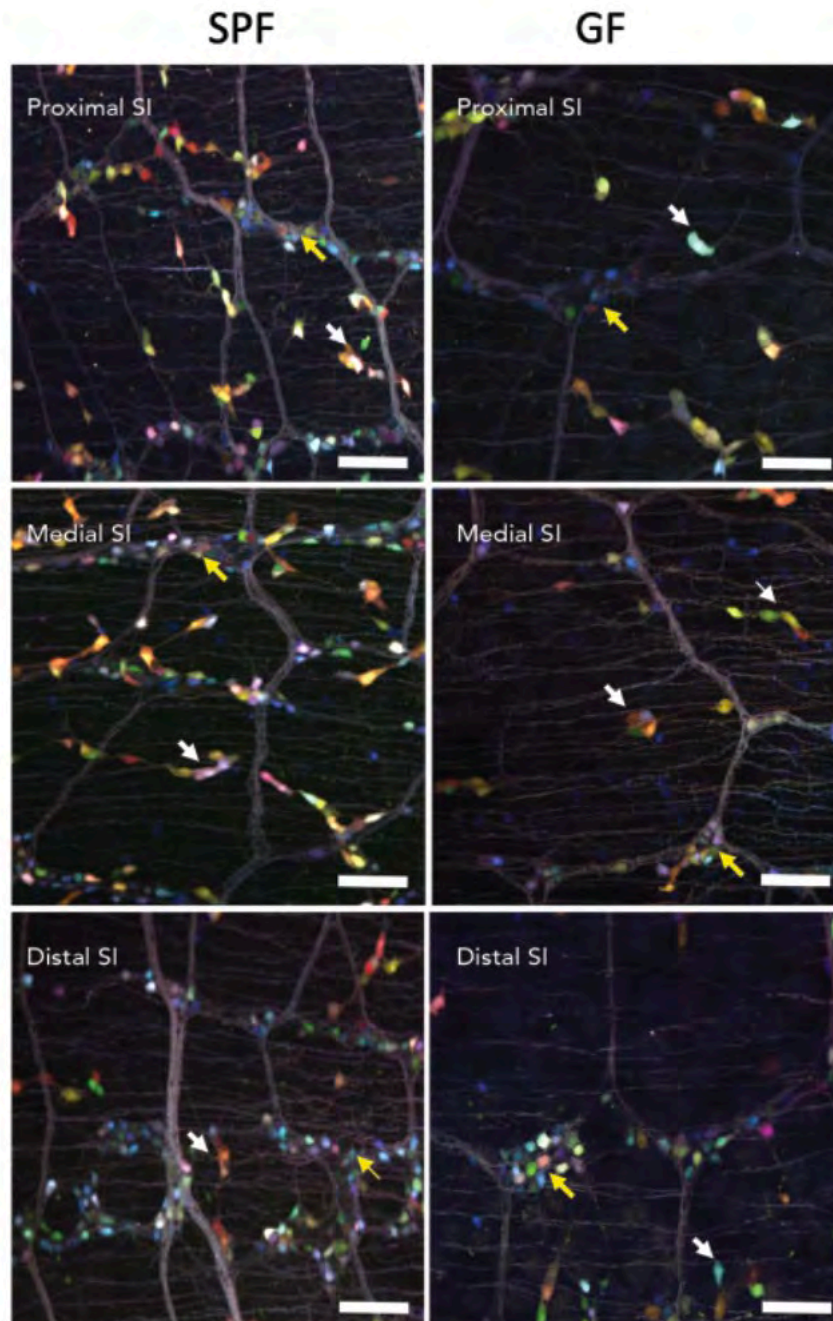
Figure 3B-3E

Quantification of neurons in 7 regions from the small intestine, and 3 regions from the large intestine, sampled proximally to distally (N = 3-4 mice per group, per intestinal region. Data points are averages from 2-3 images per mouse, per region; #: significance between regions, color of symbol corresponds to GF or SPF, *: significance between GF and SPF at each region; #,*: p<0.05, ##,**: p<0.01, ###,***: p<0.001, ####,****: p<0.001, 2-way ANOVA with Sidak's multiple comparisons test)
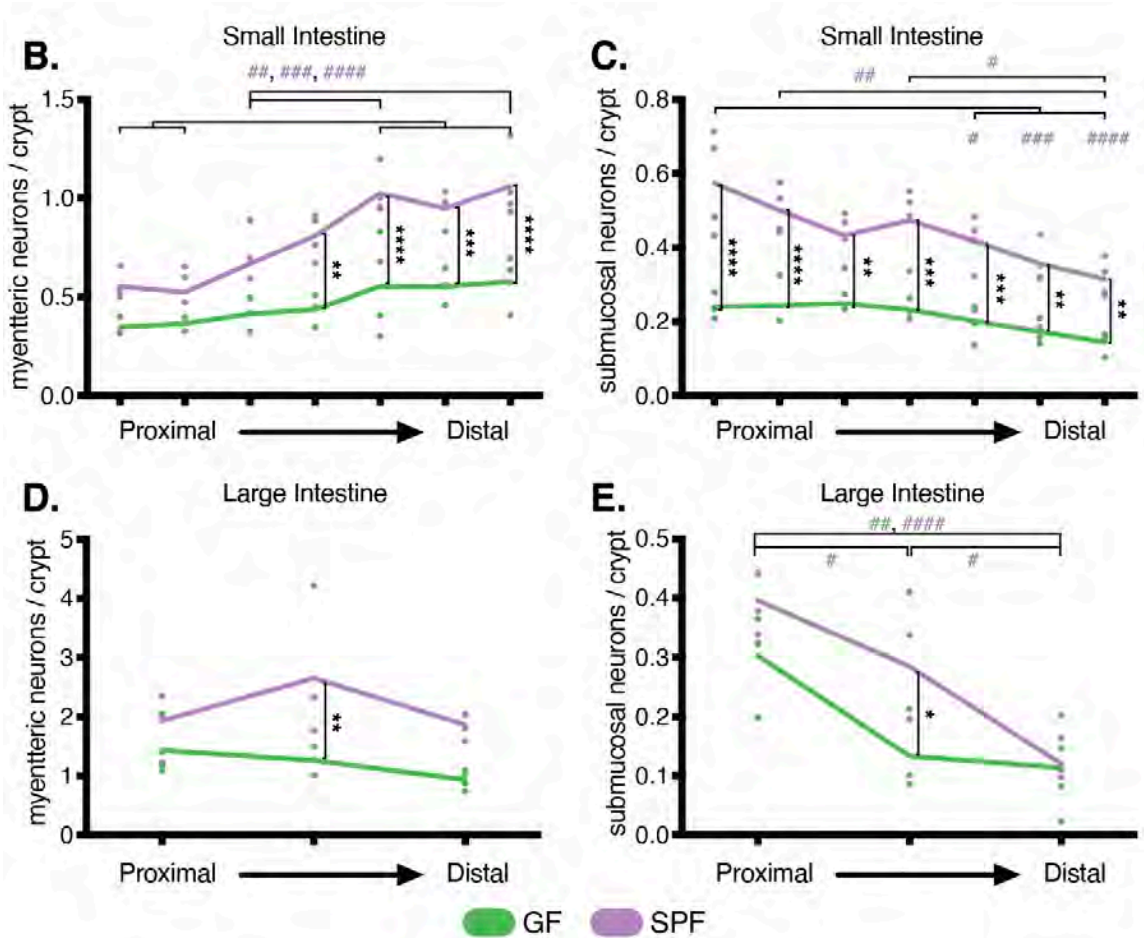
Figure 3F-3G

(F) Number of calcium peaks per minute (Data was collected from N = 54 (GF) – 68 (SPF) cells from 3 mice/group). (G) Frequency distribution of the average peak interval (time between calcium maxima) per cell. F-test measures significant differences in variances between groups. (Data was collected from N = 51 (GF) – 65 (SPF) cells from 3 mice/group, p-value determined from unpaired t-test with Welch's correction).
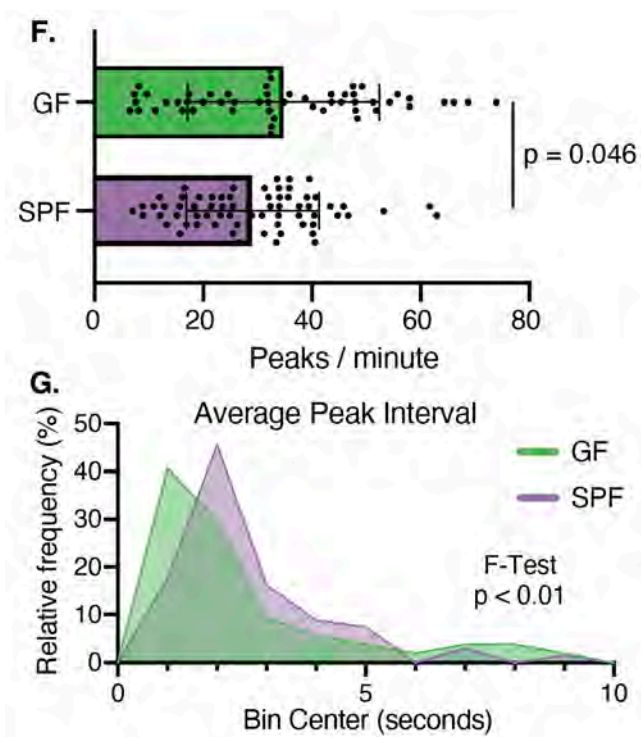
Figure 3H-3I

Heatmap of GCaMP6F fluorescence (dF/F) over time. Each row represents fluorescent time course of a single cell. Data was cutoff at 83.64 seconds.

Figure 4. Characterizing Enteric ChAT-Cre+ and TH-Cre+ Neurons and Assaying Activation-Mediated Transcriptomic Changes

Figure 4A
Representative images from cross sections (x-section), myenteric, and submucosal plexuses in ChAT-Cre and TH-Cre mice infected with AAV-PHP.S:hSYN1-DiO-XFP.
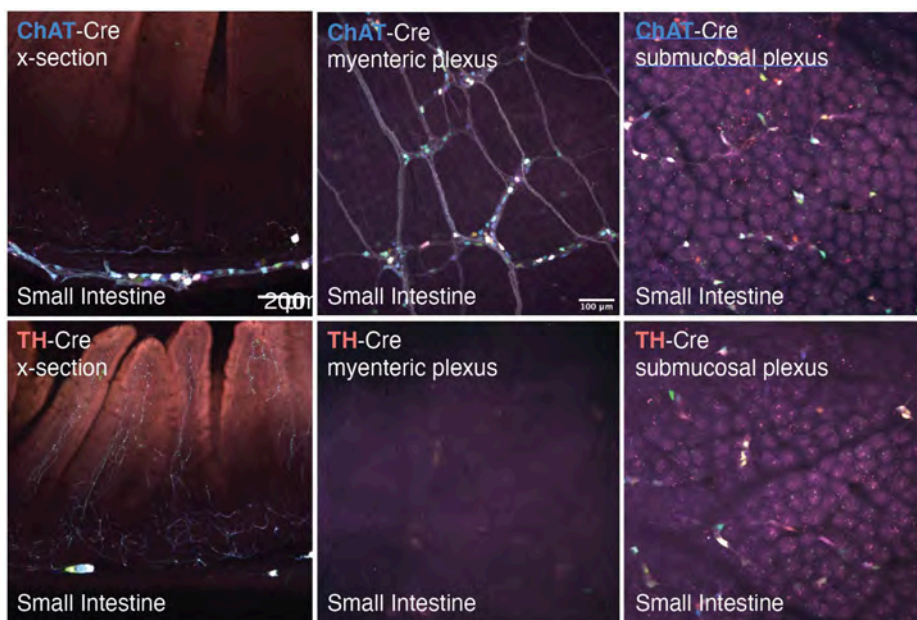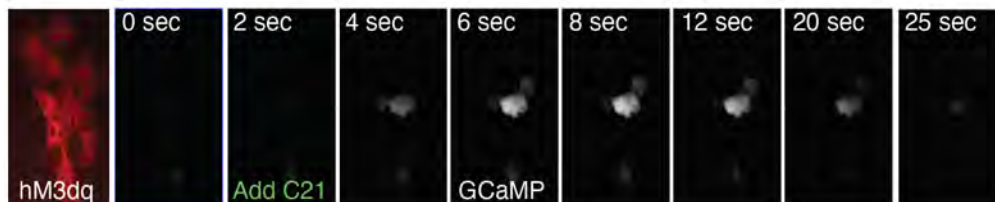

Figure 4B
Quantification of myenteric:submucosal cells ratio in ChAT- and TH-Cre mice. (N = 3 mice, each data point represent the average from 3 representative fields)
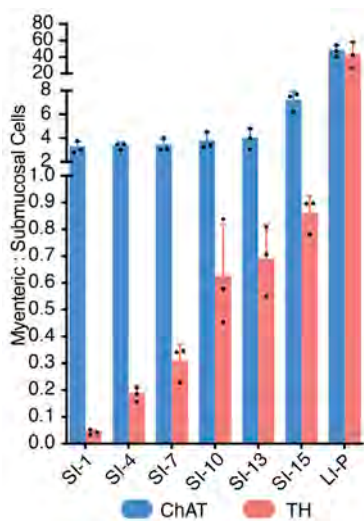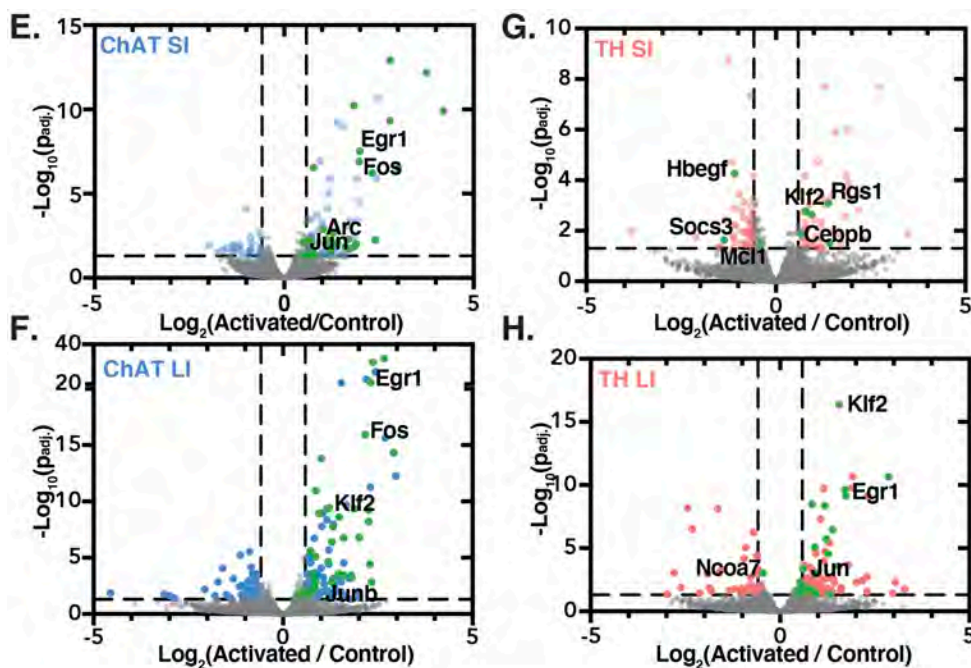
Figure 4C
Fluorescence time course of GCaMP6F in an *ex vivo* preparation of ChAT-Cre SI following C21 administration.

Figure 4D
Experimental paradigm- 10 consecutive days of C21 injections, with feces sampled in between and tissue and cecal contents collected at the end.
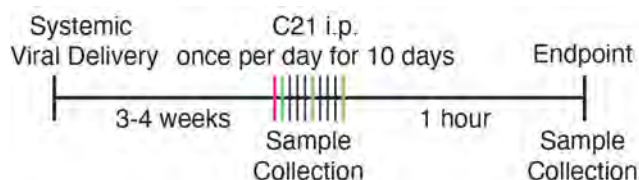

Figure 4E-4H
Volcano plots of differentially expressed genes in DREADD Activated vs Control, in (E) ChAT-Cre dSI, (F) ChAT pLI, (G) TH-Cre dSI, and (H) TH-Cre pLI. (Dotted vertical: Fold Change (FC) = +/- 1.5; Dotted horizontal: $p_{adjusted}$ <0.05. Annotated transcripts are IEGs and are highlighted in green. N = 10 mice per group)

Figure 4I
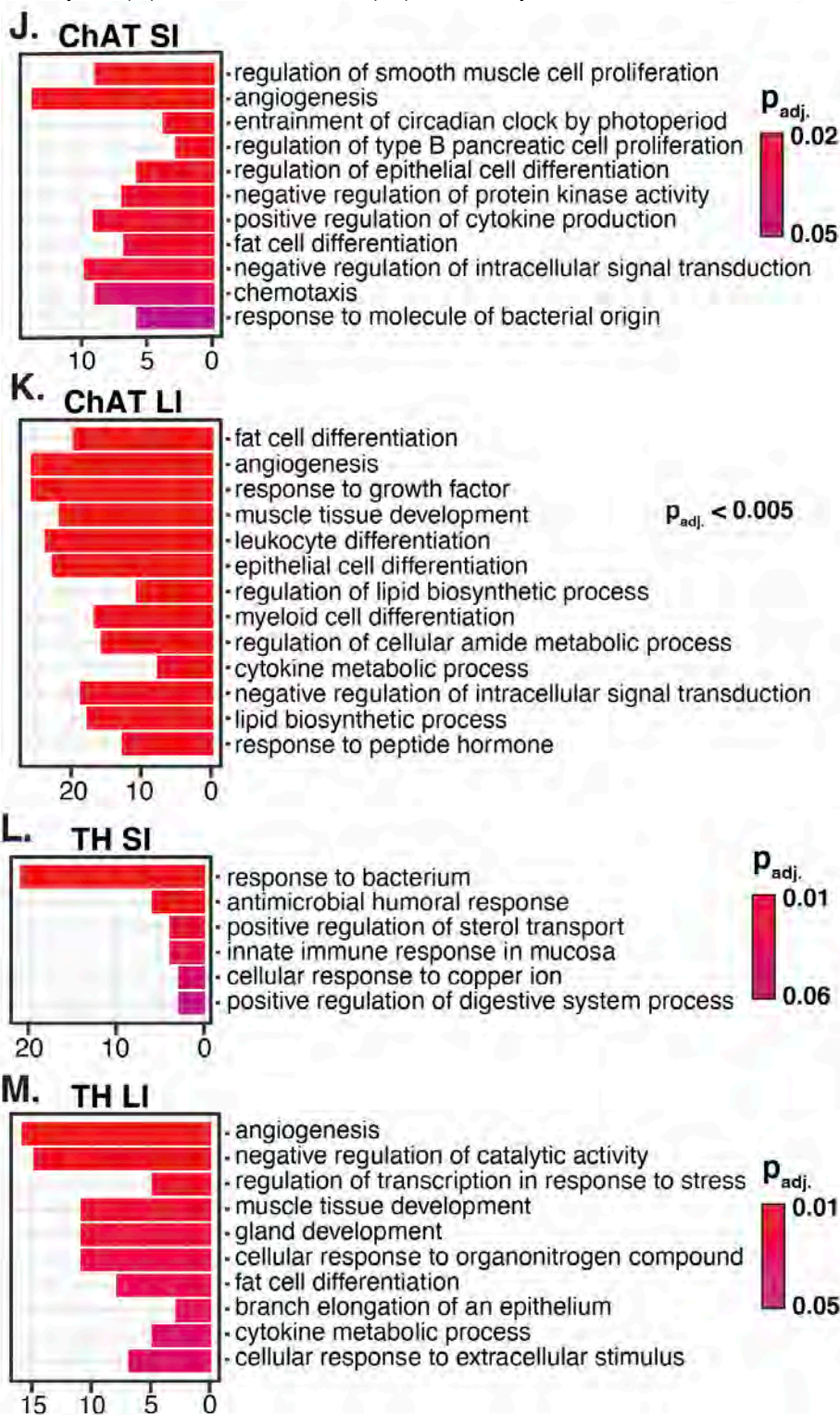Fold changes of upregulated IEGs ($p_{adj} < 0.05$) as defined by Wu et al. 2017 (31)
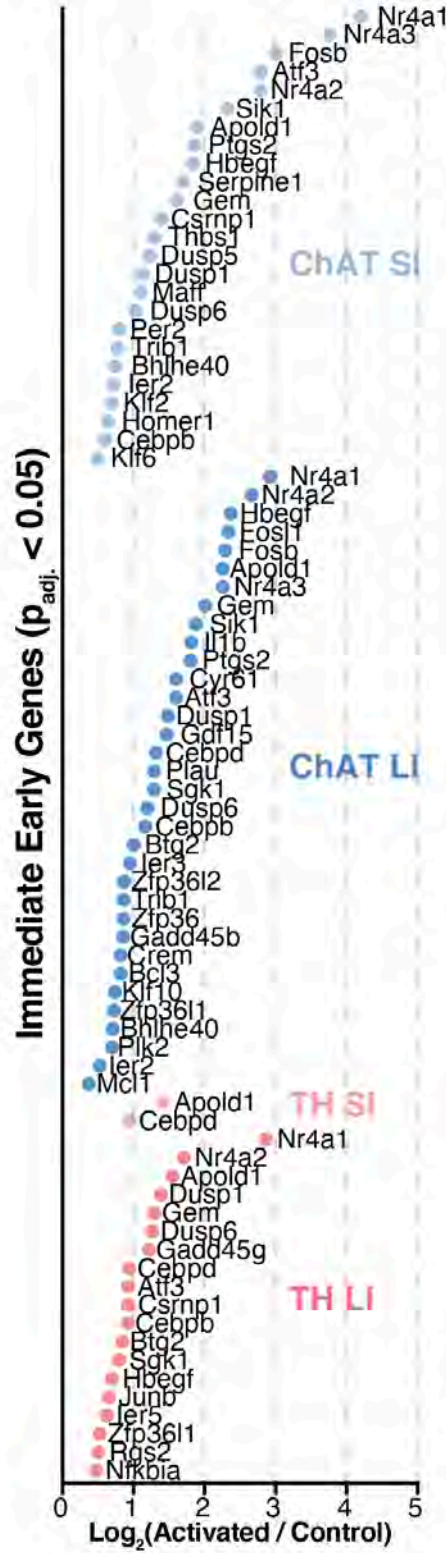
Figure 4J-4M

Gene set enrichment analysis of gene ontology (GO) terms for (J) ChAT-Cre dSI, (K) ChAT pLI, (L) TH-Cre dSI, and (M) TH-Cre pLI.

**Figure 5.** ENS Activation Alters Host and Microbe-Derived Luminal Proteins

Figure 5A
Volcano plot of differentially expressed host proteins identified in the cecal contents of Activated ChAT (N=8) vs. Control ChAT mice (N = 9 mice), 1 hour after C21 administration.
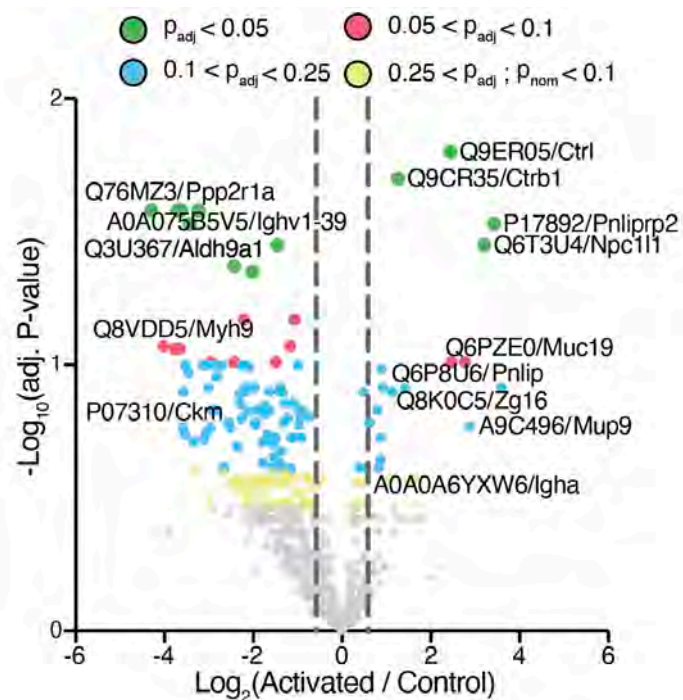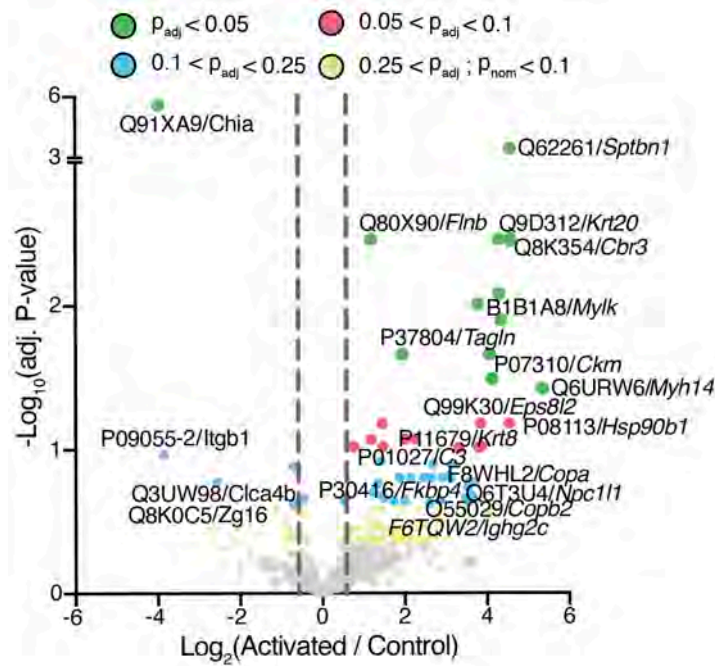

Figure 5B
STRING network analysis of host proteins that were more abundant in ChAT-activated mice ($p_{nom.} < 0.2$)
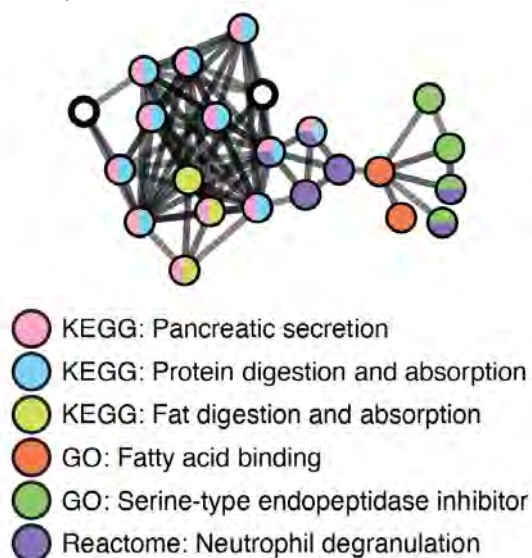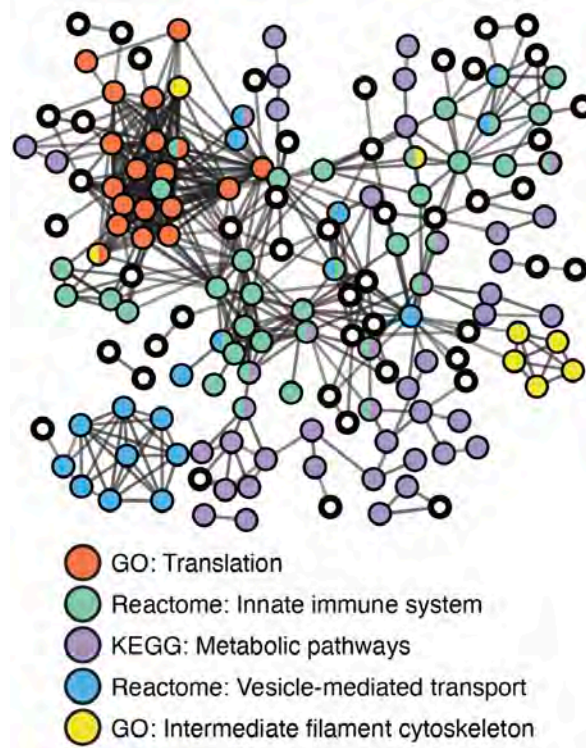
Figure 5C
Proteomic volcano plots of TH-activated vs. TH-control mice (N = 7 mice per group) after C21 administration

Figure 5D
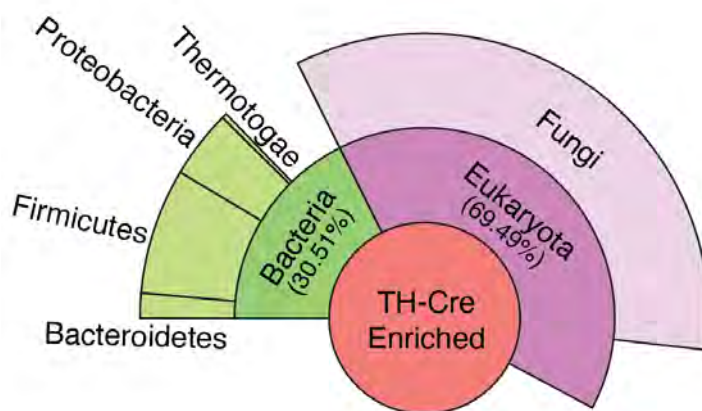STRING network analysis of upregulated host proteins in TH-activated mice ($p_{nom.} < 0.2$)

Figure 5E
Unipept metaproteomic analysis of upregulated microbial proteins ($p_{nom.} < 0.2$) in activated TH-Cre mice (N = 7-9 mice per group)
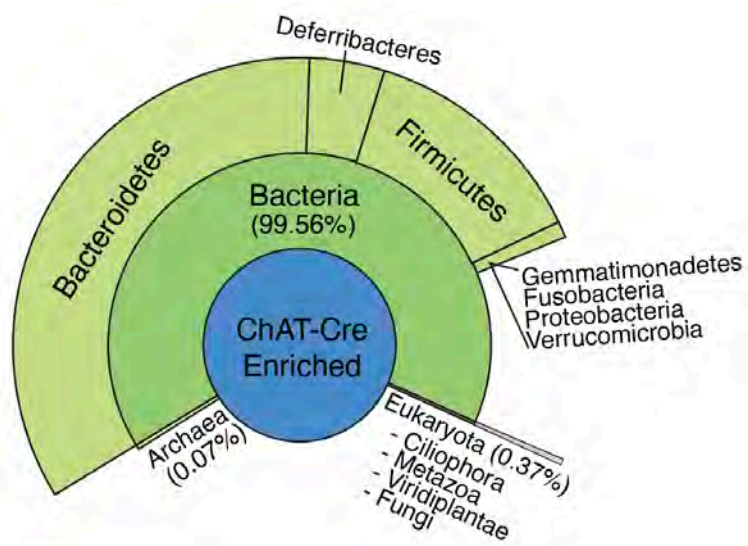

Figure 5F
Unipept metaproteomic analysis of upregulated microbial proteins ($p_{nom.} < 0.2$) in activated ChAT-Cre mice (N = 7-9 mice per group)

Figure 6. ENS Activation Alters the Microbiome

Figure 6A
Faith's phylogenetic diversity of feces and cecal contents over 10 days of neural activation in ChAT- and TH-Cre mice. Day -1 (1 day before first injection), Day +1/5/9 (1, 5, 9 days after first injection), Day +10 (Cecal contents collected at experimental endpoint) (**p<0.01, ***p<0.001 determined by Kruskal-Wallis 1-way ANOVA).
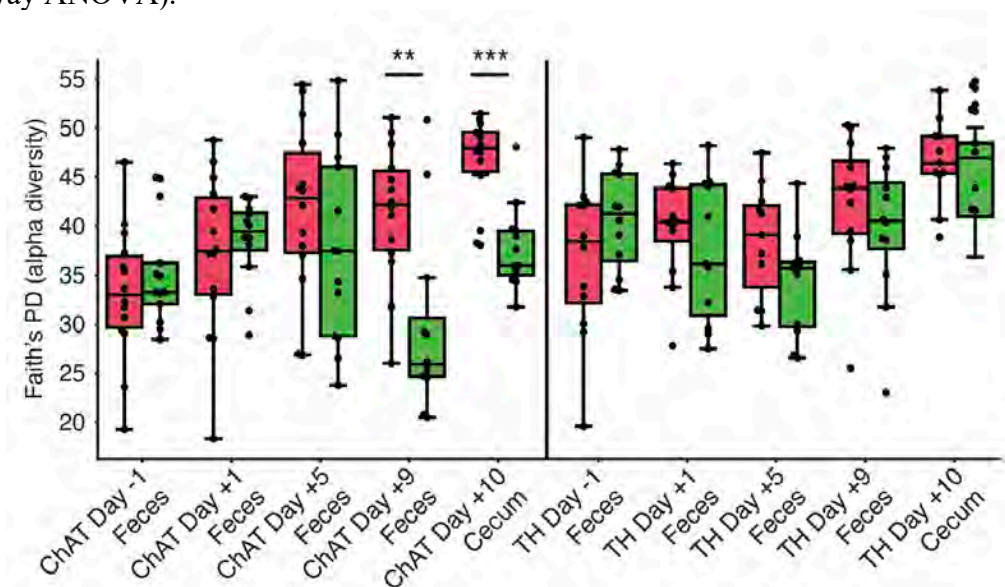
Figure 6B-6G
Weighted UniFrac principle coordinate analysis (PCA) of Activated vs. Control in ChAT- and TH-Cre mice with PERMANOVA p-values.
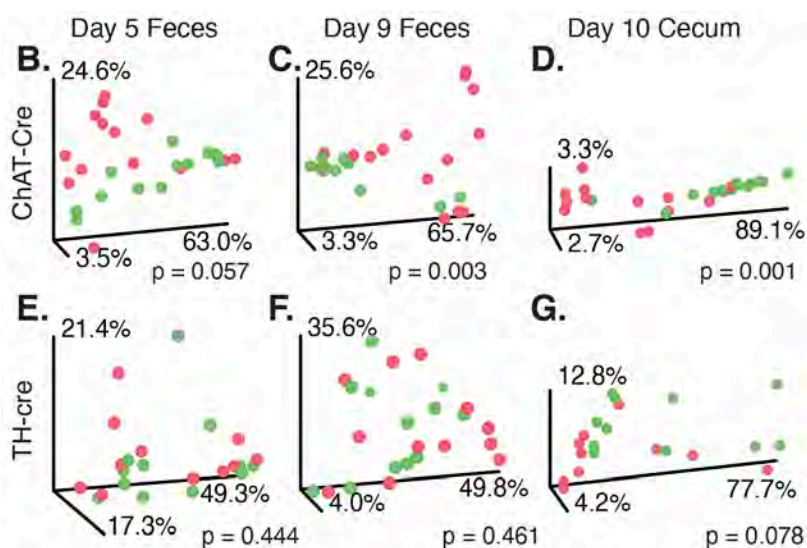
Figure 6H
Stacked bar graph showing phylum level changes in relative abundance, 5 and 9 days post-injection in feces and 10 days post-injection in cecal contents.
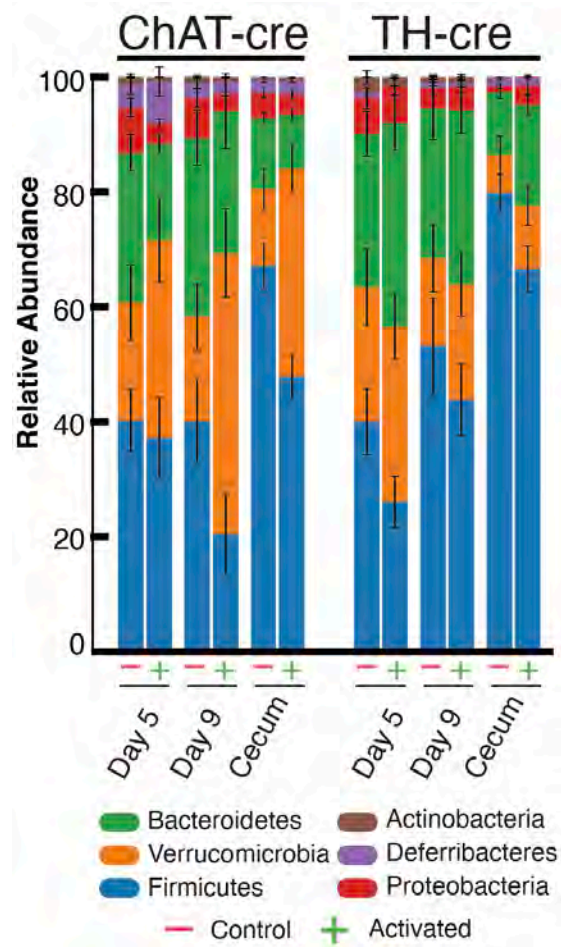
Figure 6I-6L

Cecal Microbiome LDA Effect Size (LEfSe) Analysis: (I,K) Cladograms showing differential phylogenetic clusters and (J,L) LDA plots of family level differences between Activated and Control mice (Cutoff: $\log_{10}$(LDA Score) > 2 or < -2) in (I,J) ChAT-Cre and (K,L) TH-Cre mice
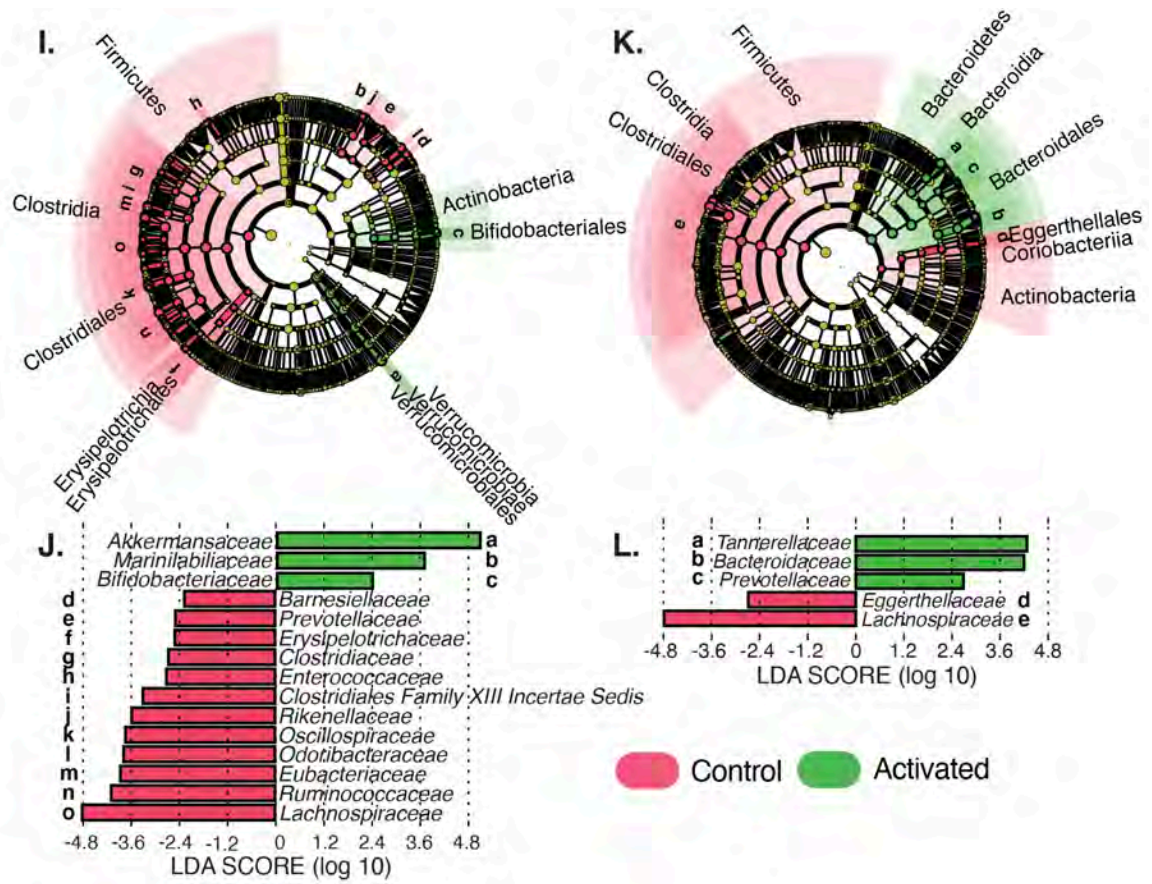
Figure 6M-6N

Changes in relative abundance of *Akkermansia muciniphila* in feces and cecal contents of (M) ChAT-Cre and (N) TH-Cre mice. (n = 11-14 mice per group, per time point; red=control, green=hM3Dq-Activated, *p<0.05, **p<0.01, significance determined by multiple t-tests with Holm-Sidak correction for multiple comparisons)
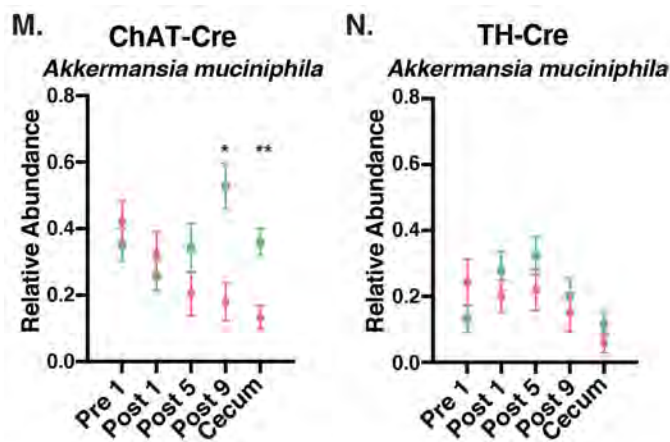
Figure 6O-6R

Beta-diversity of bacterial gene families and pathways in the (O-Q) cecum and (P-R) post-9 feces of control and activated mice. Diversity was determined with Aitchison's PCA and analyzed using the DEICODE toolbox. The direction of defining features is indicated with colored arrows. These gene families and pathways are annotated by the color of the feature arrow (Supplemental Figure 6C and 6D)
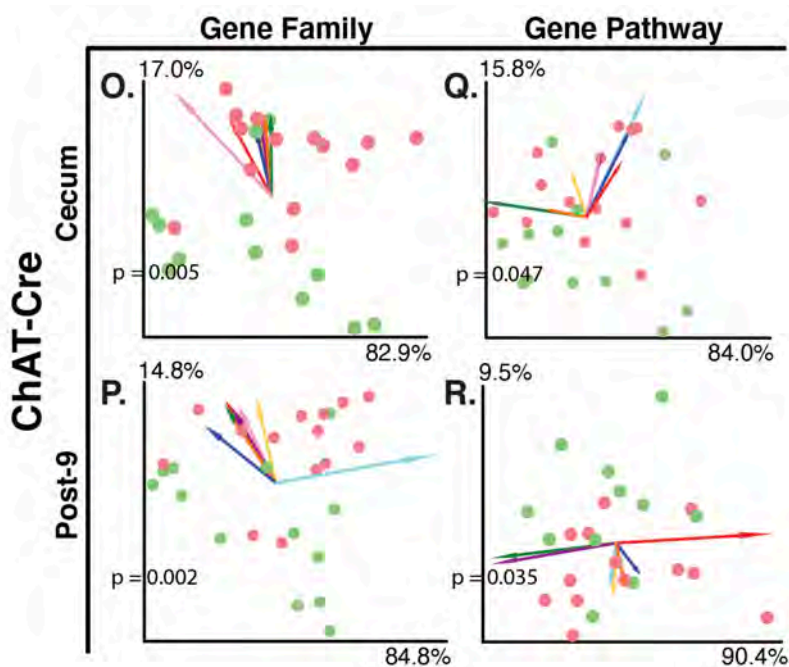
Figure 7. ENS Activation Alters the Host and Microbe-Derived Luminal
Metabolites

Figure 7A-7J
Canberra PCA of the cell-free, luminal metabolome of control (red) and activated
(green) cecal contents in ChAT-Cre and (B) TH-Cre mice. (C-J) Fecal metabolome
assayed at different timepoints before and after C21 administration in (C-F) ChAT-
Cre and (G-J) TH-Cre mice.
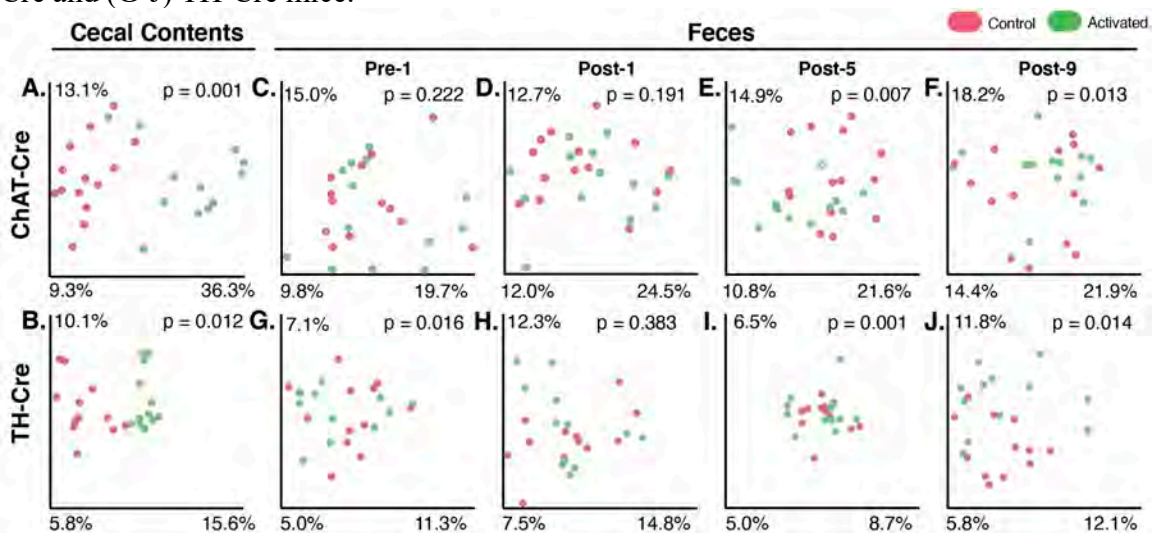
Figure 7K-7L

Metabolic networks constructed from identified cecal metabolites in (K) ChAT-Cre and (L) TH-Cre mice. Each node is labelled with an ID number, corresponding to annotations, mass-to-charge ratios, rentention times, fold changes, and significance values found in Supplemental Table 1. Each node is colored by its upregulation (green) or downregulation (red) in activated groups. IDs in bold text have an annotation in GNPS and are colored by classes class of metabolite (primary bile acids, secondary bile acids, and other metabolites). Metabolite IDs are distinct by genotype (N = 12-14 for each group analyzed, *: p<0.05, **: p<0.01)
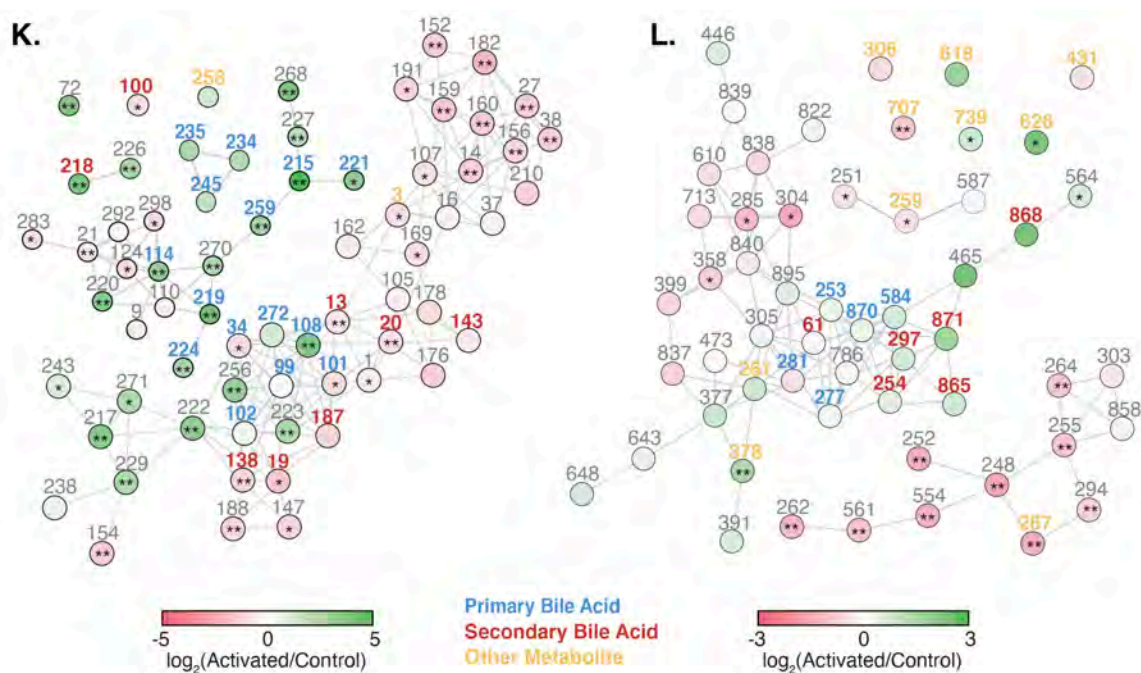
Figure 8. ENS Activation Alters Gross GI Physiologies

Figure 8A and 8B
Scatter plot of %(water content) of individual fecal pellets. (A) TH-Cre (B) ChAT-Cre mice 0-5 hours post C21 administration. (N = 10 mice per group, > 4 fecal pellets collected per mouse over 5 hour period)
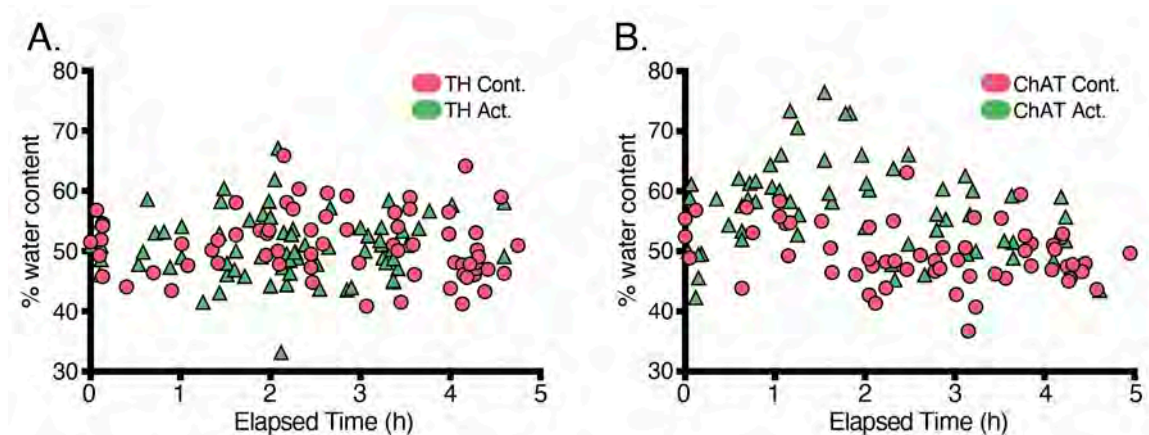
Figure 8C-8F
Linear regressions of %(water content) data from 0-2 hours (C) TH control vs. TH activated (D) ChAT control vs. ChAT activated (E) TH control vs. ChAT control (F) TH activated vs. ChAT activated . (N = 10 mice per group, > 4 fecal pellets collected per mouse over 5 hour period, p-values correspond to slopes of line of best fit)
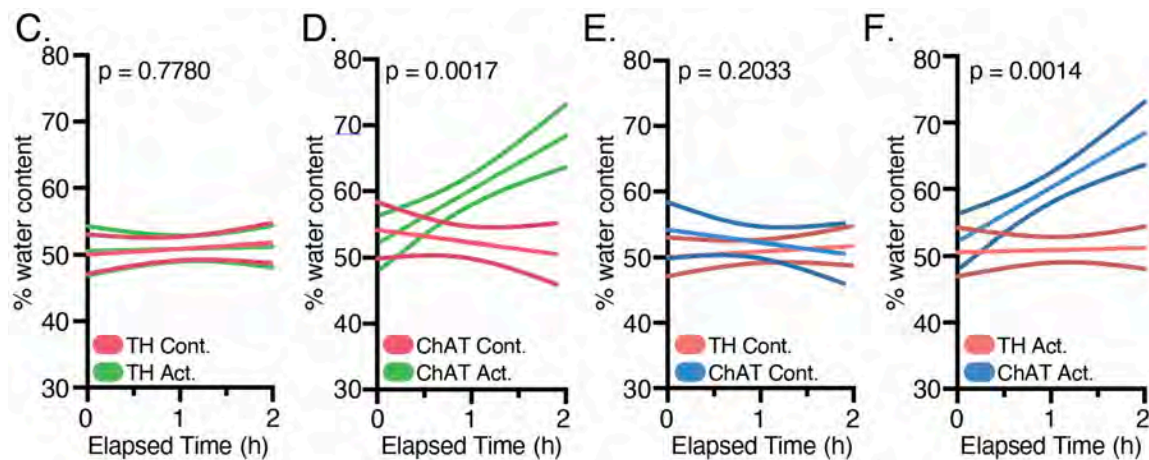
Figure 8G-8K

(G) Average %(water content) of feces from mice over a 5 hour period following C21 administration. (H) Mass Ratio of cecal contents : animal, 1 hour post C21 administration (I) GI transit time upon C21 administration. (J) Average fecal output rate upon C21 administration (G-J: N = 10-11 mice per group, statistics performed: 2way ANOVA with Sidak's method for multiple comparisons)
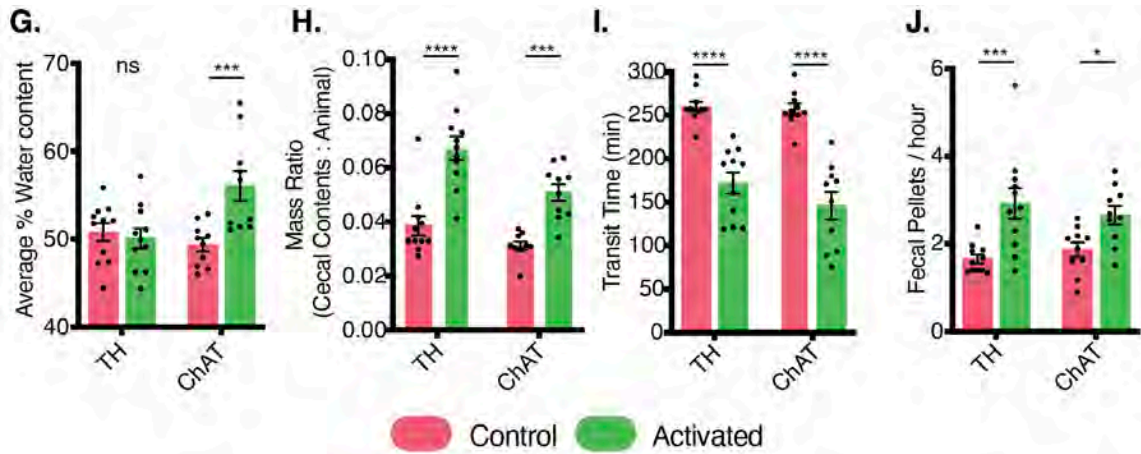
Supplemental Figures, Tables, and Legends

Supplemental Figure 1. Viral Labeling Enables a Holistic Understanding of the ENS

Supplemental Figure 1A-1D
(A-B) Tiled images of the ENS in the mouse small intestine. Mice are infected with AAV-PHP.S:hSYN1-XFP (C) Inset of panel (A) showing extrinsic nerves and neurons connecting to intrinsic ganglia of the ENS (D) Inset of panel (B) showing alterations to ENS architecture surrounding intestinal lymphoid follicles such as Peyer's patches
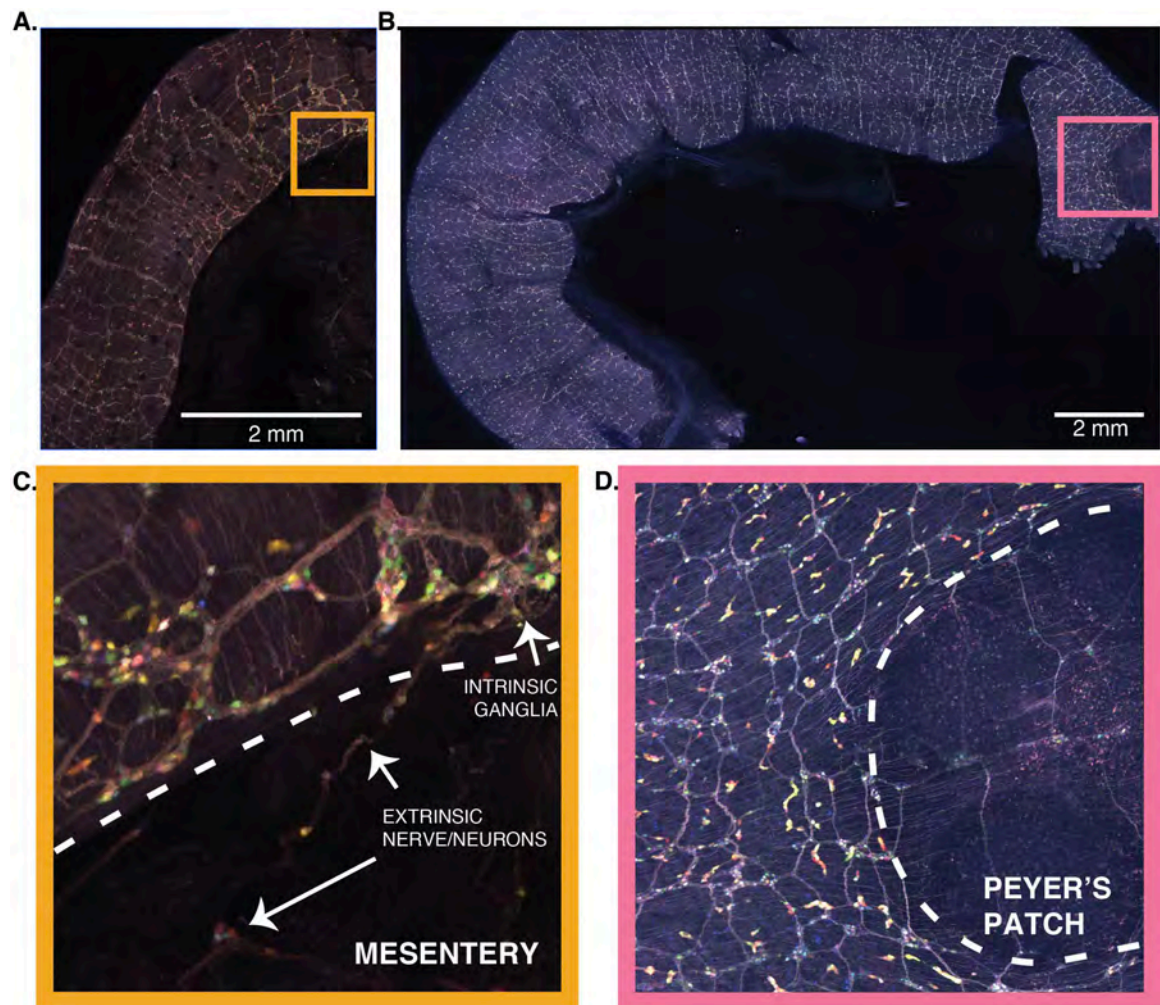
Supplemental Figure 1E-1G

(E) Tiled image of the ENS in the large intestine with insets showing how the (F) absence or (G) presence of luminal contents changes the appearance of neuronal density in the ENS.
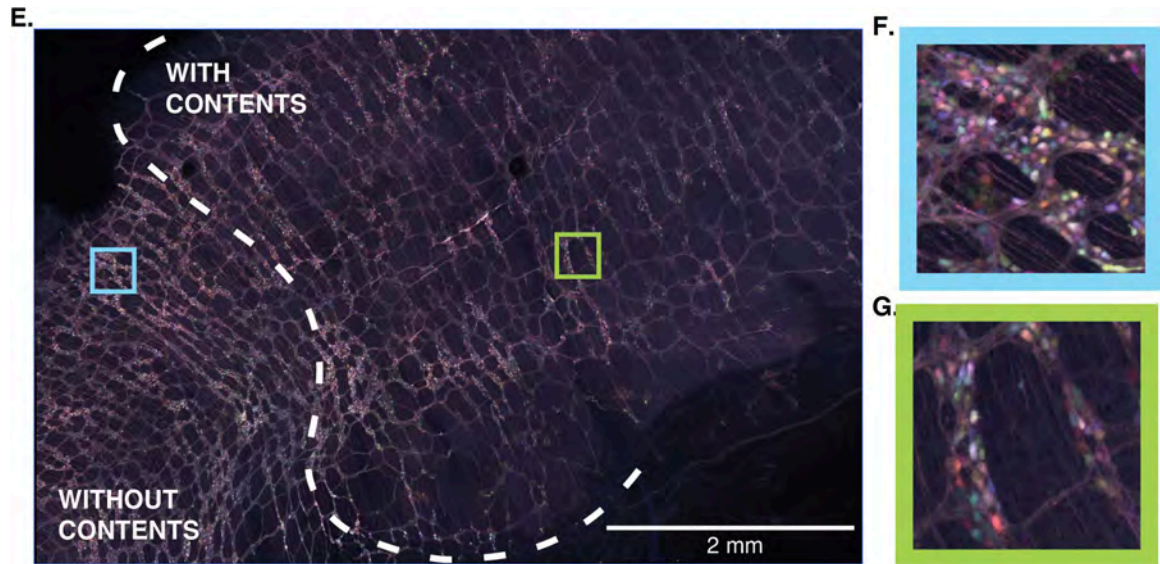
Supplemental Figure 2. Similar Viral Transduction Along the GI Tract

Supplemental Figure 2A and 2B
(A) Quantification (qPCR) of AAV transduction in different regions of the mouse small and large intestines (B) Diameter (μm) of intestinal crypts in small and large intestines (N=3-4 mice per group)
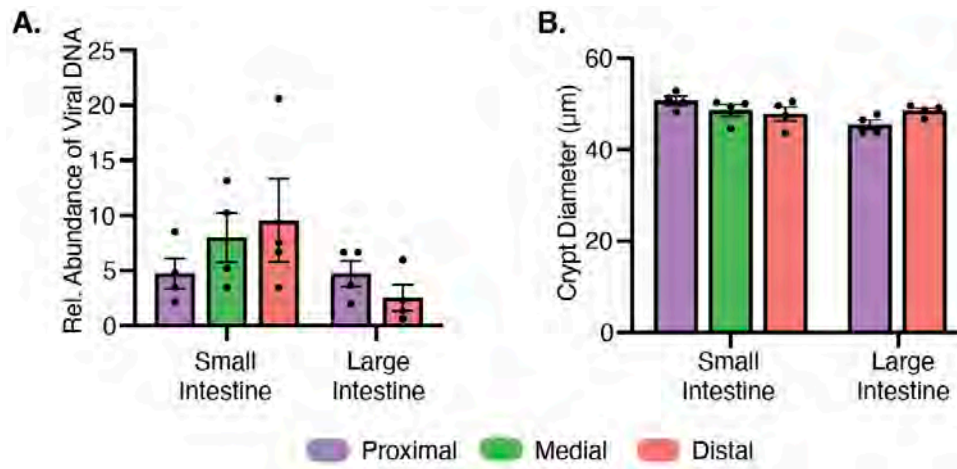
Supplemental Figure 3. Similar Viral Transduction in GF and SPF Mice

Supplemental Figure 3A and 3B
(A) qPCR of Viral DNA in GF and SPF mice in small and large intestines (B) Diameter (μm) of intestinal crypts in small and large intestines (N=3-4 mice per group)
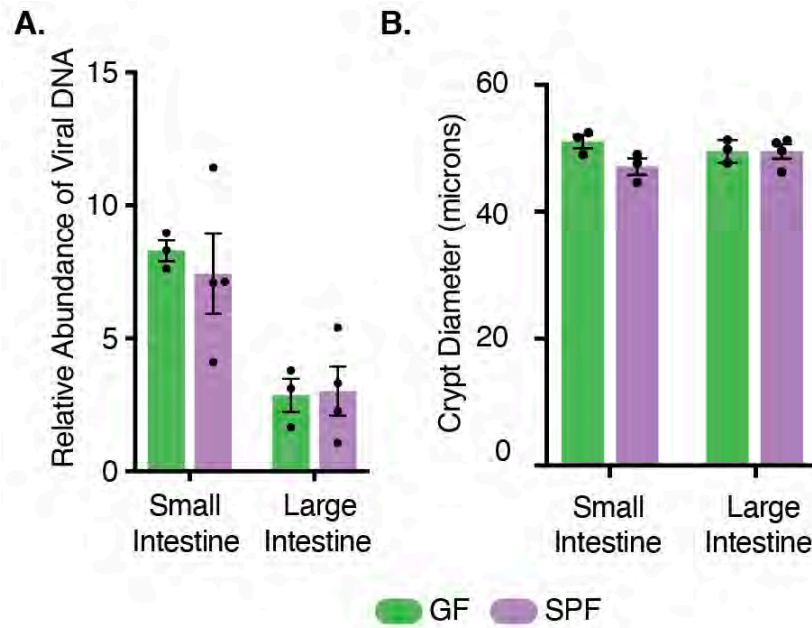
Supplemental Figure 4. AVNM Antibiotic Treatment Mirrors GF ENS Phenotype

Supplemental Figure 4A-4F

(A-F) Quantification of myenteric and submucosal neurons in GF, SPF, and antibiotic treated animals. (A,B) GF and SPF data is same data as presented in Figure 2 of manuscript. Experimental groups were conducted in parallel. (A) Myenteric and (B) submucosal neurons normalized by the number of crypts. (C) Myenteric and (D) submucosal neurons per ganglion. (E) Myenteric and (F) submucosal ganglia normalized by the number of crypts. GF: Germ Free, SPF: Specific pathogen free, 8wk-ABX: SPF AVNM treatment at 8 weeks of age, 3wk-ABX: SPF AVNM treatment at 3 weeks of age, GF-pABX: prenatal GF AVNM treatment, SPF-pABX: prenatal SPF AVNM treatment. 2way ANOVA with Dunnett's multiple comparisons tests to SPF group. N = 3-4 mice per group, per intestinal region. Values are averages from 2-3 images quantified per animal per region.
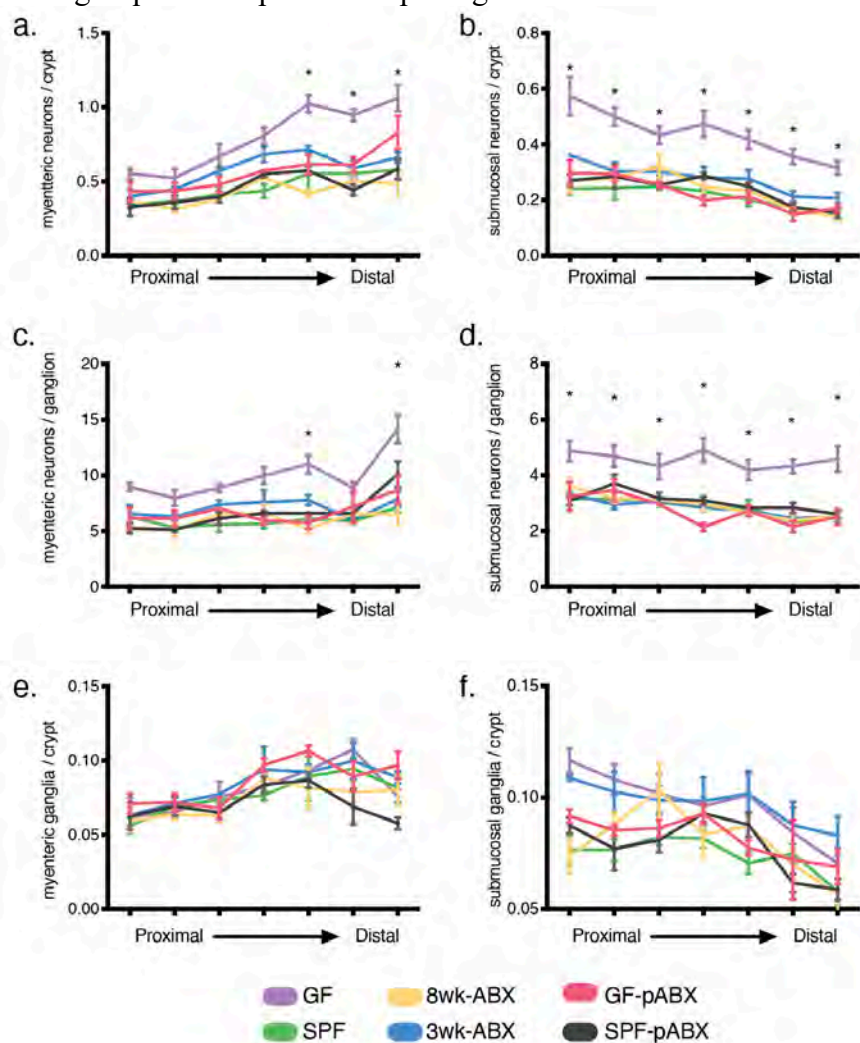
Supplemental Figure 5. GF and SPF ENS Activity Differs

Supplemental Figure 5A-5D
(A) Average, background-subtracted fluorescence for each cell over the duration of recording. (B) Time between all calcium peaks recorded from all cells. (C-D) Representative fluorescent traces of (C) GF and (D) SPF mice infected with PHPS-CAG-GCaMP6F.
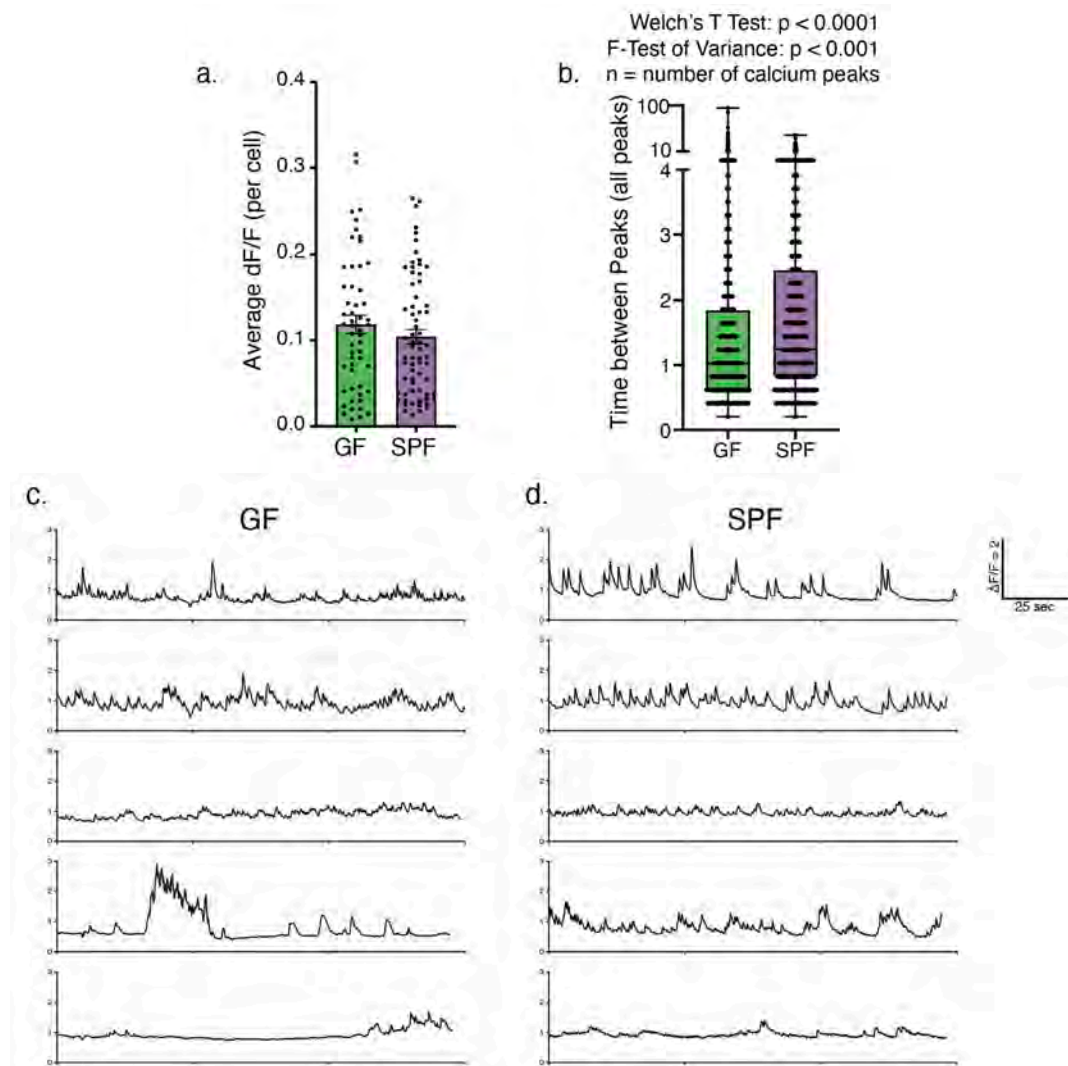
Supplemental Figure 6- Microbial GO terms Annotated from Luminal Proteins

Supplemental Figure 6A
Enriched GO terms for enriched proteins in the metaproteome identified in the
cecal contents of TH-Cre mice corresponding to Unipept analysis in Figure 4E

Count	% of Total	GO term	Name
TH-Cre Enriched Bacterial Proteins
31	17.92	GO:0071973	bacterial-type flagellum-dependent cell motility
13	7.51	GO:0005975	carbohydrate metabolic process
11	6.36	GO:0045454	cell redox homeostasis
8	4.62	GO:0032784	regulation of DNA-templated transcription, elongation
6	3.47	GO:0000160	phosphorelay signal transduction system
3	1.73	GO:0005978	glycogen biosynthetic process
2	1.16	GO:0016114	terpenoid biosynthetic process
2	1.16	GO:0050992	dimethylallyl diphosphate biosynthetic process
2	1.16	GO:0019288	isopentenyl diphosphate biosynthetic process, methylerythritol 4-phosphate pathway

Supplemental Figure 6A (continued)

Count	% of Total	GO term	Name
TH-Cre Enriched Eukaryotic Proteins			
176	44.67	GO:0006113	fermentation
77	19.54	GO:0006886	intracellular protein transport
77	19.54	GO:0016192	vesicle-mediated transport
75	19.04	GO:0006898	receptor-mediated endocytosis
71	18.02	GO:0006895	Golgi to endosome transport
52	13.20	GO:0006457	protein folding
30	7.61	GO:0051301	cell division
11	2.79	GO:0051228	mitotic spindle disassembly
11	2.79	GO:0030866	cortical actin cytoskeleton organization
9	2.28	GO:0006897	endocytosis
8	2.03	GO:0030433	ubiquitin-dependent ERAD pathway
8	2.03	GO:0030970	retrograde protein transport, ER to cytosol
8	2.03	GO:0071712	ER-associated misfolded protein catabolic process
5	1.27	GO:0016236	macroautophagy
5	1.27	GO:0097352	autophagosome maturation
5	1.27	GO:0006511	ubiquitin-dependent protein catabolic process
5	1.27	GO:0051306	mitotic sister chromatid separation
5	1.27	GO:0061166	establishment of endoplasmic reticulum localization involved in endoplasmic reticulum polarization at cell division site
5	1.27	GO:0035103	sterol regulatory element binding protein cleavage
5	1.27	GO:0034067	protein localization to Golgi apparatus

Supplemental Figure 6B
Enriched GO terms for enriched proteins in the metaproteome identified in the cecal
contents of ChAT-Cre mice corresponding to Unipept analysis in Figure 4F

ChAT-Cre Enriched Bacterial Proteins			
Count	% of Total	GO term	Name
161	11.89	GO:0005975	carbohydrate metabolic process
160	11.82	GO:0006096	glycolytic process
142	10.49	GO:0006094	gluconeogenesis
109	8.05	GO:0022900	electron transport chain
47	3.47	GO:0045333	cellular respiration
34	2.51	GO:0006457	protein folding
32	2.36	GO:0006012	galactose metabolic process
32	2.36	GO:0006090	pyruvate metabolic process
30	2.22	GO:0071973	bacterial-type flagellum-dependent cell motility
30	2.22	GO:0006044	N-acetylglucosamine metabolic process
29	2.14	GO:0019652	lactate fermentation to propionate and acetate
27	1.99	GO:0006091	generation of precursor metabolites and energy
26	1.92	GO:0006536	glutamate metabolic process
26	1.92	GO:0042026	protein refolding
23	1.70	GO:0030388	fructose 1,6-bisphosphate metabolic process
23	1.70	GO:0006007	glucose catabolic process
21	1.55	GO:0009097	isoleucine biosynthetic process
19	1.40	GO:0006189	'de novo' IMP biosynthetic process
18	1.33	GO:0019594	mannitol metabolic process
16	1.18	GO:0006108	malate metabolic process
16	1.18	GO:0019752	carboxylic acid metabolic process
16	1.18	GO:0006099	tricarboxylic acid cycle
15	1.11	GO:0009099	valine biosynthetic process
15	1.11	GO:0019262	N-acetylneuraminate catabolic process

Supplemental Figure 6B (continued)

12	0.89	GO:0006633	fatty acid biosynthetic process
12	0.89	GO:0006006	glucose metabolic process
9	0.66	GO:0006082	organic acid metabolic process
9	0.66	GO:0006085	acetyl-CoA biosynthetic process
9	0.66	GO:0006412	translation
7	0.52	GO:0006662	glycerol ether metabolic process
7	0.52	GO:0045454	cell redox homeostasis
6	0.44	GO:0009058	biosynthetic process
6	0.44	GO:0006564	L-serine biosynthetic process
6	0.44	GO:0008615	pyridoxine biosynthetic process
6	0.44	GO:0019877	diaminopimelate biosynthetic process
6	0.44	GO:0071266	'de novo' L-methionine biosynthetic process
6	0.44	GO:0009089	lysine biosynthetic process via diaminopimelate
6	0.44	GO:0009088	threonine biosynthetic process
4	0.30	GO:0009082	branched-chain amino acid biosynthetic process
3	0.22	GO:0000272	polysaccharide catabolic process
3	0.22	GO:0032259	methylation
3	0.22	GO:0055085	transmembrane transport
2	0.15	GO:0006438	valyl-tRNA aminoacylation
2	0.15	GO:0045493	xylan catabolic process
2	0.15	GO:0006310	DNA recombination
2	0.15	GO:0051301	cell division
2	0.15	GO:0006281	DNA repair
2	0.15	GO:0006260	DNA replication
2	0.15	GO:0006538	glutamate catabolic process
2	0.15	GO:0033611	oxalate catabolic process

Supplemental Figure 7. Annotated Changes to Gut Bacteria

Supplemental Figure 7A
Species-level enrichment of cecal bacteria in activated and control ChAT-Cre mice (corresponding to main text Figure 6I). Sampled 10 days after initial C21 injection
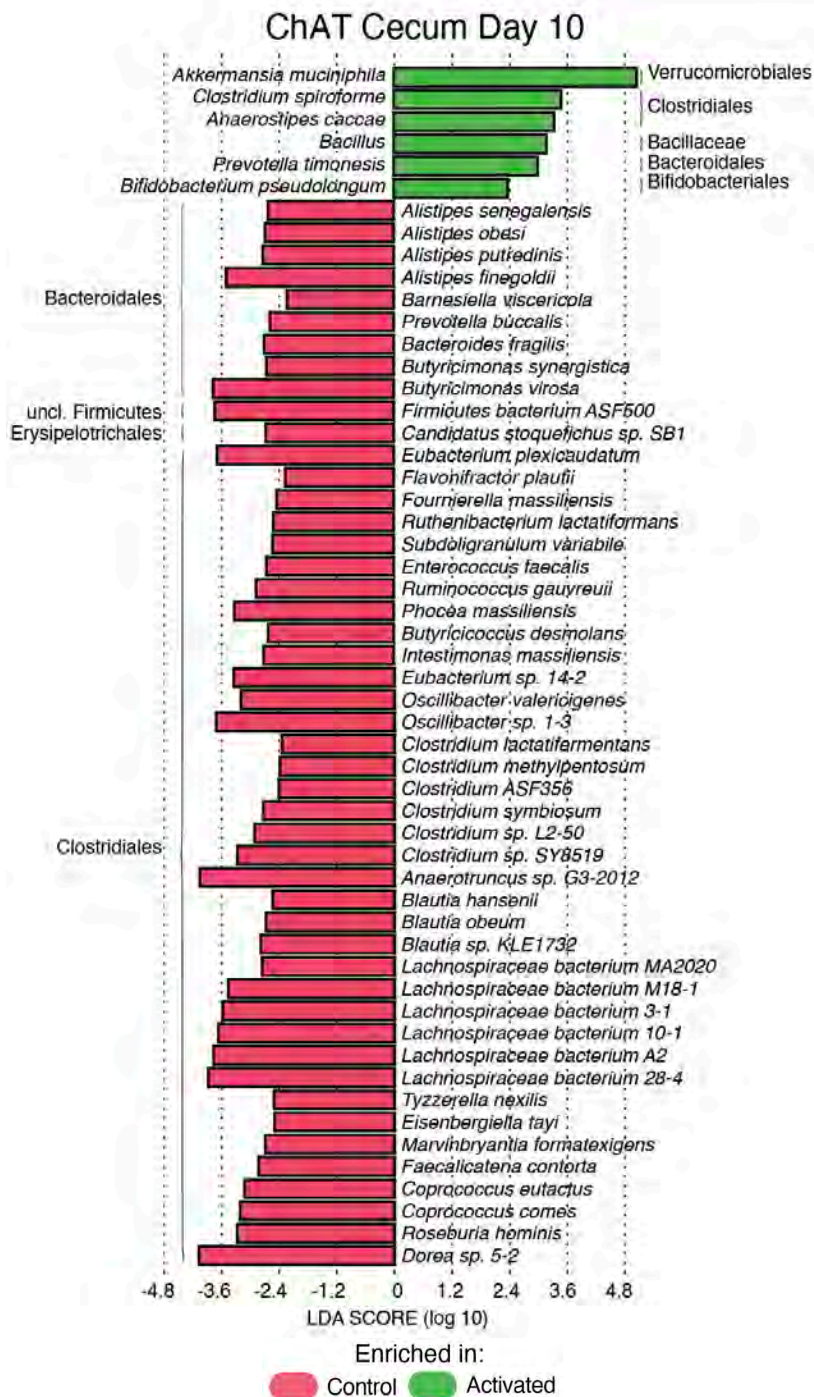
Supplemental Figure 7B

Species-levels enrichment of cecal bacteria in activated and control TH-Cre mice (corresponding to main text Figure 6J). Sampled 10 days after initial C21 injection
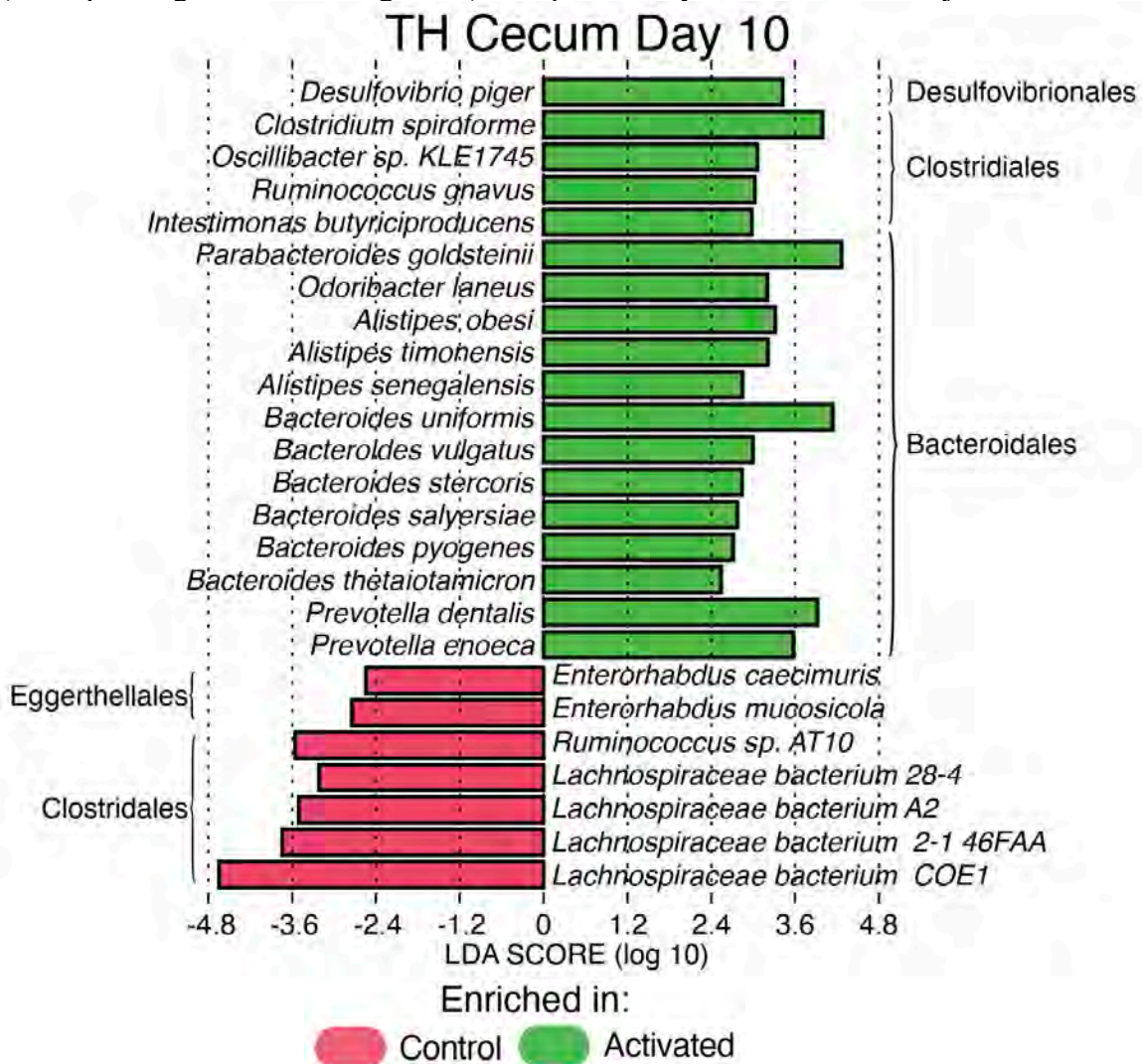
Supplemental Figure 8. ENS Activation-Mediated Changes in Feces

Supplemental Figure 8A
LEfSe Cladograms for feces on Day 9 of ChAT-Cre mice. Annotations are labelled in the tables below the cladogram
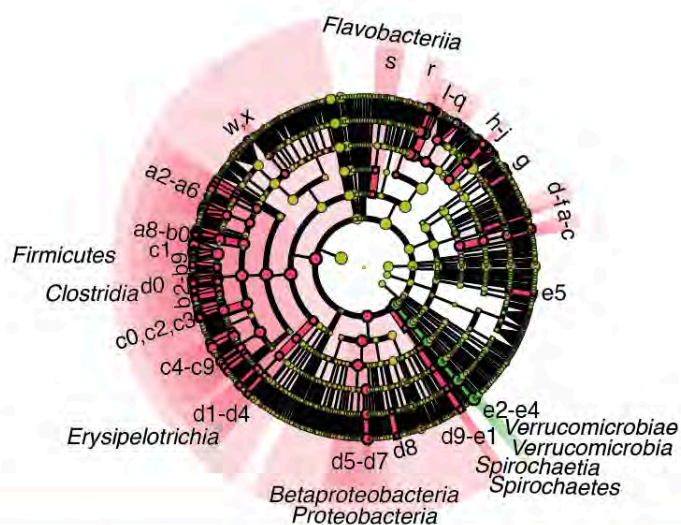
ChAT-Cre Post 9							
ID	Microbial Taxon	ID	Microbial Taxon	ID	Microbial Taxon	ID	Microbial Taxon
a	Bifidobacterium	p	Parabacteroides	b4	Dorea	d0	Clostridiales
b	Bifidobacteriaceae	q	Tannerellaceae	b5	Eisenbergiella	d1	Candidatus Stoquefichus
c	Bifidobacteriales	r	Marinilbiliales	b6	Faecalicatena	d2	Faecalitalea
d	Cellulomonas	s	Flavobacteriales	b7	Lachnoclostridium	d3	Erysipelotrichaeceae
e	Cellulomondaceae	w	Enterococcus	b8	Marvinbryantia	d4	Erysipelotrichales
f	Micrococcales	x	Enterococcaceae	b9	Sellimonas	d5	Parasutterella
g	Adlercreutzia	a2	Intestinimonas	c0	Tyzzerella	d6	Sutterellaceae
h	Barnsiella	a3	Pseudoflavonifractor	c1	Lachnospiraceae	d7	Burkholderiales
i	Coprobacter	a5	Clostridium	c2	Oscillibacter	d8	Lawsonia
j	Barnesiellaceae	a6	Clostridiaceae	c3	Oscillospiraceae	d9	Treponema
k	Prevotella	a8	Anaerofustis	c5	Anaerotruncus	e0	Spirochaetaceae
l	Prevotellaceae	a9	Eubacterium	c6	Ruminiclostridium	e1	Spirochaetales
m	Alistipes	b0	Eubacteriaceae	c7	Ruminococcus	e2	Akkermansia
n	Rikenella	b2	Blautia	c8	Ruthenibacterium	e3	Akkermansiaceae
o	Rikenellaceae	b3	Coprococcus	c9	Ruminococaceae	e4	Verrucomicrobiales
						e5	Varicellovirus

Enriched in:
Control   Activated

Supplemental Figure 8B

LEfSe Cladograms for feces on Day 5 of TH-Cre mice. Annotations are labelled in the tables below the cladogram
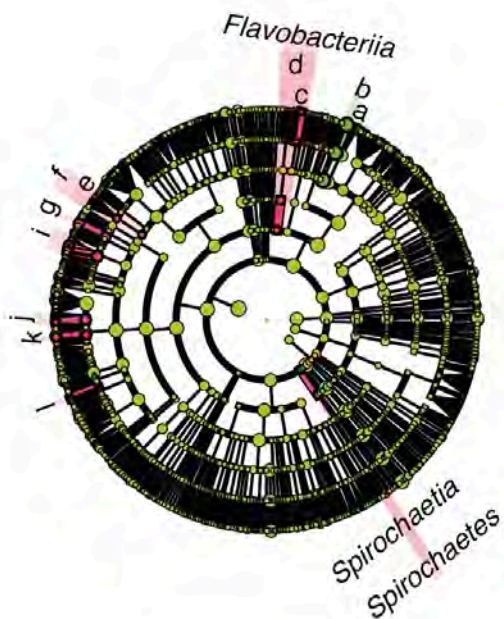
TH-Cre Post 5	
ID	**Microbial Taxon**
a	Parabacteroides
b	Tannerellaceae
c	Fluviicola
d	Flavobacteriales
e	Streptococcus
f	Streptococcaceae
g	Pseudoflavonifractor
i	Clostridium
j	Blautia
k	Eisenbergiella
l	Clostridiodes

Enriched in:

🔴 Control 🟢 Activated

Supplemental Figure 8C and 8D
Microbial gene family and pathway annotations for the defining features labelled on the DEICODE PCA plots in Figure 6O-6R. Colors in ID column refer to the color of feature arrows labelled in main figure.

C.

	ChAT-Cre Cecum	
ID	**Gene Family**	**Annotation**
1	K02003	putative ABC transport system ATP-binding protein
2	K02518	translation initiation factor IF-1
3	K02948	small subunit ribosomal protein S11
4	K02950	small subunit ribosomal protein S12
5	K02965	small subunit ribosomal protein S19
6	K03205	type IV secretion system protein VirD4
7	K03294	basic amino acid/polyamine antiporter, APA family
8	K03496	chromosome partitioning protein
ID	**Gene Pathway**	**Annotation**
1	HISDEG-PWY	L-histidine degradation I
2	ILEUSYN-PWY	L-isoleucine biosynthesis I (from threonine)
3	PWY-6122	5-aminoimidazole ribonucleotide biosynthesis II
4	PWY-6595	superpathway of guanosine nucleotides degradation (plants)
5	PWY-6606	guanosine nucleotides degradation II
6	PWY-7111	pyruvate fermentation to isobutanol (engineered)
7	PWY-7219	adenosine ribonucleotides de novo biosynthesis
8	VALSYN-PWY	L-valine biosynthesis

D.

	ChAT-Cre Post 9	
ID	**Gene Family**	**Annotation**
1	K02003	putative ABC transport system ATP-binding protein
2	K02518	translation initiation factor IF-1
3	K02913	large subunit ribosomal protein L33
4	K02946	small subunit ribosomal protein S10
5	K02948	small subunit ribosomal protein S11
6	K02950	small subunit ribosomal protein S12
7	K02965	small subunit ribosomal protein S19
8	K03205	type IV secretion system protein VirD4
ID	**Gene Pathway**	**Annotation**
1	ILEUSYN-PWY	L-isoleucine biosynthesis I (from threonine)
2	PWY-6151	S-adenosyl-L-methionine cycle I
3	PWY-6700	queuosine biosynthesis I (de novo)
4	PWY-6859	all-trans-farnesol biosynthesis
5	PWY-7111	pyruvate fermentation to isobutanol
6	PWY-7219	adenosine ribonucleotides de novo biosynthesis
7	PWY0-1296	purine ribonucleosides degradation
8	VALSYN-PWY	L-valine biosynthesis

Supplemental Figure 9. General Differences in ChAT-Cre vs. TH-Cre Metabolites Upon Activation.

Supplemental Figure 9A-9F
Canberra PCA analysis comparing activation-mediated changes to the (A-B) cecal and (C-F) fecal metabolome in ChAT-Cre versus TH-Cre mice (A) Cecal metabolome of control mice (B) Cecal metabolome of activated mice (C) Pre-C21 feces of control and (D) activated mice (E) Fecal metabolome during activation time course for control and (F) activated mice.
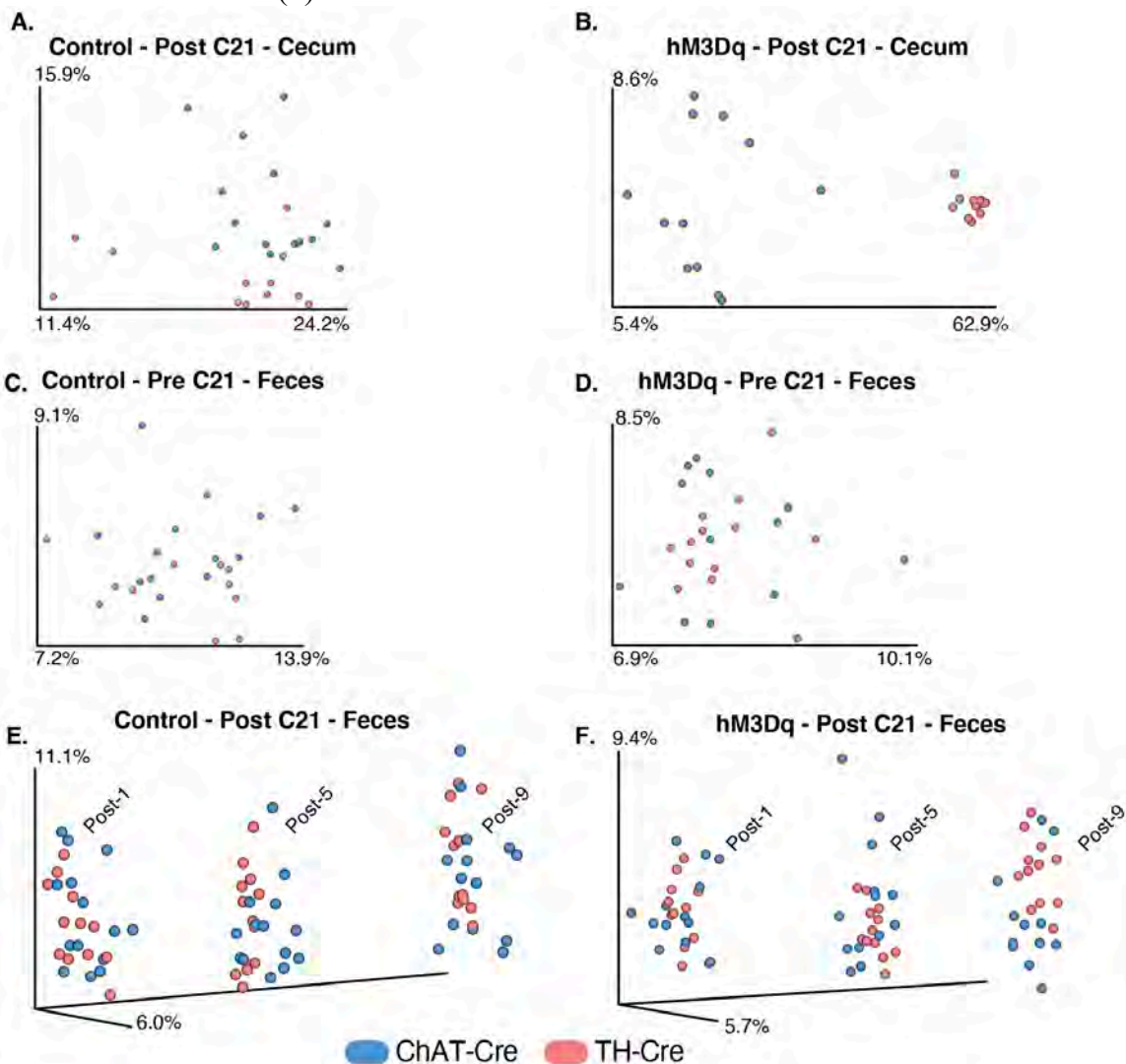
Supplemental Figure 10. ENS Activation Alters Locomotion in only ChAT-Cre Mice

Effect of DREADD activation on locomotor activity during open-field testing in TH- and ChAT-Cre mice. (A) Distance travelled (cm) in 10 minutes and (B) % of Time spent moving. (N = 10-14 mice per group; *p < 0.05; 2way ANOVA with Sidak's multiple comparisons test)
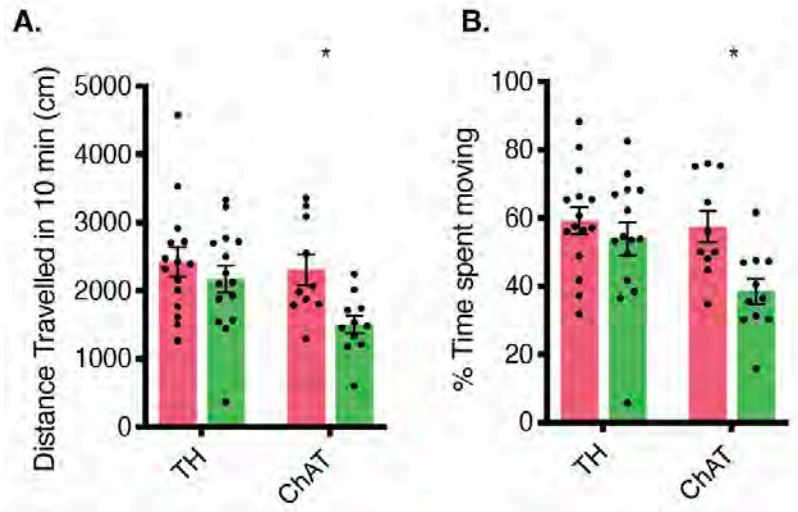
Supplemental Table 1

Extended annotations for networked (bold), MS/MS spectra in cecal luminal contents- corresponds to Figure 6K and 6L in ChAT-Cre and TH-Cre mice, respectively.

ChAT-Cre Cecum						
Activated > Control						
ID	GNPS Annotation	m/z	RT	Adduct	Log$_2$(FC)	P$_{adjusted}$
215	Cholic acid	817.5826	5.231	2M+H	5.06	0.0033
219	Cholic acid	839.5648	5.231	2M+Na	4.18	0.0015
218	7-Keto-3.alpha.,12-.alpha.-dihydroxycholanic acid	353.2467	4.903	M+H-3H2O	3.66	0.0000
108	Cholic acid	355.2627	5.222	M-3H2O+H	3.44	0.0001
221	Cholic acid	1225.87	5.231	3M+H	3.29	0.0101
114	Cholic acid	431.2766	5.22	M+Na	3.08	0.0001
259	Cholic Acid	426.3209	5.23	[M+NH4]	2.58	0.0001
224	Cholic acid	1247.854	5.231	3M+Na	2.28	0.0074
235	taurohyocholic acid	516.2984	4.019	M+H	2.18	0.1675
234	Spectral Match to Taurocholic acid from NIST14	516.2989	4.438	M+H	2.02	0.1411
248	Spectral Match to Taurocholic acid from NIST14	538.2811	4.031	M+Na	1.70	0.1717
245	taurohyocholic acid	480.2773	3.984	M-2H2O+H	1.51	0.2475
258	1-Palmitoyl-sn-glycero-3-phosphocholine	496.34	6.513	M+H	1.13	0.0840
204	Gln-Ile	260.1585	0.592	M+H	0.90	0.0173

272	Spectral Match to Cholic acid from NIST14	373.2732	4.435	M+H-2H2O	0.87	0.1293
111	N-(.alpha.-Linolenoyl)tyrosine	165.0538	0.337	M+H-C18H31ON	0.87	0.0000
48	Spectral Match to L-Tryptophan from NIST14	205.0963	0.993	M+H	0.80	0.0009
192	Ile-Thr	233.1488	0.609	M+H	0.71	0.0515
30	Spectral Match to Abrine from NIST14	188.0697	0.985	M+H-CH3NH2	0.68	0.0006
246	Val Glu Leu	360.2118	2.762	M+H	0.59	0.1675
53	Spectral Match to L-Arginine from NIST14	175.1169	0.239	M+H	0.58	0.0591
277	Gln Val Ile	359.2275	2.387	M+H	0.56	0.0840
12	Spectral Match to L-Tyrosine from NIST14	182.0803	0.336	M+H	0.47	0.0027
102	.beta.-Muricholic acid	391.2837	4.891	M+H-H2O	0.32	0.4044
99	hyocholic acid	373.2733	4.801	M-2H2O+H	0.04	0.8915

Supplemental Table 1 (continued)

ID	GNPS Annotation	m/z	RT	Adduct	Log$_2$(FC)	P$_{adjusted}$
	ChAT-Cre Cecum					
	Activated < Control					
19	Spectral Match to 12-Ketodeoxycholic acid from NIST14	391.2841	5.574	M+H	-1.57	0.0241
187	hyocholic acid	373.2733	4.749	M-2H2O+H	-1.05	0.0033
138	Spectral Match to 12-Ketodeoxycholic acid from NIST14	391.284	5.684	M+H	-1.01	0.0034
118	Spectral Match to Urobilin from NIST14	591.318	4.137	M+H	-0.94	0.0033
233	Spectral Match to Conjugated linoleic Acid (10E,12Z) from NIST14	281.2472	6.69	M+H	-0.87	0.0163
101	.beta.-Muricholic acid	355.2624	4.766	M+H-3H2O	-0.87	0.0119
34	3.alpha.-Hydroxy-7-oxo-5.beta.-cholanic acid	373.2733	6.044	M+H-H2O	-0.86	0.0371

20	.alpha.-Hyodeoxycholic acid methyl ester	357.2782	5.391	M+H-CH6O2	-0.85	0.0023
280	.gamma.-Muricholic acid/hyocholic acid	391.2835	4.781	M+H-H2O	-0.81	0.0209
3	Soyaspongenol C	441.3727	7.296	M+H	-0.74	0.0314
100	Spectral Match to Deoxycholic acid from NIST14	785.5932	6.017	2M+H	-0.73	0.0419
13	Spectral Match to Ursodeoxycholic acid from NIST14	375.2888	6.017	M+H-H2O	-0.61	0.0084
6	sphingosin C16 (Artifact)-emf	274.2734	5.273	M+H	-0.51	0.0096
143	.beta.-Hyodeoxycholic acid	375.2887	5.619	M+H-H2O	-0.45	0.1159
148	Spectral Match to Sulfadimethoxine from NIST14	311.0802	3.911	M+H	-0.39	0.1326
1	.beta.-Hyodeoxycholic acid	357.2783	6.017	M+H-2H2O	-0.37	0.0159
113	NCGC00385962-01_C16H24O3_	247.1657	12.16	M-H2O+H	-0.06	0.9123

Supplemental Table 1 (continued)

ID	GNPS Annotation	m/z	RT	Adduct	Log₂(FC)	P_adjusted
	TH-Cre Cecum					
	Activated > Control					
626	Linoelaidic acid	263.2364	8.04	M+H-H2O	2.38	0.0182
868	7-Keto-3.alpha.,12-.alpha.-dihydroxycholanic acid	353.2464	4.891	M+H-3H2O	2.37	0.3988
618	Lyso-PC(16:0)	496.3398	6.484	M+H	1.68	0.1312
871	(R)-4-((3S,5S,7R,8R,9S,10S,13R,14S,17R)-3,7-dihydroxy-10,13-dimethyl-12-oxohexadecahydro-1H-cyclopenta[a]phenanthren-17-yl)pentanoic acid	407.2789	4.906	M+H	1.64	0.1936
457	Spectral Match to Sulfamethazine from NIST14	279.0909	2.69	M+H	1.48	0.0000
378	Oleanolic acid methyl ester	411.3619	8.168	M+H-C2H4O2	1.43	0.0066
261	Soyaspongenol C	441.3727	7.293	M+H	0.76	0.0601

865	(R)-4-((3S,5S,7R,8R,9S,10S,13R,14S,17R)-3,7-dihydroxy-10,13-dimethyl-12-oxohexadecahydro-1H-cyclopenta[a]phenanthren-17-yl)pentanoic acid	407.2794	4.583	M+H	0.70	0.2134
739	Spectral Match to Coproporphyrin I from NIST14	328.1417	5.138	M+2H]	0.63	0.0475
297	Spectral Match to 12-Ketodeoxycholic acid from NIST14	391.2841	5.52	M+H	0.62	0.3677
584	(4R)-4-((3R,5R,6S,7S,9S,10R,13R,17R)-3,6,7-trihydroxy-10,13-dimethylhexadecahydro-1H-cyclopenta[a]phenanthren-17-yl)pentanoic acid	391.284	4.95	M-H2O+H	0.61	0.2347
324	Spectral Match to Urobilin from NIST14	591.3175	4.14	M+H	0.48	0.1021

279	Spectral Match to L-Tryptophan from NIST14	188.0701	0.971	M+H-NH3	0.38	0.0121
299	Spectral Match to L-Tryptophan from NIST14	205.0961	0.971	M+H	0.35	0.0263
254	Spectral Match to 12-Ketodeoxycholic acid from NIST14	391.2843	5.659	M+H	0.34	0.3055
870	(R)-4-((3R,5R,6R,7R,8S,9S,10R,13R,14S,17R)-3,6,7-trihydroxy-10,13-dimethylhexadecahydro-1H-cyclopenta[a]phenanthren-17-yl)pentanoic acid	391.2839	4.778	M-H2O+H	0.26	0.4858
253	(4R)-4-((3S,5R,6R,7S,9S,10R,13R,14S,17R)-3,6,7-trihydroxy-10,13-dimethylhexadecahydro-1H-cyclopenta[a]phenanthren-17-yl)pentanoic acid	373.2736	4.783	M-2H2O+H	0.23	0.4154

720	Spectral Match to Tyr-Val from NIST14	281.142	0.649	M+H	0.16	0.6888
280	(4R)-4-((5S,7R,9S,10S,12S,13R,14S,17R)-7,12-dihydroxy-10,13-dimethylhexadecahydro-1H-cyclopenta[a]phenanthren-17-yl)pentanoic acid	415.2818	5.984	M+Na	0.15	0.5726
277	(R)-4-((3S,5S,8R,9S,10S,12S,13R,14S,17R)-3,12-dihydroxy-10,13-dimethylhexadecahydro-1H-cyclopenta[a]phenanthren-17-yl)pentanoic acid	375.289	5.984	M-H2O+H	0.11	0.6782

Supplemental Table 1 (continued)

ID	GNPS Annotation	m/z	RT	Adduct	Log$_2$(FC)	P$_{adjusted}$
TH-Cre Cecum						
Activated < Control						
267	N-(1-Deoxy-1-fructosyl)phenylalanine	328.1393	0.524	M+H	-1.49	0.0003
707	Spectral Match to trans-Ferulic acid from NIST14	177.0535	3.149	M+H-H2O	-0.99	0.0051
306	Quinoline-2,6-diol	162.0543	2.624	M+H	-0.53	0.0728
846	Genistein-CDM-BAW-AED	271.0592	4.374	M+H	-0.46	0.0058
259	Spectral Match to Xanthine from NIST14	153.0402	0.33	M+H	-0.43	0.0439

281	(R)-4-((3R,4R,5S,8S,9S,10R,13R,14S,17R)-3,4-dihydroxy-10,13-dimethylhexadecahydro-1H-cyclopenta[a]phenanthren-17-yl)pentanoic acid	357.2786	5.375	M-2H2O+H	-0.41	0.1416
431	Trp-Val	304.1658	2.622	M+H	-0.38	0.1416
61	.alpha.-Hyodeoxycholic acid methyl ester	357.2787	5.984	M+H	-0.06	0.7655
249	Spectral Match to L-Tyrosine from NIST14	182.0811	0.335	M+H	-0.01	0.9462

Materials and Methods

Mice

All mouse experiments were performed in accordance with the NIH Guide for the Care and Use of Laboratory Animals using protocols approved by the Institutional Animal Care and Use Committee at the California Institute of Technology. TH-Cre (from Viviana Gradinaru at Caltech. Originally from Ted Ebendal B6.129X1-Thtm1(cre)Te/Kieg) (67) and ChAT-Cre mice (Jackson Laboratories, Bar Harbor, ME- Stock# 028861) were obtained from Jackson Laboratories, and homozygous Cre-mice were bred to wild-type mice to yield male and female heterozygous Cre-mice used for our studies. Wildtype specific pathogen free (SPF), C57BL/6 (Jackson Laboratories, Bar Harbor, ME Stock #000664) males and females were used for breeding and experiments involving germ free C57/B6 mice. Germ free mice were bred under gnotobiotic conditions in flexible film isolators, and once taken out were placed in sterile cages with autoclaved water supplemented with 10μg/ml erythromycin and 100μg/ml gentamicin.

Virus Production

Virus was produced using methods described in Challis et. al. (68) Briefly, human embryonic kidney (HEK293T) cells were triple-transfected with pUCmini-iCAP-AAV-PHP.S, pHelper Plasmid, and one of the following pAAV genomes (hSYN1-mRuby2, hSYN1-DiO-mRuby2, hSYN1-mNeonGreen, hSYN1-DiO-mNeonGreen, hSYN1-mTurquoise2, hSYN1-DiO-mTurquoise2, and hSYN1-DiO-hM3Dq-mRuby, CAG-GCamP6F). Cells were grown in DMEM + 5% FBS + non-essential amino acids, penicillin-streptomycin. Virus is precipitated from cells and supernatant with an 8% PEG solution (wt/vol), and purified by ultracentrifugation using 15%, 25%, 40%, and 60% stacked iodixanol gradients.

Systemic Delivery of AAV

Mice were anesthetized using 2% isoflurane. Virus was tittered to 10^{12} VGs, resuspended to a volume of 100μl with sterile PBS, and injected retro-orbitally.

Quantitative PCR of Viral Abundance

AAV-PHP.S:hSYN1-mNeonGreen was delivered systemically to WT GF and SPF mice at 6-8 weeks of age. 3-4 weeks following viral infection, 1cm of proximal, medial, and distal small and large intestines were harvested and flash frozen in TRIzol (ThermoFisher Scientific, Waltham, MA- Cat. No. 15596018) and RNA was extracted per manufacturer's instructions. Viral ssDNA is present in the RNA fraction. Contaminating RNA was eliminated with RNase treatment (ThermoFisher Scientific, Waltham, MA- Cat. No. AM228) per manufacturer's instructions. Quantitative PCR was performed on viral DNA with primers against WPRE (Forward: 5'-GGCTGTTGGGCACTGACAAT-3'; Reverse: 5'-CCGAAGGGACGTAGCAGAAG-3') and values were normalized to ubiquitous mitochondrial gene, mtRNR2 (Forward: 5'-CCGCAAGGGAAAGATGAAAA-3'; Reverse: 5'-TCGTTTGGTTTCGGGGTTTC-3'). Plotted relative abundances are mean values across three regions sampled in either small or large intestines. Threshold cycle value (Ct) for both WPRE and mtRNR2 were unchanged between GF and SPF.

Neural activation of the GI tract

TH-Cre and ChAT-Cre mice are used for these experiments. "Activated" mice are infected with AAV-PHP.S:hSYN1-DIO-hM3Dq-mRuby2 and "Control Mice" are infected with AAV-PHP.S:hSYN1-DIO-mRuby2. This is to control for both AAV-PHP.S-mediated expression and the effects of Compound 21 dihydrochloride (C21) (HelloBio, Princeton, NJ- HB6124). C21 was injected intraperitoneally at a dose of 3mg/kg in both activated and control mice. Mice for time course experiments were single housed in sterile cages and autoclaved water following first C21 administration, and administered C21 for 10 consecutive days.

GI Transit Time (Carmine Red), %(Water Content) in Feces, Fecal output rate

Mice were administered C21 (3mg/kg) intraperitoneally, and soon after were gavaged with 100µl of 6% Carmine Red in 0.5% methylcellulose in water (69). Mice

were single housed in cages void of bedding. Time of fecal pellet expulsion was recorded for each pellet, and each pellet was collected in pre-weighed, 1.5mL microcentrifuge tubes. This was done for 5 hours. Each pellet collected was checked for the presence of Carmine red, and time of initial Carmine red pellet expulsion was recorded for GI transit time. Mass of collected fecal pellets was calculated, and was left to dry in a 80ºC oven for 2 days to ensure evaporation of fecal water content. Tubes with fecal pellets were reweighed to obtain dry mass of feces, and %(water content) was calculated. Fecal output rate is the total number of pellets expelled during the 5 hour time course post-C21 administration divided by the time last fecal pellet was expelled (per mouse) during that time.

Open field testing

TH-Cre and ChAT-Cre mice were systemically infected with PHPS-hSyn-DIO-hM3Dq-mRuby2 or PHPS-hSyn-DIO-mRuby2. 3-4 weeks after infection, mice were administered C21 (3mg/kg) and 45 minutes later, were placed in a 50cm x 50cm white plexiglass arena, recorded with an overhead camera, and tracked and analyzed using the EthoVision XT 10 software package (Noldus Information Technology; Leesburg, VA, USA) for 10 minutes. The arena was disinfected between trial runs using Rescue disinfectant (Virox technologies).

Antibiotic Treatment

Broad-spectrum antibiotic cocktail consisted of ampicillin, vancomycin, neomycin, and metronidazole (AVNM). Concentrated antibiotics were filter sterilized and added to autoclaved drinking water to obtain a final concentration of 1g/L of AVNM in 2% sucrose. Antibiotics were given *ad libitum*. Wildtype, SPF animals were placed on AVNM at 3 weeks or 8 weeks of age until mice were 11-13 weeks of age. For prenatal exposure, 6-8 week old GF and SPF mice were placed on AVNM for 2-3 weeks prior to breeding. Dams will be kept on AVNM until offspring are weaned, at which point offspring will be kept on AVNM until 11-13 weeks of age.

Tissue preparation, immunohistochemistry, and Imaging

Euthasol (Virbac, Carros, France) was administered, and perfused with 30mL of phosphate buffer solution (PBS) and next with cold 4% paraformaldehyde (PFA) in PBS. GI tract was post-fixed in 4% PFA overnight at 4ºC, and stored in PBS + 0.025% sodium azide. Tissues that underwent subsequent immunohistochemistry were made transparent by use of the passive CLARITY technique (PACT) (70) .Briefly, perfused and postfixed tissues were embedded with polymerized 4% (wt/vol) acrylamide, and lipids were eliminated using 8% (wt/vol) SDS solution. Tissues were blocked in 3% donkey serum and permeabilized with PBS + 0.3% Triton (PBST). Primary antibodies were incubated in PBST for 48 hours and washed with PBST for 24 hours (replacing wash 3 times). Tissues were next incubated in secondary antibodies (and DAPI) for 24 hours and washed in PBS for 48 hours, intermittently replacing the wash solution with fresh PBS. Primary antibodies used were rabbit PGP9.5 (1:300; Millipore Sigma AB1761-I) and chicken GFAP (1:500, BioLegend Cat #829401). Secondary antibodies used were goat anti-chicken Alexa 647 (Life Technologies A-21450) and donkey anti-rabbit Alexa 568 (Life Technologies A10042). Tissues imaged just for virally expressed, endogenous fluorescence were made transparent using sorbitol-based optical clearing method, Sca*l*eS (16). Tissues were mounted in respective mounting mediums, on a glass slide with a 0.5mm spacer (iSpacer, SunJin Lab Co.). Images were acquired on Zeiss LSM 780 or 880, and microscope, laser settings, contrast, and gamma remained constant across images that were directly compared. All confocal images were taken with the following objectives: Fluar 5× 0.25 M27 Plan-Apochromat 10× 0.45 M27 (work- ing distance 2.0 mm) and Plan-Apochromat 25× 0.8 Imm Corr DIC M27 multi-immersion.

Live, *in vivo*, imaging (GCaMP6F), Video Processing, and Analysis

AAV-PHP.S-CAG-GCaMP6F (10^{12} VGs) was delivered systemically to Germ Free (GF) and specific pathogen free (SPF) mice. 3-4 weeks after infection, mice were anesthetized with 2% isoflurane on a heating pad (Kent Scientific, Torrington, CT-

DCT15) with plastic sleeve covers (Kent Scientific, Torrington, CT- DCT1520P). The abdominal cavity was surgically opened to expose the intestines. The proximal large intestine was identified, and this portion was placed on top of a stack of 4-6 glass microscopy slides (depending on size of animal) (VWR, Radnor PA- Cat. No. 48300-026). Tissue was secured onto glass slide with a biorthogonal silicon elastomer (Kwik-Sil) (World Precision Instruments, Sarasota, FL- KWIK-SIL), and a glass coverslip. Once elastomer stiffens, anesthetized mouse is placed under an upright confocal microscope (Zeiss LSM 880). Using a 10X objective, GCaMP6F fluorescence was taken at 5Hz (1 image every 200ms). Cell tracking was performed in 2D by using TrackMate ImageJ plugin (https://imagej.net/TrackMate) and fluorescence intensity was recorded from cells. Average background was determined by taking the fluorescence of a region of interest that did not contain a cell, over the duration of the video. Background was subtracted from cell fluorescence intensities.

Spike Detection

Data sets of fluorescent values recorded at a rate of 0.206 s from GCamp6f-expressing unstimulated neurons in the myenteric plexus of the proximal large intestine were analyzed with the MLspike software for Matlab downloaded from GitHub (https://github.com/MLspike/spikes) (71). MLspike determines a new baseline to subtract from the raw fluorescence data to allow accurate modelling. The software uses a version of the Viterbi algorithm to obtain the most probable spike train. From the model, fluctuating baseline, model-estimated spike train, and most probable spike times were extracted. Polynomial coefficients (p_2) was changed from 0.5 to 0.55 and (p_3) from 0.01 to 0.03 for GCaMP6F fluorescence as recommended (71). The minimum range for baseline (b_{min}) was changed from 0.7 to 0.5 as determined by observed fluorescence values.

GCaMP6F Fluorescence in Ex Vivo Intestinal Preparation

Small intestinal tissue was quickly harvested from ChAT-Cre mice, flushed and placed in oxygenated (95% O_2, 5% CO_2), ice cold Krebs-Henseleit solution for 1

hour followed by 15 min at room temperature. A segment was cut along the mesentery, and pinned flat (mucosa facing down) on a Sylgard-lined recording chamber (Warner Instruments, PH1) in oxygenated Krebs-Henseleit solution. C21 was added at 10nM and GCaMP6F fluorescence was detected on an upright microscope (Zeiss, Oberkochen, Germany- Examiner D1).

3' mRNA-sequencing

Tissue collection and RNA extraction

Mice were cervically dislocated and GI tract was removed. 1cm of tissue above and below the cecum were dissected and cleaned to represent tissue from the distal small intestine and proximal large intestine, respectively. Tissue was homogenized in TRIzol (ThermoFisher Scientific, Waltham. MA- Cat. No. 15596018) solution using bead-based homogenizing methods, and total RNA was extracted using chloroform per manufacturer's instructions.

Library Preparation, Sequencing, and Analysis

The cDNA libraries were prepared using the QuantSeq 3'mRNA-Seq Library Prep Kit FWD for Illumina (Lexogen, Greenland, NH) supplemented with UMI (unique molecular index) as per the manufacturer's instructions. Briefly, total RNA was reverse transcribed using oligo (dT) primers. The second cDNA strand was synthesized by random priming, in a manner that DNA polymerase is efficiently stopped when reaching the next hybridized random primer, so only the fragment closed to the 3' end gets captured for later indexed adapter ligation and PCR amplification. UMIs were incorporated to the first 6 bases of each read, followed by 4 bases of spacer sequences. UMIs are used to eliminate possible PCR duplicates in sequencing datasets and therefore facilitate unbiased gene expression profiling. The basic principle behind the UMI deduplication step is to collapse reads with identical mapping coordinates and UMI sequences. This step helps increase the accuracy of sequencing read counts for downstream analysis of gene expression levels. The processed libraries were assessed for its size distribution and concentration using Bioanalyzer High Sensitivity DNA Kit (Agilent Technologies, Santa Clara, CA- Cat.

No. 5067-4626 and -4627). Pooled libraries were diluted to 2 nM in EB buffer (Qiagen, Hilden, Germany, Cat. No. 19086) and then denatured using the Illumina protocol. The libraries were pooled and diluted to 2 nM using 10 mM Tris-HCl, pH 8.5 and then denatured using the Illumina protocol. The denatured libraries were diluted to 10 pM by pre-chilled hybridization buffer and loaded onto an Illumina MiSeq v3 flow cell for 150 cycles using a single-read recipe according to the manufacturer's instructions. Single-end 75bp reads (max 4.5M reads) were obtained. De-multiplexed sequencing reads were generated using Illumina BaseSpace.

UMI specific workflows that were developed and distributed by Lexogen were used to extract reads that are free from PCR artifacts (i.e., deduplication). First, the umi2index tool was used to add the 6 nucleotide UMI sequence to the identifier of each read and trims the UMI from the start of each read. This generates a new FASTQ file, which is then processed through trimming and alignment. Second, after the quality and polyA trimming by BBDuk (Website-https://jgi.doe.gov/data-and-tools/bbtools/bb-tools-user-guide/bbduk-guide/) and alignment by HISAT2 (version 2.1.0) (72) , the mapped reads are collapsed according to the UMI sequence of each read. Reads are collapsed if they have the same mapping coordinates (CIGAR string) and identical UMI sequences. Collapsing reads in this manner removes PCR duplicates. Read counts were calculated using HTSeq (73) by supplementing Ensembl gene annotation (GRCm38.78). Raw read counts were run through ShinySeq to obtain differentially expressed genes and downstream gene ontology analyses (74).

Proteome Preparation

Protein extraction

Mice were sacrificed 45 minutes after C21 administration and cecal contents were isolated and resuspended in 400ul of phosphate buffered solution, and centrifuged at x20,000g to spin down cells and lysate. Protein was isolated from resulting supernatant using Wessel-Flüegge's methanol/chloroform extraction method (75). Briefly, MeOH and chloroform was added to sample at a 4:1 and 1:1 ratio,

respectively. Next, water dH2O was added at a 3:1 ratio, samples were vortexed and centrifuged at x20,000g. Resulting precipitated protein was collected and washed with methanol. Precipitated protein was centrifuged and was left to air dry, and stored in -20C until protein digestion.

In-solution Protein Digestion and Desalting

Precipitated protein sample was dissolved in 40ul of 8M Urea (100mM Tris-HCl pH8.5). 1.25ul of 100mM Tris(2-carboxyethyl)Phosphine was added and incubated at room temperature (RT) for 20 minutes. 1.8ul of 250mM iodoactaminde was added and incubated at RT in the dark. 1ul of 0.1µg/ul of Lysyl endopeptidase was added and incubated for 4 hours in the dark. Sample was adjusted down to 2M Urea by adding 120ul of 100mM Tris-HCl pH8.5. 1.6ul of 100mM CaCl2 and 2.5ul of .2µg/ul trypsin was incubated overnight in the dark. Add 8.5ul of 100% formic acid to make a 5% FA solution. Desalt mixture by HPLC using C8 peptide microtrap (Microm Bioresources). Peptides were lyophilized and diluted to 1 ug/ul in 0.5% formic acid prior to LC-MS/MS analysis.

LC-MS/MS

Samples were analyzed on a Q Exactive HF mass spectrometer coupled to an EASY nLC 1200 liquid chromatographic system (Thermo Scientific, San Jose, CA). Approximately 200 ng of peptides were loaded on a 50 µm I.D. × 20 cm column with a 10 µm electrospray tip (PicoFrit from New Objective, Woburn, MA) in-house-packed with ReproSil-Pur C18-AQ 1.9 µm (Dr. Maisch, Ammerbuch, Germany). Solvent A consisted of 2% MeCN in 0.2% FA and solvent B consisted of 80% MeCN in 0.2% FA. A non-linear 60 minute gradient from 2% B to 40% B was used to separate the peptides for analysis. The mass spectrometer was operated in a data-dependent mode, with MS1 scans collected from 400-1650 m/z at 60,000 resolution and MS/MS scans collected from 200-2000 m/z at 30,000 resolution. Dynamic exclusion of 45 s was used. The top 12 most abundant peptides with charge states between 2 and 5 were selected for fragmentation with normalized collision energy of 28.

Peptide and Protein Identification

Thermo .raw files were converted to .ms1 and .ms2 files using RawConverter 1.1.0.18 (76) operating in data dependent mode and selecting for monoisotopic m/z. Tandem mass spectra (.ms2 files) were identified by database search method using the Integrated Proteomics Pipeline 6.5.4 (IP2, Integrated Proteomics Applications, Inc., http://www.integratedproteomics.com). Briefly, databases containing forward and reverse (decoy) (77, 78) peptide sequences were generated from in silico trypsin digestion of either the mouse proteome (UniProt; Oct. 2, 2019) or protein sequences derived from large comprehensive public repositories (ComPIL 2.0) (79). Tandem mass specta were matched to peptide sequences using the ProLuCID/SEQUEST (1.4) (80, 81) software package. The validity of spectrum-peptide matches were assessed using the SEQUEST-defined parameters XCorr (cross-correlation score) and DeltaCN (normalized difference in cross-correlation scores) in the DTASelect2 (2.1.4) (82, 83) software package. Search settings were configured as follows: (1) 5ppm precursor ion mass tolerance, (2) 10ppm fragment ion mass tolerance, (3) 1% peptide false discovery rate, (4) 2 peptide per protein minimum, (5) 600-6000Da precursor mass window, (6) 2 differential modifications per peptide maximum (methionine oxidation: M+15.994915 Da), (7) unlimited static modications per peptide (cysteine carbamidomethylation: C+57.02146 Da), and (8) the search space included half- and fully tryptic (cleavage C-terminal to K and R residues) peptide candidates with unlimited (mouse database, custom metagenomic shotgun database) or 2 missed cleavage events (ComPIL 2.0).

Differential Analysis of Detected Proteins using Peptide-Spectrum Matches (Spectral Counts)

Detected proteins were grouped by sequence similarity into "clusters" using CD-HIT 4.8.1 (84-86) at the following similarity cut-offs: 65%, 75%, 85%, and 95%. The following is an example command line input: "cd-hit -i fastafile.fasta -o outputfile -c 0.65 -g 1 -d 0". Tandem mass spectra identified as peptides (peptide spectrum matches, PSMs) were mapped to CD-HIT generated clusters. PSMs mapping to >1 cluster were discarded. Cluster-PSM tables were generated and differential analysis

was performed in DESeq2 (1.25.13) (87). Briefly, count data (PSMs) were modeled using the negative binomial distribution, and the mean-variance relationship was estimated. Variance was estimated using an information sharing approach whereby a single feature's (or cluster's) variance was estimated by taking into account variances of other clusters measured in the same experiment. Feature significance calling and ranking were performed using estimated effect sizes. Multiple testing correction was performed by Benjamini-Hochberg method within the DESeq2 package. Volcano plots were generated in Prism (GraphPad).

Differential Analysis of Detected Proteins using Ion Intensity (Precursor Intensity)

Detected proteins were grouped into "clusters" by sequence similarity using CD-HIT 4.8.1 (84-86) at the following similarity cut-offs: 65%, 75%, 85%, and 95%. The following is an example command line input: "cd-hit -i fastafile.fasta -o outputfile -c 0.65 -g 1 -d 0". Using the Census software package (88, 89) (Integrated Proteomics Pipeline 6.5.4), peptide ion intensities were calculated from .ms1 files. Peptide ion intensities were assigned to their parent peptide, then parent peptides were mapped to their appropriate CD-HIT generated clusters. Ion intensities belonging to parent peptides that map to >1 CD-HIT cluster were discarded. Cluster-ion intensity tables were generated.

Ion intensity data were analyzed using the DEP package (90) operating in R. Intensity values were automatically Log2 transformed in DEP. The cluster list was subsequently filtered with the 'filter_proteins' function such that clusters with missing values above a 65% threshold were discarded. Remaining intensities were further transformed by the 'normalize_vsn' function (91). Missing data in remaining clusters were imputed using a mixed approach. Clusters where either the control or treatment group contained only null entries were classified as 'missing not at random' (MNAR) and imputed with 0 values. All other groups were treated as 'missing at random' (MAR) and imputed using the maximum likelihood method ('MLE') (92). Note that for a given cluster, missing values for treatment groups were imputed separately by treatment group. Differential expression analyses were performed on filled-in cluster-ion intensity tables using the 'test_diff' function (93) and multiple testing

correction was performed using the 'add_rejections' function. Volcano plots, PCA plots, and heat maps were also generated using R.

Network Analysis using STRING Database

Upregulated proteins with a nominal p-value < 0.2 were searched against protein-protein interactions in the STRING database (http://www.string-db.org) where high confidence interactions were selected for. Briefly, the STRING database sources protein-protein interactions from primary databases consisting of genomic context predictions, high-throughput lab experiments, (conserved) co-expression, automated textmining, and pervious knowledge in databases (94).

Metaproteome Analysis using Unipept

Upregulated tryptic, microbial peptide sequences with nominal p-value cutoff of p < 0.2 were input into Unipept (http://unipept.ugent.be) (95, 96), equating leucine and isoleucine and filtering duplicate peptides. Briefly, Unipept indexes tryptic peptide sequences from the UniProtKB and details peptides with NCBI's taxonomic database. Lowest common ancestor is calculated for each tryptic peptide.

<ins>Metagenome Preparations</ins>

Fecal Collection

AAV-PHP.S:hSYN1-hM3Dq-mRuby (10^{12} VGs) was delivered systemically to TH-Cre and ChAT-Cre mice. 3-4 week after infection, C21 (3mg/kg) was administered daily for 10 consecutive days. Fecal pellets were collected in sterile containers one day before initial C21 dose, and between doses thereafter.

Fecal sample DNA extraction and Library Preparation

DNA was extracted with the Qiagen MagAttract PowerSoil DNA kit as previously described (Marotz et al 2017) . Our standard protocol is optimized for an input quantity of 1 ng DNA per reaction. Prior to library preparation, input DNA is transferred to a 384-well plate and quantified using a PicoGreen fluorescence assay (ThermoFisher, Inc). Input DNA is then normalized to 1 ng in a volume of 3.5 μL of molecular-grade water using an Echo 550 acoustic liquid-handling robot (Labcyte, Inc). Enzyme mixes for fragmentation, end repair and A-tailing, ligation,

and PCR are prepared and added in approximately 1:8 scale volumes using a Mosquito HV micropipetting robot (TTP Labtech). Fragmentation is performed at 37 °C for 20 min, followed by end-repair and A-tailing at 65 °C for 30 min.

Sequencing adapters and barcode indices are added in two steps, following the iTru adapter protocol (97). Universal adapter "stub" adapter molecules and ligase mix are first added to the end-repaired DNA using the Mosquito HV robot and ligation performed at 20 °C for 1 h. Unligated adapters and adapter dimers are then removed using AMPure XP magnetic beads and a BlueCat purification robot (BlueCat Bio). 7.5-µL magnetic bead solution is added to the total adapter-ligated sample volume, washed twice with 70% EtOH, and then resuspended in 7 µL molecular-grade water.

Next, individual i7 and i5 are added to the adapter-ligated samples using the Echo 550 robot. Because this liquid handler individually addresses wells, and we use the full set of 384 unique error-correcting i7 and i5 indices, we are able to generate each plate of 384 libraries without repeating any barcodes, eliminating the problem of sequence misassignment due to barcode swapping (98, 99). To ensure that libraries generated on different plates can be pooled if necessary, and to safeguard against the possibility of contamination due to sample carryover between runs, we also iterate the assignment of i7 to i5 indices each run, such that each unique i7:i5 index combination is only repeated once every 147,456 libraries. 4.5 µL of eluted bead-washed ligated samples is added to 5.5 µL of PCR master mix and PCR-amplified for 15 cycles. The amplified and indexed libraries are then purified again using magnetic beads and the BlueCat robot, resuspended in 10 µL water, and 9 µL of final purified library transferred to a 384-well plate using the Mosquito HV liquid-handling robot for library quantitation, sequencing, and storage. 384 samples are then normalized based on a PicoGreen fluorescence.

Shallow shotgun metagenome sequencing and diversity analysis

The Illumina data for each HiSeq lane was uploaded to Qiita, a tool with standardized pipelines for processing and analyzing metagenomic data (100). Adapter sequences were removed from the reads using the Atropos v.1.1.15 (101)

command (from the qp-shogun 0.1.5 pipeline) and the trimmed sequences were downloaded from Qiita. The reads for each sample were filtered of any potential mouse contamination using Bowtie2 v.2-2.2.3 (102). The filtered reads were then aligned to the Web of Life (WoL) reference phylogeny (103) with Bowtie2 using an adapted SHOGUN pipeline (104). The WoL contains 10,575 bacterial and archaeal genomes with each genome representing an OTU. Sequencing reads that did not map to a single reference genome as well as reads that mapped to multiple genomes were not included in the analysis. If an OTU had a relative abundance less than 0.01% in a given sample, the OTU was not included for that sample. Additionally, OTUs with fewer than 5 assigned reads were not considered. The samples were rarefied to a depth of 12,750 reads and those with fewer than the rarefaction depth were excluded. The QIIME2 v.2019.7 (105) DEICODE plugin was used to calculate the Aitchison distance, a compositional beta diversity metric, and perform Robust Aitchison PCA to create biplots that visualize relationships between features and samples (106). The QIIME2 diversity plugin was used to calculate the other alpha and beta diversity metrics used in this study.

Metagenomic based functional profiling

The filtered reads were also analyzed using HUMAnN2 v2.8.1 (107) to establish functional profiles for the samples. HUMAnN2 is a pipeline that begins by using MetaPhlAn 2 to compile custom databases of reference genomes based on the species detected in a sample (108). HUMAnN2 then maps the filtered onto these custom databases and the reads that do not map to any of the references are then subjected to a translated search against UniProt Reference Clusters or UniRef (109). Here, the UniRef90 database was used for the translated search and installed according to the HUMAnN2 documentation. The results from both the search performed using the custom reference genome database and the search against the UniRef90 database were combined and the gene families identified in each sample were reported in units of read per kilobase (RPKs) to account for gene length. HUMAnN2 also compared the gene families found in a sample with the MetaCyc pathways database (110) and output a table reporting the pathway abundances

found in each sample. After rarefying gene family tables to a depth of 166,000 RPKs and using a depth of 22,600 for pathway abundances, the QIIME2 diversity and DEICODE plugins were used to calculate alpha and beta diversity metrics.

Metabolomics Preparations

Sample Preparation

Frozen fecal and cecal samples were transported on dry ice for metabolomics analysis. The samples were weighed out and an extraction solvent (1:1 methanol to water with an internal standard of 1 μM sulfamethazine) was added at a 1:10 milligram to microliter ratio. The samples were then homogenized using a TissueLyser II (Qiagen) for 5 minutes at 25 hertz followed by a 15 minute centrifugation at 14,000 rpm. From the supernatant, 120 μL were transferred to a 96 deepwell plate (Eppendorf) and then these samples were lyophilized using a CentriVap Benchtop Vacuum Concentrator (Labconco) and stored at -80°C. Upon the time for data acquisition, the lyophilized plates were resuspended in a 1:1 methanol to water solvent spiked with 1 μM of sulfadimethoxine. The plates were vortexed for 2 minutes, centrifuged at 14,000 rpm for 15 minutes and 120 μL of the supernatant was transferred to a 96 well autosampler plate(Eppendorf). Plates were stored at 4 °C prior to LCMS analysis.

Data Acquisition

The untargeted metabolomics analysis was completed using an ultra-high performance liquid chromatography system (Thermo Dionex Ultimate 3000 UHPLC) coupled to ultra-high resolution quadrupole time of flight (qTOF) mass spectrometer (Bruker Daltonics MaXis HD). A Phenomenex Kinetex column (C18 1.7 μm, 2.1 mm x 50 mm) was used for chromatographic separation. An injection volume of 5 μL was used per sample and a flow-rate of 0.500 mL was used throughout the analysis. The mobile phase consisted of solvent A: 100% LC-MS grade water spiked with 0.1% formic acid and solvent B: 100% LC-MS grade acetonitrile spiked with 0.1% formic acid. The chromatographic gradient was as follows: 0.0–1.0 min, 5% B; 1.0–9.0 min, 5–100% B; 9.0-11.0 min, 100% B; 11.0-

11.5 min, 100-5% B; 11.5-12.5 min, 5% B. The data was collected using electrospray ionization in positive mode. Sample data was saved as .d file folders.

Data Processing

The raw .d data files were converted to mzXML format using Bruker Compass DataAnalysis 4.1 software. The resulting .mzXML file, the original .d file folders, and basic prep information sheet were stored on the UC San Diego MassIVE data repository under the accession number MSV000084550. For the MS1 level feature detection, the open-source software MZmine version 2.51 was used. The parameters used are as follows: 1) Mass Detection (Centroid, Noise Level MS1 1E3, MS2 1E2); 2) ADAP Chromatogram Builder (Min Group size in # of scans = 3, Group Intensity Threshold = 3E3, Min Highest Intensity = 1E3, m/z tolerance 0.01 m/z or 10.0 ppm); 3) Chromatogram Deconvolution (Local Minimum Search > Chromatographic Threshold 0.01%, Minimum in RT range 0.50 min, <Minimum Relative Height 0.01%, Minimum Absolute Height 3E3, Min Ratio of Peak Top/Edge 2, Peak Duration Range 0.05-0.50 min; m/z Calculation Auto, m/z range for MS2 pairing 0.01 Da, and RT Range for MS2 Pairing 0.1 min); Isotopic Peaks Grouper (m/z Tolerance 0.01 m/z or 10.0 ppm, Retention Time Tolerance 0.3 min, Maximum Charge 4, Representative Ion Most Intense); Join Aligner (m/z Tolerance 0.01 m/z or 10.0 ppm, Weight for m/z 75, Retention Time Tolerance 0.3 min, Weight for RT 25); Gap-Filling Peak Finder (Intensity Tolerance 20%, m/z Tolerance 0.005 m/z or 10.0 ppm, Retention Time Tolerance 0.2 min). The resulting feature table was saved as a .csv file and .mgf file for use in GNPS and MetaboAnalyst.

Molecular Networking and Statistical Analysis

Molecular networking was performing using the feature networking tool available on the Global Natural Products Social Molecular Networking portal (GNPS) accessed via the following link:

https://gnps.ucsd.edu/ProteoSAFe/index.jsp?params=%7B%22workflow%22:%22FEATURE-BASED-MOLECULAR-NETWORKING%22,%22library_on_server%22:%22d.speclibs;%22%7D.

The annotations obtained using this workflow fall under MSI level 2 or 3 and were used for feature analysis. The .mgf and .csv outputs from MZmine v2.51 were used to run the workflow. The GNPS workflow parameters used we as follows: Precursor Ion Mass 0.02 Da, Fragment Ion Mass Tolerance 0.02 Da, Min Pairs Cos 0.7, Minimum Matched Fragments 6, Maximum Shift Between Precursors 500 Da, Network TopK 10, Maximum Connected Component Size (Beta) 100, and the files were row sum normalized. Default parameters were used for the rest of the settings. The visualizations and statistical analyses were performed using QIIME 2 2019.10, MetaboAnalyst and Cytoscape v3.7.2.

REFERENCES

1.   Furness JB (2006) *The Enteric Nervous System* (Wiley-Blackwell).

2.   Grundy D, Brookes S (2011) Neural Control of Gastrointestinal Function. *Colloquium Series on Integrated Systems Physiology: From Molecule to Function* 3(9):1–134.

3.   Furness JB, Callaghan BP, Rivera LR, Cho H-J (2014) The Enteric Nervous System and Gastrointestinal Innervation: Integrated Local and Central Control. *The Enteric Nervous System*, Advances in Experimental Medicine and Biology. (Springer New York, New York, NY), pp 39–71.

4.   Schneider S, Wright CM, Heuckeroth RO (2019) Unexpected Roles for the Second Brain: Enteric Nervous System as Master Regulator of Bowel Function. *Annu Rev Physiol* 81(1):235–259.

5.   Muller PA, et al. (2014) Crosstalk between Muscularis Macrophages and Enteric Neurons Regulates Gastrointestinal Motility. *Cell* 158(5):1210.

6.   Gabanyi I, et al. (2016) Neuro-immune Interactions Drive Tissue Programming in Intestinal Macrophages. *Cell* 164(3):378–391.

7.   Bravo JA, et al. (2011) Ingestion of Lactobacillus strain regulates emotional behavior and central GABA receptor expression in a mouse via the vagus nerve. *Proceedings of the National Academy of Sciences* 108(38):16050–16055.

8.   Kotterman MA, Schaffer DV (2014) Engineering adeno-associated viruses for clinical gene therapy. *Nat Rev Genet* 15(7):445–451.

9.   Chan KY, et al. (2017) Engineered AAVs for efficient noninvasive gene delivery to the central and peripheral nervous systems. *Nat Neurosci* 20(8):1172–1179.

10.   Wess J, Nakajima K, Jain S (2013) Novel designer receptors to probe GPCR signaling and physiology. *Trends Pharmacol Sci* 34(7):385–392.

11.   Fried DE, Gulbransen BD (2015) In situ $Ca2+$ imaging of the enteric nervous system. *JoVE* (95). doi:10.3791/52506.

12.   Deverman BE, et al. (2016) Cre-dependent selection yields AAV variants for widespread gene transfer to the adult brain. *Nat Biotechnol* 34(2):204–209.

13. Benskey MJ, et al. (2015) Targeted gene delivery to the enteric nervous system using AAV: a comparison across serotypes and capsid mutants. *Mol Ther* 23(3):488–500.

14. Treweek JB, et al. (2015) Whole-body tissue stabilization and selective extractions via tissue-hydrogel hybrids for high-resolution intact circuit mapping and phenotyping. *Nature Protocols* 10(11):1860–1896.

15. Yang B, et al. (2014) Single-Cell Phenotyping within Transparent Intact Tissue through Whole-Body Clearing. *Cell* 158(4):945–958.

16. Hama H, et al. (2015) ScaleS: an optical clearing palette for biological imaging. *Nat Neurosci* 18(10):1518–1529.

17. Hansen MB (2003) The enteric nervous system II: Gastrointestinal functions. *Pharmacol Toxicol* 92(6):249–257.

18. Mowat AM, Agace WW (2014) Regional specialization within the intestinal immune system. *Nat Rev Immunol* 14(10):667–685.

19. Karhunen LJ, Juvonen KR, Huotari A, Purhonen AK, Herzig KH (2008) Effect of protein, fat, carbohydrate and fibre on gastrointestinal peptide release in humans. *Regulatory Peptides* 149(1-3):70–78.

20. Makki K, Deehan EC, Walter J, Bäckhed F (2018) The Impact of Dietary Fiber on Gut Microbiota in Host Health and Disease. *Cell Host Microbe* 23(6):705–715.

21. Giaroni C, et al. (2000) Glutamate receptors of the AMPA type modulate neurotransmitter release and peristalsis in the guinea-pig isolated colon. *Life Sciences* 67(14):1747–1757.

22. Rakhilin N, et al. (2016) Simultaneous optical and electrical in vivo analysis of the enteric nervous system. *Nature Communications* 7(1):31.

23. Chen T-W, et al. (2013) Ultrasensitive fluorescent proteins for imaging neuronal activity. *Nature* 499(7458):295–300.

24. McVey Neufeld KA, Mao YK, Bienenstock J, Foster JA, Kunze WA (2012) The microbiome is essential for normal gut intrinsic primary afferent neuron excitability in the mouse. *Neurogastroenterology & Motility* 25(2):183–e88.

25. Collins J, Borojevic R, Verdu EF, Huizinga JD, Ratcliffe EM (2013) Intestinal microbiota influence the early postnatal development of the enteric nervous system. *Neurogastroenterology & Motility* 26(1):98–107.

26. De Vadder F, et al. (2018) Gut microbiota regulates maturation of the adult enteric nervous system via enteric serotonin networks. *Proceedings of the National Academy of Sciences* 115(25):6458–6463.

27. Kulkarni S, et al. (2017) Adult enteric nervous system in health is maintained by a dynamic balance between neuronal apoptosis and neurogenesis. *Proceedings of the National Academy of Sciences* 114(18):E3709–E3718.

28. McVey Neufeld KA, Mao YK, Bienenstock J, Foster JA, Kunze WA (2013) The microbiome is essential for normal gut intrinsic primary afferent neuron excitability in the mouse. *Neurogastroenterol Motil* 25(2):183–e88.

29. McVey Neufeld KA, Perez-Burgos A, Mao YK, Bienenstock J, Kunze WA (2015) The gut microbiome restores intrinsic and extrinsic nerve function in germ-free mice accompanied by changes in calbindin. *Neurogastroenterol Motil* 27(5):627–636.

30. Thompson KJ, et al. (2018) DREADD Agonist 21 Is an Effective Agonist for Muscarinic-Based DREADDs in Vitro and in Vivo. *ACS Pharmacol Transl Sci* 1(1):61–72.

31. Wu YE, Pan L, Zuo Y, Li X, Hong W (2017) Detecting Activated Cell Populations Using Single-Cell RNA-Seq. *Neuron* 96(2):313–329.e6.

32. Ramirez-Carrozzi VR, et al. (2009) A Unifying Model for the Selective Regulation of Inducible Transcription by CpG Islands and Nucleosome Remodeling. *Cell* 138(1):114–128.

33. Bahrami S, Drabløs F (2016) Gene regulation in the immediate-early response process. *Advances in Biological Regulation* 62:37–49.

34. Miano JM, et al. (1993) Smooth muscle cell immediate-early gene and growth factor activation follows vascular injury. A putative in vivo mechanism for autocrine growth. *Arterioscler Thromb* 13(2):211–219.

35. Flandez M, Guilmeau S, Blache P, Augenlicht LH (2008) KLF4 regulation in intestinal epithelial cell maturation. *Experimental Cell Research* 314(20):3712–3723.

36. Albenberg LG, Wu GD (2014) Diet and the intestinal microbiome: associations, functions, and implications for health and disease. *Gastroenterology* 146(6):1564–1572.

37.   Jia L, Betters JL, Yu L (2011) Niemann-pick C1-like 1 (NPC1L1) protein in intestinal and hepatic cholesterol transport. *Annu Rev Physiol* 73(1):239–259.

38.   Rodríguez-Piñeiro AM, et al. (2013) Studies of mucus in mouse stomach, small intestine, and colon. II. Gastrointestinal mucus proteome reveals Muc2 and Muc5ac accompanied by a set of core proteins. *American Journal of Physiology - Gastrointestinal and Liver Physiology* 305(5):G348–G356.

39.   Matsushima S, Hori S, Matsuda M (1986) Conversion of 4-aminobutyraldehyde to gamma-aminobutyric acid in striatum treated with semicarbazide and kainic acid. *Neurochem Res* 11(9):1313–1319.

40.   Nakamura A, Ooga T, Matsumoto M (2019) Intestinal luminal putrescine is produced by collective biosynthetic pathways of the commensal microbiome. *Gut Microbes* 10(2):159–171.

41.   McConnell RE, Benesh AE, Mao S, Tabb DL, Tyska MJ (2011) Proteomic analysis of the enterocyte brush border. *American Journal of Physiology - Gastrointestinal and Liver Physiology* 300(5):G914–26.

42.   Donowitz M, et al. (2007) Proteome of murine jejunal brush border membrane vesicles. *J Proteome Res* 6(10):4068–4079.

43.   Macpherson AJ, et al. (2000) A primitive T cell-independent mechanism of intestinal mucosal IgA responses to commensal bacteria. *Science* 288(5474):2222–.

44.   vanderWaaij LA, Limburg PC, Mesander G, vanderWaaij D (1996) In vivo IgA coating of anaerobic bacteria in human faeces. *Gut* 38(3):348–354.

45.   Macpherson AJ (2004) Induction of Protective IgA by Intestinal Dendritic Cells Carrying Commensal Bacteria. *Science* 303(5664):1662–1665.

46.   Donaldson GP, et al. (2018) Gut microbiota utilize immunoglobulin A for mucosal colonization. *Science* 360(6390):795–800.

47.   Segata N, et al. (2011) Metagenomic biomarker discovery and explanation. *Genome Biol* 12(6):R60.

48.   Everard A, et al. (2013) Cross-talk between Akkermansia muciniphila and intestinal epithelium controls diet-induced obesity. *Proc Natl Acad Sci USA* 110(22):9066–9071.

49.   Plovier H, et al. (2017) A purified membrane protein from Akkermansia muciniphila or the pasteurized bacterium improves metabolism in obese and diabetic mice. *Nature Medicine* 23(1):107–113.

50.   Cekanaviciute E, et al. (2017) Gut bacteria from multiple sclerosis patients modulate human T cells and exacerbate symptoms in mouse models. *Proc Natl Acad Sci USA* 114(40):10713–10718.

51.   Jangi S, et al. (2016) Alterations of the human gut microbiome in multiple sclerosis. *Nature Communications* 7(1):12015–11.

52.   Olson CA, et al. (2018) The Gut Microbiota Mediates the Anti-Seizure Effects of the Ketogenic Diet. *Cell* 173(7):1728–1741.e13.

53.   Wang M, et al. (2016) Sharing and community curation of mass spectrometry data with Global Natural Products Social Molecular Networking. *Nat Biotechnol* 34(8):828–837.

54.   Nothias LF, et al. (2019) Feature-based Molecular Networking in the GNPS Analysis Environment. *bioRxiv* 38:812404.

55.   Pluskal T, Castillo S, Villar-Briones A, Oresic M (2010) MZmine 2: Modular framework for processing, visualizing, and analyzing mass spectrometry-based molecular profile data. *BMC Bioinformatics* 11(1). doi:10.1186/1471-2105-11-395.

56.   Sumner LW, et al. (2007) Proposed minimum reporting standards for chemical analysis Chemical Analysis Working Group (CAWG) Metabolomics Standards Initiative (MSI). *Metabolomics* 3(3):211–221.

57.   Sakai K, Makino T, Kawai Y, Mutai M (1980) Intestinal microflora and bile acids. Effect of bile acids on the distribution of microflora and bile acid in the digestive tract of the rat. *Microbiol Immunol* 24(3):187–196.

58.   Aries V, Crowther JS, Drasar BS, Hill MJ (1969) Degradation of bile salts by human intestinal bacteria. *Gut* 10(7):575–576.

59.   Walsh KT, Zemper AE (2019) The Enteric Nervous System for Epithelial Researchers: Basic Anatomy, Techniques, and Interactions With the Epithelium. *Cellular and Molecular Gastroenterology and Hepatology* 8(3):369–378.

60.   Fung TC, Olson CA, Hsiao EY (2017) Interactions between the microbiota, immune and nervous systems in health and disease. *Nat Neurosci* 20(2):145–155.

61. Carabotti M, Scirocco A, Maselli MA, Severi C (2015) The gut-brain axis: interactions between enteric microbiota, central and enteric nervous systems. *Ann Gastroenterol* 28(2):203–209.

62. Yissachar N, et al. (2017) An Intestinal Organ Culture System Uncovers a Role for the Nervous System in Microbe-Immune Crosstalk. *Cell* 168(6):1135–1148.e12.

63. Kaelberer MM, et al. (2018) A gut-brain neural circuit for nutrient sensory transduction. *Science* 361(6408):eaat5236.

64. Lai NY, et al. (2019) Gut-Innervating Nociceptor Neurons Regulate Peyer's Patch Microfold Cells and SFB Levels to Mediate Salmonella Host Defense. *Cell* 180(1):33–49.e22.

65. Matheis F, et al. (2020) Adrenergic Signaling in Muscularis Macrophages Limits Infection-Induced Neuronal Loss. *Cell* 180(1):64–78.e16.

66. Jarret A, et al. (2020) Enteric Nervous System-Derived IL-18 Orchestrates Mucosal Barrier Immunity. *Cell* 180(1):50–63.e12.

67. Lindeberg J, et al. (2004) Transgenic expression of Cre recombinase from the tyrosine hydroxylase locus. *Genesis* 40(2):67–73.

68. Challis RC, et al. (2019) Systemic AAV vectors for widespread and targeted gene delivery in rodents. *Nature Protocols* 14(2):379–414.

69. Yano JM, et al. (2015) Indigenous Bacteria from the Gut Microbiota Regulate Host Serotonin Biosynthesis. *Cell* 161(2):264–276.

70. Treweek JB, et al. (2015) Whole-body tissue stabilization and selective extractions via tissue-hydrogel hybrids for high-resolution intact circuit mapping and phenotyping. *Nature Protocols* 10(11):1860–1896.

71. Deneux T, et al. (2016) Accurate spike estimation from noisy calcium signals for ultrafast three-dimensional imaging of large neuronal populations in vivo. *Nature Communications* 7(1):12190–17.

72. Kim D, Langmead B, Salzberg SL (2015) HISAT: a fast spliced aligner with low memory requirements. *Nat Methods* 12(4):357–360.

73. Anders S, Pyl PT, Huber W (2015) HTSeq--a Python framework to work with high-throughput sequencing data. *Bioinformatics* 31(2):166–169.

74. Sundararajan Z, et al. (2019) Shiny-Seq: advanced guided transcriptome analysis. *BMC Res Notes* 12(1):432–5.

75.   Wessel D, Flügge UI (1984) A method for the quantitative recovery of protein in dilute solution in the presence of detergents and lipids. *Analytical Biochemistry* 138(1):141–143.

76.   He L, Diedrich J, Chu Y-Y, Yates JR (2015) Extracting Accurate Precursor Information for Tandem Mass Spectra by RawConverter. *Anal Chem* 87(22):11361–11367.

77.   Peng J, Elias JE, Thoreen CC, Licklider LJ, Gygi SP (2003) Evaluation of multidimensional chromatography coupled with tandem mass spectrometry (LC/LC-MS/MS) for large-scale protein analysis: the yeast proteome. *J Proteome Res* 2(1):43–50.

78.   Elias JE, Gygi SP (2007) Target-decoy search strategy for increased confidence in large-scale protein identifications by mass spectrometry. *Nat Methods* 4(3):207–214.

79.   Park SKR, et al. (2018) ComPIL 2.0: An Updated Comprehensive Metaproteomics Database. *J Proteome Res* 18(2):616–622.

80.   Xu T, et al. (2006) ProLuCID, a fast and sensitive tandem mass spectra-based protein identification program.

81.   Xu T, et al. (2015) ProLuCID: An improved SEQUEST-like algorithm with enhanced sensitivity and specificity. *J Proteomics* 129:16–24.

82.   Tabb DL, McDonald WH, Yates JR (2002) DTASelect and Contrast: tools for assembling and comparing protein identifications from shotgun proteomics. *J Proteome Res* 1(1):21–26.

83.   Cociorva D, L Tabb D, Yates JR (2007) Validation of Tandem Mass Spectrometry Database Search Results Using DTASelect. *Current Protocols in Bioinformatics* 16(1). doi:10.1002/0471250953.bi1304s16.

84.   Li W, Godzik A (2006) Cd-hit: a fast program for clustering and comparing large sets of protein or nucleotide sequences. *Bioinformatics* 22(13):1658–1659.

85.   Fu L, Niu B, Zhu Z, Wu S, Li W (2012) CD-HIT: accelerated for clustering the next-generation sequencing data. *Bioinformatics* 28(23):3150–3152.

86.   Li W, Jaroszewski L, Godzik A (2001) Clustering of highly homologous sequences to reduce the size of large protein databases. *Bioinformatics* 17(3):282–283.

87. Love MI, Huber W, Anders S (2014) Moderated estimation of fold change and dispersion for RNA-seq data with DESeq2. *Genome Biol* 15(12):1–21.

88. Park S, Aslanian A, McClatchy DB, Han X, 2014 Census 2: isobaric labeling data analysis. *academicoupcom*

.

89. Park SK, Venable JD, Xu T, Yates JR (2008) A quantitative analysis software tool for mass spectrometry–based proteomics. *Nat Methods* 5(4):319–322.

90. Zhang X, et al. (2018) Proteome-wide identification of ubiquitin interactions using UbIA-MS. *Nature Protocols* 13(3):530–550.

91. Huber W, Heydebreck von A, Sültmann H, Poustka A, Vingron M (2002) Variance stabilization applied to microarray data calibration and to the quantification of differential expression. *Bioinformatics* 18 Suppl 1(Suppl 1):S96–104.

92. Gatto L, Lilley KS (2012) MSnbase-an R/Bioconductor package for isobaric tagged mass spectrometry data visualization, processing and quantitation. *Bioinformatics* 28(2):288–289.

93. Ritchie ME, et al. (2015) limma powers differential expression analyses for RNA-sequencing and microarray studies. *Nucleic Acids Res* 43(7):e47–e47.

94. Szklarczyk D, et al. (2019) STRING v11: protein-protein association networks with increased coverage, supporting functional discovery in genome-wide experimental datasets. *Nucleic Acids Res* 47(D1):D607–D613.

95. Mesuere B, et al. (2015) The Unipept metaproteomics analysis pipeline. *Proteomics* 15(8):1437–1442.

96. Gurdeep Singh R, et al. (2019) Unipept 4.0: Functional Analysis of Metaproteome Data. *J Proteome Res* 18(2):606–615.

97. Glenn TC, et al. (2019) Adapterama I: universal stubs and primers for 384 unique dual-indexed or 147,456 combinatorially-indexed Illumina libraries (iTru & iNext). *PeerJ* 7:e7755.

98. Costello M, et al. (2018) Characterization and remediation of sample index swaps by non-redundant dual indexing on massively parallel sequencing platforms. *BMC Genomics* 19(1):332–10.

99.   Sinha R, et al. (2017) Index switching causes "spreading-of-signal" among multiplexed samples in Illumina HiSeq 4000 DNA sequencing. 29:1072–29.

100.   Gonzalez A, et al. (2018) Qiita: rapid, web-enabled microbiome meta-analysis. *Nat Methods* 15(10):796–798.

101.   Didion JP, Martin M, Collins FS (2017) Atropos: specific, sensitive, and speedy trimming of sequencing reads. *PeerJ* 5(10):e3720.

102.   Langmead B, Salzberg SL (2012) Fast gapped-read alignment with Bowtie 2. *Nat Methods* 9(4):357–359.

103.   Zhu Q, et al. (2019) Phylogenomics of 10,575 genomes reveals evolutionary proximity between domains Bacteria and Archaea. *Nature Communications* 10(1):5477–14.

104.   Hillmann B, et al. (2018) Evaluating the Information Content of Shallow Shotgun Metagenomics. *mSystems* 3(6):457.

105.   Bolyen E, et al. (2019) Reproducible, interactive, scalable and extensible microbiome data science using QIIME 2. *Nat Biotechnol* 37(8):852–857.

106.   Martino C, et al. (2019) A Novel Sparse Compositional Technique Reveals Microbial Perturbations. *mSystems* 4(1):813.

107.   Franzosa EA, et al. (2018) Species-level functional profiling of metagenomes and metatranscriptomes. *Nat Methods* 15(11):962–968.

108.   Truong DT, et al. (2015) MetaPhlAn2 for enhanced metagenomic taxonomic profiling. *Nat Methods* 12(10):902–903.

109.   Suzek BE, Huang H, McGarvey P, Mazumder R, Wu CH (2007) UniRef: comprehensive and non-redundant UniProt reference clusters. *Bioinformatics* 23(10):1282–1288.

110.   Caspi R, et al. (2018) The MetaCyc database of metabolic pathways and enzymes. *Nucleic Acids Res* 46(D1):D633–D639.

Chapter 5

CONCLUSION

Conclusion

Neurons, in general, detect chemical stimuli and transmit electrical impulses over large biological distances at remarkable speeds (1). In the brain, experiential stimuli motivate neural plasticity and learning, and this defines the network by which information is propagated from one cell to another, resulting in predictable physiological or behavioral outputs (2). In the GI tract, the ENS adapts and responds to incredibly diverse molecular cues and must do so throughout the entire length and surface area of the intestines- the largest and most expansive internal organ. Often coined as the "second brain" (3), perhaps it is the exposure and entrainment of GI neurons to molecular stimuli, over brief and lengthy biological time scales, that establishes its physiological "identity". These exposure events could ultimately determine the host's response, tolerance, and susceptibility to the environment and disease. And as we process these complex and dynamic molecular environments, and work to maintain host and microbial homeostasis, aging and neurodegeneration of the GI nervous system are not so different from that found in the brain.

The CNS is responsible for reacting and adapting to environmental cues processed by our physical senses. The GI nervous system integrates such signals from the brain but receives additional molecular input from the luminal environment. The brain dictates the environments we are exposed to and our initial reactions to it. However, it is the GI tract, and innervation of it, that processes the chemical cues and propagates this information as electrical impulses throughout the body. It is through this network that the GI tract is inextricably linked to the rest of the body. Thus, dysregulation of the GI nervous system may have a larger role, than previously believed, in impacting GI physiology and beyond. As advances in experimental tools help us understand the active role that GI innervation has in shaping the intestinal tissue, luminal environment, and the systemic milieu, novel hypotheses on disease etiologies will emerge, promoting the study of therapeutics that target the ENS for both GI and peripheral related diseases.

References

1. Groh JM, Gazzaniga MS (2003) How the Brain Keeps Time. *Daedalus* 132(2):56–61.

2. Bruel-Jungerman E, Davis S, Laroche S (2016) Brain Plasticity Mechanisms and Memory: A Party of Four. *Neuroscientist* 13(5):492–505.

3. Gershon MD (2015) The Enteric Nervous System: A Second Brain. *Hospital Practice* 34(7):31–52